PUBLISHER:

Address of Publisher & Editor's Office:

GDAŃSK UNIVERSITY
OF TECHNOLOGY
Faculty
of Ocean Engineering
& Ship Technology

ul. Narutowicza 11/12
80-233 Gdańsk, POLAND
tel.: +48 58 347 13 66
fax: +48 58 341 13 66
e-mail: office.pmr@pg.gda.pl

Account number:
BANK ZACHODNI WBK S.A.
I Oddział w Gdańsku
41 1090 1098 0000 0000 0901 5569

Editorial Staff:

Tadeusz Borzęcki Editor in Chief

Przemysław Wierzchowski Scientific Editor

Jan Michalski Editor for review matters

Aleksander Kniat Editor for international relations

Kazimierz Kempa Technical Editor

Piotr Bzura Managing Editor

Cezary Spigarski Computer Design

Domestic price:
single issue: 25 zł

Prices for abroad:
single issue:
- in Europe EURO 15
- overseas USD 20

ISSN 1233-2585

POLISH MARITIME RESEARCH
in internet
www.bg.pg.gda.pl/pmr/pmr.php

POLISH MARITIME RESEARCH

No 4 (80) 2013 Vol 20

CONTENTS

Editorial

POLISH MARITIME RESEARCH is a scientific journal of worldwide circulation. The journal appears as a quarterly four times a year. The first issue of it was published in September 1994. Its main aim is to present original, innovative scientific ideas and Research & Development achievements in the field of :

Engineering, **Computing & Technology**, **Mechanical Engineering**,

which could find applications in the broad domain of maritime economy. Hence there are published papers which concern methods of the designing, manufacturing and operating processes of such technical objects and devices as : ships, port equipment, ocean engineering units, underwater vehicles and equipment as well as harbour facilities, with accounting for marine environment protection.
The Editors of POLISH MARITIME RESEARCH make also efforts to present problems dealing with education of engineers and scientific and teaching personnel. As a rule, the basic papers are supplemented by information on conferences , important scientific events as well as cooperation in carrying out international scientific research projects.

Scientific Board

On October 14th, 2013
at the age of 70, passed suddenly away

Editor in Chief of the Quarterly “Polish Maritime Research”

Tadeusz Borzecki, PhD, MSc

Photo: L. Nadolny

Mr Tadeusz Borzecki was a academic teacher at Faculty of Ocean Engineering and Ship Technology, Gdansk University of Technology (GUT) Poland.

He was awarded a Master of Science (Naval Architect) degree by GUT in 1966 and a Doctor of Engineering in 1975. He was the Vice-Dean of Faculty of Ocean Engineering and Ship Technology in 2005-2008.

Member of international Boards and editorial staffs,
Honoured with many distinctions.

Dean

Faculty of Ocean Engineering
and Ship Technology,
Gdansk University of Technology

Editorial Board

Polish Maritime Research

POLISH MARITIME RESEARCH 4(80) 2013 Vol 20; pp. 4-17
10.2478/pomr-2013-0035

Influence of viscosity and compressibility of aerated oil on determination of volumetric losses in a variable capacity piston pump

Jan Koralewski, M. Sc.,
Gdansk University of Technology, Poland

ABSTRACT

Modulus B of the liquid volume elasticity of non-aerated and aerated oil is defined in the paper as relation to the indicated increase of pressure in the pump working chambers, with the change of oil temperature and degree of aeration. In evaluation of the losses due to oil compressibility in a variable capacity displacement pump, the volume of compressed liquid at each pump setting is taken into account. Volumetric losses have been divided into leakage losses in the pump chambers and losses due to liquid compressibility. The need of accounting for only the leakage losses for pump evaluation is pointed out.

Keywords: hydrostatic drive, variable capacity displacement pump, liquid aeration, method of determining the degree of liquid aeration

INTRODUCTION

In references [1–3] the Author presented results of investigations of the influence of hydraulic oil viscosity on volumetric losses in a variable capacity piston pump. The tests were carried out with a HYDROMATIK A7V.58.1.R.P.F.00 type pump of bent axis design, without taking into account the hydraulic oil compressibility. The investigations were performed on a test stand in the Hydraulic and Pneumatics Laboratory of the Faculty of Mechanical Engineering and the results were elaborated in the Chair of Marine Mechatronics of the Faculty of Ocean Engineering and Ship Technology of the Gdansk University of Technology.

The tests were performed with:

- 8 hydraulic oil temperatures ϑ (oil kinematic viscosity ν):
  $\vartheta = 20°C$ ($\nu = 120.40$ mm^{2}s^{-1}), $\vartheta = 24°C$ ($\nu = 91.16$ mm^{2}s^{-1}),
  $\vartheta = 30°C$ ($\nu = 65.37$ mm^{2}s^{-1}), $\vartheta = 36°C$ ($\nu = 47.05$ mm^{2}s^{-1}),
  $\vartheta = 43°C$ ($\nu = 34.68$ mm^{2}s^{-1}), $\vartheta = 50°C$ ($\nu = 26.41$ mm^{2}s^{-1}),
  $\vartheta = 60°C$ ($\nu = 18.77$ mm^{2}s^{-1}), $\vartheta = 68°C$ ($\nu = 14.53$ mm^{2}s^{-1}),
- 8 values of increase Δp_P pressure in the pump:
  $\Delta p_P = 1.6$ MPa, $\Delta p_P = 3.2$ MPa, $\Delta p_P = 6.3$ MPa,
  $\Delta p_P = 10$ MPa, $\Delta p_P = 16$ MPa, $\Delta p_P = 20$ MPa,
  $\Delta p_P = 25$ MPa, $\Delta p_P = 32$ MPa,
- 7 values of pump capacity coefficient b_P:
  $b_P = 0.225$; $b_P = 0.361$; $b_P = 0.493$;
  $b_P = 0.623$; $b_P = 0.752$; $b_P = 0.880$; $b_P = 1$.

The Author presents in this paper results of the investigations of the effect of viscosity and compressibility of non-aerated and aerated oil on determination of volumetric losses in a variable capacity piston pump.

The problem of effect of compressibility of the non-aerated and aerated working liquid on volumetric and mechanical losses in a variable capacity displacement pump has been undertaken by Zygmunt Paszota [4-10].

In reference [13] Z. Paszota presented his method of determining the degree of aeration of liquid flowing in a variable capacity displacement pump.

The Author is the first user of the method in his research work into the influence of liquid aeration and viscosity on mechanical and volumetric losses in the pump.

LIQUID COMPRESSIBILITY IN A VARIABLE CAPACITY PISTON PUMP

The term „compressibility" defines susceptibility of liquid to volumetric strain with changing pressure. The measure of strain is compressibility coefficient β defined as:

$$\beta = -\frac{1}{V_0}\frac{dV}{dp} \tag{1}$$

For finite increments, relations may be used of change of initial volume V_0 with increase of pressure by a value Δp:

$$\Delta V = -\beta V_0 \Delta p \tag{2}$$

The inverse of compressibility coefficient is modulus B of the liquid volume elasticity:

$$B = 1/\beta \tag{3}$$

For mineral oils, modulus B depends on pressure p and temperature ϑ. These relations are illustrated in diagrams (Fig. 1 and Fig. 2).

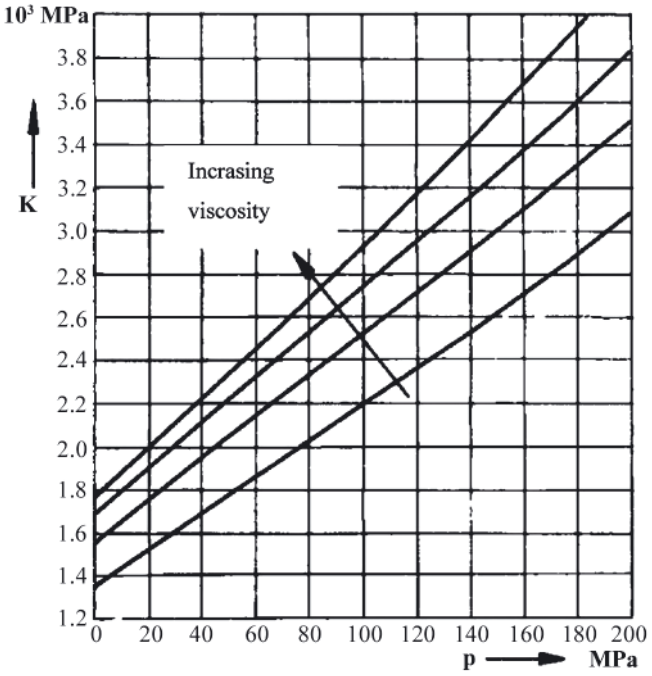

Fig. 1. Relation of modulus K of volumetric strain K of mineral oils to pressure and viscosity [12]

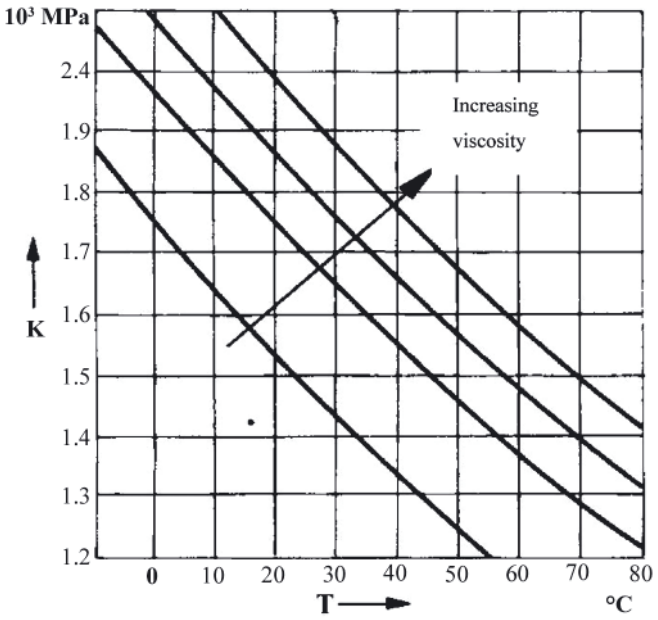

Fig. 2. Relation of modulus K of volumetric strain of mineral oils to temperature and viscosity [12]

Numerical values of modulus B of the used hydraulic oils are the following [11]:

- at the normal temperature (20°C), close to B = 1500 MPa,
- B increases with the pressure (by about 1% every 2 MPa up to 20 MPa (a_p = 0.005/1 MPa)),
- B decreases when the temperature increases (about 1% every 2°C up to 100°C (a_ϑ = -0.005/1°C)).

In working chambers of the tested piston pump during their connection with the inlet channel was slight overpressure $p_{P1i} \approx 0.05$ MPa (i.e. absolute pressure $p_{P1ia} \approx 0.15$ MPa). Let's assume that the value of modulus B of the hydraulic oil volume elasticity, at the temperature ϑ = 20°C, equals to:

$$B_{|p_{P1ia} \approx 0.15MPa;\, \vartheta = 20°C} = 1500\,MPa \tag{4}$$

Therefore, the dependence of modulus B of oil on the increase Δp_{Pi} of pressure in the working chambers and on the increase $\Delta\vartheta$ of oil temperature may be described by the expression:

$$B = B_{|p_{P1ia} \approx 0.15MPa;\, \vartheta = 20°C}(1 + a_p\,\Delta p_{Pi} + a_\vartheta\,\Delta\vartheta) \tag{5}$$

The hydraulic oil compressibility depends to a great extent on the contents of non-dissolved air. The measure of non-dissolved air in oil is the oil aeration coefficient ε – ratio of the volume V_a of air to the volume $V_0 = V_o + V_a$ of mixture equal to the sum of oil volume V_o and air volume V_a:

$$\varepsilon = \frac{V_a}{V_o + V_a} = \frac{V_a}{V_0} \tag{6}$$

The oil aeration coefficient ε is determined at the absolute pressure p_{P1ia} in the pump working chambers during their connection with the inlet channel.

An increase Δp_{Pi} of pressure in the pump working chambers causes a decrease of the oil and air mixture volume by the value ΔV (assuming a hypothesis of compression of air pV_a = cte) equal to:

$$\Delta V = \Delta V_o + \Delta V_a = \frac{V_o}{B}\Delta p_{Pi} + \frac{V_a}{p_{P1ia} + \Delta p_{Pi}}\Delta p_{Pi} \tag{7}$$

If the aeration coefficient ε is small, which is a general case, V_o is close to V_0. Therefore, it can, be written [11]:

$$\Delta V = V_0\left(\frac{1}{B} + \frac{\varepsilon}{p_{P1ia} + \Delta p_{Pi}}\right)\Delta p_{Pi} \tag{8}$$

Modulus B' of aerated hydraulic oil volume elasticity is defined by the expression:

$$\frac{1}{B'} = \frac{1}{B} + \frac{\varepsilon}{p_{P1ia} + \Delta p_{Pi}} \tag{9}$$

or, in the conditions of changing the aerated oil pressure and temperature, by the expression:

$$\frac{1}{B'} = \frac{1}{B_{|p_{P1ia} \approx 0.15MPa,\, \vartheta = 20°C}(1 + a_p\Delta p_{Pi} + a_\vartheta\Delta\vartheta)} + \frac{\varepsilon}{p_{P1ia} + \Delta p_{Pi}} \tag{10}$$

Fig. 3 presents modulus B of non-aerated (ε = 0) oil volume elasticity and modulus B' of aerated (ε > 0) oil volume elasticity as dependent on the indicated increase Δp_{Pi} of pressure in the pump working chambers with the hydraulic oil temperature limit values ϑ = 20°C and ϑ = 68°C assumed during the tests.

In a variable capacity pump, the initial oil volume V_0 (Fig. 4), subjected to compression in effect of increase Δp_{Pi} of pressure in the chambers, corresponding to setting q_{Pgv} of variable geometrical working capacity, is equal to:

$$V_0 = 0.5q_{Pt} + 0.5q_{Pgv} \tag{11}$$

When the variable (set) geometrical working capacity q_{Pgv} reaches the maximum value equal to the pump theoretical working capacity q_{Pt} ($q_{Pgv} = q_{Pt}$), the compressed oil volume V_0 has the value:

$$V_0 = 0.5q_{Pt} + 0.5q_{Pt} = q_{Pt} \tag{12}$$

The change ΔV of liquid volume due to compression of liquid as an effect of increase Δp_{Pi} of pressure in the pump chambers (presented in Fig. 4) equals to the volumetric losses q_{Pvc} due to compression of oil during one pump shaft revolution:

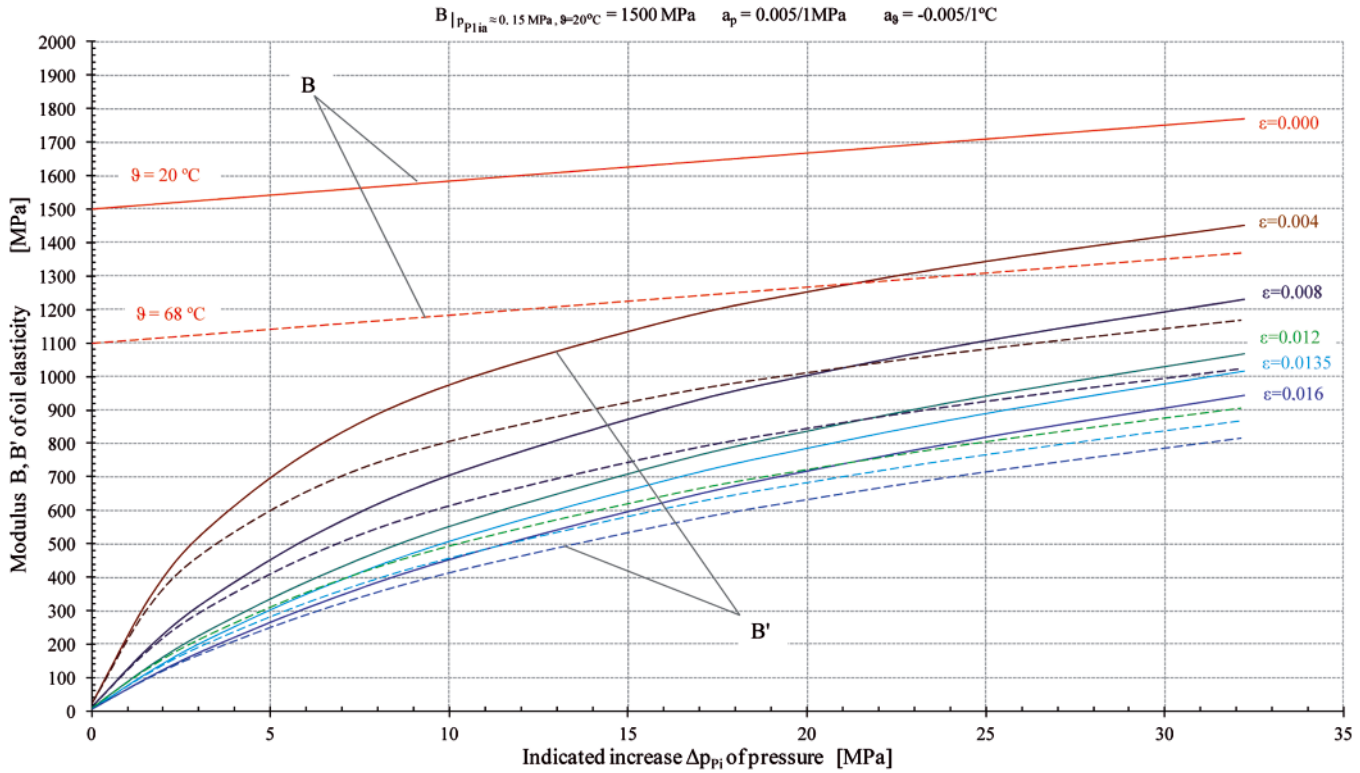

Fig. 3. Modulus B of volume elasticity of non-aerated hydraulic oil (ε = 0) and modulus B' of aerated oil (ε > 0) as relations dependent on indicated increase Δp_{Pi} of pressure in the pump working chambers, with limit values ϑ = 20°C (continuous line) and ϑ = 68°C (dashed line) of hydraulic oil temperature adopted during the investigations. It was assumed that modulus B of oil volume elasticity at absolute pressure $p_{P1ia} \approx 0.15$ MPa in the pump working chambers during their connection with the inlet channel and at oil temperature ϑ = 20°C is equal to B = 1500 MPa. Also assumed was the value of coefficient a_p = 0.005/1 MPa of the change of modulus B of oil due to increase Δp_{Pi} of pressure in the working channels and coefficient a_ϑ = - 0.005/1°C of the change of modulus B due to change of oil temperature ϑ

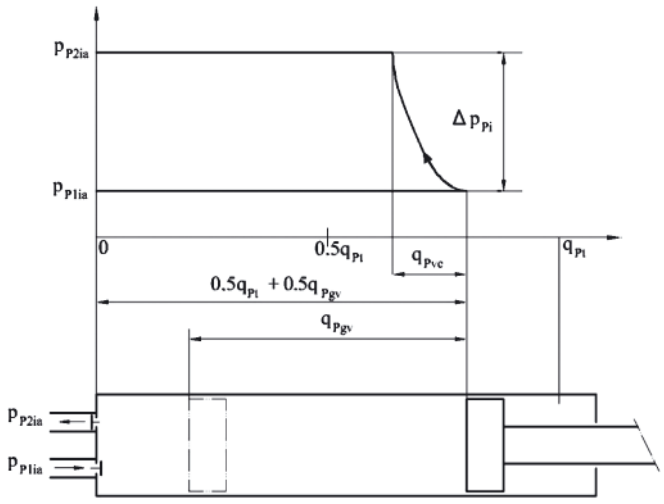

Fig. 4. Initial oil volume ($0.5q_{Pt} + 0.5q_{Pgv}$) subjected to compression in a variable capacity displacement pump in effect of increase Δp_{Pi} of pressure in the chambers, corresponding to setting q_{Pgv} of variable geometrical working capacity

$$\Delta V = q_{Pvc} \tag{13}$$

The losses q_{Pvc} of pump capacity per one shaft revolution (Fig. 4) due to compressibility of non-aerated (or aerated) oil, occurring with setting q_{Pgv} of variable geometrical capacity, is determined (in reference to (7) and (8)) by the formula:

$$q_{Pvc} = \frac{(0.5q_{Pt} + 0.5q_{Pt})\,\Delta p_{Pi}}{B'} \tag{14}$$

and with $q_{Pgv} = q_{Pt}$ by the formula:

$$q_{Pvc} = \frac{q_{Pt}\,\Delta p_{Pi}}{B'} \tag{15}$$

after replacing 1/B' by expression (10), by the formula:

$$q_{Pvc} = (0.5q_{Pt} + 0.5q_{Pgv}) \cdot \left[\frac{1}{B_{|p_{P1ia} \approx 0.15\,\mathrm{MPa}, \vartheta = 20°C}\,(1 + a_p \Delta p_{Pi} + a_\vartheta \Delta\vartheta)} + \frac{\varepsilon}{p_{P1ia} + \Delta p_{Pi}} \right] \Delta p_{Pi} \tag{16}$$

and, with $q_{Pgv} = q_{Pt}$, by the formula:

$$q_{Pvc} = q_{Pt} \cdot \left[\frac{1}{B_{|p_{P1ia} \approx 0.15\,\mathrm{MPa}, \vartheta = 20°C}(1 + a_p \Delta p_{Pi} + a_\vartheta \Delta\vartheta)} + \frac{\varepsilon}{p_{P1ia} + \Delta p_{Pi}} \right] \Delta p_{Pi} \tag{17}$$

Fig. 5 presents an example (with assumed oil aeration coefficient ε = 0.0135) of calculations of the losses $q_{Pvc} = f(\Delta p_{Pi})$ of pump capacity per one pump shaft revolution, taking into account formula (16) for cases of variable geometrical working capacity settings q_{Pgv} and formula (17) for the maximum setting $q_{Pgv} = q_{Pt}$, i.e. pump theoretical working capacity.

The change of losses q_{Pvc} of pump capacity per one shaft revolution due to the liquid compressibility, as a relation to the indicated increase Δp_{Pi} of pressure in the working chambers, presented in Fig. 5, takes into account the influence of changing volumes V_0 (Fig. 4) of liquid in working chambers subjected to compression and being an effect of operation of

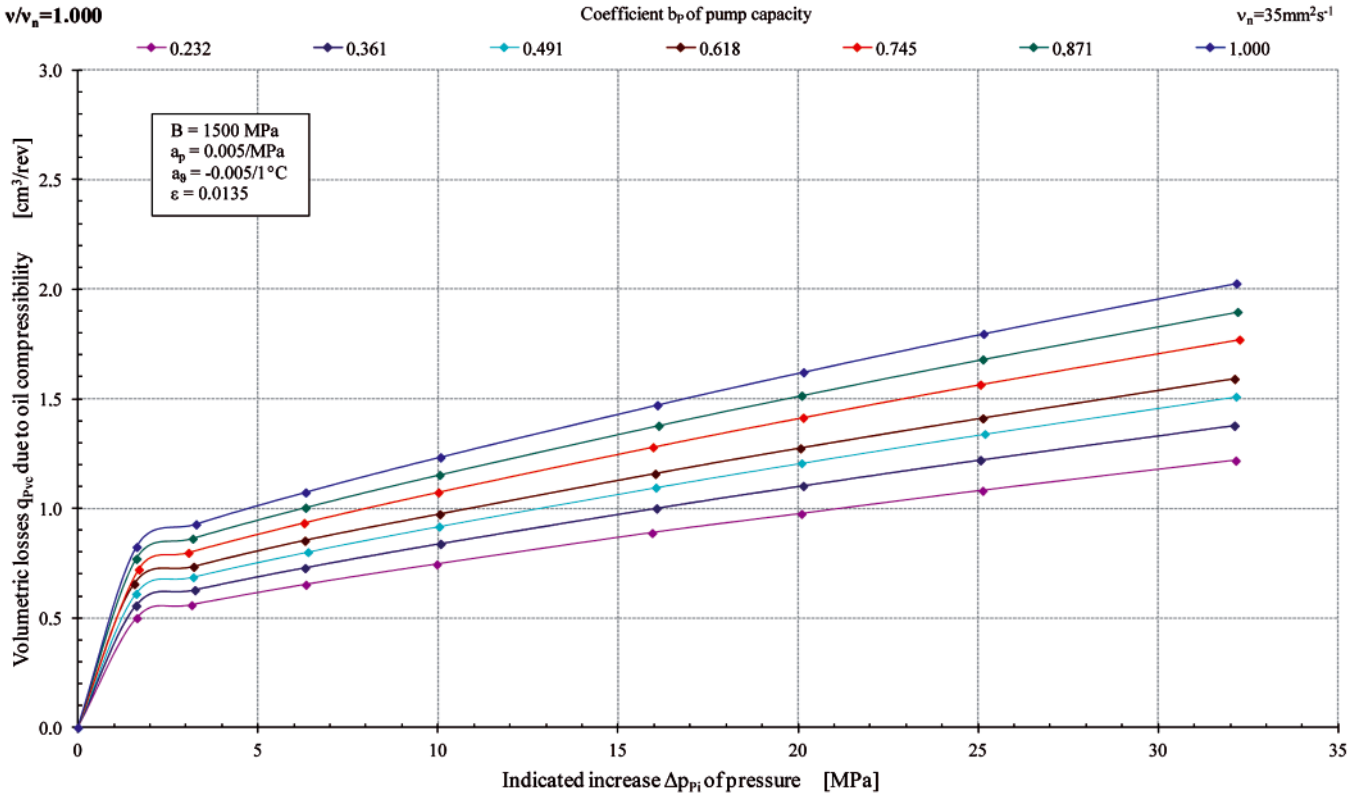

Fig. 5. Losses q_{Pvc} of pump capacity during one pump shaft revolution due to compressibility of aerated ($\varepsilon = 0.0135$) liquid, decreasing the active volume of liquid displaced by the pump compared with the theoretical working capacity q_{Pt} ($b_P = 1$) or geometrical working capacity q_{Pgv} ($0 \le b_P \le 1$) (pump of HYDROMATIK A7V.DR.1.R.P.F.00 type)

a variable capacity q_{Pgv} (variable b_P coefficient) per one shaft revolution.

The losses q_{Pvc} of pump capacity per one shaft revolution due to the liquid compressibility reduces the active volume of liquid displaced by the pump compared with the theoretical working capacity q_{Pt} or geometrical variable working capacity q_{Pgv} (determined at $\Delta p_{Pi} = 0$). This fact must be taken into account in evaluation of intensity $q_{Pv} = Q_{Pv}/n_P$ of volumetric losses in working chambers and in evaluation of the increase $\Delta M_{Pm|\Delta p_{Pi}}$ of torque of mechanical losses in the „working chambers - shaft" assembly, the losses caused by the increase Δp_{Pi} of pressure in the pump working chambers.

DETERMINING THE PUMP GEOMETRICAL VARIABLE WORKING CAPACITY q_{Pgv} AND THEORETICAL WORKING CAPACITY q_{Pt}

It is essential, particularly in evaluation of operating characteristics of a displacement pump with variable capacity per one shaft revolution, to determine precisely the pump theoretical working capacity q_{Pt} and geometrical working capacities q_{Pgv} . The geometrical working capacities q_{Pgv} change in the $0 \le q_{Pgv} \le q_{Pt}$ range and the corresponding coefficients $b_P = q_{Pgv}/q_{Pt}$ of pump capacity change in the $0 \le b_P \le 1$ range. The precise evaluation of $b_P = q_{Pgv}/q_{Pt}$ coefficient depends on the precise evaluation of q_{Pgv} and q_{Pt}.

The pump theoretical working capacity q_{Pt} and geometrical working capacities q_{Pgv} are evaluated at the indicated increase Δp_{Pi} of pressure in the working chambers equal zero ($\Delta p_{Pi} = 0$). Their values are determined by approximation at $\Delta p_{Pi} = 0$ point of the $q_P = Q_P/n_P = f(\Delta p_{Pi})$ line describing, with the fixed pump setting (but not known exactly value of b_P coefficient), the value q_P displaced in one shaft revolution as a relation to Δp_{Pi}. The line $q_P = f(\Delta p_{Pi})$ is determined by measurement points obtained from the tests.

Fig. 6 presents an example of the relation $q_P = f(\Delta p_{Pi})$ of capacity q_P per one shaft revolution of the tested axial piston pump to the indicated increase Δp_{Pi} of pressure in working chambers with coefficients $b_P = 0.225$ and $b_P = 1$ of pump capacity per one shaft revolution. Therefore, these examples present searching for geometrical working capacity q_{Pgv} and theoretical working capacity q_{Pt} per one shaft revolution as well as evaluation of the subdivision of the intensity q_{Pv} of volumetric losses per one shaft revolution into the volumetric losses q_{Pvl} due to oil leakage in working chambers and volumetric losses q_{Pvc} due to compressibility of non-aerated (or aerated) oil.

The losses $q_{Pvc} = f(\Delta p_{Pi})$ per one shaft revolution determined by formula (16), resulting from the liquid compressibility, occurring with setting q_{Pgv} of the pump variable geometrical working volume (or by formula (17) with setting q_{Pt} of the pump theoretical working volume) are added to capacity $q_P = f(\Delta p_{Pi})$ per one shaft revolution determined by the line drawn through the measurement points. The result of adding $q_{Pvc} = f(\Delta p_{Pi})$ to $q_P = f(\Delta p_{Pi})$ is the line $q_{P\text{ without compressibility}} = f(\Delta p_{Pi})$ of pump capacity as a difference between q_{Pgv} (or q_{Pt}) and the volumetric losses q_{Pvl} due to oil leakage (independent of the liquid compressibility):

$$(q_{P\text{ without compressibility}} = q_{Pvc} + q_P) = f(\Delta p_{Pi}) \qquad (18)$$

$$(q_{P\text{ without compressibility}} = q_{Pgv}\ (\text{or } q_{Pt}) - q_{Pvl}) = f(\Delta p_{Pi}) \qquad (19)$$

Approximation of the line $q_{P\text{ without compressibility}} = f(\Delta p_{Pi})$ with $\Delta p_{Pi} = 0$ allows to determine the value q_{Pgv} (or q_{Pt}):

$$q_{P\text{ without compressibility}|\Delta p_{Pi} = 0} = q_{Pgv}\ (\text{or } q_{Pt}) \qquad (20)$$

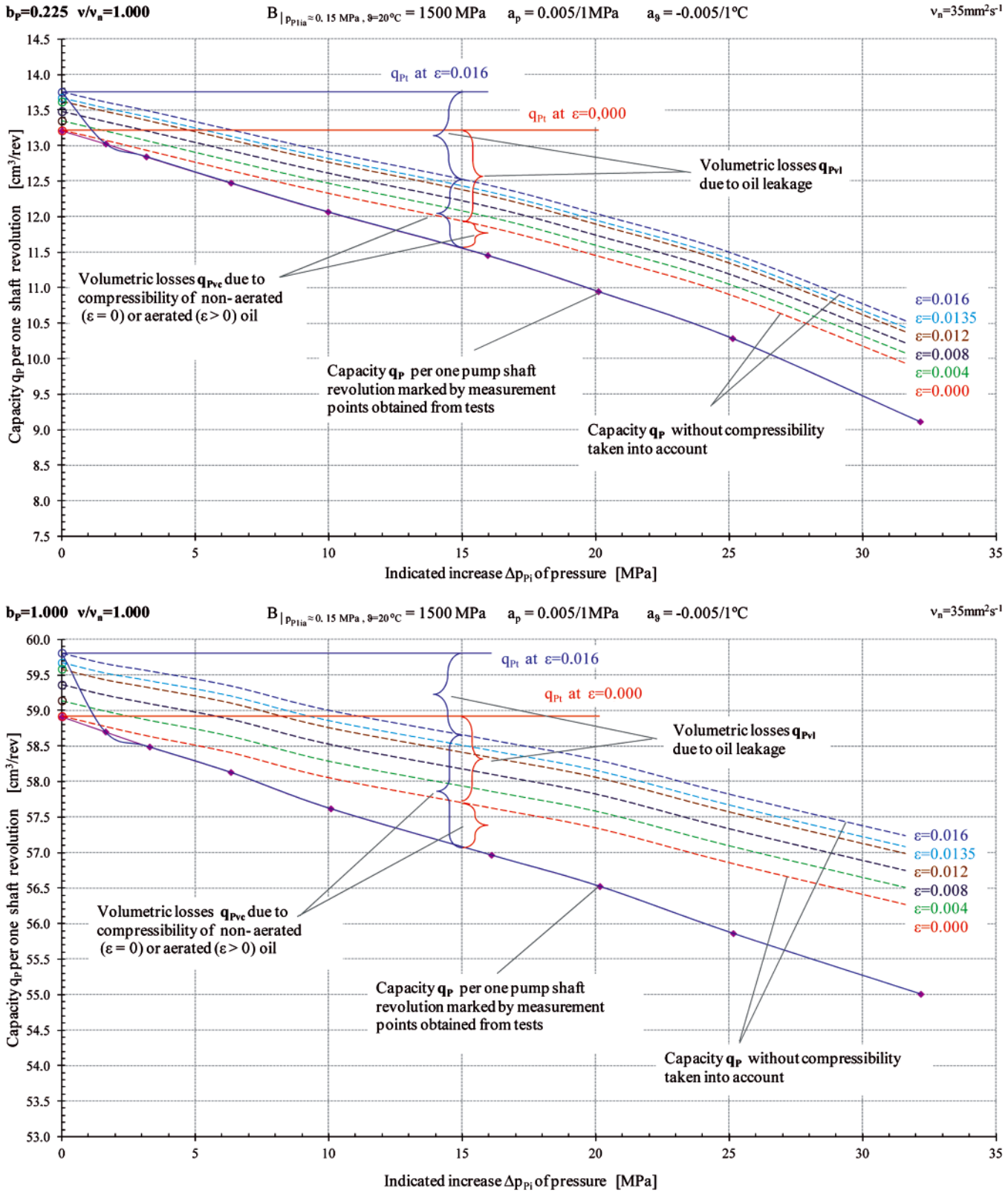

Fig. 6. Dependence of pump capacity q_P per one shaft revolution on the indicated increase Δp_{Pi} of pressure in the working chambers, at the coefficients b_P = 0.225 and b_P = 1 of pump capacity; the values q_{Pgv} of geometrical working volume and q_{Pt} of theoretical working volume per one shaft revolution (determined at Δp_{Pi} = 0) and subdivision of the intensity $q_{Pv} = q_{Pvl} + q_{Pvc}$ of volumetric losses per one shaft revolution into volumetric losses q_{Pvl} due to oil leakage in the chambers and volumetric losses q_{Pvc} due to compressibility of non-aerated (or aerated) oil dependent on the value of oil aeration coefficient ε (ε = 0 to 0.016); viscosity coefficient ν/ν_n = 1, oil temperature ϑ = 43°C (pump of the HYDROMATIK A7V.DR.1.R.P.F.00 type)

As shown in Fig. 6, the pump theoretical working capacity q_{Pt}, determined by approximation at point $\Delta p_{Pi} = 0$ of the line $q_P = f(\Delta p_{Pi})$ obtained from tests and taking into account the liquid compressibility, as well as the line ($q_{P\ without\ compressibility} = q_{Pvc} + q_P$) = $f(\Delta p_{Pi})$ taking into account the compressibility of non-aerated (ε = 0) oil has practically the same value q_{Pt} = 58.9 cm³/rev. Approximation of the line ($q_{P\ without\ compressibility} = q_{Pvc} + q_P$) = $f(\Delta p_{Pi})$ at point Δp_{Pi} = 0, made with allowing for compressibility of aerated oil, shows the increase of q_{Pt} practically proportional to oil aeration coefficient ε. This is clearly presented in Fig. 7. For example, with ε = 0.0135, takes the value q_{Pt} = 59.57 cm³/obr.

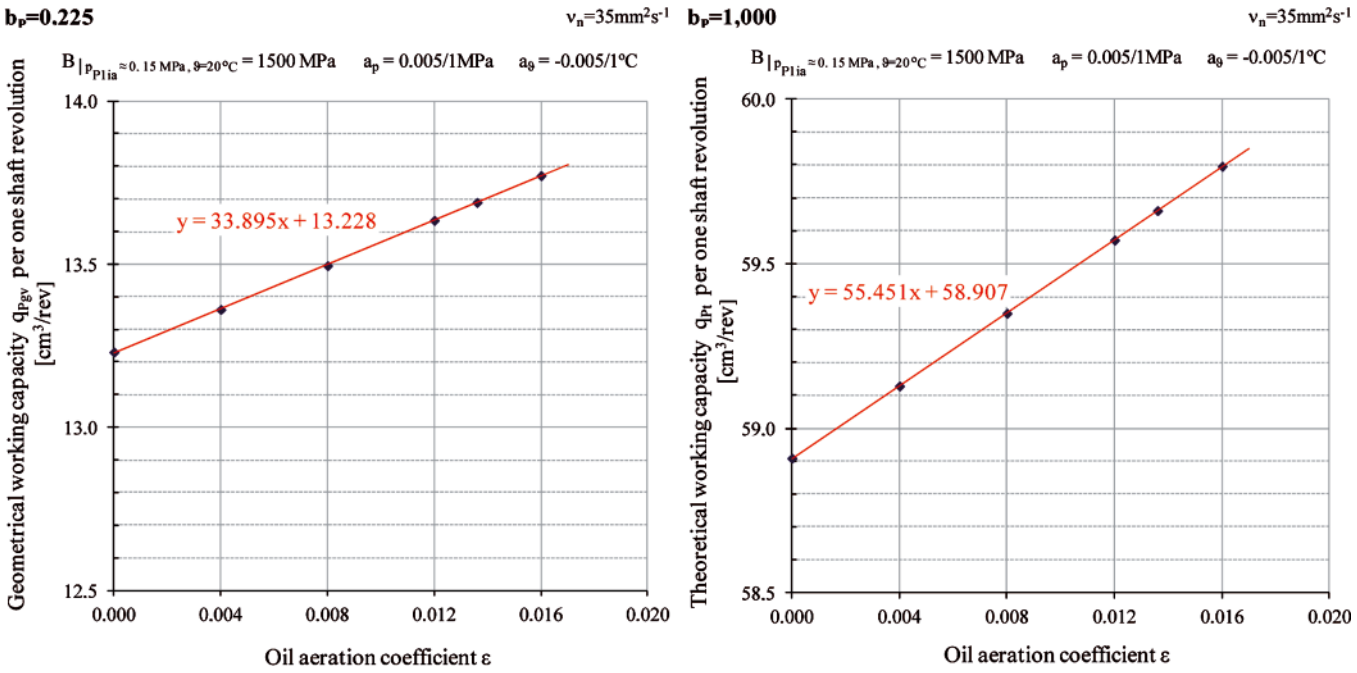

Fig. 7. *Effect of evaluation of geometrical working capacity q_{Pgv} and theoretical working capacity q_{Pi} per one pump shaft revolution resulting from assumption of aeration coefficient ε of the pump displaced oil; evaluation of qPgv and qPt (Fig. 7 and Fig. 8) is a result of approximation, at $\Delta p_{Pi} = 0$, of the relation of pump capacity q_P per one shaft revolution to the indicated increase Δp_{Pi} of pressure in the working chambers taking into account the aerated oil compressibility (at a given oil aeration coefficient ε) (pump HYDROMATIK A7V.DR.1.R.P. F.00 type)*

Fig. 8a and Fig. 8b present the values of geometrical working capacity q_{Pgv} (b_p = 0.225) and theoretical working capacity q_{Pt} (b_p = 1) per one shaft revolution obtained with different values of the oil viscosity ratio ν/ν_n and also average values q_{Pgv} and q_{Pt} obtained with assumed. Values of the modulus of liquid volume elasticity B = ∞, B = 1500 MPa, with assumed values of the oil aeration coefficient ε = 0, ε = 0.008 and ε = 0.0135.

RESULTS OF THE VOLUMETRIC LOSS INVESTIGATIONS

Fig. 9a and 9b present the subdivision of volumetric losses $q_{Pv} = f(\Delta p_{Pi})$ per one shaft revolution into losses $q_{Pvc} = f(\Delta p_{Pi})$ due to oil compressibility and losses $q_{Pvl} = f(\Delta p_{Pi})$ due to oil leakage with different values of oil aeration coefficient ε in the pump, with geometrical working capacity q_{Pgv} and theoretical working capacity q_{Pt} per one shaft revolution. The figures show, with different values of the aeration coefficient ε, unchanging characteristics of the losses $q_{Pvl} = f(\Delta p_{Pi})$ due to oil leakage and changing characteristics of the losses $q_{Pvc} = f(\Delta p_{Pi})$ due to oil compressibility, and also characteristics $(q_{Pv} = q_{Pvl} + q_{Pvc}) = f(\Delta p_{Pi})$ of the volumetric losses $q_{Pv} = f(\Delta p_{Pi})$ in the pump as a sum of the losses $q_{Pvl} = f(\Delta p_{Pi})$ due to leakage and the losses $q_{Pvc} = f(\Delta p_{Pi})$ due to oil compressibility.

Fig. 10a and Fig. 10b present the dependence of volumetric losses q_{Pv} per one shaft revolution (with the assumption of B = ∞) or the dependence of volumetric losses q_{Pvl} per one shaft revolution due to oil leakage (with the assumption of B = 1500 MPa, a_p = 0.005/1 MPa, a_ϑ = -0.005/1°C) on the indicated increase Δp_{Pi} of pressure in the pump working chambers, with different values ν/ν_n of oil viscosity ratio, with coefficient b_P = 0.225 and b_P = 1 of pump capacity q_{Pgv} per one shaft revolution. With taking into account the oil compressibility, losses due to oil leakage in the pump working chambers appear evidently smaller.

Fig. 11a and Fig. 11b present the high share of volumetric losses q_{Pvc} per one shaft revolution due to compressibility of non-aerated (ε = 0) and aerated (ε = 0.0135) oil as a component of the volumetric losses $q_{Pv} = q_{Pvl} + q_{Pvc}$ in the tested pump. With coefficient of pump capacity b_P = 1 and coefficient of non-aerated oil ε = 0, that share was in the 30 to 40 % range. With the aeration coefficient ε = 0.0135, the share changes from 40 ÷ 50 % to 80 ÷ 90 %. With coefficient b_P = 0.225 of pump capacity, the share is a little lower but still high.

Fig. 12 presents the volumetric losses q_{Pvl} per one shaft revolution due to oil leakage as a dependence on the indicated increase Δp_{Pi} of pressure in the working chambers with different values of the pump capacity coefficient b_P and different values of oil viscosity ratio ν/ν_n. Decreasing oil viscosity ν has a clear influence on the increase of leakage in the pump, but change of pump capacity coefficient b_P has practically no influence on leakage in the chambers.

CONCLUSIONS

1. Ability of determining the aeration of working liquid and resulting liquid compressibility makes it possible to determine the volumetric losses q_{Pv} in the pump working chambers and subdivision of the losses into losses q_{Pvl} due to leakage in the pump chambers and losses q_{Pvc} due to liquid compressibility in the chambers which are not connected with displacement pump construction.
2. The influence of liquid compressibility on the evaluation of volumetric losses in the pump with the oil aeration coefficient ε = 0.0135 was remarkable. Losses due to liquid compressibility amounted to 30 ÷ 90 % of volumetric losses depending on the value of increase Δp_{Pi} of pressure in the working chambers, the oil viscosity ratio ν/ν_n and the pump capacity coefficient b_P.
3. Knowledge of the compressibility of non-aerated liquid makes it possible to determine the volumetric losses due to leakage in the pump working chambers.
4. Volumetric losses due to leakage and volumetric losses due to liquid compressibility must be clearly separated and only the losses due to leakage should be taken into account for pump evaluation.

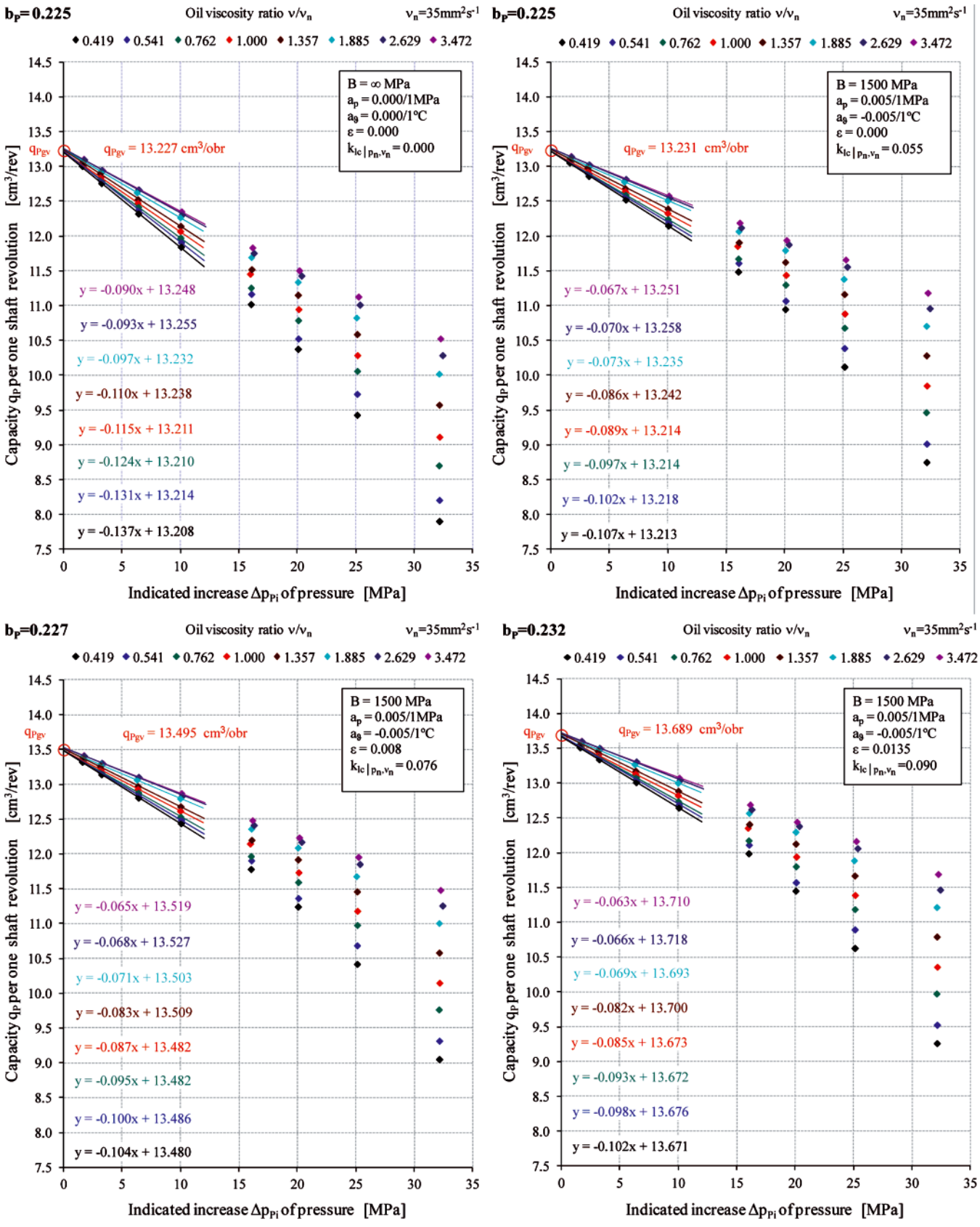

Fig. 8a. *Determination of the pump geometrical variable working capacity q_{Pgv} ($q_{Pgv} = b_P \cdot q_{Pt}$) and the value of pump capacity coefficient b_P from the dependence of pump capacity q_P per one shaft revolution on the indicated increase Δp_{Pi} of pressure in the pump working chambers with different values of oil viscosity ratio ν/ν_n and average value of q_{Pgv}; assumed values B = ∞ and B = 1500 MPa, assumed values ε = 0, ε = 0.008, ε = 0.0135, b_P = 0.225 to 0.232 (pump HYDROMATIK A7V.DR.1.R.P. F.00 type)*

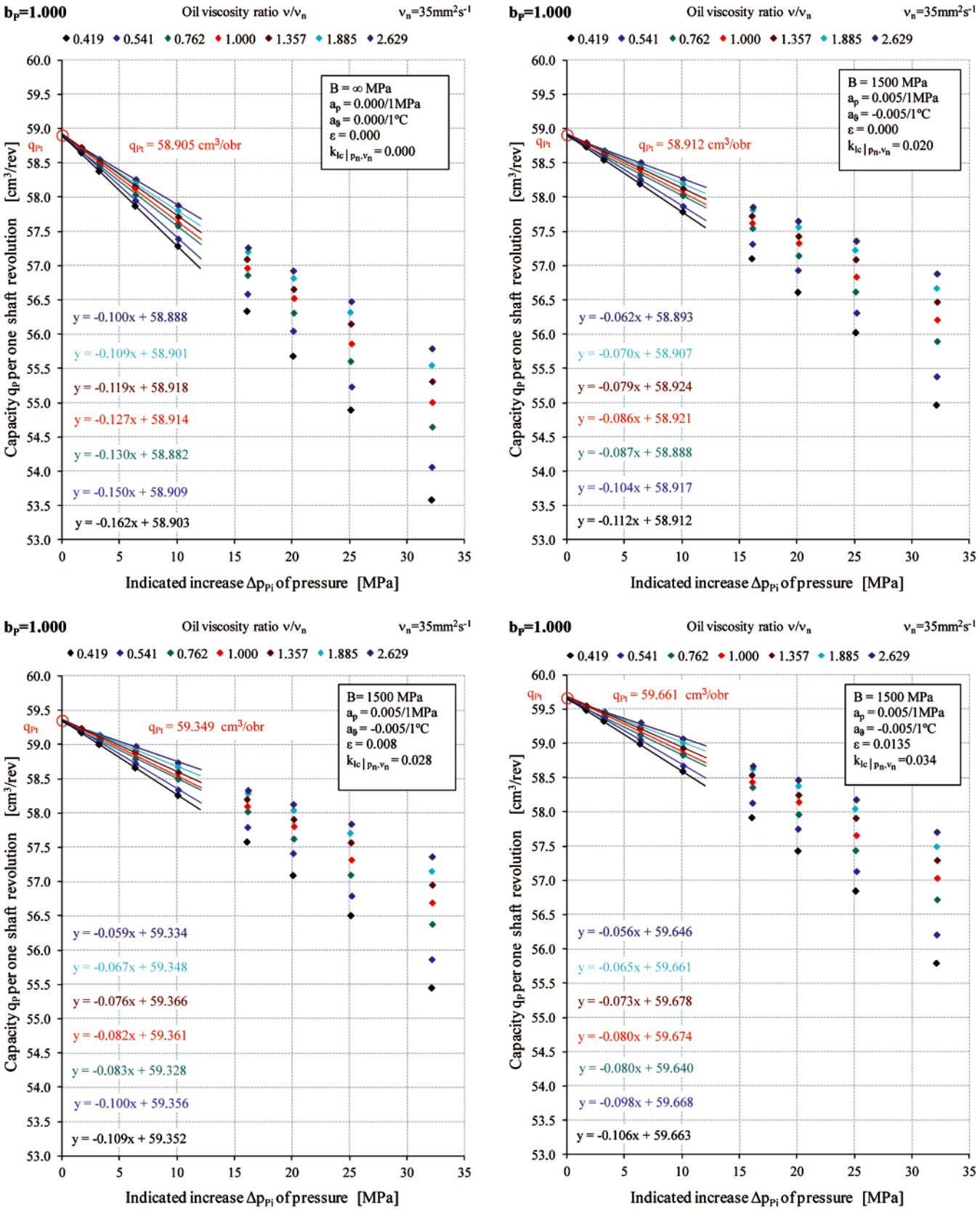

Fig. 8b. *Determination of the pump theoretical working capacity q_{Pt} (pump capacity coefficient b_P = 1) from the dependence of pump capacity q_P per one shaft revolution on the indicated increase Δp_{Pi} of pressure in the pump working chambers, with different values of oil viscosity ratio ν/ν_n and average value of q_{Pt}; assumed values B = ∞ and B = 1500 MPa, assumed values ε = 0, ε = 0.008, ε = 0.0135 (pump HYDROMATIK A7V.DR.1.R.P. F.00 type)*

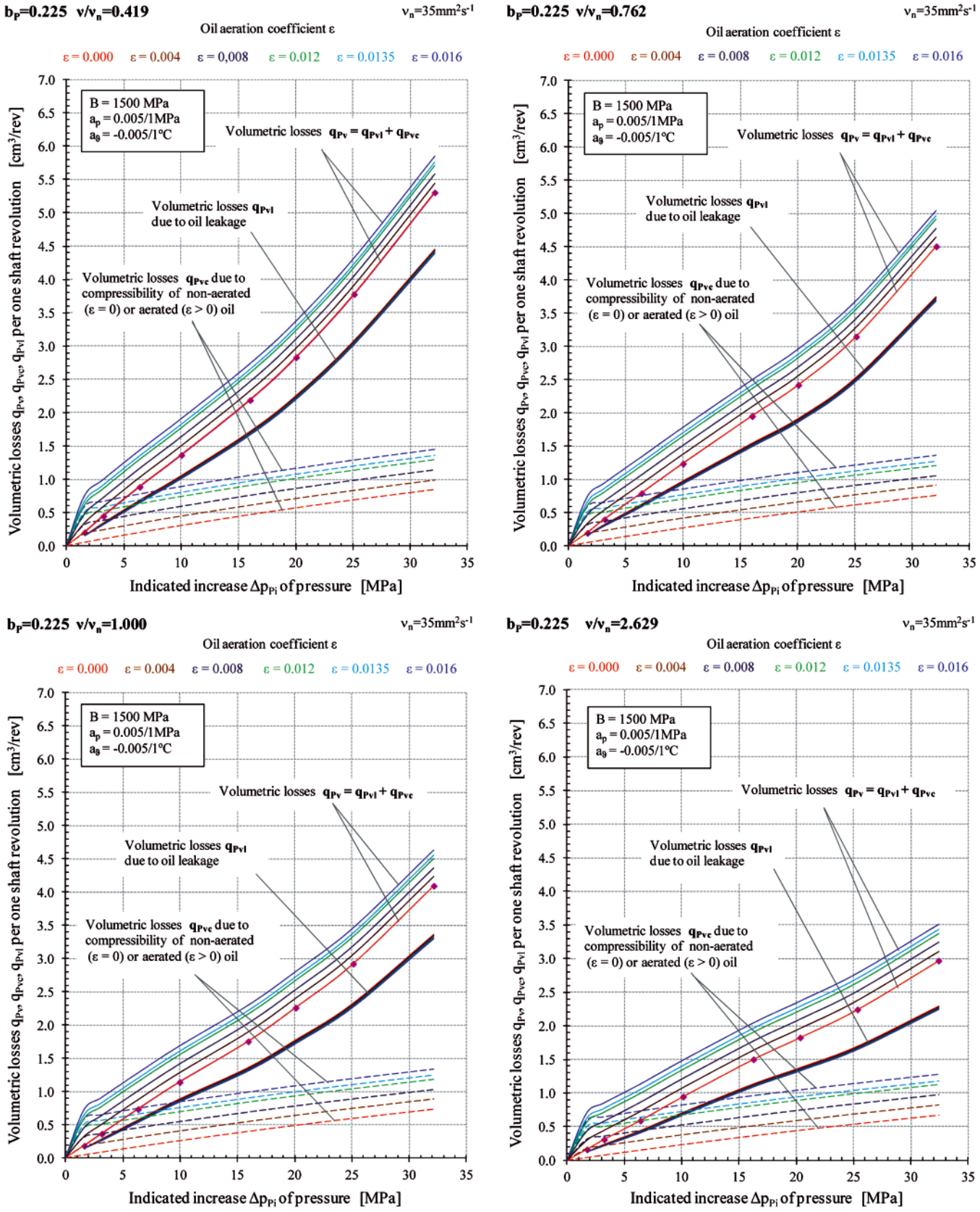

Fig. 9a. *Subdivision of volumetric losses $q_{Pv} = f(\Delta p_{Pi})$ per one shaft revolution in the pump working chambers into losses $q_{Pvc} = f(\Delta p_{Pi})$ due to oil compressibility and losses $q_{Pvl} = f(\Delta p_{Pi})$ due to oil leakage at different values of oil aeration coefficient ε and different values of oil viscosity ratio ν/ν_n in the tested pump with the pump geometrical working capacity q_{Pgv} (b_P = 0.225) (pump HYDROMATIK A7V.DR.1.R.P.F.00 type)*

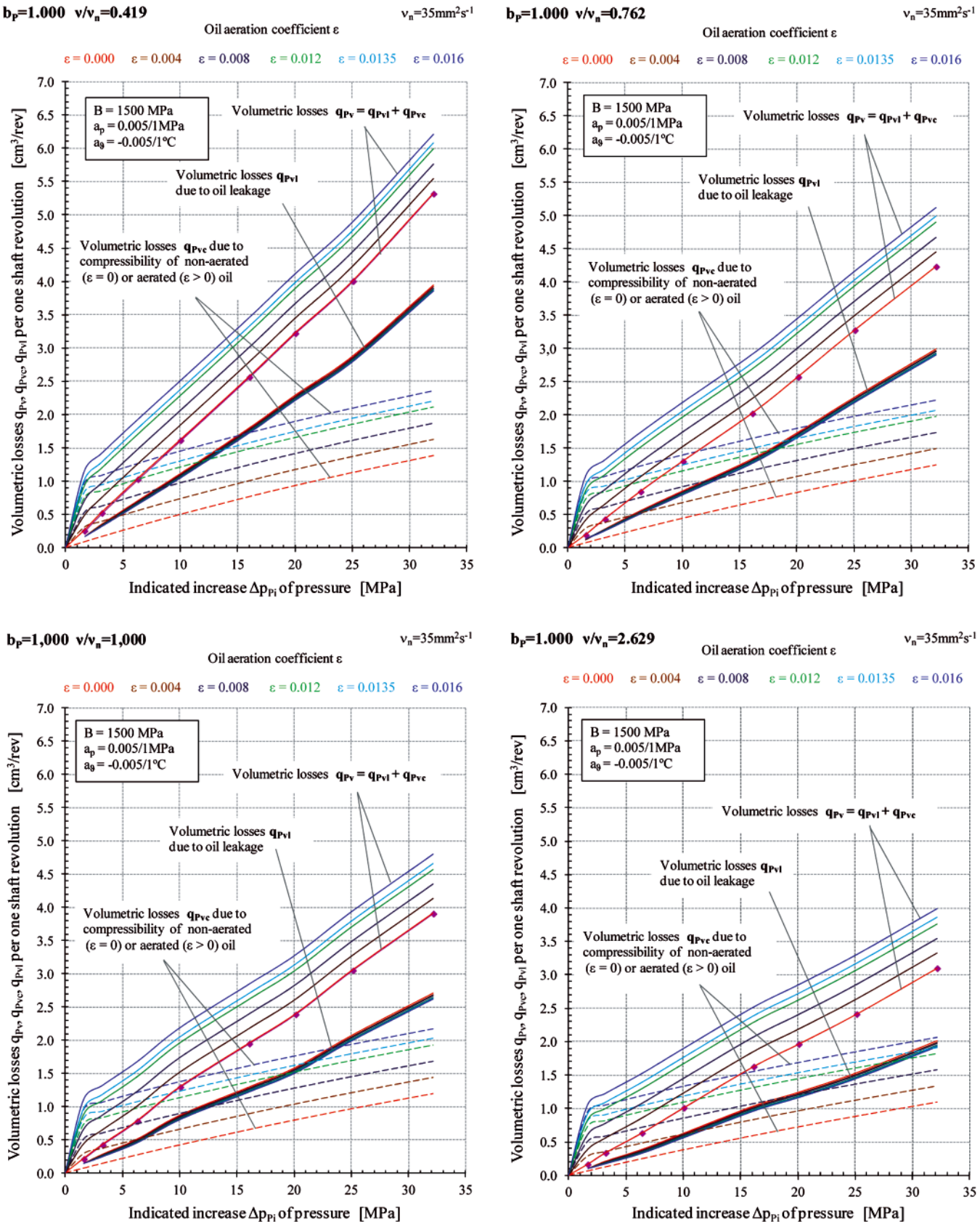

Fig. 9b. *Subdivision of volumetric losses $q_{Pv} = f(\Delta p_{Pi})$ per one shaft revolution in the pump working chambers into losses $q_{Pvc} = f(\Delta p_{Pi})$ due to oil compressibility and losses $q_{Pvl} = f(\Delta p_{Pi})$ due to oil leakage at different values of oil aeration coefficient ε and different values of oil viscosity ratio v/v_n in the tested pump with the pump theoretical working capacity q_{Pt} (b_P = 1) (pump HYDROMATIK A7V.DR.1.R.P.F.00 type)*

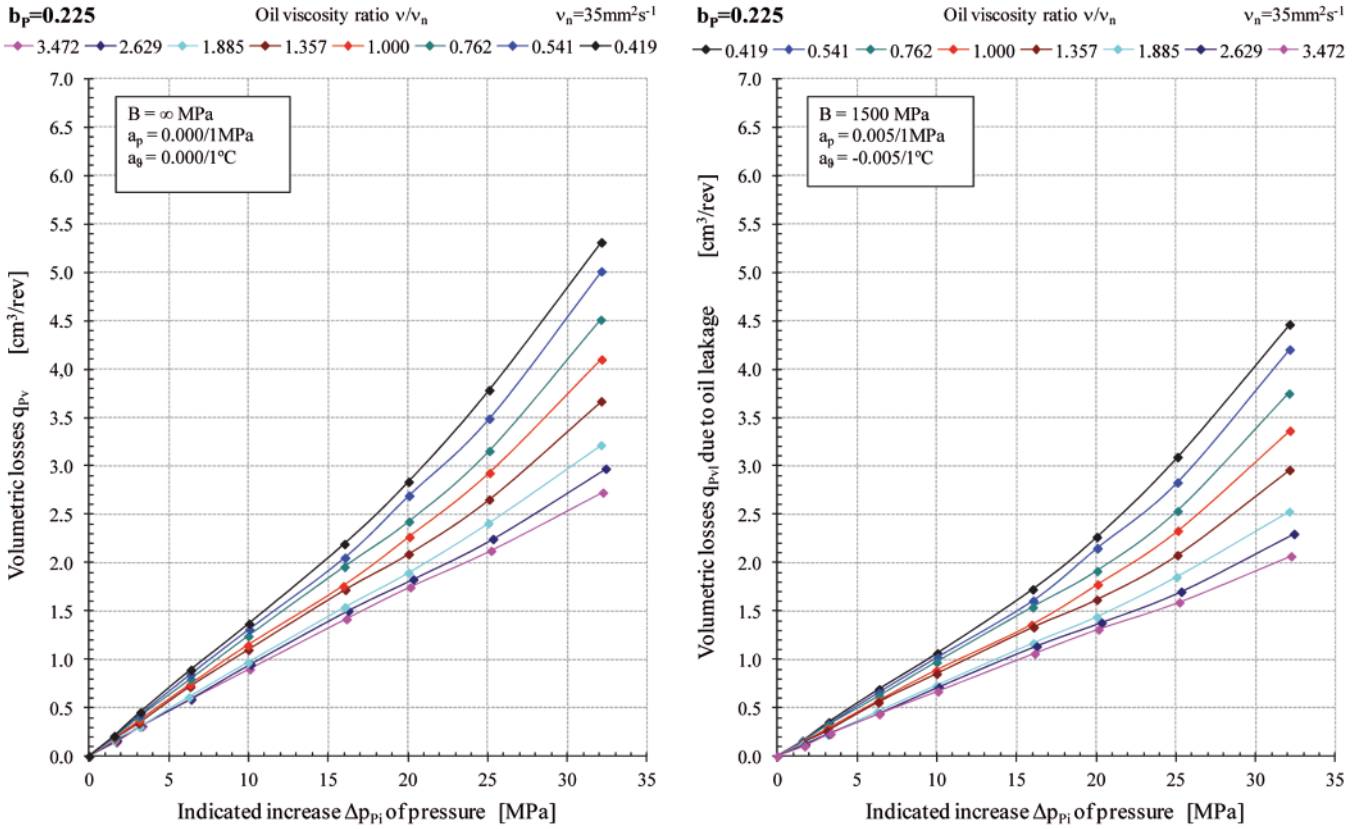

Fig. 10a. *Volumetric losses q_{Pv} per one shaft revolution (with the assumption B = ∞) or volumetric losses q_{Pvl} per one shaft revolution due to oil leakage (with the assumption of B = 1500 MPa, a_p = 0.005/1 MPa, $a_ϑ$ = - 0.005/1 °C) as dependent on the indicated increase $Δp_{Pi}$ of pressure in the pump working chambers, with different values of oil viscosity ratio ν/ν$_n$, with coefficient b_P = 0.225 of pump capacity q_{Pgv} per one shaft revolution ($b_P = q_{Pgv}/q_{Pi}$) (pump HYDROMATIK A7V.DR.1.R.P. F.00 type)*

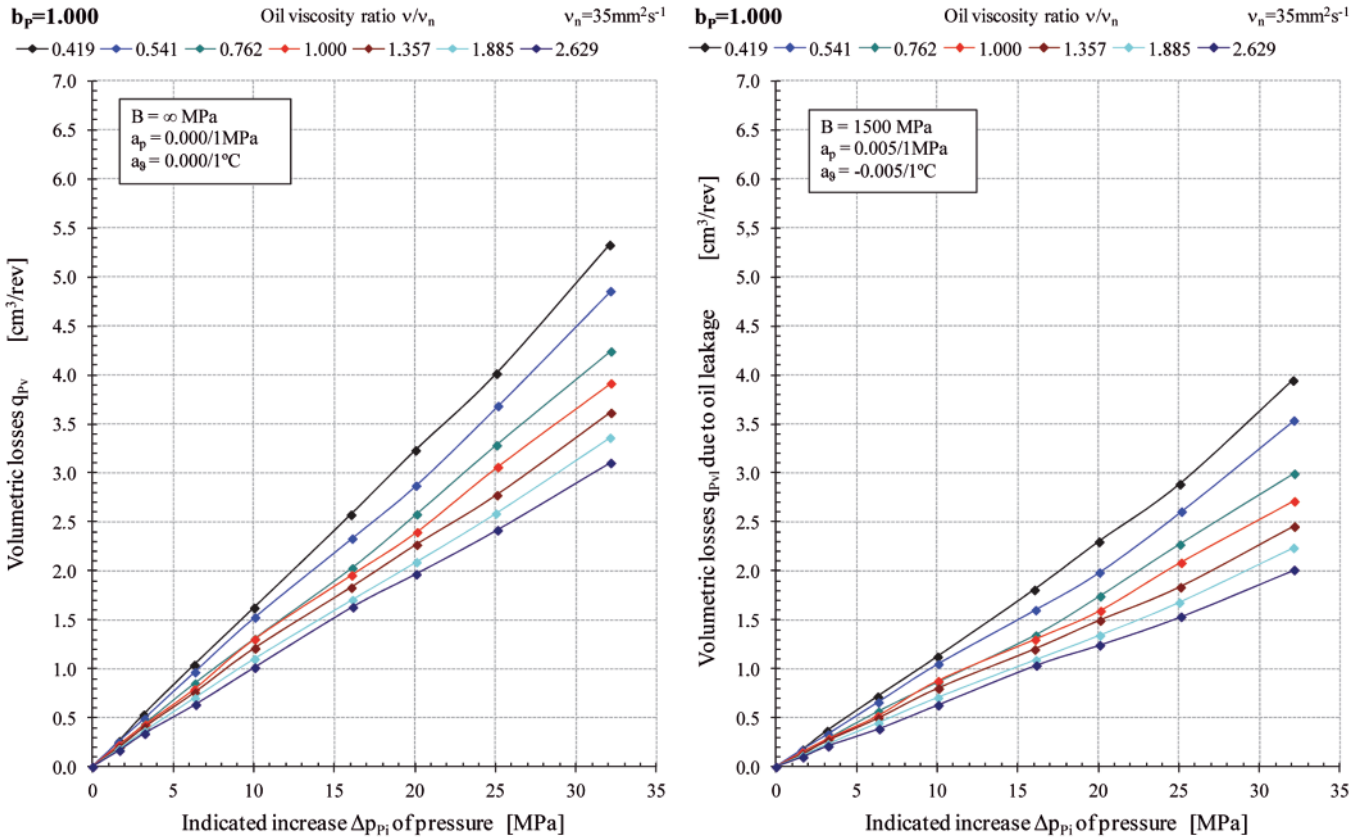

Fig. 10b. *Volumetric losses q_{Pv} per one shaft revolution (with the assumption B = ∞) or volumetric losses q_{Pvl} per one shaft revolution due to oil leakage (with the assumption of B = 1500 MPa, a_p = 0.005/1 MPa, $a_ϑ$ = - 0.005/1 °C) as dependent on the indicated increase $Δp_{Pi}$ of pressure in the pump working chambers, with different values of oil viscosity ratio ν/ν$_n$, with coefficient b_P = 1 of pump capacity q_{Pgv} per one shaft revolution ($b_P = q_{Pgv}/q_{Pi}$) (pump HYDROMATIK A7V.DR.1.R.P. F.00 type)*

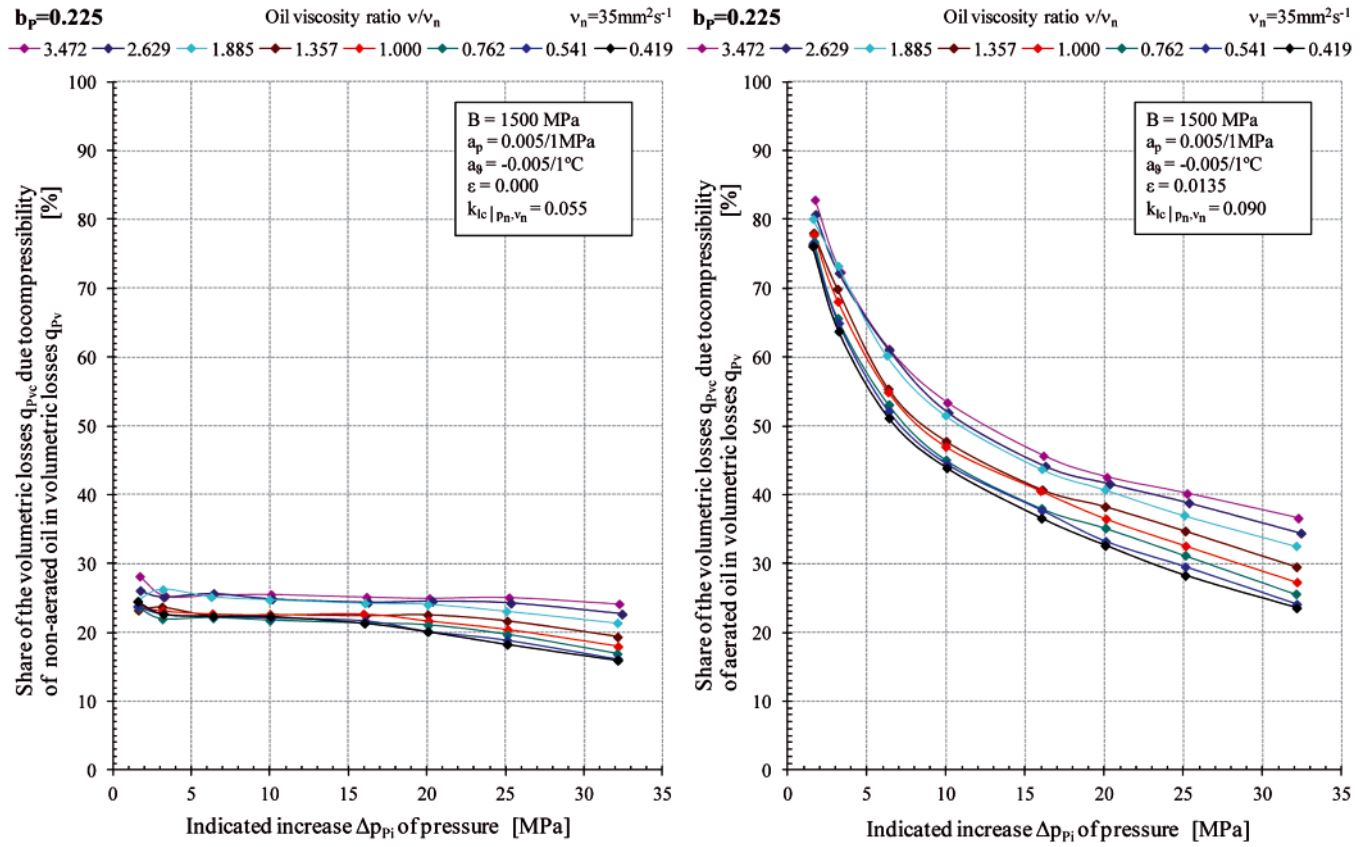

Fig. 11a. *Share of the volumetric losses q_{Pvc} per one shaft revolution due to compressibility of non-aerated (ε = 0) and aerated (ε = 0.0135) oil in the pump volumetric losses q_{Pv}, with the pump capacity coefficient b_P = 0.225 (pump HYDROMATIK A7V.DR.1.R.P.F.00 type)*

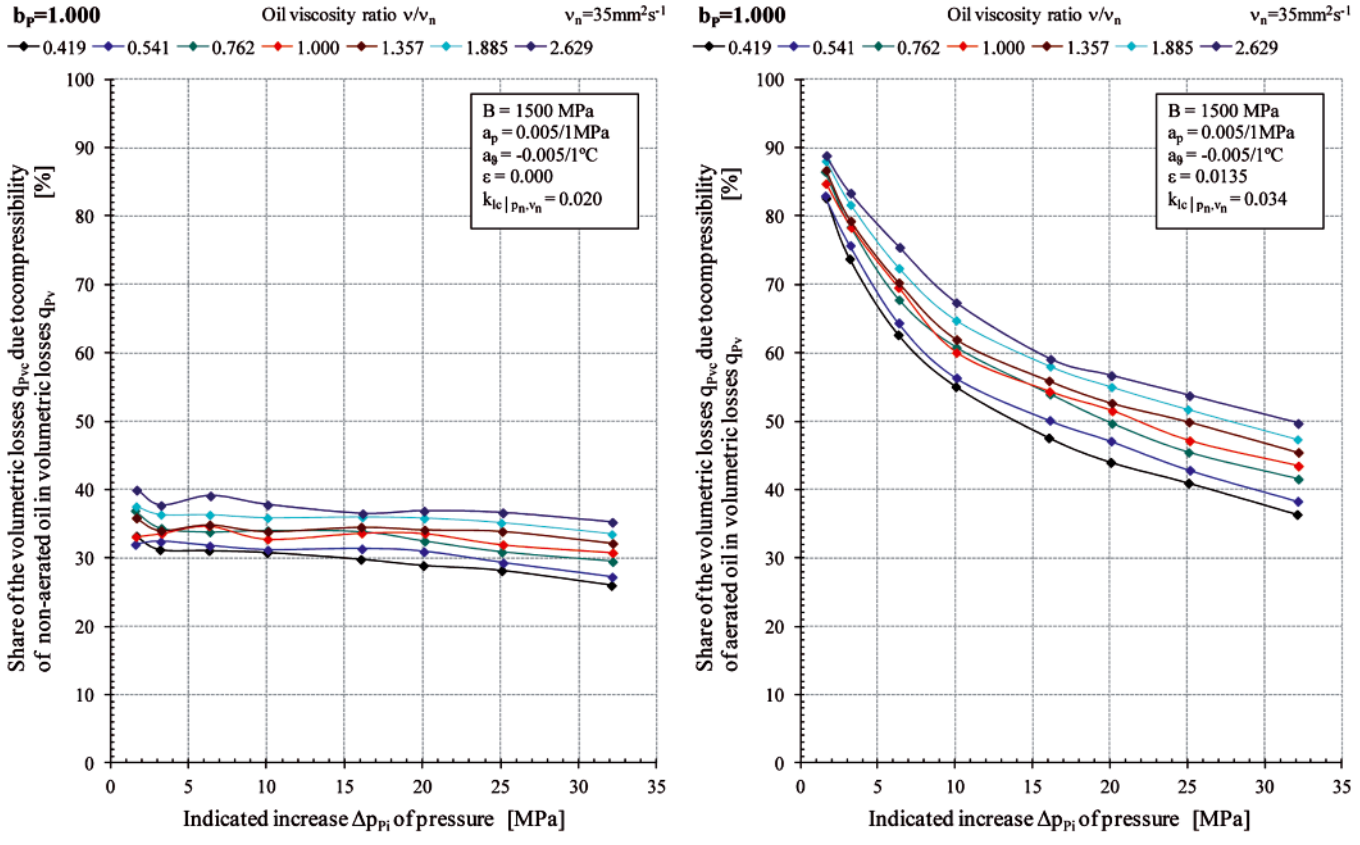

Fig. 11b. *Share of the volumetric losses q_{Pvc} per one shaft revolution due to compressibility of non-aerated (ε = 0) and aerated (ε = 0.0135) oil in the pump volumetric losses q_{Pv}, with the pump capacity coefficient b_P = 1 (pump HYDROMATIK A7V.DR.1.R.P.F.00 type)*

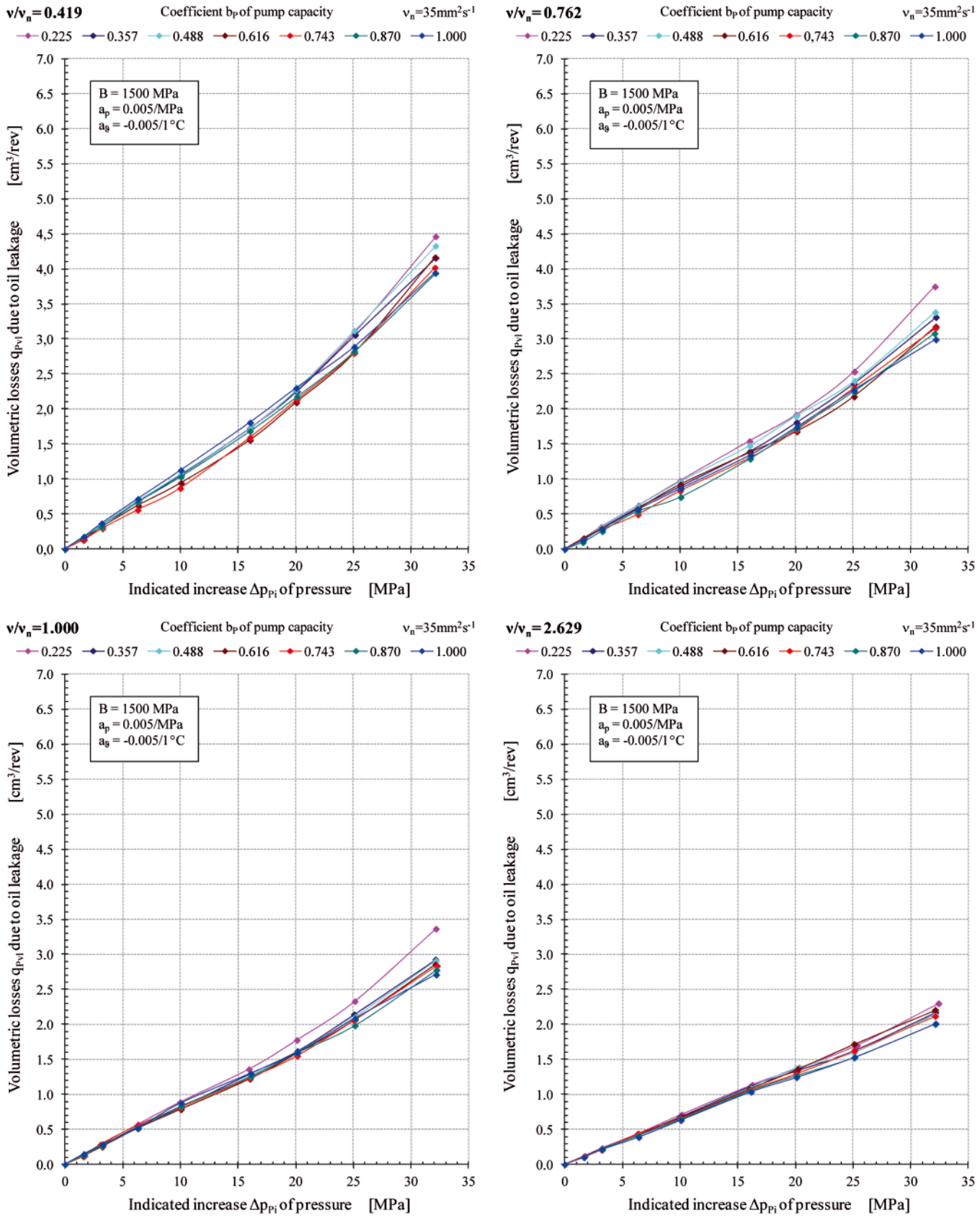

Fig. 12. *Volumetric losses q_{Pvl} per one shaft revolution due to oil leakage as dependent on the indicated increase Δp_{Pi} of pressure into the pump working chambers, with different values of pump capacity coefficient b_P and different values ν/ν_n ratio of oil viscosity; losses q_{Pvl} are practically independent of the pump capacity coefficient b_P (pump HYDROMATIK A7V.DR.1.R.P.F.00 type)*

BIBLIOGRAPHY

1. Koralewski J.: *Influence of hydraulic oil viscosity on the volumetric losses in a variable capacity piston pump*. Chapter in the monograph: „Research, design, production and operation of hydraulic systems" (in Polish) Adam Klich, Antoni Kozieł and Edward Palczak editors. „Cylinder" Library. „Komag" Mining Mechanisation Centre, Gliwice 2011
2. Koralewski J.: *Influence of hydraulic oil viscosity on the volumetric losses in a variable capacity piston pump*. „Napędy i sterowanie", scientific monthly, 9 /2011
3. Koralewski J.: *Influence of hydraulic oil viscosity on the volumetric losses in a variable capacity piston pump*. Polish Maritime Research 3, 2011, Vol. 18
4. Paszota Z.: *Effect of the working liquid compressibility on the picture of volumetric and mechanical losses in a high pressure displacement pump used in a hydrostatic drive. Part I Energy losses in a drive system, volumetric losses in a pump*//International Scientific-Technical Conference Hydraulics and Pneumatics, Wrocław, 16 – 18 maja 2012 / Ośrodek Doskonalenia Kadr SIMP - Wrocław : ODK SIMP we Wrocławiu, 2012,
5. Paszota Z.: *Effect of the working liquid compressibility on the picture of volumetric and mechanical losses in a high pressure displacement pump used in a hydrostatic drive. Part II Mechanical losses in a pump* //International Scientific-Technical Conference Hydraulics and Pneumatics, Wrocław, 16 – 18 maja 2012 / Ośrodek Doskonalenia Kadr SIMP - Wrocław : ODK SIMP we Wrocławiu, 2012,
6. Paszota Z.: *Effect of the working liquid compressibility on the picture of volumetric and mechanical losses in a high pressure displacement pump used in a hydrostatic drive. Part I Energy losses in a drive system, volumetric losses in a pump*// Polish Maritime Research 2/2012, Vol. 19
7. Paszota Z.: *Effect of the working liquid compressibility on the picture of volumetric and mechanical losses in a high pressure displacement pump used in a hydrostatic drive*. *Part II Mechanical losses in a pump* // Polish Maritime Research 3, 2012, Vol.19
8. Paszota Z.: *Theoretical and mathematical models of the torque of mechanical losses in the pump used in a hydrostatic drive* (in Polish). Chapter in the monograph: „Research, design, production and operation of hydraulic systems" (in Polish) Adam Klich, Antoni Kozieł and Edward Palczak editors. „Cylinder" Library. „Komag" Mining Mechanisation Centre, Gliwice 2011
9. Paszota Z.: *Theoretical and mathematical models of the torque of mechanical losses in the pump used in a hydrostatic drive*. (in Polish). „Napędy i sterowanie", scientific monthly 10/2011
10. Paszota Z.: *Theoretical models of the torque of mechanical losses in the pump used in a hydrostatic drive*. Polish Maritime Research 4 / 2011, Vol. 18
11. Guillon M.: *Theory and calculation of hydraulic systems* (in Polish). Wydawnictwa Naukowo-Techniczne Warszawa 1967
12. Osiecki A.: *Hydrostatic drive of machine* (in Polish). Wydawnictwa Naukowo-Techniczne Warszawa 2004
13. Paszota Z.: *Method of determination the degree of liquid aeration in a variable capacity displacement pump*. //Polish Maritime Research 3/2013, vol.20

CONTACT WITH THE AUTHOR

Jan Koralewski, M. Sc.
Faculty of Ocean Engineering
and Ship Technology
Gdansk University of Technology
Narutowicza 11/12
80-233 Gdansk, POLAND
e-mail: jkoral@pg.gda.pl

POLISH MARITIME RESEARCH 4(80) 2013 Vol 20; pp. 18-24
10.2478/pomr-2013-0036

The semi-Markov model of the process of appearance of sea-going ship propupsion system ability and inability states in application to determining the reliablity of these systems

Jerzy Girtler, Prof.,
Gdansk University of Technology, Poland

ABSTRACT

The article presents possible application of the theory of semi-Markov processes in creating the eight-state model of the process of appearance of the propulsion systems ability and inability states on sea-going vessels performing transportation tasks in a relatively long operating time t ($t \to \infty$). The model has been proved to be able to be successfully used for determining the reliability of the abovementioned systems. The probability of faultless operation in time t was assumed the measure of system reliability. Operating situations of sea-going vessels were characterised, with special attention being paid to the fact that the loads of propulsion system components of these vessels are of random nature. These loads lead to damages which for this reason were also considered random events. It was also assumed that the damages provoke the appearance of states of inability of particular ship propulsion system components which means that these states are random events as well. The states of ability of a given ship propulsion system have been assumed to exist when all components of this system are in the state of ability. In case when at least one component is in the state of inability, the entire system is in the state of inability. Conditions were formulated for the reliability model of an arbitrary system to be able to be worked out in the form of the semi-Markov process. The need for the use of technical diagnostics in reliability examination of sea-going ship propulsion systems was indicated. In conclusions, certain qualities of the article were highlighted which are, in author's opinion, of highest importance in reliability examination of sea-going ship propulsion systems.

Key words: reliability, semi-Markov process, state of ability, state of inability, sea-going ship, ship propulsion system

INTRODUCTION

Sea-going ships perform transportation tasks in remarkably different weather and sea conditions, which generally depend on: wind force and direction, sea undulation level (height, length and direction of waves), speed and direction of sea currents, level of underwater hull section overgrowing with algae and crustaceans, ship over-icing, and type of the water region in which the ship sails while performing the transportation task [9, 10, 19]. Extremely unfavourable conditions of ship operation have place when the ship performs the transportation task in storm: at the wind (hurricane) flowing with the speed which can exceed 29 m/s in extreme cases and reveal a heavily destructive potential, and on the sea with waves of over 300 m in length and 10 m in height. What is more, in such cases the hurricane carries such huge amounts of water dust with the air that the visibility is practically equal to zero. The situation at sea which corresponds to slightly better conditions of ship sailing is shown in Fig. 1. It has place when waves of over 5 m in height and 100 m in length become steep and the whitecaps on wave crests start arranging in strips. This state of sea is characterised by loud noise of breaking waves which can be heard even from a large distance and is additionally intensified by extremely strong wind having the speed over 12 m/s.

Fig. 1. *Situation at sea in storm conditions in which the container ship performs the transportation task (the situation which is at least dangerous)*

Performing transportation tasks by any ship in the conditions of strong undulation of surface sea layers (Fig. 1) creates unfavourable conditions for operation of all power conversion system equipment installed on the ship, in particular for its propulsion system with the main engine. This sometimes causes damage to system components, most frequently the main engine (Fig. 2) which as a rule leads to sea disaster. It is possible to prevent such unfavourable and even dangerous events once we know, among other factors, the probability of occurrence of such random events considered the states of ability and inability of the ship propulsion system. To assess those probabilities we need a relevant model of the process of appearance of the abovementioned states. And to work out this model, in turn, we should identify sea and weather conditions in which transportation tasks are performed by ships, and attribute relevant reliability states of ship propulsion systems to those conditions.

SEA AND WEATHER CONDITIONS DURING SHIP VOYAGES AND RELIABILITY STATES OF SHIP PROPULSION SYSTEMS

The sea and weather conditions in which the transportation tasks are performed by sea-going ships may differ considerably. In the temperate climate, surface layers of the sea water are, as a rule, turbulent in spring and autumn. Impetuous action of the undulated sea on the ship hull is additionally intensified by strong wind, the gusts of which can reach 24.4 m/s (strong gale, 9 in Beaufort scale), 28.4 m/s (whole gale, 10 in Beaufort scale), 32.5 m/s (violent storm, 11 in Beaufort scale), or as much as 36.6 m/s (hurricane, 12 in Beaufort scale) [10]. Such a situation is a threat to ship's safety and frequently leads to its sinking. As a rule, the ship sinks when one of some components of its main propulsion system are damaged. As a result of this damage, power transmission to the screw propeller (7) is stopped and the thrust force (T) and the driving force component (T_N) which balances the resistance (R_x) and allows the ship to sail with speed v (Fig. 2) are not generated any longer. Generally, the force T_N, along with the force acting on the rudder, secure relevant course stability (steering quality) of the ship.

The forces R_{ha} and R_{G1} which act at a right angle to the lever arm a generate the ship trim by the stern, which is additionally increased by forces T_N and R_x acting at a right angle to the arm b. All this leads to sometimes heavy reduction of the driving force (T_N), which in turn remarkably decreases the course stability of the ship and, finally, its safety.

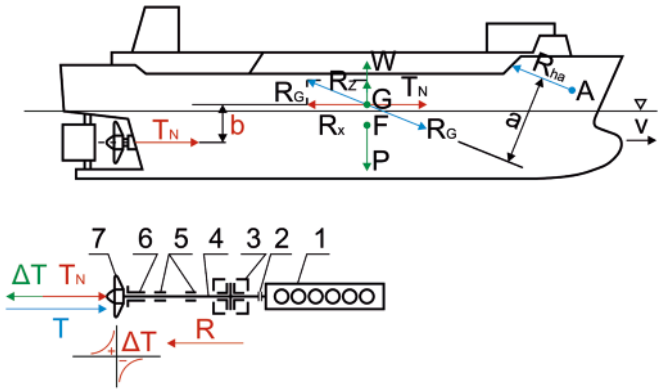

Fig. 2. Scheme of forces and moments acting on the ship: ***T*** *– thrust force,* ***T_N*** *– driving force,* ***ΔT*** *– thrust deduction,* ***R = R_x*** *– overall ship hull resistance which is balanced by force* ***T_N****,* ***R_{ha}*** *– resultant force of all hydro- and aerodynamic forces acting on the ship,* ***R_z*** *– hydro- and aerodynamic lift,* ***P*** *– ship weight,* ***W*** *– ship's buoyancy force,* ***G*** *– ship's centre of gravity,* ***F*** *– ship's centre of buoyancy,* ***a*** *– arm of action of forces* ***R_{ha}*** *and* ***R_{Gl}****,* ***b*** *– arm of action of thrust generating forces* ***T_N*** *and* ***R_x****,* ***1*** *– main engine,* ***2*** *– coupling,* ***3*** *– thrust bearing with (thrust) shaft,* ***4*** *– propeller shaft,* ***5*** *– radial bearings,* ***6*** *– stuffing-box,* ***7*** *– screw propeller*

Many sea disasters taking the form of: 1) ship's running aground on rocky or sandy shallows, or 2) ship's collision with underwater rock or coral reef, or 3) ship's turn over during the storm, or, finally, 4) collision of two ships, are likely to take place when the main engines cannot be loaded, due to their bad technical state, within the entire load range for which they were preconditioned in the design and production process (Fig. 3). This situation is a threat to ship's stability, and the ship's voyage performed in such conditions at heavy sea frequently end with a disaster.

One of main causes of sea disasters is worsened technical condition of ship propulsion systems, especially the main engines used for ship driving. Bad technical condition of these systems is the reason why they cannot be loaded with full load, and consequently a sufficiently large thrust force T cannot be generated by the screw propeller (Fig. 2). In such cases, even the maximum rudder deflection is not sufficient to generate forces which will compensate the action of wind and undulated sea. As a consequence, the ship firstly loses its steering qualities (course stability) and cannot move any longer in the assumed direction, and then it loses its transverse stability. The appearance of the backstay wind along with the following waves during strong sea undulation makes the ship turn over, as a rule [9].

The course stability can be kept by the ship only when the main engine can be loaded within the entire load range to which it was preconditioned in the design and production phase, i.e. within the working area 1-E-2-3-1 limited by external speed characteristics: h_{max} = idem and h_{min} = idem, and controller speed characteristics NR_{max} = idem and NR_{min} = idem in Fig. 3 [16, 18]. If the propulsion system can be loaded within the above range, we can assume that the system is in the state of ability. If it can be loaded only within a limited range, for instance along an external main engine characteristic h_{nom} = idem or h_t = idem (Fig. 3), and, simultaneously, with the power much smaller than N_{en} or N_{et}, we have to assume that the propulsion system is in the state of inability. This conclusion results from the fact that when the system is loaded within a limited range, for instance along the line segment A-D of the controller characteristic (Fig. 3), the generated thrust force T (Fig. 2) and its component T_N (being the driving force) are not large enough to balance, in storm conditions, the force R_x which is the total hull resistance at ship's speed v. Nevertheless in good weather conditions, safe ship sailing along the line segment A-B or even A-C of the abovementioned characteristic is still quite possible. Obviously, the state of ability of the propulsion system can be defined in another way, for instance assuming that it is reached when the main engine can be loaded in accordance with the engine speed characteristics which allow it to fulfil one of the following criterion functions (Fig. 3): optimal overall propulsion efficiency $\eta_{n(opt)}$, optimal overall engine efficiency $\eta_{o(opt)}$, or optimal driving efficiency $\xi_{o(opt)}$ [16, 18]. Controlling the engine operation according to the curve of optimal engine efficiency $\eta_{o(opt)}$ makes it possible to reach the minimal specific consumption of the fuel (heavy oil or diesel oil), while controlling it in accordance with the curve of optimal driving efficiency $\xi_{o(opt)}$ leads to the minimal effective power of the engine for the a priori assumed speed of ship motion. Clearly, in this case the specific fuel consumption is larger than when the engine operates according to the curve $\eta_{o(opt)}$. It is also clear that controlling the engine operation should consist in such selection of injection pump setting h = idem and the screw pitch setting (H/D) = idem, that the optimal overall propulsion efficiency $\eta_{n(opt)}$ is obtained for given external conditions WZ (sailing conditions), and not only the

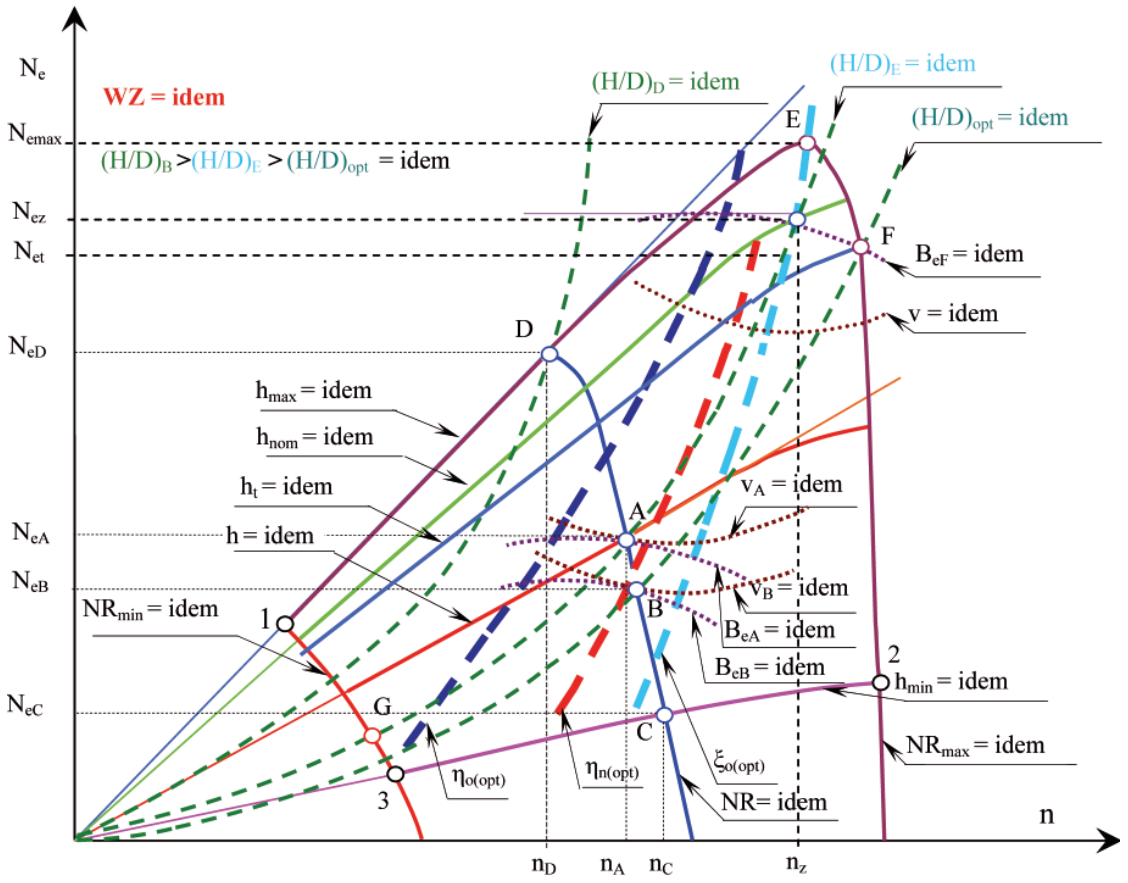

Fig. 3. *Sample motion characteristic of the propulsion system for WZ = idem:* ***H/D*** *– adjustable blade propeller pitch coefficient,* $(H/D)_{opt}$ *– optimal adjustable blade propeller pitch coefficient,* ***WZ*** *– external conditions of ship motion,* B_e *– engine's diesel oil consumption per hour,* B_{eA} *– diesel oil consumption per hour at point A of engine operation,* B_{eB} *– diesel oil consumption per hour at point B of engine operation,* B_{eF} *– diesel oil consumption per hour at point F of engine operation,* v *– ship speed,* v_A *– ship speed when the engine works at point A,* v_B *– ship speed when the engine works at point B,* ***NR*** *– rotational speed controller setting,* NR_{max} *– maximal rotational speed controller setting,* NR_{min} *– minimal rotational speed controller setting,* h_{max} *– maximal fuel bar setting,* h_{nom} *– nominal fuel bar setting,* h_{min} *– minimal fuel bar setting,* h_t *– fuel bar setting which enables obtaining continuous effective power (*N_{et}*),* h *– fuel bar setting,* N_e *– effective power of the engine,* N_{ez} *– nominal effective power,* N_{et} *– continuous effective power,* N_{eA} *– effective power at point A of engine operation,* N_{eB} *– effective power at point B of engine operation,* N_{eC} *– effective power at point C of engine operation,* N_{eD} *– effective power at point D of engine operation,* n *– rotational speed of the engine,* n_n *– nominal rotational speed,* n_A *– rotational speed at point A of engine operation,* n_C *– rotational speed at point C of engine operation,* n_D *– rotational speed at point D of engine operation,* $\eta_{o(opt)}$ *– optimal overall engine efficiency,* $\eta_{n(opt)}$ *– optimal overall propulsion efficiency,* $\xi_{o(opt)}$ *– optimal driving efficiency*

optimal overall engine efficiency $\eta_{o(opt)}$ nor optimal driving efficiency $\xi_{o(opt)}$ [18]. However, being of high importance for the realisation of the rational engine operation process in normal conditions, such methods are not applicable when the ship safety is under threat in storm conditions, as in those cases (Fig. 3) the engine is to be loaded not only with the full nominal effective power (N_{ez}) at the nominal speed (n_z), but also with larger powers, including the maximal power (N_{emax}) (point E).

The above analysis reveals that the main engine (1) transmitting mechanical energy to the screw propeller (7) can be loaded at different effective powers (N_e) and rotational speeds (n). Possible ways of main engine loading are shown in Fig. 3, which illustrates a sample motion characteristic of the ship propulsion system. It is noteworthy that the load reveals a random nature, which causes the wear of the engine and other propulsion system components, and leads to propulsion system damages, considered the random events.

Therefore of high importance is the knowledge on ship propulsion system reliability, which can be interpreted in a descriptive sense as the system property which secures its ability to be loaded within the entire engine performance range (Fig. 3) in a defined time [2, 3]. At the same time in the normative sense, the system reliability can be calculated as the probability of maintaining the ability to be loaded within the entire engine performance range in certain time and given ship operation conditions.

It results from the proposed interpretation of ship propulsion system reliability that the reliability of the system of this type is maintained when it can be loaded within the entire range of loads to which it was preconditioned in the design and production phase. With the reference to [3, 4] we can state that this means that the reliability of the main engine and entire propulsion system requires maintaining the state of its ability (s_0). In case the engine or another component of the ship propulsion system cannot be loaded within the entire load range due to their worsened technical condition, we have to assume that the system is in the state of inability (s_i, i = 1, 2, …, 7) [16, 18].

The reliability states and time intervals of their duration can be recognised using relevant diagnostic systems (*SDG*), such as for instance: *CoCoS* (*Computer Controlled Surveillance System*) produced by *MAN*, or *CBM* (*Condition-Based Maintenance*) produced by *Wartsila* [22, 23] for marine engine diagnostics.

The above considerations reveal that changes of the both technical and energetic state of the propulsion systems of sea-going ships (including also their individual components) are random events. These changes, when analysed during the operation of systems of this type, can be considered the

realisations having the form of stochastic processes which are discrete in states and continuous in time. Worsening of the technical condition of these systems is mainly affected the conditions in which they work [5, 16, 18].

These conditions can change from most favourable to most difficult [9, 10, 16, 18]. In this situation the use of technical diagnostics with relevant diagnosing systems (SDG) is necessary. SDG's are needed for identifying technical states of the propulsion systems being the diagnosed systems (SDN). They are also needed for recording times when these states appear and time intervals of their duration. The task consists in determining the states which compose the set:

$$S = \{ s_0, s_1, s_2, s_3, s_4, s_5, s_6, s_7\} \quad (1)$$

having the following interpretation (Fig. 2):

- s_0 – state of ability of the propulsion system, which lasts when the main engine (and, consequently, all other system components) can be loaded within the entire range to which the system was preconditioned in the design and production phase,
- s_1, s_2, s_3, s_4, s_5, s_6, s_7 – states of inability of the system, which appear and last when: the main engine, the coupling, the thrust bearing, the propeller shaft, the propeller shaft bearings, and/or the propeller shaft screw propeller stuffing-box cannot be loaded within the entire range, although they can be loaded within a limited range.

Additionally, recording the times τ_j (j = 0, 1, 2,.., n) of the appearance of states s_i (i = 0, 1, 2, …, 7) and time intervals of their duration t_j(j = 0, 1, 2,.., n) makes it possible to use the theory of semi-Markov processes for working out the semi-Markov model of the process of state changes $s_i \in S$ (i = 0, 1, 2, …, 7). This model is necessary for determining the reliability of the analysed propulsion systems.

THE SEMI-MARKOV MODEL OF CHANGES OF TECHNICAL STATES OF SHIP PROPULSION SYSTEMS

The semi-Markov model of changes of the technical state of an arbitrary propulsion system provides opportunities for determining its reliability taking into account both preventive services oriented on protecting against damages, and those forced by the damages. Both types of services are needed for system regeneration. The regeneration of the system takes place after each service, either preventive or forced. In order to determine the reliability of the ship propulsion system, the semi-Markov model of the process of changes of its technical states (in the reliability aspect) can be presented in the form of the semi-Markov process {W(t): t ≥ 0} with the set of states S = { s_0, s_1, s_2, s_3, s_4, s_5, s_6, s_7} (1). Changes of the above named states s_i (i = 0, 1, 2,..., 7) take place in consecutive times t_n (n ∈ N). In time t_0 = 0 the system is in the state s_0 which lasts until the damage of any system component takes place, while the states s_i (i = 1, 2,..., 7) last until the damaged component is regenerated. The system is damaged when any of its components is damaged, which means that the reliability structure of the propulsion system is a series structure. As a consequence, the state s_0 exists when all components of the propulsion system are new, or the degree of their wear is so low that the system can be loaded within the entire range to which it was preconditioned in the design and production phase. At the same time the states s_i (i = 1, 2, …, 7) take place when the abovementioned propulsion system components (Fig. 2) are in the condition which make it impossible to use the system within the entire range of loads. These states are recognised by relevant diagnosing systems (SDG) in time intervals between consecutive preventive services of the system. Taking into account this situation in the phase of propulsion system operation requires a probabilistic description of the process of its state changes s_i (i = 0, 1, 2, 3, …, 7) including the probability of the appearance of these states in particular times t_0, t_1,..., t_{n-1}, t_n of system operation.

It is possible to construct the semi-Markov model of a real process of ship propulsion system state changes, because these states can be defined in such a way that the duration time of the state existing at time τ_n and the state which can be obtained at time τ_{n+1} do not depend stochastically on earlier states and time intervals of their duration. The semi-Markov model {W(t): t ≥ 0} of the real process of reliability state changes in the phase of propulsion system operation was constructed based on the theory of semi-Markov processes. The proposed model is characterised by the following properties [12, 13, 15, 17]:

1) the Markov condition is met which says that the future evolution of the process of operational changes of ship propulsion system states for which the semi-Markov model was constructed depends only on the system state at a given time, and not on the past system operation, consequently the future of this system depends on the present and not on the past,
2) random variables: T_i which represents the duration time of the state s_i irrespective of the fact which state will be the next, and T_{ij}, which represents the duration time of the state „s_i" given that the next state of this process is the state „s_j", have distributions different than the exponential distribution.

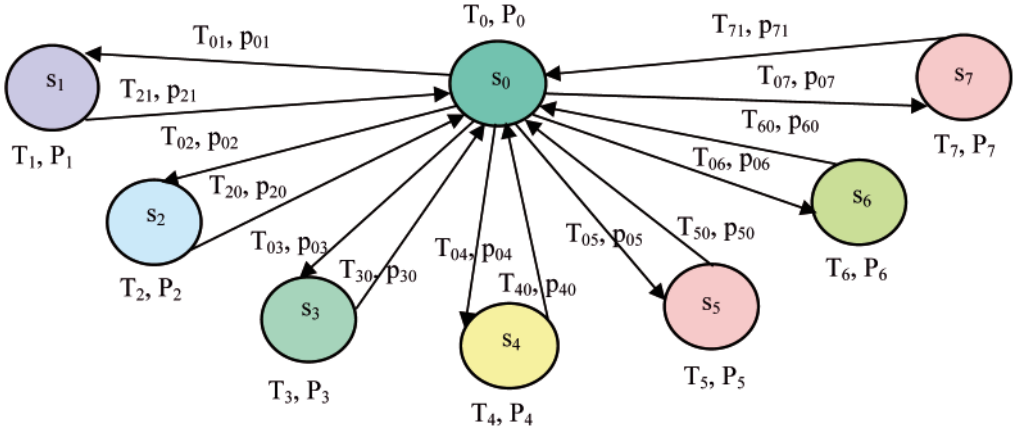

Fig. 4. *Graph of state changes in process {W(t): t ≥ 0}: s_0 – state of ability of the propulsion system, s_1 – state of inability of the main engine, s_2 – state of inability of the coupling, s_3 – state of inability of the thrust bearing, s_4 – state of inability of the propeller shaft, s_5 – state of inability of the propeller shaft bearings, s_6 – state of inability of the propeller shaft stuffing-box, $s_{2(7)}$ – state of inability of the screw propeller, T_i, P_i (i = 0, 1, ..., 7) – times and probabilities of propulsion system existence in states $s_i \in S$(i = 0, 1, ..., 7), T_{ij}, p_{ij} – times and probabilities of propulsion system existence in states $s_i \in S$(i = 0, 1, ..., 7) given that the next system state is s_j, j = 0, 1, ..., 7; i ≠ j*

Modelling which resulted in the construction of the semi-Markov model of changes of ship propulsion system states took into account the results of the analysis of changes of these states [1, 3, 10, 18, 23]. These states were recognised as essential in the examination of a real process of their appearance, observed in the system operation phase.

The empirical investigations have proved that we can assume that the state of an arbitrary propulsion system, including that shown in Fig. 2 in the form of a functional scheme, at time t_{n+1} and the time interval of duration of the state reached at earlier time t_n do not depend on states taking place at times $t_0, t_1,..., t_{n-1}$ and their duration times. Therefore the process $\{W(t): t \geq 0\}$ is the semi-Markov process [1, 2, 5, 6, 7, 8, 11, 12, 16, 17]. The graph of state changes in this process is shown in Fig. 4.

The initial distribution of this process is the following:

$$P\{W(0) = s_i\} = \begin{cases} 1 \text{ for } i = 0 \\ 0 \text{ for } i = 1, 2, ..., 7 \end{cases} \tag{2}$$

while the functional matrix has the form:

$$\mathbf{Q(t)} = \begin{bmatrix} 0 & Q_{01}(t) & Q_{02}(t) & Q_{03}(t) & Q_{04}(t) & Q_{05}(t) & Q_{06}(t) & Q_{07}(t) \\ Q_{10}(t) & 0 & 0 & 0 & 0 & 0 & 0 & 0 \\ Q_{20}(t) & 0 & 0 & 0 & 0 & 0 & 0 & 0 \\ Q_{30}(t) & 0 & 0 & 0 & 0 & 0 & 0 & 0 \\ Q_{40}(t) & 0 & 0 & 0 & 0 & 0 & 0 & 0 \\ Q_{50}(t) & 0 & 0 & 0 & 0 & 0 & 0 & 0 \\ Q_{60}(t) & 0 & 0 & 0 & 0 & 0 & 0 & 0 \\ Q_{70}(t) & 0 & 0 & 0 & 0 & 0 & 0 & 0 \end{bmatrix} \tag{3}$$

The functional matrix **Q(t)** represents the model of reliability state changes of the ship propulsion system with the functional scheme shown in Fig. 2. Non-zero elements $Q_{ij}(t)$ of the matrix **Q(t)** depend on distributions of random variables T_i (i = 0, 1, 2,..., 7), which are the time intervals when the process $\{W(t): t \geq 0\}$ is in particular states $s_i \in S$(i = 0, 1,..., 7). Elements of the functional matrix **Q(t)** are the probabilities of transition of the abovementioned process from state s_i to state s_j ($s_i, s_j \in S$) in time not longer than t. These probabilities are defined in the following way [11, 12]:

$$Q_{(ij)}(t) = P\{W(\tau_{n+1}) = s_j, \tau_{n+1} - \tau_n < t | W(\tau_n) = s_i\} = p_{ij}F_{ij}(t) \tag{4}$$

where:

p_{ij} – probability of uniform Markov chain transition in one step;

$p_{ij} = P\{Y(\tau_{n+1}) = s_j | Y(\tau_n) = s_i\} = \lim_{t \to \infty} Q_{ij}(t)$;

$F_{(ij)}(t)$ – distribution function of random variable $T_{(ij)}$ representing the time when the process $\{W(t): t \geq 0\}$ is in state s_i given that the next state is s_j.

Since the functional matrix **Q(t)** (3) is the stochastic matrix, then the matrix **P** (7) of the probabilities of transitions of the Markov chain placed into this process consists of terms which are [1, 3, 4] the probabilities p_{ij}: $p_{00} = 0$, $p_{i0} = Q_{i0}(t) = 1$ (i = 1, 2, …, 7) and $p_{0j} = Q_{0j}(t)$ (j = 1, 2, …, 7), for $i \neq j$.

The process $\{W(t): t \geq 0\}$ is irreducible [1, 3, 4] and the random variables $T_{(ij)}$ have limited and positive expected values. Therefore its limiting distribution [11, 12]

$$P_j = \lim_{t \to \infty} P_{ij}(t) = \lim_{t \to \infty} P\{W(t) = s_j\}$$
$$s_j \in S(j = 0, 1,...,7) \tag{5}$$

has the following form [12]:

$$P_j = \frac{\pi_j E(T_j)}{\sum_{l=0}^{7} \pi_l E(T_l)} \tag{6}$$

The probabilities π_j(j = 0, 1, 2,..., 7) in formula (6) are the limiting probabilities of the Markov chain placed into the process $\{W(t): t \geq 0\}$, while $E(T_j)$ and $E(T_l)$ are the expected values of the random variables T_j and T_l, respectively, representing time intervals spent by the propulsion system in states s_j and s_l independently on what the next state is. Determining the limiting distribution (6) requires solving the system of equations with the abovementioned limiting probabilities π_j (j = 0, 1,..., 7) of the placed Markov chain and the matrix **P** of the probabilities of transition from state s_i to state s_j. This equation system has the following form:

$$\left.\begin{aligned} &[\pi_0, \pi_1, \pi_2, \pi_3, \pi_4, \pi_5, \pi_6, \pi_7] = [\pi_0\ \pi_1, \pi_2, \pi_3, \pi_4, \pi_5, \pi_6, \pi_7] \cdot \mathbf{P} \\ &\sum_{k=1}^{4} \pi_k = 1 \end{aligned}\right\} \tag{7}$$

where, taking into account the fact that matrix (3) is the stochastic matrix, matrix **P** has the following form:

$$\mathbf{P} = \begin{bmatrix} 0 & p_{01} & p_{02} & p_{03} & p_{04} & p_{05} & p_{06} & p_{07} \\ 1 & 0 & 0 & 0 & 0 & 0 & 0 & 0 \\ 1 & 0 & 0 & 0 & 0 & 0 & 0 & 0 \\ 1 & 0 & 0 & 0 & 0 & 0 & 0 & 0 \\ 1 & 0 & 0 & 0 & 0 & 0 & 0 & 0 \\ 1 & 0 & 0 & 0 & 0 & 0 & 0 & 0 \\ 1 & 0 & 0 & 0 & 0 & 0 & 0 & 0 \\ 1 & 0 & 0 & 0 & 0 & 0 & 0 & 0 \end{bmatrix}$$

After solving the equation system (7) and making use of the formula (6) we get the following relations:

$$\left.\begin{aligned} P_0 &= \frac{E(T_0)}{E(T_0)+\sum_{l=0}^{7} p_{0l}E(T_l)}, \quad P_1 = \frac{p_{01}E(T_1)}{E(T_0)+\sum_{l=0}^{7} p_{0l}E(T_l)}, \\ P_2 &= \frac{p_{02}E(T_2)}{E(T_0)+\sum_{l=0}^{7} p_{0l}E(T_l)}, \quad P_3 = \frac{p_{03}E(T_3)}{E(T_0)+\sum_{l=0}^{7} p_{0l}E(T_l)}, \\ P_4 &= \frac{p_{04}E(T_4)}{E(T_0)+\sum_{l=0}^{7} p_{0l}E(T_l)}, \quad P_5 = \frac{p_{05}E(T_5)}{E(T_0)+\sum_{l=0}^{7} p_{0l}E(T_l)}, \\ P_6 &= \frac{p_{06}E(T_6)}{E(T_0)+\sum_{l=0}^{7} p_{0l}E(T_l)}, \quad P_7 = \frac{p_{07}E(T_7)}{E(T_0)+\sum_{l=0}^{7} p_{0l}E(T_l)}. \end{aligned}\right\} \quad (8)$$

The probability P_0 is the limiting probability that in a longer time interval of operation (theoretically for $t \to \infty$) the propulsion systems is in state $s_{(0)}$. Thus this probability defines the serviceability of the system at arbitrary time t of its operation, i.e. the ability of the system to perform a task. At the same time the probabilities P_j(j = 1, 2,..., 7) are the limiting probabilities of the existence of states $s_j \in S$ of the analysed system when $t \to \infty$, i.e. the probabilities of the existence of situations when some system components (and, consequently, the entire system due to its series reliability structure) are in states of inability.

Calculating the probabilities P_0 and P_j(j = 1, 2, …, 7) requires assessing probabilities p_{ij} and the expected values $E(T_j)$, which is expensive and time consuming.

Collecting the information necessary for assessing the above probabilities and expected values requires the use of relevant (SDG) systems to diagnose particular propulsion system elements, which are the diagnosed systems (SDN) in this case [5].

FINAL REMARKS AND CONCLUSIONS

The semi-Markov processes are becoming more and more frequently used for solving problems concerning reliability, general service and diagnostics of various devices, diesel engines for instance.

The use of the semi-Markov process, instead of the Markov process, as the model of reliability state changes of propulsion systems working on sea-going ships in a given time results from the fact that we have to expect that the random variable $T_{(ij)}$ which represents the time interval when the system is in state s_i given that the next state is s_j, and the random variable T_i which is the time interval when the system is in state s_i(i = 0, 1, 2, …, 7) independently on what the next state is, have arbitrary concentrated distributions in set $R_+ = [0, +\infty)$. The use of the Markov process in this case would be justified when we could assume that the random variables $T_{(ij)}$ and T_i have exponential distributions.

The presented model is of certain practical importance, because of its easiness to estimate the transition probabilities p_{ij} being the elements of matrix **P** (7) and the expected values $E(T_j)$. We should keep in mind here that the point estimation of the expected value $E(T_j)$ does not provide opportunities for assessing the accuracy of its estimation. This accuracy is only secured in the interval estimation, in which the confidence interval $[t_{dj}, t_{gj}]$ with random endpoints is calculated. This confidence interval contains the unknown expected value $E(T_j)$ with certain probability (confidence level) β.

The semi-Markov processes are stochastic processes which reveal specific properties. In publications on this subject different definitions of the semi-Markov process, with different levels of generality and precision levels, can be found. For the purpose of modelling the operation process of the ship propulsion system and other devices, the semi-Markov process (family of random variables) $\{W(t): t \geq 0\}$, can be defined using a so-called uniform Markov regenerative process [11, 12, 17].

It results from the definition of the semi-Markov process that it is the stochastic process with a discrete set of states, and its realisations are interval constant functions (having constant values in operating time intervals being the random variables), which are right-continuous. It also results from this definition that the process is well defined when its initial distribution $P_i = P\{W(0) = s_i\}$ is known, along with (in the analysed case) the functional matrix $\mathbf{Q(t)} = [Q_{ij}]$ $(i \neq j; i, j = 0, 1, 2,..., 7)$, the elements of which are the probabilities of process transition from state "s_i" to state "s_j" in time not longer than t (4), being the non-decreasing functions of time t and denoted as $Q_{ij}(t)$ [1, 6, 11, 12].

BIBLIOGRAPHY

1. Girtler J.: *Applicability of semi-Markov processes as models of machine operation processes* (in Polish). Machine Operation Issues (Zagadnienia Eksploatacji Maszyn), Warsaw 1996, z.3(107) pp. 419-428.
2. Girtler J.: *Reliability model of two-shaft turbine combustion engine with heat regenerator*. Journal of KONES Powertrain and Transport, Vol. 132, No. 4, 2006, pp.15-22.
3. Girtler J.: *Possibility of defining theoretical operation for diesel engines in energy terms*. Combustion Engines (Silniki Spalinowe), no. 3, 2011, pp. 1-9 [pdf].
4. Girtler J.: *A method for evaluating the performance of a marine piston internal combustion engine used as the main engine on a ship during its voyage in different sailing conditions*. Polish Maritime Research, Vol. 17 No. 4, 2010, pp. 31-38.
5. Girtler J.: *Diagnostics as the condition for controlling the operation of marine internal combustion engines* (in Polish). PNA studies, (Studia WSM) No. 28, Szczecin 1997.
6. Girtler J.: *Physical aspects of application and usefulness of semi-Markov processes for modeling the processes occurring in operational phase of technical objects*. Polish Maritime Research, Vol. 11, No 3, 2004, pp. 25-30.
7. Girtler J.: *Quantum issues in diagnostics of marine energy machines and devices*. Scientific Journals of the Maritime University of Szczecin. – No 30(102).
8. Girtler J.: *Aspects of quantum diagnostics of machines* (in Polish). XXXIX Machine Diagnostics Symposium. Wisla, 04÷10.03. 2012, Materials issued as article abstracts and on CD, 23 p. Publications of the Faculty of Transport of the

Silesian University of Technology (Wyd. Wydział Transportu Politechniki Śląskiej), Katowice 2012.
9. Girtler J., Kitowski Z., Kuriata A.: *Ship safety at sea. System approach* (in Polish). WKiŁ, Warsaw1995.
10. Girtler J., Kuszmider S., Plewiński L.: *Selected issues of sea-going ship operation in the aspect of safety of sailing*. Monograph (in Polish). WSM, Szczecin 2003.
11. Grabski F.: *Semi-Markov models of reliability and operation* (in Polish). PAN IBS, Series: System Research (Badania Systemowe) vol. 30, Warsaw 2002.
12. Grabski F.: *Theory of semi-Markov processes of technical object operation* (in Polish). Scientific Reports of PNA (Zeszyty Naukowe AMW), no. 75A, Gdynia 1982.
13. Jadźwiński J., Borgoń J: *Operating reliability and safety of flights* (in Polish). WKiŁ, Warsaw 1989.
14. Kiliński A.: *Descriptive and normative definitions of the idea of reliability* (in Polish). Quality Issues (Problemy Jakości), No. 3, Warsaw 1972, pp.5−13.
15. Limnios N., Oprisan G.: *Semi-Markov Processes and Reliability*. Boston, Birkhauser 2001.
16. Piotrkowski I., Witkowski K.: *Operation of marine internal combustion engines* (in Polish). AM Gdynia 2002.
17. Сильвестров Д. С.: Полумарковские процессы с дискретным множеством состояний. Издательство „Советское Радио". Москва, 1980.
18. Wojnowski W.: *Marine power plants* (in Polish). Part. I. PNA Publications (wyd. AMW), Gdynia 1998.
19. Wiśniewski B.: *Wind undulation* (in Polish). Scientific publications of SU (Wyd. Naukowe USz)., Szczecin 1998.
20. *Machine diagnostics engineering (in Polish)*. Collective work, editors: B. Żółtowski and C. Cempel. PTDT. Wyd. ITE, Warsaw, Bydgoszcz, Radom 2004.
21. *Reliability manual* (in Polish). Collective work, editor: J. Migdalski. Publications of Machine Industry (Wydawnictwa Przemysłu Maszynowego) „WEMA", Warsaw 1982
22. *MAN B&W Diesel A/S: CoCoS Maintenance*, Designed for Maintenance Excellence, Copenhagen 2005.
23. Wartsila Corporation: *Service News from Wartsila Corporation* 2 2002/1 2003, CBM for two stroke engines, Kaidara Software, Wartsila Corporation Helsinki, March 2003.

CONTACT WITH THE AUTHOR

Jerzy Girtler, Prof.
Department of Ship Power Plants
Faculty of Ocean Engineering and Ship Technology
Gdansk University of Technology
Narutowicza 11/12
80-233 Gdansk, POLAND
e-mail: jgirtl@pg.gda.pl

POLISH MARITIME RESEARCH 4(80) 2013 Vol 20; pp. 25-33
10.2478/pomr-2013-0037

The influence of efficiency of the cooling system on the thermodynamic parameters and performance of a two - stage VC 20.96 reciprocating compressor designed to serve as a marine engine starter

Mateusz Grzelczak, Ph.D.,
Poznan University of Technology, Poland

ABSTRACT

The paper presents results of the research related to the analysis of the thermodynamic and flow processes occurring in a prototype VC 20.96 two-stage liquid-cooled reciprocating compressor. The compressor has been developed and manufactured by H. Cegielski Poznan metal works in collaboration with the Poznan University of Technology. The research related to the VC compressor was realized within the KBN 3127/C.T07-6/2002 project titled "Development of design of type-series of reciprocating compressors and their implementation in production". The basic task of the project was to develop two type-series of liquid- and air- cooled reciprocating compressors of the V- and W- arrangement, designed to serve as marine engine starters. The result of the design work was the manufacturing of two compressors: the VC 20.96 liquid-cooled compressor and the WP 18.80 air-cooled one. The main aim of the research described in this paper was to evaluate the efficiency of the cooling system which uses inter-coolers integrated with the compressing stages and the cooperation of the compressing stages in terms of pressure ratio distribution. Owing to the cooling method, the applied design assumptions enabled to develop a compact compressor fulfilling the assumed operating parameters.

Key words: reciprocating compressor; liquid-cooled compressor; efficiency; polytropic exponent

INTRODUCTION

The requirements set for the compressing machines installed in marine engine rooms force the designers to develop simple and reliable design solutions with particular focus on their limited size. Additionally, low electrical energy consumption and low coolant flow per unit of compressed gas are required from the compressing units.

In light of the above given conditions the engineers aimed at ensuring the assumed parameters such as pressure increments and volumetric flow rates of the compressed gas, thus guaranteeing high efficiency of the process through the improvement of the cooling.

In the VC compressor has been implemented a solution that consists in integrating the inter-cooler and the after-cooler with the compressing stages. This required developing complex casts of the cylinder heads and coolers.

The applied uneven distribution of pressure ratio between the first and the second stage contributed to the development of excessively high temperatures in the second stage compression chamber. Another problem yet occurred - the air in the second stage suction chamber heated up. Hence, the main task described in the paper was the analysis of the inter-cooling system and the cooling of the cylinder walls, based on the measurements of the thermodynamic parameters and pressures in function of crankshaft angle for each of the compressing stages. The obtained indicator diagrams enabled to verify the efficiency of the cooling of the cylinder walls, based on the determined polytropic exponents of the compression process. Prior to modifying the design that consisted in development of a new compressing stage of the piston diameter of 86 mm, tests were performed for three values of the clearance volume of the second stage. The tests were aimed at determining the minimum amount of coolant fulfilling the condition of similar temperature values at the end of compression in each of the stages.

TECHNICAL SPECIFICATION OF THE COMPRESSOR

The VC20.96 liquid-cooled compressor reaches the discharge pressure of $P_t = 30$ bar at the flow rate $q_v = 220$ m³/h and the compressor speed N = 1800 rpm. Below in Tab. 1 are shown the basic geometrical and operating parameters obtained from the design calculations.

Tab. 1. VC20.96 compressor design specification

No.	Quantity	Unit	Compressor crankshaft speed N [rpm]			
			1000	1200	1500	1800
1.	Air suction parameters: - pressure p_o - temperature t_o - relative humidity φ	 bar °C %	 1.0 20 ÷ 45 10.0 ÷ 95.0			
2.	Air compression parameters: - nominal discharge pressure p_D - maximum temperature $t_{D,\,max}$	 bar °C	 30 90			
3.	Air volumetric flow rate q_v for the nominal discharge pressure p_D = 30 bar and ambient parameters: - t_o = 20°C, φ = 50.0% - t_o = 45°C, φ = 50.0%	 m³/h m³/h	 128 105	 154 126	 192 158	 229 189
4.	Design parameters: - cylinder bore of 1 st stage, D_1 - cylinder bore of 2 nd stage, D_2 - piston stroke s - clearance volume of 1st stage, $V_{C,1}$ - clearance volume of 2nd stage, $V_{C,2}$ - length of the connecting rod, $l_{1,2}$	 mm mm mm m³ m³ mm	 200 90 96 $2.35\ 10^{-4} \div 2.51\ 10^{-4}$ $3.25\ 10^{-5} \div 3.58\ 10^{-5}$ 284			
5.	Pressure ratio of 1st stage, ε_1, for the ambient parameters: - t_o = 20°C, φ = 0.0% - t_o = 45°C, φ = 50.0%	 - -	 5.34 5.28	 5.36 5.31	 5.38 5.37	 5.41 5.40
6.	Cooling water: - temperature at inlet t_w - volumetric flow rate $q_{v\,w}$	 °C l/min	 15 ÷ 40 140	 115	 95	 75

Fig. 1 presents the image of the prototype VC compressor manufactured by H. Cegielski Poznan S.A.

Fig. 1. *The prototype VC 20.96 reciprocating compressor*

THE SCOPE OF THE RESEARCH AND THE TEST STAND

The research program comprised the thermodynamic, flow, dynamic and acoustic measurements.

The basis for the performance of the research was the work titled 'The program of trials of the prototype of the VC20.96 compressor' and the PN-ISO 1217:1999 and PN-93/M-53950/01 standards.

The above mentioned standards are related to acceptance tests carried out on positive displacement compressors, i.e mainly to determining the efficiency and power at a given pressure during compression. The scope of the tests on the VC20.96 compressor has been thus extended in relation to this standard. Additionally, the standard related to the vibration and noise measurements (PN-84/N-01330) has been applied.

The trials covered the compression process in the individual compression stages and the whole compressor, as well as the cooling process (inter-cooling and after-cooling).

The tests were carried out for the ambient conditions close to normal: p_o = 1 bar, t_o = 20°C, and the relative humidity φ = 60%, and also for the tropical conditions, i.e. the ambient temperature t_o = 45°C.

The trials were performed for varying cooling rates in a wide range of cooling-water flow and a full range of pressures during compression: 5, 10, 15, 20, 25 and 30 bar for four crankshaft speeds: 1000, 1200, 1500 and 1800 rpm.

The tests were divided into two stages [phases]. In the first stage phase the basic quantities were measured such as discharge pressure, volumetric flow rate and power at assumed speeds. The second stage phase was related to the pressure and temperature measurements in the suction and compression chambers of each of the compression stages, the measurements of the hydraulic resistance in the form of pressure drops and the measurement of temperatures upstream and downstream the coolers and the mass of the condensed liquid downstream the coolers.

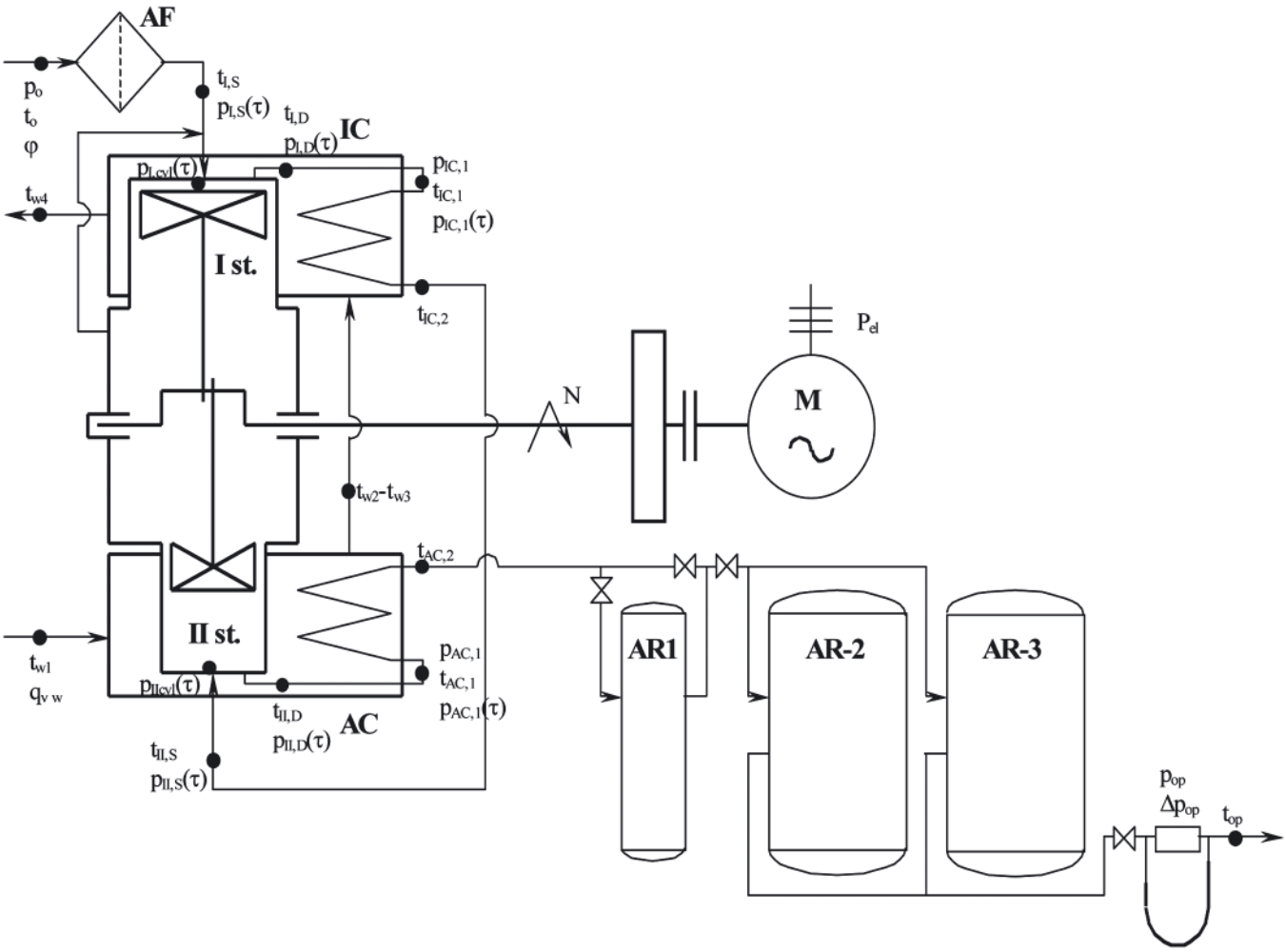

Fig. 2. *Schematic diagram of the research stand for measuring stationary thermodynamic and mechanical parameters and the runs of pressure in function of crankshaft angle*

Within the thermodynamic and flow investigations of the compressor the runs of pressure in function of crankshaft angle were measured in order to obtain the indicator diagrams of the compression process. The runs of pressure were measured inside the cylinders and in selected cross sections of the air ducts of the first and second stages of the compressor for the following operating conditions: discharge pressure of 15 and 30 bar, crankshaft speed of 1500 and 1800 rpm. The tests were extended by the measurements of the runs of pressure for two diameters of cylinder bore of the second stage: d_I = 90 mm and d_{II} = 86 mm.

The measurement of the runs of pressure in function of crankshaft angle was realized by using two ENDEVCO 8540 piezoresistive pressure transducers (differing in the measurement range). The pressure measurement in the first stage was carried out with the transducer operating in the range of 0 ÷ 689.5 kPa of the absolute pressure, and in the second stage with the transducer operating in the range of 0 ÷ 3447.4 kPa of the absolute pressure.

The above mentioned pressure converters have a calibration certificate issued by National Institute of Standards and Technology (NIST) USA and accordance with MIL-STD-45662A (MILITARY STANDARD - Calibration Systems Requirements).

The measurement of the values varying in time was realized according to the schematic diagram presented in Fig. 3. The electrical signal from the pressure transducers and the voltage signal from the photoelectric probe designed to measure the crankshaft angle,were converted into a digital signal in the Iotech ADC 488/8SA converter. The signal was converted through an amplifier also operating as a ENDEVCO 136 charger. The A/C converter used in the measurements also recorded each of the three measured quantities with the frequency of f = 20 kHz. The digital signal obtained through the internal controller card was saved on a PC.

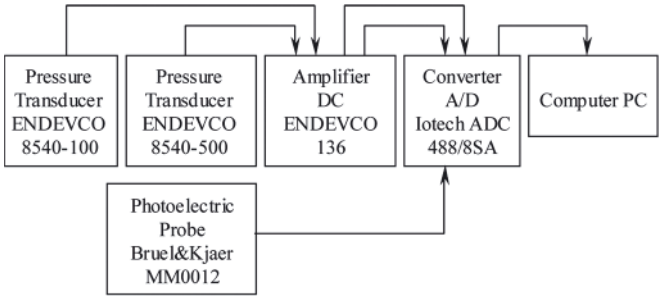

Fig. 3. *Schematic diagram of the measurement track for recording the values in function of crankshaft angle*

EXPERIMENTAL RESULTS

The division of the VC compressor research into two stages phases enabled an independent interpretation of the physical quantities which describe the issue of heat exchange in the coolers and through the cylinder walls of each of the compressing stages. The first stage phase of the research consisted in the measurement of the stationary parameters such as temperatures, pressures, volumetric flow rate of air and coolant in the characteristic control cross-sections of the

reciprocating compressor. The parameters enabled to make an analysis of the efficiency of the inter-cooler and after-cooler. The second stage phase of the research included the measurements of the pressures inside the cylinder in function of crankshaft angle, on the basis of which the p-V diagrams have been developed. The obtained pressure runs allowed to evaluate the flow of heat transferred through the cylinder walls from the compressed gas to the coolant. The evaluation has been carried out based on the comparison of the obtained values of the polytropic exponents of the compression and expansion processes for each of the stages.

In the first place, the paper presents the results of the measurements such as characteristics of the discharge pressure in function of the volumetric flow rate of air at the suction (Fig. 4). The obtained results have been presented for four crankshaft speeds. From comparison of the measured volumetric flow rate with the design values it turns out that the chosen assumptions have been satisfied except the crankshaft speed of N = 1200 rpm. The relative difference between the design volumetric flow rate and the measured one for that speed is 12 %. In the case of tropical conditions the situation is more advantageous as the design assumptions related to the volumetric flow rate have been fulfilled for the whole range of speeds.

The characteristics of the discharge pressure presented in Fig. 4 in function of the air volumetric flow rate show the specificity of the positive displacement machine for which a drop of the volumetric flow rate occurs as the discharge pressure grows. It has been observed that it is a result of a leakage between the piston and cylinder wall or a leakage in the discharge valves. A relative difference of the volumetric flow rate for a compressor producing the extreme value of pressure at discharge, p_D = 0.5 and 3.0 MPa, is equal to maximum 15 %.

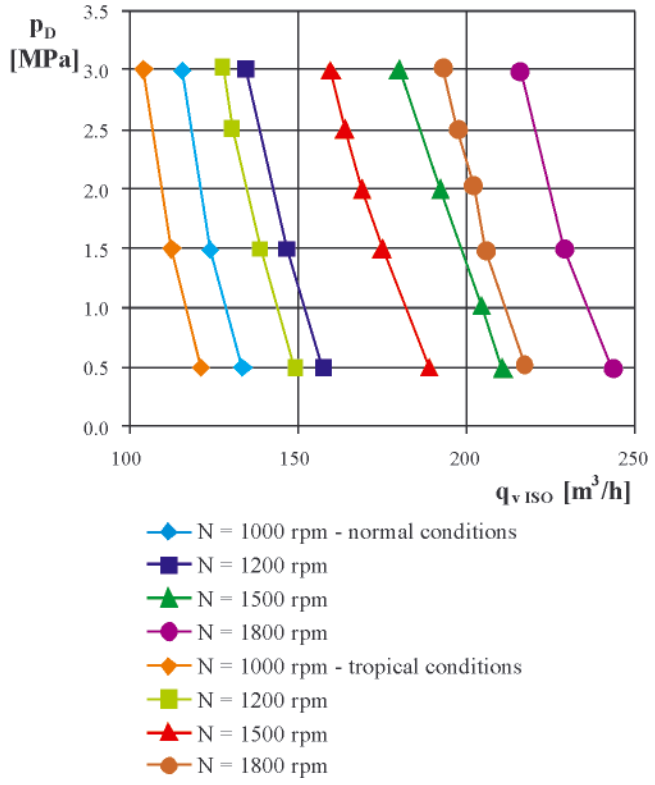

Fig. 4. Characteristics of the compressor discharge pressure in function of the volumetric flow rate for four crankshaft speeds and both the nominal and tropical conditions taken into account

Prior to interpretation of the results (efficiency of the coolers) the values of the discharge temperature and pressure ratios of each of the stages were compared (Fig. 5 and 6). The comparison takes into account the run of the above mentioned parameters in function of the discharge pressure for two volumetric flow rates of the cooling water. The first flow rate was $q_{v1,w}$ = 30 l/min and corresponded to the minimum amount of cooling water and the second value of the flow rate was three times greater and amounted to $q_{v1,w}$ = 90 l/min.

In the case of the run of temperature shown in Fig. 5, can be observed a greater temperature drop as the cooling water flow rate increases in the second compressing stage in comparison to the first stage. This results from a lower temperature of the cooling water supplied to the inter-cooler of the first stage, which consequently contributes to the obtaining of a lower temperature of air downstream the inter-cooler as well as in the suction chamber of the second stage. Additionally, the lower temperature values at the end of the compression process result from the increased heat transfer through the cylinder walls to the coolant.

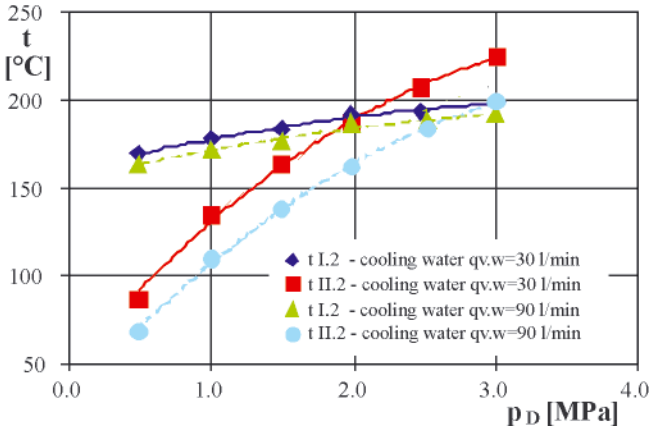

Fig. 5. Comparison of the air temperature runs in the discharge chambers of the first and second stages for the volumetric flow rate of the cooling water qv,w = 30 and 90 l/min, at the maintained values of t_{ol} = 15°C and N = 1500 rpm

Another parameter that changed its value due to the increase of the cooling water flow rate is the pressure ratio. More advantageous cooling conditions of the second stage resulted in the increase of the pressure ratio in this stage and a drop of the pressure ratio in the first stage (Fig. 6). This results from the increase of the heat-up volumetric coefficient of the second stage the consequence of which was the distribution of the pressure ratios.

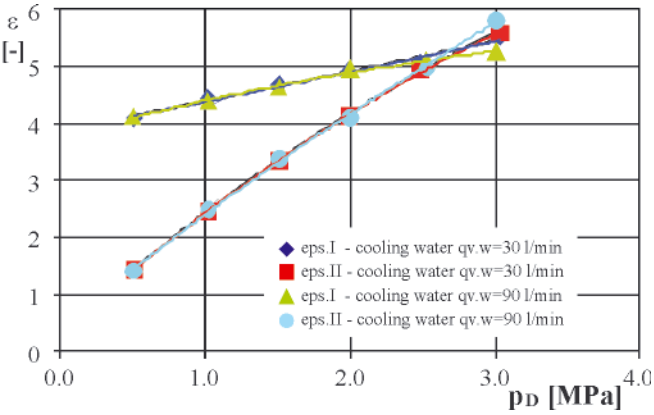

Fig. 6. The comparison of pressure ratios of the first and second stages in function of pressure for the cooling water flow qv,w = 30 and 90 l/min, at the maintained values of t_o = 15°C and N = 1500 rpm

Based on the obtained measurement results in the form of temperatures of the compressed air and cooling water in the inlet and outlet cross-sections of the inter-cooler and the after-cooler, the values of efficiency of the coolers were determined.

Below the values of the efficiency of the coolers have been shown for two volumetric flow rates of the cooling water: $q_{v1,w} = 30$ l/min and $q_{v2,w} = 90$ l/min. For the calculations, the definition of the efficiency of the heat exchanger operating in the cross current configuration has been selected. This has been chosen because, despite the fact that the inflow of the coolant fulfilled the cross-flow condition, in the majority of the volume of the coolers a cross-current flow was realized. The dependence on the basis of which the efficiency was determined, is as follows:

$$E_{IC} = \frac{T_{IC,1} - T_{IC,2}}{T_{IC,1} - T_{w3}} \qquad E_{AC} = \frac{T_{AC,1} - T_{AC,2}}{T_{AC,1} - T_{w1}}$$

The efficiency of the inter-cooler for the cooling water flow rate $q_{v1,w} = 30$ l/min and $q_{v2,w} = 90$ l/min is, respectively:

$$E_{IC,n,30} = 0.88 \qquad E_{IC,n,90} = 0.91$$

The efficiency of the after-cooler for the same water flow rates is:

$$E_{AC,n,30} = 0.77 \qquad E_{AC,n,90} = 0.82$$

As a complement, based on the obtained measurement results, the values of the efficiency of the inter-cooler and after-cooler have been presented for tropical conditions at the maintained value of the cooling water flow rate $q_{v,w} = 140$ l/min.

The efficiency of the inter-cooler is:

$$E_{IC,t,140} = 0.92$$

The efficiency of the aftercooler is:

$$E_{AC,t,140} = 0.87$$

The uneven distribution of the pressure ratio assumed at the design stage led to an excess of the admissible temperature for the second stage of the compressor. For this reason the interpretation of the results took a form of discharge temperatures, values of the pressure ratios, air volumetric flow rate and electrical power of the compressor in the whole range of the volumetric flow rate of the cooling water. The complement of the analysis was the inclusion of three values of clearance volume for the second stage. The assumed strategy aimed at selecting a new diameter of the second-stage cylinder that would allow a distribution of pressure ratios so that the admissible discharge temperature is not exceeded at maintaining the minimum possible value of the volumetric flow rate of the cooling water, in the same time.

Fig. 7 ÷ 9 present the above mentioned thermodynamic parameters for the designed value of the clearance volume marked V_C on the graphs and two outstanding volumes extended by 50 % and 100 % as compared to the design value ($V_{C1} = V_C$, $V_{C2} = 1{,}5V_C$ and $V_{C3} = 2{,}0V_C$). The developed measurement results prove that the distribution of the pressure ratios obtained for the lowest clearance volume fulfills the design assumptions (Fig. 8.). The average value of the pressure ratio for the first stage was $\varepsilon_I = 4.9$, and, the pressure ratio of the second stage is greater and amounts to $\varepsilon_{II} = 6.3$. An uneven distribution of the pressure ratios and the excess temperature in the suction chamber of the second stage have led to an excess of the admissible air temperature ($t_{max} = 230$ °C) (which may reduce compressor mechanical durability and worsen oil lubricating properties). Based on the performed measurements for the design clearance volume, the temperature of the second stage was on the admissible level but the discharge temperature of the first stage at the volumetric water flow rate $q_{v,w} = 60$ l/min was lower by Δt 38 °C (Fig. 7). Unfortunately, approximating lower values of the volumetric cooling water flow rate would clearly lead to the excess of the admissible temperature of the first stage. As a complement, the value of the electrical power being the highest due to the compressed air flow rate reaching $q_{v,w} = 180$ m³/h, has been presented in Fig. 9. This results from the maintaining of the highest value of the volumetric coefficient of clearance volume of the second stage when applying the design value of the clearance volume.

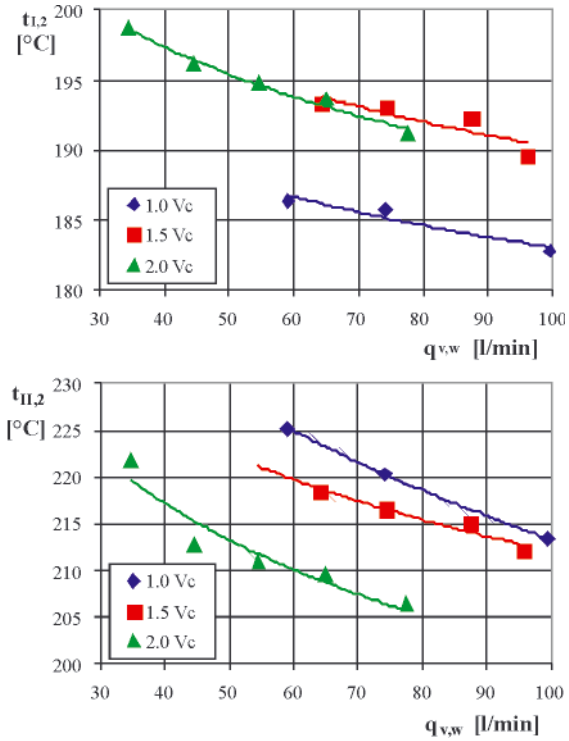

Fig. 7. The comparison of the runs of air temperature in the compression chambers of the first and second stages in function of the volumetric flow rate of the cooling water $q_{v,w}$ for three values of the clearance volume V_C at the maintained values: $t_o = 15$ °C and $N = 1500$ rpm

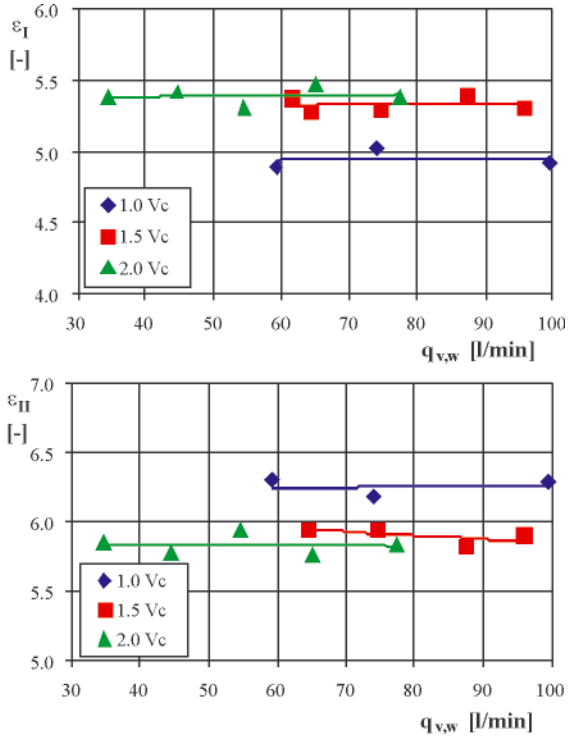

Fig. 8. The comparison of the runs of pressure ratio of the first and second stages in function of the volumetric flow rate of the cooling water $q_{v,w}$ for three values of the clearance volume V_C, at the maintained values: $t_o = 15$ °C and $N = 1500$ rpm

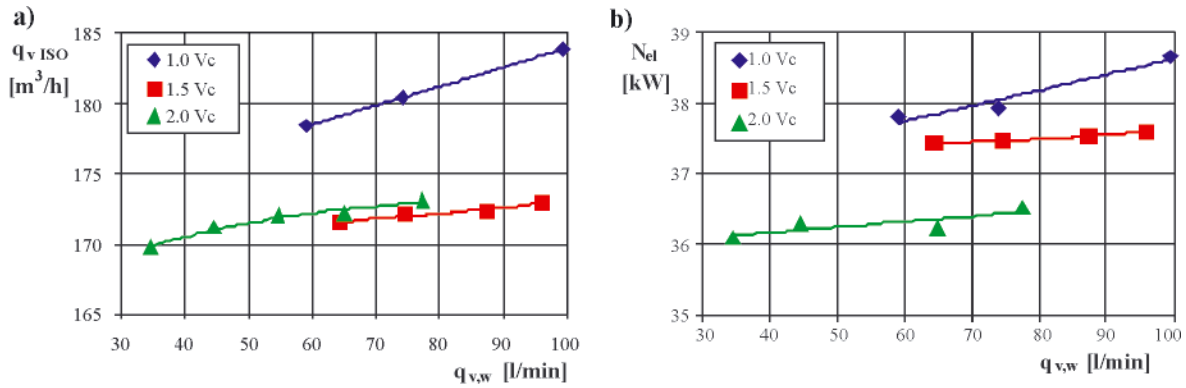

Fig. 9. The comparison of the runs of the compressed air volumetric flow rate (a) and the electric power (b) measured at the electric motor terminals in function of the volumetric flow rate of the cooling water $q_{v,w}$ for three values of the clearance volume V_C, at the maintained values: t_o = 15 °C and N = 1500 rpm

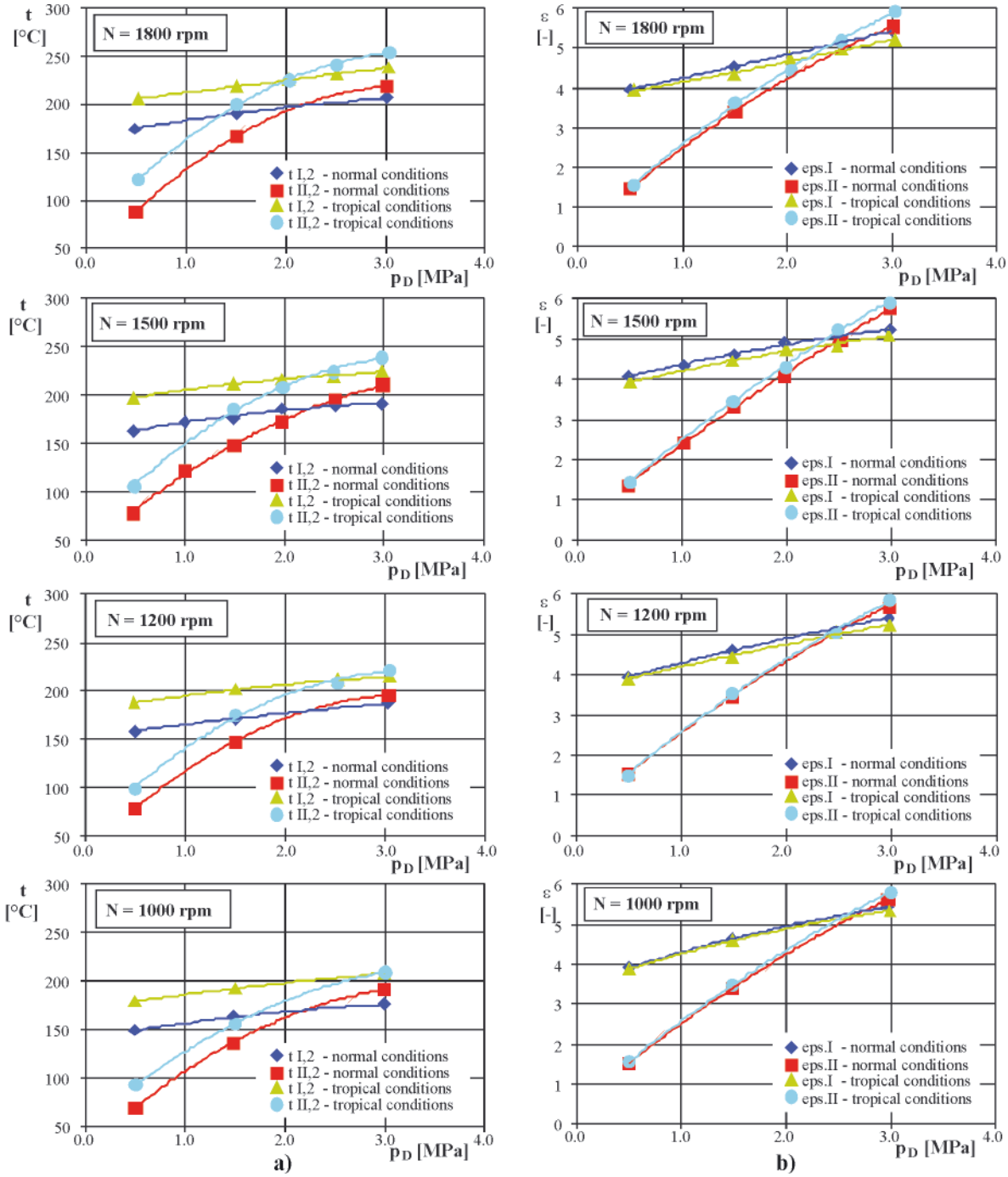

*Fig. 10. The comparison of the runs of air temperature in the compression chambers of the first and second stages (**a**) and the pressure ratio (**b**) in function of discharge pressure for normal conditions: t_o = 15 °C, tropical conditions: t_o = 45 °C, and four crankshaft speed values: N = 1800, 1500, 1200 and 1000 rpm, at the maintained constant value of the volumetric cooling-water flow rate $q_{v,w}$ = 140 l/min*

As a result of increasing the clearance volume of the second stage a drop in the operating parameters such as the volumetric flow rate or compressing power (Fig. 9), must be expected. In the case of extreme values of the clearance volumes (V_C and 2.0 V_C) the difference between the clearance volumes and the electric power demand amounts to Δq_v = 4 %, ΔN_{el} = 4.5 %, respectively. The application of a greater clearance volume enables to obtain a less varied pressure ratio distribution (Fig. 8) that consequently contributes to a reduction of differences in the temperatures between the first and the second stages (Δt = 22 °C) and to the simultaneous reduction of the volumetric flow rate of the cooling water to the value of $q_{v,w}$ = 35 l/min (Fig. 7). The lower amount of cooling water ensures a better index of cooling water per unit of compressed air, not exceeding the admissible temperature in any of the stages.

The next stage [phase] of the research consisted in performing measurements in tropical conditions. For the evaluation of the compressor cooling system under tropical conditions the author used the runs of the discharge temperatures in function of discharge pressure for each of the compressing stages and of the distribution of pressure ratios in function of discharge pressure. The obtained results were subjected to the analysis for four crankshaft speeds: 1000; 1200; 1500 and 1800 rpm, which is presented in Fig. 10 in the form of graphs.

Basing on the runs of the discharge temperatures in function of discharge pressure one can observe higher values for tropical conditions in the whole adjustable range. A disadvantageous fact is the excess of the admissible temperature in the second stage at the crankshaft speed of 1800 and 1500 rpm, which exceeds 250 °C at the speed of N = 1800 rpm. Moving towards lower speeds one can observe a drop in the temperature and the even more important fact that the discharge temperature of the first and second stages levels and does not exceed 210 °C. Such a great drop in the discharge temperature for each of the stages results from the drop of the temperature at the suction to the second stage and a growth in the heat exchange rate through the cylinder walls as a result of the lower value of the cooling-water temperature in the inter-cooler.

Subsequently, analyzing the graphs showing the runs of pressure ratio in function of discharge pressure for the tropical conditions one can observe a greater pressure ratio diversification as compared to normal conditions. The reason for this is the reduction of the heat-up volumetric coefficient of the first stage, particularly at the speed N = 1800 rpm. The relative difference between the pressure ratios at this speed is $\delta\varepsilon$ = 15 % and for N = 1000 rpm this difference is twice lower and amounts to $\delta\varepsilon$ = 8 %.

The concluding element of the research are the measurements of the pressure in function of crankshaft angle. On the basis of the obtained results indicator diagrams were drawn for two crankshaft speeds N = 1800 and 1500 rpm and two values of the discharge pressure p_D = 1.5 and 3.0 MPa. The diagrams were drawn in the form of a run of pressure in the cylinder in function of volume. The obtained diagrams are presented in Fig. 11 through 18. On each of the diagrams the thermodynamic processes responsible for the process of compression and expansion of gas inside the cylinder, are depicted. The reference point for the curves describing the processes occurring in the compressor are the isentropic (n = κ) and isothermal (n = 1) processes. The reflecting of the process along the curve of compression and expansion carries an error resulting from the application of approximation consisting in describing the polytropic exponent of the whole process by a single value based on the below presented equation of polytropic process:

$$p_1 V_1^n = p_2 V_2^n = \text{const}$$

The obtained results are first presented for the first stage (Fig. 11 ÷ 14). Fig. 15 through 18 show the results for the second stage with taking into account the same discharge pressures and crankshaft speeds as for the first stage.

Analyzing the compression process in the first stage one can observe very good conformity of the line of actual process with the polytropic process of the exponent n in the range n = 1.4 ÷ 1.44. Such high values of the polytropic exponents result from a low intensity of the heat transfer through the

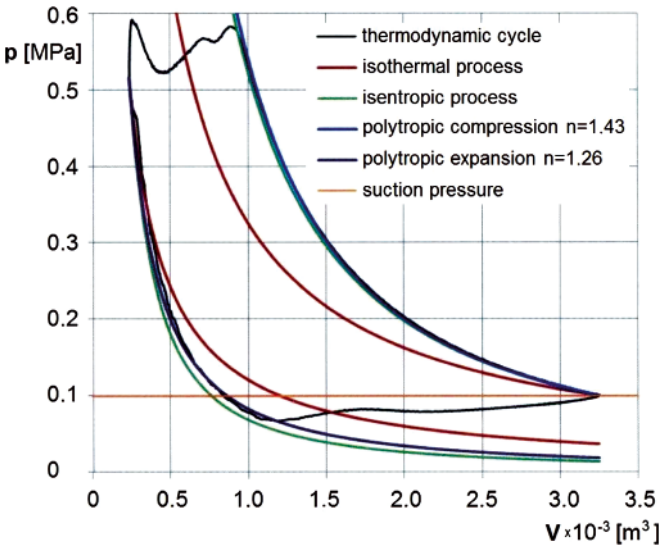

Fig. 11. Indicator diagram for the first stage, N = 1500 rpm, p_D = 1.5 MPa

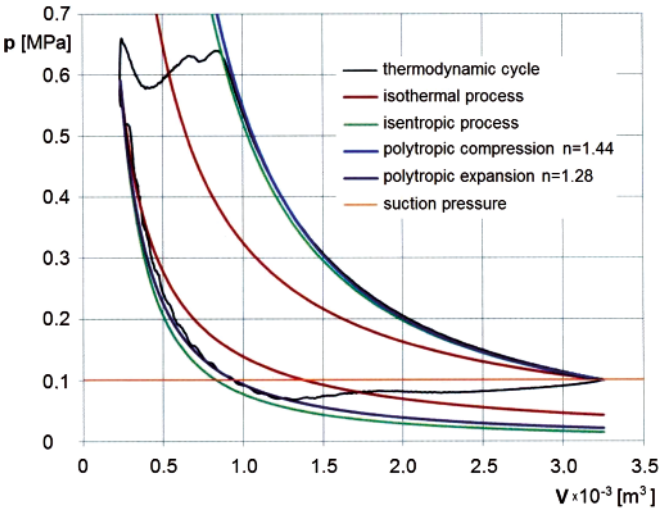

Fig. 12. Indicator diagram for the first stage, N = 1500 rpm, p_D = 3.0 MPa

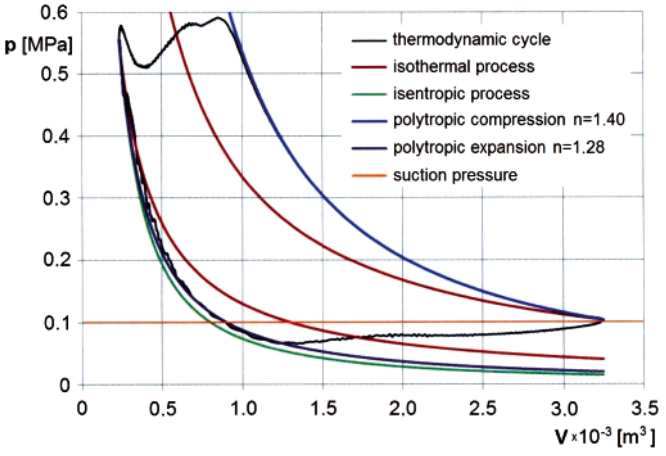

Fig. 13. Indicator diagram for the first stage, N = 1800 rpm, p_D = 1.5 MPa

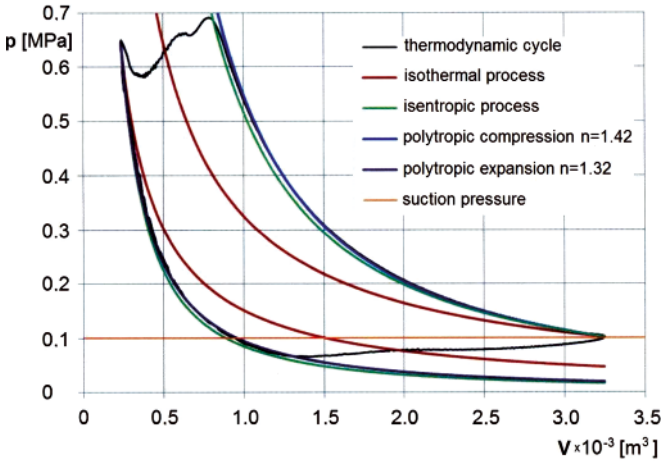

Fig. 14. Indicator diagram for the first stage, N = 1800 rpm, p_D = 3.0 MPa

cylinder walls, which results mainly from the relationship between the cylinder volume and the area of heat exchange (area of the cylinder walls).

The process of expansion takes place at lower values of the polytropic exponents within the range of n = 1.26 ÷ 1.32.

A much more advantageous, in terms of the polytropic exponents, is the second stage. In Fig. 15 ÷ 18 which take into account different parameters of the compressor, are shown the results obtained by the author, namely the range of the polytropic exponent n = 1.24 ÷ 1.31. The obtained value results from a more advantageous relation ratio of the cylinder volume and the area of the cylinder walls. Hence, the

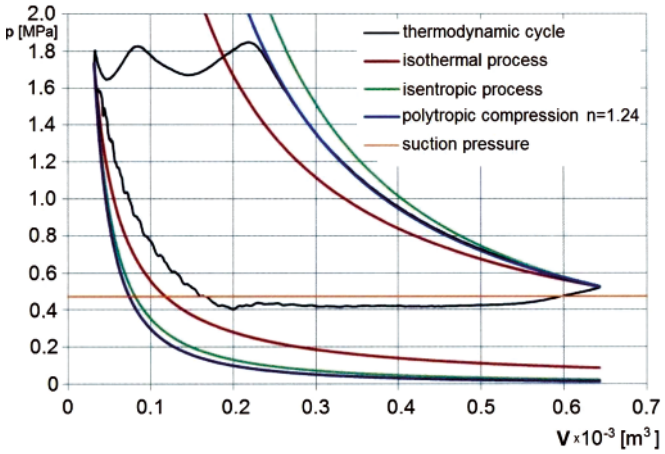

Fig. 15. Indicator diagram for the second stage, N = 1500 rpm, p_D = 1.5 MPa

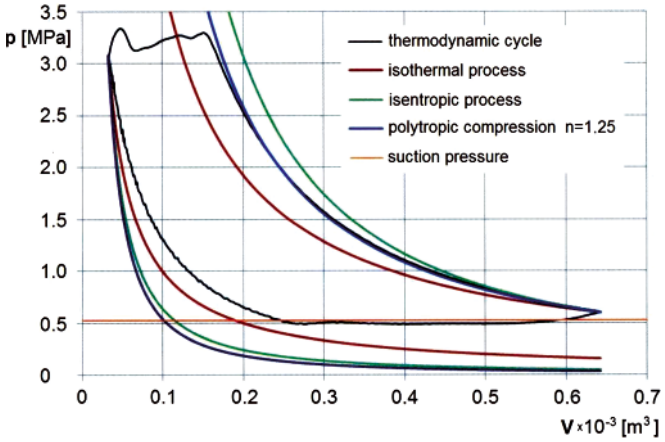

Fig. 16. Indicator diagram for the second stage, N = 1500 rpm, p_D = 3.0 MPa

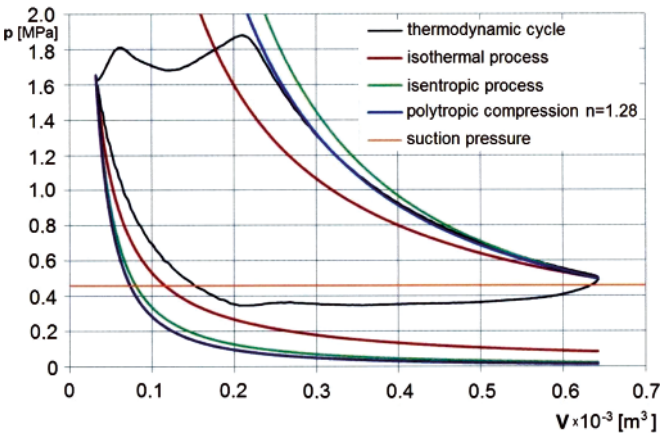

Fig. 17. Indicator diagram for the second stage, N = 1800 rpm, p_D = 1.5 MPa

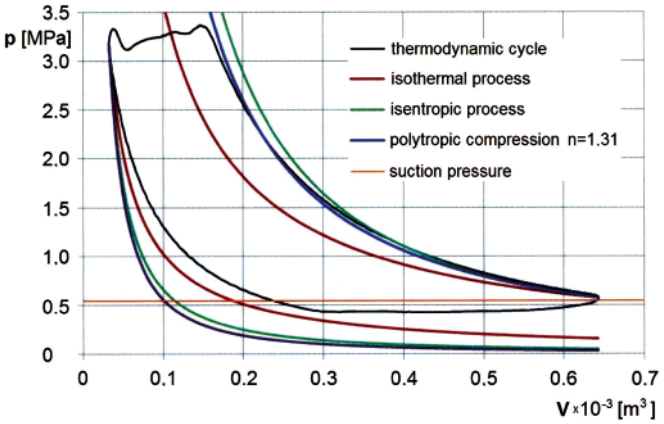

Fig. 18. Indicator diagram for the second stage, N = 1800 rpm, p_D = 3.0 MPa

closer the compression process to isothermal one the greater thermodynamic efficiency of the second stage.

In the case of the second stage an uncertainty as to the determined polytropic exponents appears because the run of the pressure in function of volume confirms that the leakage from the discharge valve occurs. This is revealed in the form of a significant divergence between the lines of the actual process and the isothermal one (the actual process line is on the right of the isothermal one, which does not take place in the thermodynamic sense but only confirms occurrence of the said leakage from the discharge valve).

In order to complement the interpretation of the values of the polytropic exponents, were made calculations consisting in determining the exponents based on the average values of the thermodynamic parameters recorded during the research investigations. The parameters are temperature and pressure values in the suction and discharge chamber of each of the stages. The equation for the determination of the polytropic exponents is presented below:

$$n = \frac{1}{1 - \frac{\ln \frac{T_2}{T_1}}{\ln \frac{p_2}{p_1}}}$$

The obtained values are shown in Fig. 19 in the form of curves representing the polytropic exponent in function of crankshaft speed. The presented results were complemented with results of the run of the polytropic exponents for tropical conditions. For both normal and tropical conditions one can observe a drop in the polytropic exponent towards lower

crankshaft speeds. The observed trend is correct due to the approximation of the thermodynamic processes along with the decrease in the crankshaft speed to quasi-statistical processes. A more intense change of the polytropic exponent took place for the first compressing stage and the value of the polytropic exponent amounted to n = 1.46 for the highest crankshaft speed (N = 1800 rpm) and n = 1.39 for the speed N = 1000 rpm. As for the second stage, a drop in the value of the polytropic exponent occurred at the extreme crankshaft speed and amounted to $\Delta n = 0.023$.

The obtained values of the polytropic exponent for tropical conditions confirm a more advantageous heat transfer through the cylinder walls to the cooling water. There are several factors influencing the values of the exponents. The first and most important is the assumption of the temperature of the cooling water in the tropical conditions by 5°C lower than that at the intake. Another factor to the benefit of the tropical conditions is a higher oil temperature that lowers the surface friction losses in the piston-cylinder assembly.

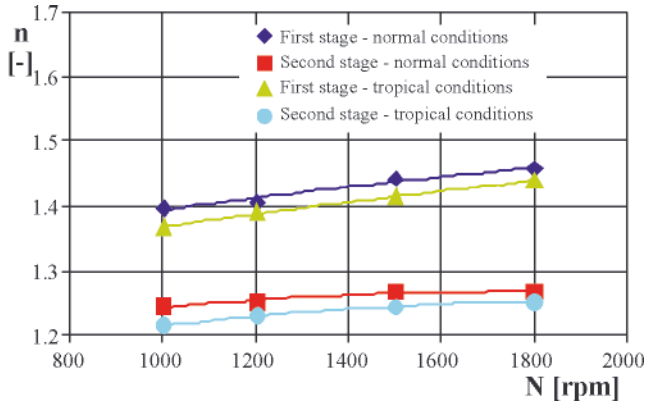

Fig. 19. *The runs of the polytropic exponents in function of compressor crankshaft speed for normal and tropical ambient conditions*

SUMMARY AND CONCLUSIONS

On the basis of the performed research investigations and the analysis of the obtained calculation results of the physical quantities which influence the evaluation of the compressor cooling system, the following conclusions were drawn:

- the compressor coolers reach high efficiency (in particular the inter-cooler whose lowest efficiency value amounts to E = 0.88) at the cooling- water volumetric flow rate $q_{v,w}$ = 30 l/min;
- the system of coolers ensures sufficient cooling for the compressor at a minimum amount of water, with the flow rate of $q_{v,w}$ = 35 l/min for the normal ambient conditions, at the maintaining an even pressure ratio distribution between the stages.
- under the tropical ambient conditions the admissible discharge pressure in the second stage was exceeded at the crankshaft speed values: N = 1500 and 1800 rpm.

The prototype of the VC compressor, apart from the trials carried out in H. Cegielski Poznan S.A., was subjected to trials under supervision of PRS (Polish Register of Shipping) and the trials on the ferry *POMERANIA*. All the trials were successful. The only unfavourable effect which happened during the trials was the overheating of the concentric valve of the second stage. It was caused by an insufficient amount of cooling water supplied to the system. Eventually, upon the conclusion of the trials, Polska Żegluga Bałtycka S.A. (Polish Baltic Shipping Co - Polferries) has stated in its letter directed to H.Cegielski S.A., that the compressor fully meets the Company's expectations.

BIBLIOGRAPHY

1. Hagel R., Zakrzewski J.: *Dynamic metrology* (in Polish). WNT,Warszawa 1984
2. Fodemski T. et al.: *Thermal measurements* (in Polish). WNT, Warszawa 2001
3. Walczak J., Tyrcha J., Grzelczak M.: *Elaboration of construction of series of types of special purpose piston compressors and putting it into production* (in Polish). Report No. KBN 3127/ C.T07-6/2002
4. Wiśniewski S., Wiśniewski T. S.: *Heat exchange* (in Polish). WNT, Warszawa 2000.

CONTACT WITH THE AUTHOR

Mateusz Grzelczak, Ph.D.
Faculty of Machines and Transportation
Poznan University of Technology
Piotrowo 3
60-965 Poznan, POLAND
e-mail: mateusz.grzelczak@put.poznan.pl

POLISH MARITIME RESEARCH 4(80) 2013 Vol 20; pp. 34-38
10.2478/pomr-2013-0038

Calculations of labyrinth seals with and without diagnostic extraction in fluid-flow machines

Paweł Kaszowski, Ph.D.,
Marek Dzida, Assoc. Prof.,
Gdansk University of Technology, Poland
Piotr Krzyślak, Assoc. Prof.,
Poznan University of Technology, Poland

ABSTRACT

Labyrinth seals are essential components of steam turbine unit constructions. Two types of labyrinth seals can be named, the first of which is the seal without diagnostic steam extraction, and the second – with extraction. The distribution of flow parameters along the packing is affected remarkably by the average seal clearance. The presence of diagnostic extraction leads to the equation system which is determinable and can be inversed to calculate the average seal clearance Si. Analysing the obtained results leads to the conclusion that the information about this parameter provides opportunities to monitor the current state of the packing in real time. The applied calculation procedure bases on the de Saint - Venant equation. The article also includes a brief description of both types of seals.

Key words: labyrinth seals; Fanno curve; diagnostic extraction

INTRODUCTION

Steam turbines constitute fluid flow machines used for propelling ships and offshore oil platforms as well as for driving electric generators in power industry. Labyrinth seals are turbine elements responsible for minimization of heat steam leakage losses.

The labyrinth seals are classified as those with and without steam extraction. If a seal without extraction is selected then it is not possible to fully determine parameters occurring along the packing. However a seal with extraction gives such possibility. To this end a suitable calculation model is necessary.

DESCRIPTION OF PACKING

Among labyrinth seals two types are distinguished: the first is not fitted with a diagnostic extraction and the other is fitted with a diagnostic extraction.

Fig. 1 presents the schematic diagram of labyrinth seal without diagnostic extraction as well as distribution of pressure drop in particular seal chambers. Flux of mass flowing through the seal is determined by Fanno line presented in Fig. 2, and described by the function (1):

$$\dot{m} = f(p_0, p_k, h_0, S_n, \mu) \tag{1}$$

where:
$\dot{m}$ – mass flux flowing through seal
p_o – steam pressure before seal

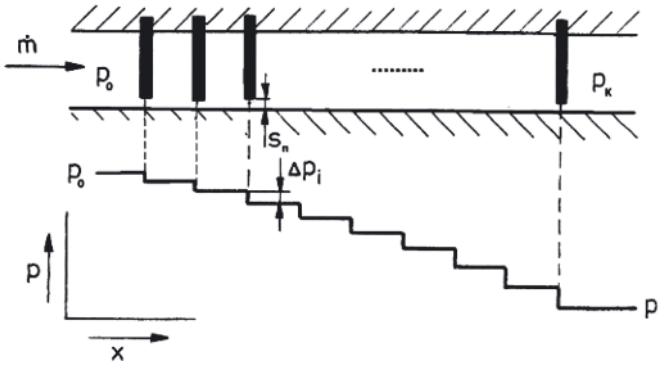

Fig. 1. *Schematic diagram of labyrinth seal without diagnostic extraction*

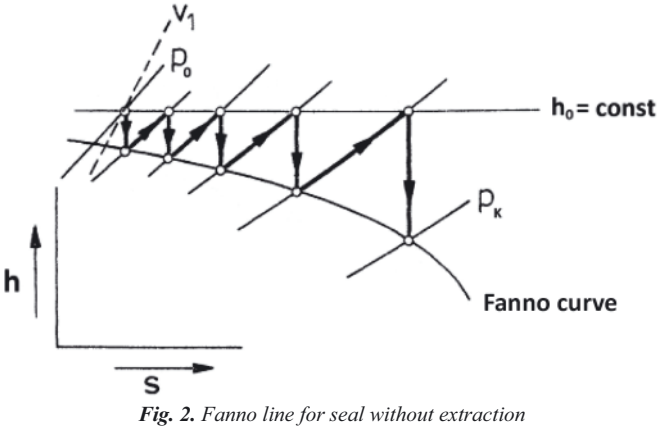

Fig. 2. *Fanno line for seal without extraction*

p_k – steam pressure behind seal
h_o – initial medium enthalpy before seal
s_n – mean clearance of seal
μ – flow rate for seal

The above given function which describes mass flux flowing through seal, is determined by mean clearance of seal. Values of mass flux and mean clearance are unknowns closely mutually connected. Despite the known values of pressure and temperature present before and behind the seal it is not possible to unambigously assess mass flux in the case if the mean value of clearance is not known. It means that to determine medium flow through such seal to know complete input data is necessary.

Lack of any initial parameter makes determining the value of interest not possible. If in the equation of mass flux through the seal one unknown appears then it is not possible to control state of wear of the seal.

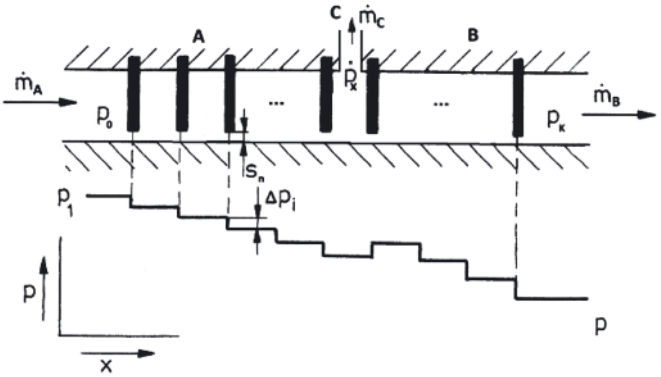

Fig. 3. Schematic diagram of labyrinth seal with diagnostic extraction

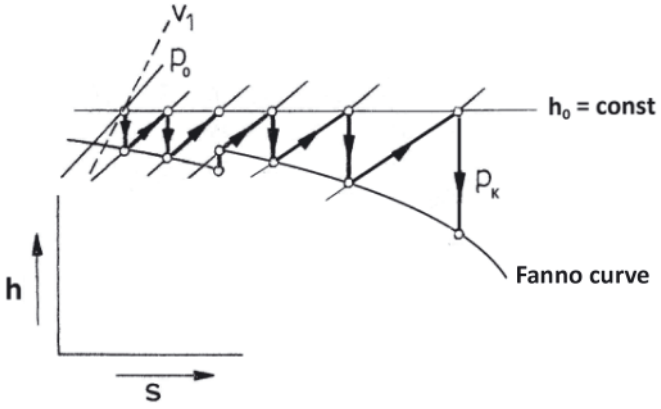

Fig. 4. Fanno line for seal with extraction

Fig. 3 presents the labyrinth seal with diagnostic extraction. An example run of Fanno curve for such packing is shown in Fig. 4.

The diagnostic channels are aimed at the disturbing of chocking process within the seal, realized by providing them an appropriate geometry, for instance by application of a nozzle. Location of steam extraction and pressure measurement channels is to be so optimized as to ensure, on the basis of thermodynamic and fluid mechanic relationships, maximum possible accuracy and sensitivity of diagnostic apparature. Role of extraction channels is more thoroughly described in the publication [3].

A seal can be divided into segments. The segment A is a seal fragment between the inlet to packing and diagnostic extraction channel. The next segment, marked B, is situated between the diagnostic channel and the outlet from the seal. And, the segment C comprises the mass extraction channel. To the labyrinth packing with diagnostic extraction the following set of equations is applicable:

$$\dot{m}_C = \dot{m}_A - \dot{m}_B$$
$$\dot{m}_A = f(p_0, p_x, h_0, S_n, \mu) \quad (2)$$
$$\dot{m}_B = f(p_x, p_k, h_0, S_n, \mu)$$

where:
$\dot{m}_A$ – mass flux flowing through the seal segment A
$\dot{m}_B$ – mass flux flowing through the seal segment B
$\dot{m}_C$ – mass flux flowing through the diagnostic extraction channel
p_o – steam pressure before seal
p_k – steam pressure behind seal
p_x – steam pressure occurring in the space from which $\dot{m}_C$ mass flux is discharged
h_o – initial medium enthalpy before seal
s_n – mean clearance of seal
μ – flow rate for seal

If a value of $\dot{m}_C$ steam mass flux through extraction channel is known then the above given set of equations is solvable and it makes it possible to determine value of mean seal clearance and values of leakges through the segments A and B. Owing to the knowlege of parameters occurring in a seal its wear state can be determined and consequently its overhaul schedule planned. In the case of a seal without diagnostic channel such task is not feasible.

CALCULATIONS OF STEAM THERMODYNAMIC PARAMETERS ALONG THE LABYRINTH SEAL WITHOUT DIAGNOSTIC EXTRACTION

The gas thermodynamic parameters were determined in particular points of the seal in accordance with Fig. 1.

The pressure drop in successive gaps of the seal, assumed linear, is calculated by means of the following formula:

$$\Delta p = \frac{p_0 - p_k}{z} \quad (3)$$

where:
z – number of seal stages

The seal gap cross-section area A is determined by the mean seal clearance S_n and seal diameter D:

$$A = \pi D S_n \quad (4)$$

Value of the specific steam volume and the steam enthropy s_o was read from steam tables. This way all the parameters necessary for determining location of the point 0 at the h – s diagram (see Fig. 5), were found.

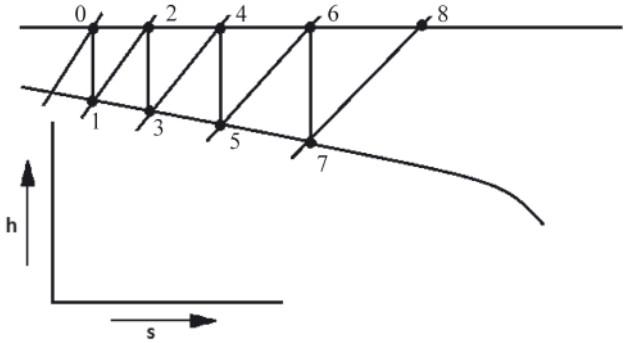

Fig. 5. Way of determining Fanno line for a seal

Change of steam parameters during isenthropic process of expansion between the points (0 - 1) was determined by using the flow equation as follows:

$$\frac{c}{v} = \frac{\dot{m}_n}{A} = K = idem \tag{5}$$

where:

υ – specific volume of steam flowing through a seal segment

Gas velocity at outlet from the seal segment is determined by the equation:

$$c = v\frac{\dot{m}_n}{A} \tag{6}$$

Drop of enthalpy in the seal segment by the equation:

$$\Delta h = \frac{c^2}{2} \tag{7}$$

or, if the seal parameters are taken into account, by the equation:

$$\Delta h = v^2\frac{\dot{m}_n^2}{2A^2} \tag{8}$$

By taking into account the enthalpy drop in the first seal segment the location of the point 1 at the h – s diagrams, i.e. the outlet from the first segment, is obtained.

The process between the points 1 – 2 was assumed the isobaric braking of the flow from the contraction ($p_1 = p_2$). This way kinetic energy conversion into heat by lowering flow velocity due to friction with simultaneous lack of environmental heat exchange, was asssumed. During the process the steam enthalpy, at outlet from the seal, increases up to the value equal to that before the medium inlet to the seal.

$$h_2 = h_1 + \frac{c_2^2}{2} = h_0 \tag{9}$$

Before each successive contraction the medium is assumed to be of the constant enthalpy value equal to initial one. Steam temperature value is read from steam tables. Location of all the points along the seal was determined by making use of the assumption that the mass braking occurs in the isobaric process, and of the prior calculated pressure distribution in the seal, as well as the presented way of calculating.

Next, values of mass flow rate in every gap of the seal were determined by means of de'Saint – Venant equation:

$$\dot{m}_i = A\sqrt{2g\frac{\kappa}{\kappa-1}\left[\left(\frac{p_{i+1}}{p_i}\right)^{\frac{2}{\kappa}} - \left(\frac{p_{i+1}}{p_i}\right)^{\frac{\kappa-1}{\kappa}}\right]\frac{p_i}{v_i}} \tag{10}$$

where:

i – number of seal segment

The steam flow differences in particular seal stages were this way obtained. As results from the calulations the pressure distribution in successive seal segments is not unambigous. To the seal calculations some pressure corrections should be introduced.

PRESSURE CORRECTION

Mass flux flowing through every contraction is described by Eq.(10) from which it results that flow through every gap is directly dependent on the pressure before the obstruction, p_i, and that behind it, p_{i+1}. For the assumed linear pressure drop the mass flux flowing through every contraction is not constant. For the searched-for pressure distribution the mass flux flowing through every contraction should be the same,which results from the mass conservation law. In order to obtain it a pressure correction should be made for every chamber.

By making use of the de Saint – Venant equation for z stages of the packing the set of (z – 1) equations describing the leakage from the whole seal, is obtained.

The relation (10) is developed into Taylor series, but only up to 1st order derivatives, as the so obtained accuracy is sufficient; this way the linear equation of the following form is found:

$$d\dot{m} = \frac{\partial\dot{m}}{\partial p_i}dp_i + \frac{\partial\dot{m}}{\partial p_{i+1}}dp_{i+1} \tag{11}$$

This operation makes it possible to determine the pressure corrections $\Delta p_1, \Delta p_2, \ldots, \Delta p_z$. The partial derivatives appearing in Eq. (11) are as follows:

$$\frac{\partial\dot{m}}{\partial p_i} = \frac{A}{2}\sqrt{2g\frac{\kappa}{\kappa-1}\frac{1}{v_i p_i}}\frac{1}{\sqrt{\left(\frac{p_{i+1}}{p_i}\right)^{\frac{2}{\kappa}} - \left(\frac{p_{i+1}}{p_i}\right)^{\frac{\kappa+1}{\kappa}}}}\times$$

$$\times\left[\left(1-\frac{2}{\kappa}\right)\left(\frac{p_{i+1}}{p_i}\right)^{\frac{2}{\kappa}} + \left(\frac{\kappa+1}{\kappa}-1\right)\left(\frac{p_{i+1}}{p_i}\right)^{\frac{\kappa+1}{\kappa}}\right] \tag{12}$$

$$\frac{\partial\dot{m}}{\partial p_{i+1}} = \frac{A}{2}\sqrt{2g\frac{\kappa}{\kappa-1}\frac{p_i}{v_i}}\frac{1}{\sqrt{\left(\frac{p_{i+1}}{p_i}\right)^{\frac{2}{\kappa}} - \left(\frac{p_{i+1}}{p_i}\right)^{\frac{\kappa+1}{\kappa}}}}\times$$

$$\times\left(\frac{1}{p_i}\right)\left[\frac{2}{\kappa}\left(\frac{p_{i+1}}{p_i}\right)^{\frac{2}{\kappa}} + \frac{\kappa+1}{\kappa}\left(\frac{p_{i+1}}{p_i}\right)^{\frac{\kappa+1}{\kappa}}\right]$$

The general form of Eq. (11), on the assumption that the increments Δp and $\Delta\dot{m}$ are sufficenty small, describes a change of mass flux flowing through *i*-th contraction depending on pressure changes before and behind the contraction:

$$\Delta\dot{m}_i = \frac{\partial\dot{m}}{\partial p_i}\Delta p_i + \frac{\partial\dot{m}}{\partial p_{i+1}}\Delta p_{i+1} \tag{13}$$

Eq. (13) is formed separately for every gap in the seal:

$$\Delta\dot{m}_1 = \frac{\partial\dot{m}_1}{\partial p_0}\Delta p_0 + \frac{\partial\dot{m}_1}{\partial p_1}\Delta p_1$$

$$\ldots \tag{14}$$

$$\Delta\dot{m}_z = \frac{\partial\dot{m}_n}{\partial p_{i-1}}\Delta p_{i-1} + \frac{\partial\dot{m}_n}{\partial p_i}\Delta p_i$$

and also:

$$\Delta\dot{m}_1 = \dot{m}_1 - \dot{m}_2$$

$$\ldots \tag{15}$$

$$\Delta\dot{m}_i = \dot{m}_i - \dot{m}_{i+1}$$

In order to obtain a correct pressure distribution in the packing the same mass flux flowing through every contraction

should be achieved. After completing the calculations the difference $\Delta\dot{m}_i = \dot{m}_i - \dot{m}_{i+1}$ is to be close to zero. This way the set of (z – 1) linear equations is obtained:

$$\dot{m}_1 - \dot{m}_2 = \frac{\partial \dot{m}_1}{\partial p_0}\Delta p_0 + \frac{\partial \dot{m}_1}{\partial p_1}\Delta p_1$$
$$\cdots \qquad (16)$$
$$\dot{m}_i - \dot{m}_{i+1} = \frac{\partial \dot{m}_i}{\partial p_{i-1}}\Delta p_{i-1} + \frac{\partial \dot{m}_i}{\partial p_i}\Delta p_i$$

The above given set of equations is solved by transforming the task to the matrix problem as follows:

$$\boldsymbol{A} \cdot \boldsymbol{X} = \boldsymbol{B} \qquad (17)$$

where the square matrix **A** is built of the components of Eq. (17), except of the unknowns Δp_1, arranged as follows:

$$\boldsymbol{A} = \begin{bmatrix} \frac{\partial \dot{m}_1}{\partial p_1} & \cdots & 0 \\ \vdots & \ddots & \vdots \\ 0 & \cdots & \frac{\partial \dot{m}_{z-1}}{\partial p_{z-1}} \end{bmatrix} \qquad (18)$$

The vector **X** is built of the searched-for values of the unknown pressure drops Δp_1 , Δp_2 , ... , Δp_z:

$$\boldsymbol{X} = \begin{bmatrix} \Delta p_1 \\ \vdots \\ \Delta p_{z-1} \end{bmatrix} \qquad (19)$$

And, the matrix **B** is composed of the mass flux differences:

$$\boldsymbol{B} = \begin{bmatrix} -(\dot{m}_1 - \dot{m}_2) \\ \vdots \\ -(\dot{m}_{z-1} - \dot{m}_z) \end{bmatrix} \qquad (20)$$

Next, in order to determine the unknowns Δp_1 , Δp_2 , ... , Δp_{z-1} from the set of matrix equations the inverse matrix is applied:

$$\boldsymbol{X} = \boldsymbol{A}^{-1} \cdot \boldsymbol{B} \qquad (21)$$

The so calculated values constitute corrections for the pressure drop initially assumed linear, in successive labyrinth packing chambers. The calculations are performed by using iterations up to reaching an assumed accuracy of calculations.

In the above presented way were performed calculations for the interbody seal of the HP turbine of 200MW power and the following parameters:

Pressure before the seal	p_o	9.861	MPa
Steam temperature before the seal	t_o	522.5	°C
Enthalpy before the seal	h_o	3433	kJ/kg
Pressure behind the seal	p_2	4.204	MPa
Steam flow rate through the seal	$\dot{m}n$	2.228	kg/s
Shaft diameter	D	475	mm
Nominal clearance of the seal	S_n	1.0	mm
Number of seal stages	z	80	

Fig. 6 and 7 present diagrams of pressure distribution and mass flux flowing through the seal. The results before introduction of the correction are marked red, and those after the correction - blue. It can be observed that the pressure distribution, as results from Eq. (10), is directly connected with the pressure occurring in the chambers before and behind seal stage. The corrections were performed iteratively up to reaching the accuracy of $\Delta m/m_n = 10^{-3}$.

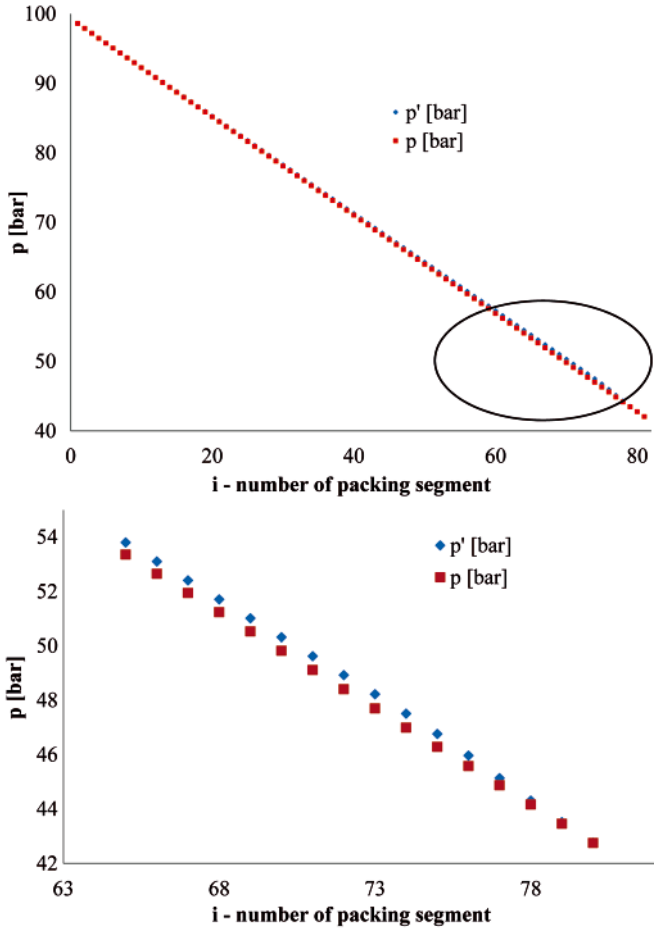

*Fig. 6. Comparison of pressure distributions along the seal before and after introduction of corrections; **p** – pressure distribution before correction, **p'** – pressure distribution after introduction of correction*

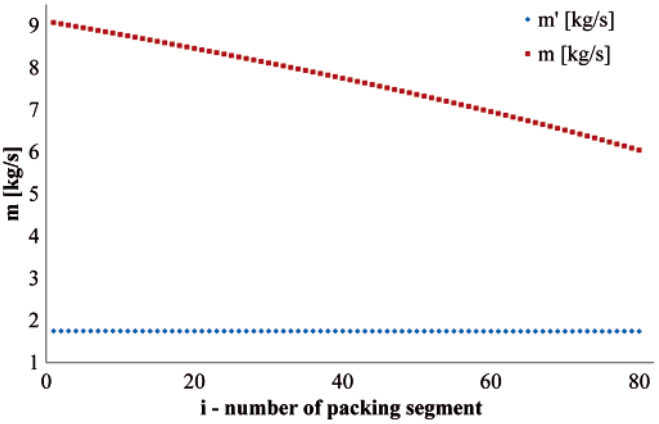

*Fig. 7. Comparison of mass fluxes flowing through the seal gaps; **m** – before correction, **m'** – after introduction of correction*

Calculations of steam thermodynamic parameters along the packing with diagnostic extraction were performed. The additional steam extraction of 0.4 kg/s flow rate will cause disturbances of medium flow through seals by extracting a part of steam from space between contractions, located between 70th and 71st seal stage. It is assumed that the temperature and pressure occurring in the space from which the mass flux is extracted, is not changeable, i.e. the isobaric decreasing of gas velocity occurs. The smaller steam flux flowing through

successive gaps will cause a smaller pressure drop in the gap at isenthropic expansion. It will result in a noticeable increase of pressure in the place where the diagnostic extraction is located (Fig. 8).

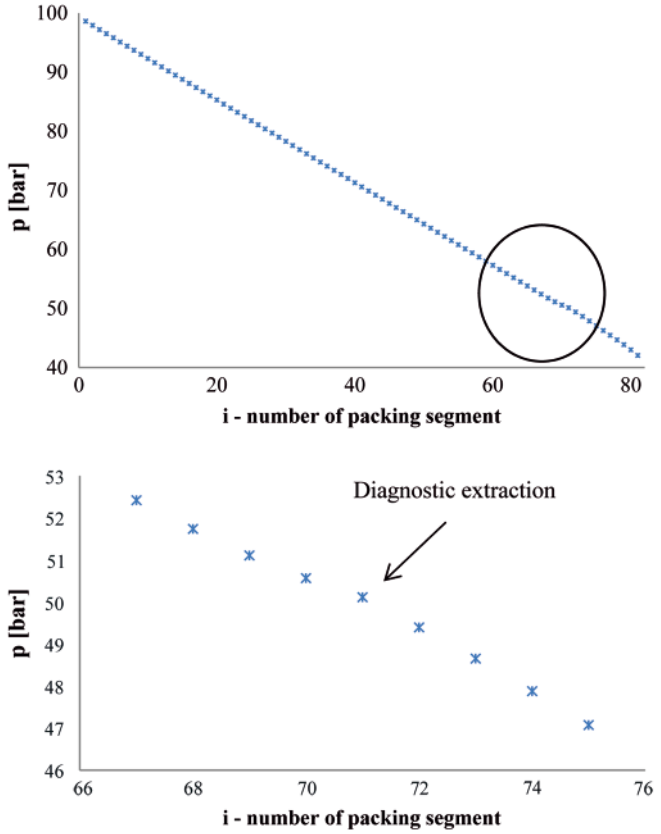

Fig. 8. Pressure distribution in the seal with diagnostic extraction

At the remaining segment of the packing, i.e. that measured from the extraction up to the end of the seal, flow drag of the decreased mass flux will be lower because of lower flow velocities. The mass flux flowing through the seal without diagnostic extraction as well as that for the seal with extraction is presented in Fig. 9. In the case of the seal with diagnostic extraction, behind 70th seal stage can be observed a drop in value of the mass flux flowing through the seal by the value extracted through the diagnostic channel. The spread of results for this seal fragment is associated with the assumed calculation accuracy and computing power of the used computer. It does not result from accuracy of the calculation method.

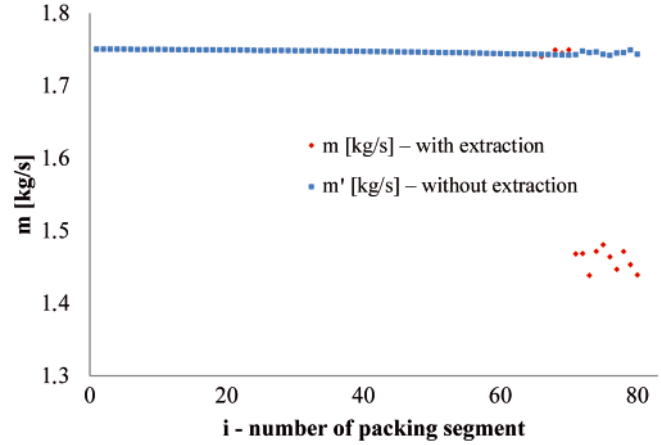

Fig. 9. Mass flux flowing through the seal with and without diagnostic extraction

The run of Fanno line was presented for both the cases in Fig. 10. The Fanno line for the seal without diagnostic extraction is marked black, in red is depicted the Fanno line for the packing with diagnostic extraction, and in blue colour is shown the inital enthalpy value.

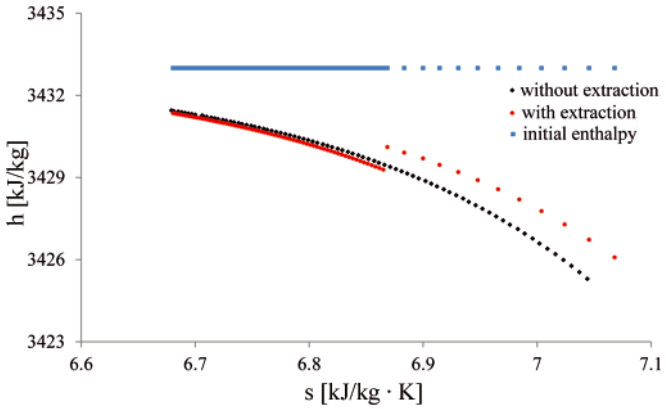

Fig. 10. Fanno line for labyrinth seal without and with diagnostic extraction

SUMMARY

In the case of the labyrinth seal with extraction the elaborated set of equations is determinate. It makes it possible to exactly determine values of parameters occurring along the seal, in contrast to that without extraction. This is the unambigous equation system which can be inverted in order to determine the mean seal clearance: $Si = f(p_o, p_x, h_o, \dot{m}, \mu)$.

Knowledge of this parameter makes real-time diagnosing state of labyrinth seal, possible. It allows for planning repair and maintenance time without necessity of stopping the turbines, as well as for determining state of seal wear.

BIBLIOGRAPHY

1. Chmielniak T.: *Steam turbines: theoretical background* (in Polish). Wydawnictwo Politechniki Śląskiej (Publishing House of Silesian University of Technology),Gliwice, 1998
2. Kaszowski P.: *Analysis of operation of labyrinth seals with extraction* (in Polish). M.Sc. Thesis, Gdańsk University of Technology, Department of Energy Engineering and Industrial Apparatures, Gdańsk, 2011
3. Krzyślak P., Winowiecki M.: *A method of diagnosing labyrinth seals in fluid-flow machines*. Polish Maritime Research 3(57) Vol. 15, 2008, pp. 38-41
4. Perycz S.: *Steam and gas turbines* (in Polish). Wydawnictwo Politechniki Gdańskiej (Publishing House of Gdańsk University of Technology), Gdańsk 1988
5. Trütnovsky K.: *Berührungsfreie Dichtungen, Grundlagen und Anwendungen der Strömung durch Spalte und Labirynthe* (in German). VDI – VERLAG bh; (Verlag des Vereins Deutscher Ingeniuere), Düsseldorf, 1964

CONTACT WITH THE AUTHORS

Paweł Kaszowski, Ph.D.
Marek Dzida, Assoc. Prof.
Faculty of Ocean Engineering
and Ship Technology
Gdansk University of Technology
Narutowicza 11/12
80-233 Gdansk, POLAND
e-mail: dzida@pg.gda.pl

Piotr Krzyślak, Assoc. Prof.
Faculty of Machines and Transportation
Poznan University of Technology
Piotrowo 3
60-965 Poznan, POLAND

POLISH MARITIME RESEARCH 4(80) 2013 Vol 20; pp. 39-44
10.2478/pomr-2013-0039

Stress-corrosion resistance of the EN AW-AlZn5Mg1,5CuZr alloy in different heat treatment states

Lesław Kyzioł, Assoc. Prof.,
Gdynia Maritime University

ABSTRACT

The effect of heat treatment of the plastically worked 7000 series Al-Zn-Mg aluminium alloy system on its stress-corrosion resistance is examined. For the same chemical constitution, the effect of heat treatment on mechanical and corrosion properties of Al-Zn-Mg alloys systems is remarkable. It was proved that a parameter having significant effect on corrosion properties of the alloy is the rate of alloy cooling after heat treatment. This conclusion is confirmed by observation of structural forms which fully reflect mechanical and corrosion properties of the alloy.

Key words: heat treatment; stress corrosion; alloy structures; corrosion resistance

INTRODUCTION

Due to their favourable mechanical properties, plastically worked 7000 series aluminium alloys have recently become an object of intensive examination, especially abroad. In Poland, the 7000 series alloy was used, among other applications, for building the superstructure of the 620 project vessel. Generally, the vessel's hull, (including the superstructure), is subject to heavy dynamic loads in unfavourable sea environment, which lead to high material effort. One of unfavourable properties of the plastically worked 7000-series aluminium alloys is their susceptibility to corrosion, especially layer corrosion in sea water environment. A rigorous parameter which determines usability of a given material for constructions which are subject to loading in sea environment is its stress-corrosion resistance. The article aims at determining the stress-corrosion resistance of the EN AW-AlZn5Mg1,5CuZr alloy in the aspect of micro-structural changes resulting from the applied heat treatment.

THE ESSENCE OF STRESS CORROSION OF 7000 SERIES ALUMINIUM ALLOYS

Material stress corrosion is the synergic action of the corrosion environment and mechanical stress. It manifests itself by the appearance of cracks in the metal or alloy caused by the corrosion environment and static tensile stress. The cracks resulting from the stress corrosion are situated perpendicular to the direction of tensile stress action and can have the inter-crystalline, intracrystalline, or mixed form. Observations of stress cracks have revealed that a period of incubation frequently takes place before the appearance of a detectable crack. The intensity of microcracks forming in this period can be evaluated by examining changes of mechanical properties caused by structural changes of the alloy over different time-intervals of the stress-corrosion test.

The plastically worked Al-Zn-Mg alloy systems which are to be used in marine constructions should reveal sufficiently high mechanical properties along with high resistance to cracking in the conditions of simultaneous action of mechanical stresses and corrosion environment.

Publications [1-6, 13] present the effect of selected media on the resistance of Al-Zn-Mg alloys to stress corrosion.

The present article mainly focuses on determining the effect of heat treatment on the resistance of the examined aluminium alloy to stress corrosion. The effect of heat treatment parameters on mechanical properties of this alloy was discussed in this article.

The results of the investigations have shown that in the Al-Zn-Mg alloy systems with total contents of Zn + Mg > 5 % better stress-corrosion resistance is obtained, along with good mechanical properties, when a special heat treatment is applied which includes cooling with a "stop". This procedure preserves both good mechanical properties and high stress-corrosion resistance [7].

The type of aging after heat treatment remarkably affects the resistance of Al-Zn-Mg alloy systems to stress corrosion. Low aging temperatures (< 100 °C), in combination with longer times of aging, worsen the stress-corrosion resistance [2, 3, 6], while two-stage aging in temperatures close to the critical temperature of GP zone solubility, especially at, $t_s > t_k$ increases the resistance to stress-corrosion cracking of the majority of alloys [2].

Heat treatment introduces changes in the structure of the metal. The stress-corrosion cracking is affected by the following factors:
- the PFZ width along the wide-angle grain boundaries;
- the structure of dislocations and vacancies caused by cooling after heat treatment;
- the structure of precipitates inside the matrix;
- the size and concentration of precipitates on grain boundaries [3].

Another parameter which affects stress-corrosion cracking is the presence of time-dependent tensile stresses. In aluminium alloys the increased tensile stresses almost always lead to the reduction of material durability [8, 9]. The relation between the crack appearance time and the stress σ which is proposed for the majority of materials has the form [10]

$$\sigma = -k \cdot \log t + c \tag{1}$$

where:
k, c – experimental constants.

In publication [10] the following relation is given:

$$\sigma = t^{-n} \tag{2}$$

where:
n – experimental constant.

Taking into account the effect of the examination temperature (T) leads to the relation [11]:

$$\frac{1}{t} = K_1 \cdot e^{-\frac{Q_a}{R_s T}} \cdot e^{c\sigma} \tag{3}$$

where:
K_1, c – experimental constants,
R_s – gas constant,
Q_a – energy of activation (9 ÷ 20 kcal/mol).

Publication [12] proposes the following empirical relation

$$\sigma = k \cdot t^{-a} \tag{4}$$

where:
k, a – empirical constants.

MATERIAL USED FOR TESTS. CHARACTERISTICS OF HEAT TREATMENT PARAMETERS APPLIED TO EN AW-ALZN5MG1,5CUZR ALLOY

The stress-corrosion resistance of Al-Zn-Mg alloy systems was examined using 10 mm thick sheets of EN AW-AlZn5Mg1,5CuZr alloy. At delivery conditions, the above alloy was artificially precipitation hardened (supersaturated at the temperature of 480 °C/30 min., cooled in water of temperature of 20 °C, naturally aged during 48 hours, and finally artificially aged in two stages: 90 °C/8 h+135 °C/28 h). In order to determine the effect of alloy heat treatment on stress corrosion the alloy was exposed to various heat treatments. The chemical constitution of the alloy and parameters of the applied heat treatments are given in Table 1.

The materials after heat treatment were used for cutting samples from aluminium sheets in the direction perpendicular to the direction of rolling. Mechanical properties were examined on the universal testing machine MTS 810.12, for sample loads ranging up to 100 kN and the traversing speed equal to 2 mm/min, according to the PN-ISO 377-1:1994 standard.

The stress corrosion at constant load (F = const) was tested in a rig consisting of 12 independent sections which provided opportunities for simultaneous tests of 12 samples. The corrosion solution was the 3 % solution of NaCl, refreshed after each 7 days. The testing time was 1500 h. The temperature

Tab. 1. *Chemical constitution and heat treatment parameters used in tests of samples cut from 10 mm thick sheets of EN AW-AlZn5Mg1,5CuZr alloy*

State	Heat treatment parameters	Chemical constitution [%]										No of batch and certificate
		Zn	Mg	Cr	Zr	Mn	Mg	Fe	Cu	Ti	Remainders	
T61	supersaturating at temp. 450 °C/1,5 h, cooling in water at temp. 20 °C, natural aging in 6 days, artificial aging 95 °C/15 h + 150 °C/10 h (artificial precipitation hardening)	5.3	2.13	0.17	0.19	0.04	0.27	0.15	0.046	0.006	remainders	6.229.001/OM
T62	supersaturating at temp. 450 °C/1,5 h, cooling in water at temp. 80 °C, natural aging in 6 days, artificial aging 95 °C/15 h + 150 °C/10 h (artificial precipitation hardening)											
T63	supersaturating at temp. 450 °C/1,5 h, cooling in air, natural aging in 6 days artificial aging 95 °C/15 h + 150 °C/10 h (artificial precipitation hardening)											
T4	supersaturating at temp. 450 °C/1,5 h, cooling in air, natural aging in 3 months (precipitation hardening)											

of the corrosion environment ranged within 20 ÷ 22 °C. The initial stress was set with respect to the yield point at the level of $\sigma_0 = (0.4 \div 1.0)R_{0.2}$.

RESULTS OF TESTS AND THEIR ANALYSIS

Mechanical properties of the EN AW-AlZn5Mg1,5CuZr alloy were tested in different heat treatment states (Table 1). Table 2 collects the average values of mechanical properties of the examined alloy for different heat treatments.

Tab. 2. *Collection of average values of mechanical properties of the EN AW-AlZn5Mg1,5CuZr alloy for different heat treatments*

State	Mechanical properties			
	R_m [MPa]	$R_{0.2}$ [MPa]	A_5 [%]	Z [%]
T61	479	442	9	22
T62	442	397	10	34
T63	362	295	12	33
T4	399	247	14	31

The heat treatment parameters (T61, T62, T63), excluding the variant labelled as T4 (natural aging), significantly differ between each other only by the rate of cooling after heat treatment.

The mechanical properties of the examined alloy recorded for different heat treatment states are given in Table 2. The tests have proved that after the heat treatment denoted as T63 (cooled in air after heat treatment) the examined alloy had relatively poor mechanical properties, but remarkable plastic elongation (contraction).

In state T62 (cooled in hot water after heat treatment) the alloy had much better mechanical properties and good plastic properties, but the same alloy in state T61 (cooled in cold water after heat treatment) revealed the best mechanical properties and the worst plastic properties. In state T4 (natural aging), the alloy revealed relatively high tensile strength, but the lowest yield point.

In order to recognise possible reasons for such large differences of mechanical properties revealed by the examined alloy, the chemical constitution of which remained unchanged in all tests, the structural analysis of samples representing different heat treatments was conducted.

Metallographic specimens for microanalysis were polished and then etched using the Wasserman's reagent. Photos were taken and observations were performed in the optical microscope Neophot – 2. Moreover, the microstructures of the examined alloy were observed on thin foils in the transmission electron microscope Tesla-300. The foils were prepared on abrasive papers using a standard method, and then were electro-polished in the solution having the following composition: 20 % perchloric acid, 80 % ethyl alcohol. The temperature of the electrolyte was approximately equal to –40 °C.

Analysing microstructures of the EN AW-AlZn5Mg1,5CuZr alloy for different heat treatment states. Figures 1 ÷ 3 show the alloy microstructures for selected heat treatments.

The conducted microanalysis has made it possible to determine the PFZ width of the examined aluminium alloy for different heat treatments. The results are given in Table 3.

Tab. 3. *PFZ width of the EN AW-AlZn5Mg1,5CuZr alloy, in dependence on the applied heat treatment*

Heat treatment state	T63	T62	T61	T4
PFZ width, nm	425.0	125.8	70.5	80.0

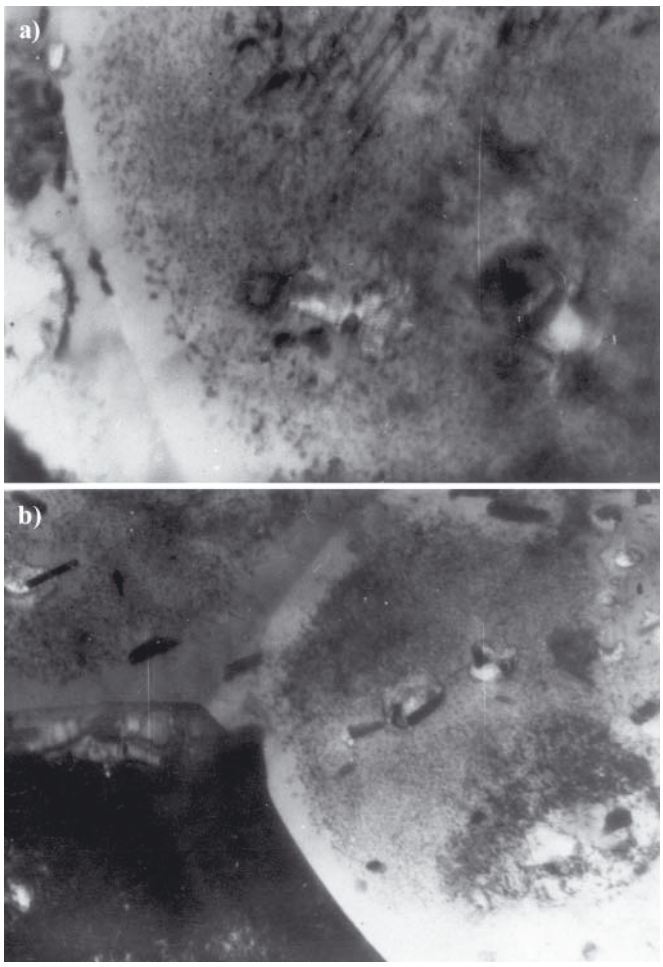

Fig. 1. *Microstructure of EN AW-AlZn5Mg1,5CuZr T63 alloy, thin foil.* ***a)*** *magnified 32.000x,* ***b)*** *magnified 44.000x*

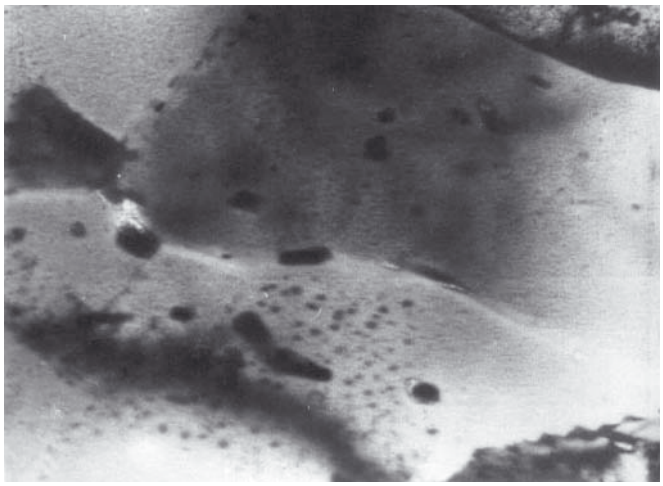

Fig. 2. *Microstructure of EN AW-AlZn5Mg1,5CuZr T62 alloy, thin foil, magnified 32.000x*

The conducted microanalysis has indicated clear correlation of the structure and mechanical properties of the examined Al-Zn-Mg alloy with the type of the performed heat treatment. The static tensile test has shown that in state T61 the alloy has better mechanical properties than in states T62 and T63. Separation of GP zones was observed in the alloy structure obtained as a result of cooling in cold water after heat treatment (T61) (Fig. 6). Their presence could be concluded from the so-called "tweed structure", being the effect of the first decomposition of solid solution. The observed precipitate free zones (PFZ) adjacent to grain boundaries had the width of 50 ÷ 80 nm.

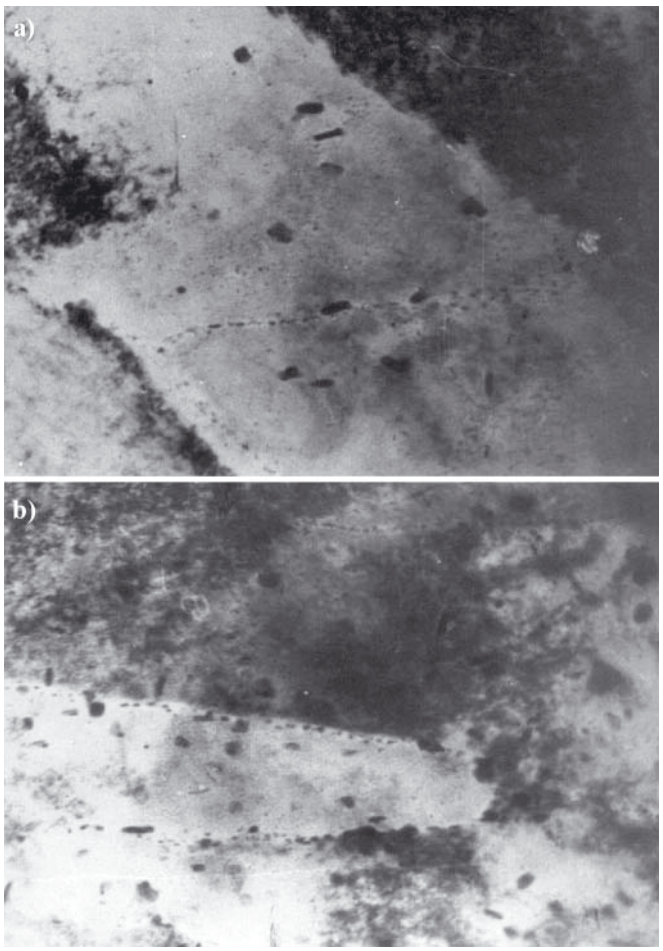

Fig. 3. *Microstructure of EN AW-AlZn5Mg1,5CuZr T61 alloy, thin foil,* ***a)*** *magnified 32.000x,* ***b)*** *magnified 60.000x*

Larger $MgZn_2$ phase precipitates could be observed at grain boundaries. In the material which was air cooled after heat treatment (state T63 – Fig. 4) remarkable decomposition of the solid solution took place. Observed were fine precipitates of the transient phase η′ and the equilibrium phase T which separated directly from the solid solution during slow cooling after heat treatment. PZF zones of 400 ÷ 600 nm in width were observed as well.

In the microstructure of the aluminium alloy in state T62 (cooling in hot water after heat treatment) shown in Fig. 5 fine precipitates of the transient phase η′ were observed inside the grains. The η phase ($MgZn_2$) precipitates which were observed at grain boundaries were arranged in rows. The PFZ width was of an order of 120 ÷ 200 nm.

The microstructure of the aluminium alloy in state T4 (natural aging after heat treatment) was characteristic for the presence of continuous η phase precipitates at grain boundaries. Inside the grains, the observed "tweed structure" testified to the presence of GP zones.

Figure 4 illustrates the effect of the PFZ width on mechanical properties of the examined aluminium alloy. The conducted microstructure analysis and static mechanical tests of the EN AW-AlZn5Mg1,5CuZr alloy have made the basis for determining the relation between the width of the precipitate free zone (PFZ) and mechanical properties. The microanalysis has showed that the PFZ width depends on the method of alloy cooling after heat treatment (more precisely: on the cooling rate). The increasing rate of cooling after heat treatment results in smaller PFZ width, which manifests itself by increased mechanical properties and decreased plasticity.

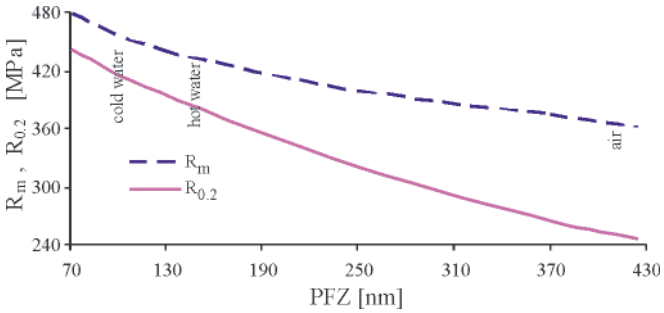

Fig. 4. *PFZ width vs. mechanical properties of EN AW-AlZn5Mg1,5CuZr alloy cooling in cold water (T = 20 °C), cooling in hot water (T = 80 °C), cooling in air*

Stress-corrosion resistance of EN AW-AlZn5Mg1,5CuZr alloy in different heat treatment stages

The stress corrosion of the alloy was examined in different heat treatment states for the initial stress level $\sigma_0/R_{0.2}$ = = 0.60 ÷ 1.0 in time t = 1500 h. After being exposed to corrosion, samples were torn on a universal testing machine MTS 810.12 in order to determine their mechanical properties.

From among 12 samples tested in state T61, 4 samples cracked in time t < 1100 h. The average durability of the material used for preparing samples did not exceed t = 1000 h at stress level σ_0 = 332 MPa, and t = 2000 h at stress level σ_0 = = 100 MPa (Fig. 5).

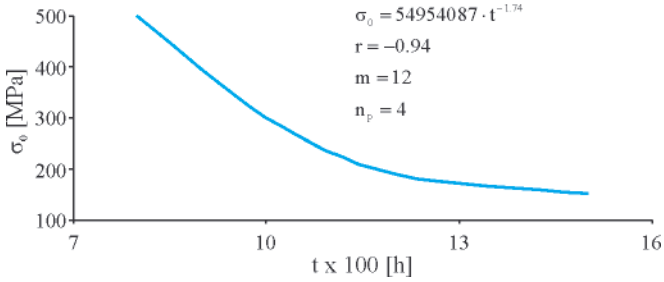

Fig. 5. *Stress-corrosion durability of EN AW-AlZn5Mg1,5CuZr T61 alloy exposed to corrosion in 3 % NaCl solution*

Figure 5 shows the curve of stress-corrosion durability of the aluminium alloy for the state T61. The accompanied changes of mechanical properties of the examined alloy after stress-corrosion exposition are given in Table 4.

Stress-corrosion tests of the alloy in state T63 have shown that none of the tested samples cracked during the testing time t = 1500 h. Symptoms of layer corrosion on samples were not observed either. The heat treatment remarkably affected the stress-corrosion resistance. The stress-corrosion tests have made the basis for determining mechanical properties of the examined samples (Table 4).

Like for state T63, also in state T62 the examined alloy did not reveal symptoms of layer corrosion. None of the tested samples was damaged in time t = 1500 h. For this state, the improvement of alloy resistance to stress corrosion was observed, as compared to state T61. Like in the previous case, the stress-corrosion tests have made the basis for determining mechanical properties of the examined samples (Table 4).

As a result of alloy tests in state T4, 50 % of the tested samples cracked in time t < 1100 h. The symptoms of layer corrosion were clearly observed on the samples. Figure 10 shows the curve of stress-corrosion durability, while Table 4 collects mechanical properties of the examined samples after stress-corrosion exposition.

Tab. 4. *Percent decrease of mechanical properties of the EN AW-AlZn5Mg1,5CuZr alloy after stress-corrosion exposition, in dependence on the applied heat treatment (for stress level $\sigma_0/R_{0.2} = 0.80$)*

Test	State	Mechanical properties			
		R_m [MPa]	$R_{0.2}$ [MPa]	A_5 [%]	Z [%]
before stress corrosion	T61	479	442	9	22
	T62	442	397	19	34
	T63	362	295	12	33
	T4	399	247	14	31
after stress corrosion	T61	460	421	3	10
	T62	426	377	3	9
	T63	303	242	6	15
	T4	150	130	1	8
		Relative change of mechanical properties			
		$\delta R_m = \Delta R_m/R_m$ [%]	$\delta R_{0.2} = \Delta R_{0.2}/R_{0.2}$ [%]	$\delta A_5 = \Delta A_5/A_5$ [%]	$\delta Z = \Delta Z/Z$ [%]
Change of mechanical properties for given heat treatment state	T61	↓4	↓4	↓66	↓55
	T62	↓4	↓5	↓70	↓74
	T63	↓16	↓18	↓50	↓55
	T4	↓62	↓48	↓93	↓74

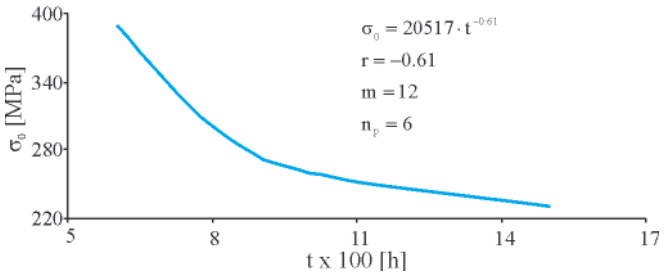

Fig. 6. *Stress-corrosion durability of EN AW-AlZn5Mg1,5CuZr T4 alloy exposed to corrosion in 3 % NaCl solution*

Analysing the obtained results of testing the effect of heat treatment of the EN AW-AlZn5Mg1,5CuZr alloy on its stress-corrosion resistance leads to the conclusion that for the state T62 (cooling in hot water after heat treatment) the alloy's resistance to stress corrosion was improved with respect to the alloy in state T61 (cooling in cold water).

Like in state T62, the reduced cooling rate after heat treatment (air cooling) in state T63 remarkably improved alloy's resistance to corrosion cracking. Both heat treatments T62 and T63 secured good alloy resistance to corrosion cracking. Moreover, each of given methods of artificial aging after heat treatment eliminated alloy's tendency to layer corrosion.

In the aspect of structural analyses, the resistance of the EN AW-AlZn5Mg1,5CuZr alloy to corrosion cracking is explained as the effect of non-uniform concentration of inter-metallic phases (especially η phase) and different PFZ widths.

In states T61 and T4, the η phase precipitates at grain boundaries have continuous structure, while in states representing higher stress-corrosion resistance (T62, T63) they are not continuous any longer. Moreover, corrosion resistance of the examined aluminium alloy subjected to different cooling procedures after heat treatment increased with the increased width of the PFZ zone.

CONCLUSIONS

Mechanical properties and stress-corrosion resistance of the examined aluminium alloy EN AW-AlZn5Mg1,5CuZr depend remarkably on the applied heat treatment. Artificial aging after heat treatment makes it possible to reach higher conventional yield point $R_{0,2}$, than in case of natural aging. The investigations have indicated low resistance of the alloy in state ta to stress corrosion.

In the examined artificially aged alloys (T6) mechanical properties and corrosion crack resistance depend on the cooling rate after heat treatment (aging conditions were the same for all artificially precipitation hardened states). The higher the cooling rate after heat treatment, the better the mechanical properties and the worse the stress-corrosion resistance.

The type of heat treatment affects the nature of the material structure, especially the concentration and size of inter-metallic phases, and the PFZ width. The increased rate of cooling after heat treatment, followed by artificial aging, lead to the decrease of the PFZ width. The nature of η phase precipitates at grain boundaries also affects the corrosion resistance of the alloy. Moreover, phase precipitates revealing continuous nature worsen alloy's resistance to stress corrosion as well.

That is why the type of heat treatment (in particular the cooling rate after the heat treatment) is to be selected in such a way as to secure simultaneously high mechanical properties and good stress-corrosion resistance of the alloy at relatively low cost of the entire process. In these terms, the best results can be achieved using hot water as the cooling medium after heat treatment (state T62). The heat treatment labelled as T62 makes it possible to obtain good mechanical properties ($R_m \approx 440$ MPa, $R_{0,2} \approx 400$ MPa) and stress-corrosion durability (at $\sigma_0 = 320$ MPa, $t > 1500$ h).

After the heat treatment T62, the examined aluminium alloy with Cr and Zr additives had the structure which secured good mechanical properties and high resistance to stress-corrosion cracks. This structure revealed uniform distribution of η phase without continuous precipitates at grain boundaries, along with satisfactory PFZ width, approximately equal to 120 nm.

BIBLIOGRAPHY

1. Gruhl W.: *The stress corrosion behaviour of high strength AlZnMg alloys*. Aluminum, 5, 1978.
2. Sinavskij V. S., Valkov V. D.: *Korrozja i zaŝĉita aluminiovych splavov*. Metallurgija, Moskva, 1986.
3. Strabawa J.: *Structural analysis of stress-corrosion development in K63Cu alloy*. Ph.D. thesis (in Polish), AGH, Cracow, 1974.
4. Charbonier J. C., Marandet B., Sanz G.: *Methodes d'essais utilisees pour la determination de K_{ISCC} en milieu salin:*

application au cas de guelgues aciers a˙tres haute resistance. Mateaux, 50, No 599-600, 1975.
5. Cudny K., Puchaczewski N.: *Metal alloys for ship hulls* (in Polish). Wydawnictwo Morskie, Gdańsk 1989.
6. Bugłacki H.: *The effect of heat treatment and chemical constitution on mechanical properties and stress corrosion of the AlZn5Mg1 alloy in welded ship constructions*. Ph. D. thesis (in Polish). Gdansk University of Technology. Gdańsk, 1981.
7. Cudny K et. al.: *Summary of examination of weldability and corrosion resistance of the AlZn5Mg3 alloy. Scientific research report* (in Polish). WSMW, Gdynia 1984.
8. Cudny K., Wójcik J.: *Testing the tendency to hot crack of the AlZn5Mg1 alloy welded with AlMg5 and AlMg5Zn2 binders with different zirconium content* (in Polish). Zeszyty Naukowe WSMW, Gdynia Nr 1/60, 1979.
9. Report on scientific research "Light alloys", stage II, (in Polish). WSMW Gdynia, 1982.
10. Yoshimitsu M.: *Influence of applied stress and test temperature on stress corrosion cracking of Al-Zn-Mg alloy*. Journal Japan Institute Light Metals, No 12, 1976.
11. Brown B F.: *A new stress-corrosion cracking test for high strength alloys*. Material Research and Standards, No 3, 1966.
12. Kowarsch A., Bugłacki H.: *Testing the effect of stress corrosion on strength of precipitation hardened Al-Zn-Mg alloys* (in Polish). Ochrona przed korozją, Nr 1, 1979.
13. Kyzioł L., Czapczyk K.: *Influence of heat treatment on stress -corrosion resistance of EN AW-AIZn5Mg1,5CuZr alloy*, Solid State Phenomena, Mechatronic System and Materials Vol. 199, 2013, pp. 424-429.

CONTACT WITH THE AUTHOR

Lesław Kyzioł, Assoc. Prof.
Faculty of Marine Engineering,
Gdynia Maritime University
Morska 81/87
81-225 Gdynia, POLAND
e-mail: lkyz@am.gdynia.pl

POLISH MARITIME RESEARCH 4(80) 2013 Vol 20; pp. 45-51
10.2478/pomr-2013-0040

Test research on the resistance performance of high-speed trimaran planing hull

Weijia Ma*, Ph.D.,
Harbin Engineering University, China
Huawei Sun*, Ph.D.,
AVIC Aerodynamics Research Institute, China
Jin Zou, Prof.,
Heng Yang, Ph.D.,
Harbin Engineering University, China

ABSTRACT

In order to identify high-speed navigation ability of trimaran planing hull, as well as investigate the characteristics of its resistance and hull form, ship model tests were conducted to measure resistance, trim and heaving under different displacements and gravity centre locations. The test results were then used to study the influence of spray strips on resistance and sea-keeping qualities. Moreover, different planing surfaces were compared in the model tests which helped to look into influence of steps on hull resistance and its moving position. Also, the resistance features of monohull and trimaran planing hulls, both with and without steps, were compared to each other. From the tests it can be concluded that: the two auxiliary side hulls increase aerodynamic lift at high-speed motion, which improves the hydrodynamic performance; the trimaran planing hull has also excellent longitudinal stability and low wave-making action; when $Fr_{\nabla} > 8$*, its motion is still stable and two distinct resistance peaks and two changes of sailing state (the second change is smaller) appear; spray strips are favourable for sea-keeping qualities at high speed. The change trends before the second resistance peak as to the resistance and sailing behaviour of trimaran planing hull without steps are the same as for monohull planing hull without steps. but when steps in both hulls exist the change trends are different; more specifically: trimaran planing hull with steps has only one resistance peak and its resistance increases along with its speed increasing, and the resistance is improved at the increasing speed as the number of steps increases.*

Key words: trimaran planing hull; side hulls; high speed; step; resistance; model test

INTRODUCTION

Trimaran planing hull has excellent navigation performance. It is constituted of a main ship hull and two auxiliary side hulls. The trimaran planing hull in combination of normal planing hull, high-speed multihull vessel and gas - layer - reducing - resistance ship, owns advantages of the three ship types. It has good hydrodynamical and aero-dynamical performance and operates in planing mode at normal stage of navigation. Due to its high speed and easy adjustment to different sea states trimaran planing hulls are applicable both to military and civil missions.

Currently, in some foreign countries design technology of trimaran planing hulls has been highly developed [1]. It not only has won frequently the championship in different boat races but also has been used as a unmanned weapon platform. Because of its high superiority, published technical papers are - for the sake of confidentiality- limited to real ship photos or introductory materials. Several Chinese researchers studied the design and performance of catamaran scooters by model and real ship tests [2-5]. Features of tri-wave-elimination planing boat were also analyzed [6]. At the same time, the operating principle, ship type character and general performance of channel-hydrofoil planing boat were explored [7-8]. And, experiments were also conducted on the hydrodynamic performance of high-speed craft [9]. Then resistance characteristics of channel-hydrofoil planing boat were studied [10]. In the paper [11] the effect of bottom steps on propulsion efficiency of high speed planing craft with outboard engine was analyzed. The operating principle and technology points of trimaran wave-absorption planing craft were then researched [12]. Effects of different locations of gravity centre, step patterns, air flow rates and air injection ways on resistance of stepped planing boat were studied comprehensively [13-18]. Further, its propulsion system was investigated by using a real craft [19]. A resistance regression formula for double stepped planing craft, based on data from the model tests [20], was elaborated. So far, there has been no Chinese paper related to trimaran planing crafts. Since resistance performance is significant for evaluating a new ship type, in this paper are discussed model resistance experiments carried out with the aim to check the high speed navigation ability of trimaran planing craft and its resistance performance with and without spray strips at different displacements and gravity centre locations. The model tests have been also used to explore the effect of steps on its resistance and voyage state. Finally, the test results and observed phenomena are combined in analyzing this ship type.

* These authors contributed to the work equally and should be regarded as co-first authors

TESTED MODEL AND ITS TESTING SCHEMES

The moulded lines of the trimaran planing hull considered in this paper are shown in Fig. 1. Its features are as follows: the channels placed from bow to stern at both sides of the monohull planing hull, divide the hull into the main ship hull and two auxiliary side hulls. They make up two trumpet-like channels and form the hull cross sections similar to the shape of M.

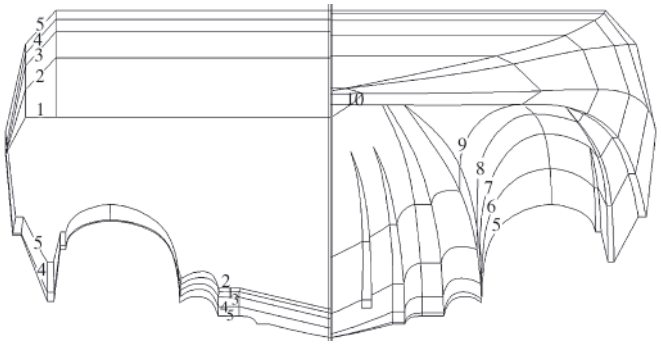

Fig. 1. *Moulded lines of tested model*

The ship model is made of FRP (fibreglass reinforced plastic) and its main hull is slender body whose length/width ratio is 7.32. The cross section of the auxiliary appendage is an inverse trapezoid with a bevel in both sides. Displacement of the auxiliary side hulls accounts for about 10 % of the total displacement. The moulded lines and ship model are shown in Fig. 1 and Fig. 2, respectively. For comparison, the wooden spray strips are separately formed into two pairs of pyramid-like elements of the length/ship length ratio of 0.47 and 0.213, respectively, and their pressurized-water angles are equal to 10°. The channel has a dome-roof with S-shape top body lines.The model has ten ordinates spaced by 240 mm, and its stem is the tenth ordinate. The scheme of the model with three steps has the transverse steps (of 12 mm in height) set up at the ordinates: 2⅓, 3⅔, 5, respectively. On the projection of ship bottom, the projection line of the steps at tail end is vertical to keel line, as shown in Fig. 3.

Fig. 2. *The model of trimaran-planing boat*

Fig. 3. *Three transverse steps on the model body*

The scheme of the model with two steps has the declined steps (of 6 mm in height) set up at the ordinates: 2⅓, 3⅔, respectively. On the projection of ship bottom,the angle between projection line of the step at tail end and keel line is equal to 60°, as shown in Fig. 4.

Fig. 4. *Two declined steps on the model body*

The scheme of the model with one step has the transverse step (of 6 mm in height) set up at the ordinate 3⅔, as shown in Fig. 5.

Fig. 5. *One transverse step on the model body*

The principal dimensions of the ship model are given in Tab.1.

Tab. 1. *Principal dimensions of the ship model*

Principal dimension	Value
Length L (m)	2.40
Moulded breadth B (m)	0.640
Bevel line breadth of main hull Bm (m)	0.297
Ordinate spacing ΔL (mm)	240
Average dead rise angle β (°)	13
Scale ratio	1: 6.46

One of the main characteristic features of the trimaran planing hull is its excellent rapidity. During the test, towing speed is brought to the limitation of the model tank before porpoising behaviour turns up. The resistance, trim and heaving in different states were examined by using four model tests in which the trimaran planing hull model was basically the same but the difference between them consisted in that one was without steps and the other ones with three different types of steps. The testing schemes are shown in Tab. 2.

TEST RESULTS AND ANALYSES

The model tests were carried out in the high-speed hydrodynamic tank of Aviation Industry Institute 605, Jingmen, China. The resistance, trim and heaving were tested by free towing method. In detail, the resistance was measured by means of an electrometric device with 0.2 % accuracy; trim - by tilt sensor with 0.1° accuracy and the up-pitch was taken positive; heaving was measured by a heave meter with 1 % accuracy and rising was taken positive. The test results of the drag/lift ratio R/Δ, the trim α and the heave amplitude H against the change of the volumetric Froude number Fr_∇ are shown in Fig. 6 through Fig. 8.

Tab. 2. Testing schemes

No. of scheme	Δ [kg]	l [m]	d [m]	θ [°]	Remarks
1	40	0.62	0.144	3	No spray strips
2	40	0.62	0.144	3	Two pairs of spray strips
3	50	0.64	0.159	3	Two pairs of spray strips
4	60	0.66	0.171	3	Two pairs of spray strips
5	40	0.63	0.145	3	No steps
6	40	0.63	0.145	3	3 transverse steps of 12 mm height
7	40	0.63	0.145	3	2 declinate steps of 6 mm height
8	40	0.63	0.145	3	1 transverse step of 6 mm height

where: Δ - stands for the weight of trimaran planing hull, l - represents the distance between centre of gravity and stern transom plate, d - shows designed draught, θ is trim when the ship model stands still

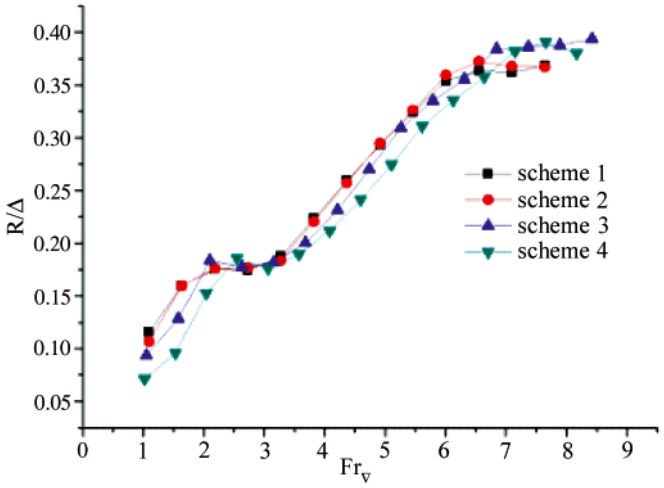

Fig. 6. Changes in drag/lift ratio for different testing schemes

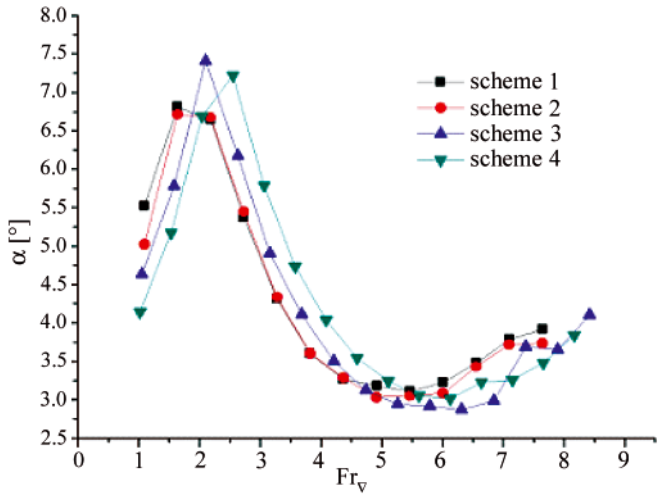

Fig. 7. Changes in trim for different testing schemes

The maximum towing speed allowable for the above mentioned tank is 16 m/s. In the testing scheme 1 and 2 when the towing speed reaches 15 m/s ($Fr_\nabla = 8.2$), porpoising behaviour appears; while in the scheme 3 and 4 when the towing speed reaches 16 m/s and the volumetric Froude number reaches 8.42 and 8.17, respectively, the model behaviour is stable without porpoising motion. Generally, when the volumetric Froude number becomes greater than 5, common planing crafts often show porpoising behaviour, while planing hulls with steps and catamaran planing crafts may also show porpoising behaviour at a low planning speed [20].

In several testing schemes the volumetric Froude number is greater than 8, this shows that as for the longitudinal stability the trimaran planing hull performs better than the general monohull and catamaran planing crafts and has excellent capability of developing super-high speeds.

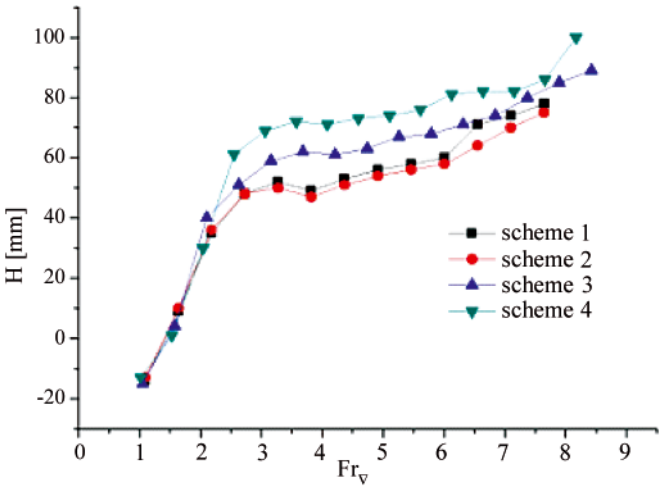

Fig. 8. Changes in heave amplitude for different testing schemes

As shown in Fig. 6, the resistance curve of the trimaran planing hull is similar to that of a seaplane in the first three phases of taking-off, as both of them have two drag humps [21]. But the drag humps of the trimaran planing hull are more distinct. The model speed when drag hump appears in different tests is shown in Tab. 3.

Tab. 3. Model speed when resistance crests appear

	Fr_∇ at the first resistance crest	Fr_∇ at the second resistance crest
Displacement: 40 kg, no spray stripes	2.15	6.6
Displacement: 40 kg, with spray stripes	2.15	6.6
Displacement: 50 kg, with spray stripes	2.2	7.1
Displacement: 60 kg, with spray stripes	2.6	7.7

It can be seen from Tab.3 that as the displacement increases and the gravity centre moves forward, the drag hump moves backwards and the volumetric Froude number needed to cross drag hump Increased, the drag hump increases continually. And, the fact whether the spray strips are installed or not has a little effect on the resistance and ship behaviour until the second drag hump appears when the resistance of model with spray strips increases by 2.5 %. But the spray strips have no effect on the position of drag hump.

As shown in Fig. 7, the trim of the trimaran planing hull, unlike the monohull planing crafts [22], has two peaks and the second peak is distinctly lower than the first one in navigation. As shown in Fig. 8, the trimaran planing craft is greatly uplifted two times; the first uplifting happens before getting into planning and the second happens when crossing the second drag hump; but the value of the second uplifting is smaller than the first one. The spray strips has no effect on trim and heaving before planning. But they become smaller after planning in the case of application of spray stripes when the curves are comparatively flat. It will greatly improve navigation ability of the high-speed trimaran planing hull as the aerodynamic lift cannot be ignored when the volumetric Froude number is greater than 6.

The following phenomena were observed in the tests: the channels at both sides are immersed in water when the ship model stands still; the wetted breadth of the channel and auxiliary side hulls decreases with the increasing of model speed when the model is in hull-borne and semi-planing stage ($0 < Fr_\nabla \leq 3.0$); the channel are fully ventilated with its top above water surface when the model starts to plane ($Fr_\nabla \approx 3.0$). Apart from the wave induced by ship motion, there appears transverse flow forming spray in the channels due to pressure difference between planing surface and ambient pressure. As shown in Fig. 9, both sides demonstrate distinct wave-making and a little spray, which then forms "chicken wake" behind the stern. With the increase of speed the wave-making declines while the spray - forming increases, and the distance between the "chicken wake" and the stern rises gradually.

Fig. 9. *Phenomena during the test at $Fr_\nabla = 2.2$*

As shown in Fig. 10, in the planing stage ($3.0 < Fr_\nabla < 6.0$) the splashing rises further, while the "chicken wake" decreases gradually and the wake furls to the middle part. In this stage the resistance is approximately proportional to Fr_∇. The channels are filled with air-water mixture and the wetted breadth of the auxiliary side hulls decreases with the increasing of model speed.

As shown in Fig. 11 the model is in the high-speed planing stage ($Fr_\nabla > 6.0$). With the increase of speed the model hull uplifts and the auxiliary side hulls get out of the water gradually till only the after body touches the water surface. The wave-making and splashing caused by the main hull are absorbed and obstructed by the auxiliary side hulls. Air layer, air-water mixture layer and splashing layer are formed from top to bottom in the channels. The water escapes in the form of spray column at the stern and the wake is relatively flat.

Fig. 10. *Phenomena during the test at $Fr_\nabla = 3.8$*

Fig. 11. *Phenomena during the test at $Fr_\nabla = 7.6$*

It can be seen from the above decribed tests that: the main hull offers most of the effective buoyancy when the model is in still-stand and hull-borne mode; when the model is in high-speed mode, i.e. the main hydrodynamic planing surface is formed, the main hull produces most of the hydrodynamic lift. In the high-speed mode the hull is supported by hydrodynamic and aerodynamic lift, so the main hull will have enough dynamic lift even if it is narrow. The main effect of the channels at both sides consists in producing the aerodynamic lift at high velocity, which supports the hull and improves its seaworthiness. When the ship model is still standing or at a low speed the auxiliary side hulls are all immersed in water giving extra static buoyancy; and, at high speed they obstruct wave-making and splashing.

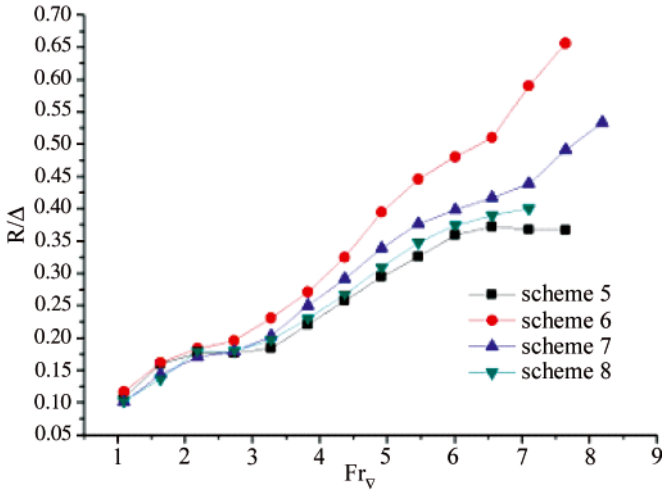

Fig. 12. *Effect of steps on the drag/lift ratio*

The drag/lift ratios R/Δ (where R and Δ stands for the total resistance and the model weight, respectively) versus the volumetric Froude number are shown in Fig. 12. When $Fr_\nabla < 2.18$ the change trend of the drag/lift ratio for the model

with three transverse steps is in compliance with that for the model without steps; the resistance of the model with three steps is a little bigger, and the resistance of the model with one or two steps is somewhat smaller, compared with that for the model without steps. When $Fr_\nabla > 2.18$ the resistance of all models with steps is bigger than that of those without steps, especially the resistance of the model with three steps, which is by 78.78 % larger when $Fr_\nabla = 7.65$. The resistance of the model without steps decreases when $Fr_\nabla > 6.55$, and the resistance of that with two steps increases sharply; and, the resistance of the model with one step also increases and its porpoising behaviour appears when $Fr_\nabla = 7.65$.

General monohull planing crafts in motion have only one drag hump, and after crossing the drag hump the resistance increases monotonically. Trimaran planing hulls without steps have two distinct drag humps between which the resistance increases monotonically, and after crossing the second drag hump the resistance tends to drop.

When the monohull planing craft enters planing state the resistance changes a little with the increasing of speed in a certain range. The planning efficiency rises and the resistance decreases with increasing number of steps. The resistance curve of trimaran planing hull with steps has only one drag hump. When it enters planing state the resistance increases distinctly. The more the steps the greater the resistance in high speed.

In Fig. 13 is shown the curve of trim against different values of the volumetric Froude number. In the process of towing two peaks can be observed for the none-step scheme in which the trim is larger than that in three-step scheme and in two-step scheme. The second peak appeared in the following order of the schemes: that of three-steps, two-steps and none-step. Particularly, porpoising behaviour turns out for one-step scheme at $Fr_\nabla = 7.65$, which results in only one peak; and the trim, if compared to that for none-step scheme, is smaller at $Fr_\nabla < 2.18$ and $Fr_\nabla > 3.82$ but almost the same at $2.18 < Fr_\nabla < 3.82$.

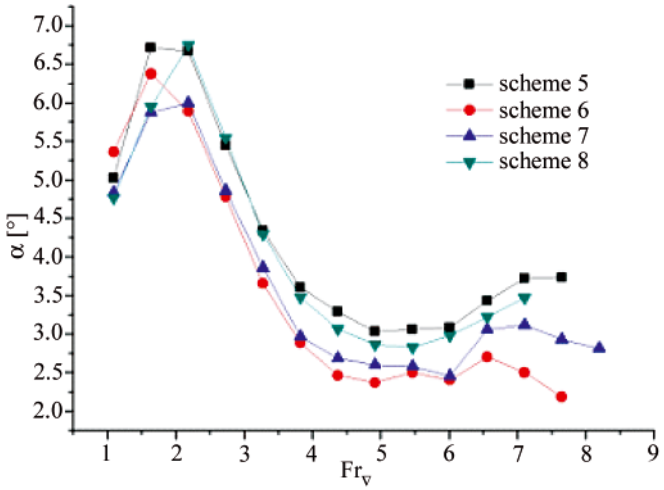

Fig. 13. *Effect of number of steps on trim*

Fig. 14 shows the heaving H against different values of the volumetric Froude number for four schemes. The heaving for three-step scheme is smaller than that for none-step scheme and, the first crest and trough are not distinct. As to the two-step scheme, its heaving curve is partly different from that of none-step scheme; their change trends at $Fr_\nabla < 3.28$ are the same and the heaving values differ a little; their first peaks are at $Fr_\nabla = 3.82$ and $Fr_\nabla = 3.28$, respectively, and their second peaks are at $Fr_\nabla = 5.46$ and $Fr_\nabla = 6$, respectively. The heaving curve for one-step scheme is in accordance with that for none-step scheme whose heaving value is a little bigger.

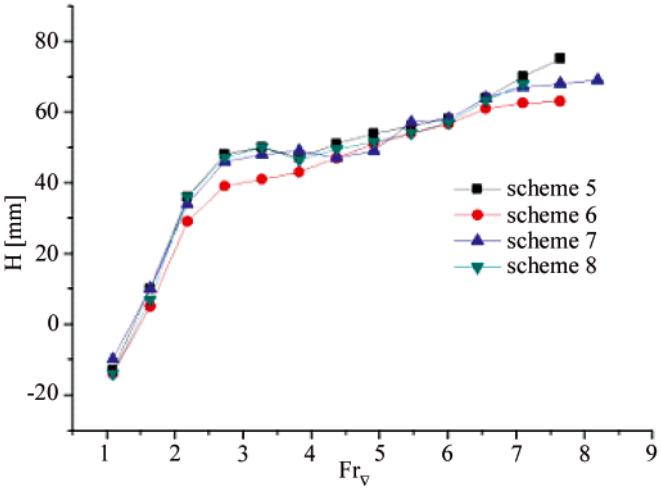

Fig. 14. *Effect of number of steps on heaving*

In hull-borne and semi-planing state, as the velocity grows, the trim of general monohull planing craft increases distinctly and the hull uplifts rapidly. After entering planing state, its trim decreases gradually and the hull uplifts slowly.

As the two curves indicate, the voyage states of trimaran planing crafts without steps could be divided into three stages: in the first stage, when the vessel is in hull-borne and semi-planing mode, its trim rises fast and the hull uplifts dramatically. The second stage comes after entering planing, when the trim decreases steadily and the uplifting amplitude also decreases. The third stage occurs before crossing the second resistance crest, when the trim rises again and the uplifting amplitude increases, but the trim and heaving are smaller than in the first stage.

The voyage states of monohull planing hull with steps can be also divided in three stages over the whole speed range. The first stage ends before the drag hump, when the trim and heaving increases gradually with the rise of speed. The second stage comes after the drag hump in planing state, when the trim sustains nearly unchanged and the hull uplifts steadily. In the third stage ($Fr_\nabla > 7.5$), the hull uplifts further and the trim falls a little, when the full-breadth planing becomes part-breadth planing in which the kinetic stability may be lost. The only difference between trimaran planing hull with steps and that without steps is that the velocity is different when trim and heaving changes. Except the one-step scheme where porpoising behaviour appears at $Fr_\nabla = 7.65$, the other two schemes are excellent as to motion stability of the crafts.

During the tests the spray is observed at the sides of the trimaran planing hull. Generally, regardless of whether monohull planing crafts have steps or not, strong spray will occur at high speed. As to none-step trimaran planing crafts, with the rise of speed at $Fr_\nabla > 6$, the auxiliary side hulls take slowly off the water surface and the wave-making and splashing caused by the main hull are absorbed and obstructed by them, as seen in Fig. 15; and, air-cushion layer is formed in the top of the channels and the flow of air-water mixture is totally free. As to other schemes with steps, the spray splashes out of the border, which leads to vortex and turbulence. Therefore, the none-step scheme has a much smaller wet area than other schemes, thereby has a smaller frictional resistance, which could be one of the reason why the resistance of none-step scheme is lower than that for other schemes.

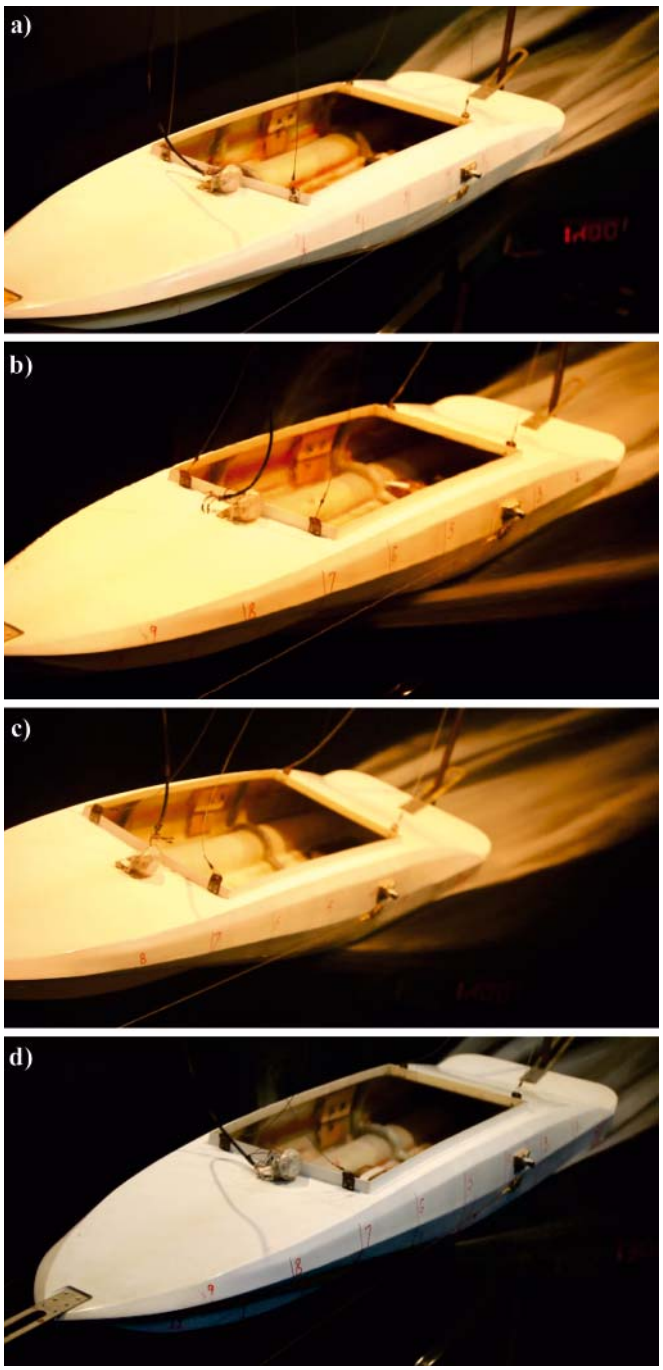

Fig. 15. *Spray forming at the sides for different model schemes.* ***a)*** *none-step model,* $Fr_{\nabla} = 7.6$; ***b)*** *three-step model,* $Fr_{\nabla} = 7.6$; ***c)*** *two-step model,* $Fr_{\nabla} = 7.6$; ***d)*** *one-step model,* $Fr_{\nabla} = 7.1$

CONCLUSIONS

This article mainly discusses the resistance performance of trimaran planing vessels. The resistance tests took into consideration several factors, including steps (applied or not), step patterns, and types of planing surface. Also, water splash beside the hulls under high speed was observed.

On the basis of the obtained test results the following conclusions can be offered:

1) The trimaran planing crafts have good longitudinal stability and high-speed navigation ability.
2) Influenced by aerodynamic lift, the trimaran planing hull has two distinct resistance crests. At high speed it sustains stable and its pitch and heave are small.
3) In the performed tests the influence of spray strips on the trimaran planing hull resistance performance appeared not distinct, but it can improve its navigation ability when the vessel enters planing.
4) Static buoyancy and dynamic lift supporting trimaran planing hulls are mainly provided by the main hull. The added auxiliary side hulls on one hand constitute - together with the main hull - the flow channel to generate aerodynamic lift; on the other hand they obstruct wave-making and splashing at high speed.
5) Trimaran planing hull without steps has two distinct resistance crests within the navigation range and the resistance between the two resistance peaks increases almost linearly. The pitch angle curve has also two peaks and the change of amplitude of the second peak is smaller than that of the first one; The heaving values, relative to pitch angle changes, increased greatly two times within the testing range. When steps are added to the hull, its resistance becomes larger,the second resistance hump disappears, the resistance increases with the increasing number of steps, the pitch angle and heaving displacement are both smaller than for the scheme without steps and the change trend of their curves is basically identical; and, the second peak of pitch angle and the second large rise of heaving appear earlier with the increasing number of steps.
6) The change trends before the second resistance crest of resistance and sailing behaviour of trimaran planing hull without steps are the same as for monohull planing hull without steps.
7) The greater number of steps of the craft, the larger its resistance. Installing the steps does not cause porpoising behaviour to emerge earlier, and, the longitudinal stability of the craft maintains excellent.
8) The trimaran planing crafts without steps, opposite to monohull planing hulls (both with and without steps) and trimaran planing crafts with steps, keep the splash within the channel, thus make it low, and form an air cushion layer which reduces the resistance.

BIBLIOGRAPHY

1. Lorne Frederick Campbell: *Entrapment Tunnel Monohull Optimized Waterjet and High Payload*. 7418915B2, 2007.9.20, USA.
2. Liu Qian, Hou Yutang, Wang Zhentao, et al.: *Development of high-speed twin-hulled planing boat*. Ship Engineering, 2,1999.
3. Liu Qian, Hou Yutang, Zhao Hua, et al: *Design and experimental research of catamaran planing boat on plateau water.* Shipbuilding of China, 3, 1999.
4. Liu Qian, Hou Yutang, YU Wudi, et al.: *Effects of principal dimensions, moulded lines and parameters of channel on speed and powering of catamaran planing boat*. Shipbuilding of China, 3, 1998.
5. LIU Qian, Wang Zhentao: *The distinguishing features, uses and development trends of high-speed planing catamaran*. Jiangshu Ship, 15(1), 1998.
6. Liu Qian, Pang Liguo, Lei Yunhong: *Research on working principle and technical features of tri-wave-elimination planing boat*. Jiangshu Ship, 17(1),2000
7. Su Yongehang, Zhao Lianen: *A study on characters of high performance channel type planing boat*. Shipbuilding of China, 1, 1996.
8. Zhao Lianen, Li Jide, He Yi: *A study on performance of channel-hydrofoil-type planing boat*. Shipbuilding of China, 3, 1997.
9. CHI Yunpeng, Meng Xianqin: *Experimental investigation on resistance an seakeeping performance for high speed channel crafts*. Ship Engineering, 3. 1995.

10.Zhao Zhiping: *Characteristics of resistance for channel type planing boat*. Journal of Dalian Fisheries University, 12(4),1997.
11..Huang Zhengang:*The effect of bottom steps to the propulsion efficiency of high speed planing craft with outboard engine*. Ship, (3),1996.
12.Liu Qian, Pang Liguo: *The operating principle and technology points of trimaran wave-absorption planing craft*. Jiangsu Ship, 17(1), 2000.
13.Dong Wencai, Guo Rixiu: *Effects of Different Air Injection Techniques on Resistance of Stepped Planing Boat*. Shipbuilding of China, 41(2), 2000.
14.Dong Wencai,Guo Rixiu: *Air injection on the bottom of stepped planing craft and its effect on resistance*. Journal of Ship Mechanics, 4(3), 2000.
15.Dong Wencai, Guo Rixiu: *Study on the mechanism of resistance reduction to the stepped planing craft by air injection.* Journal of Ship Mechanics, 6(6), 2002.
16.Dong Wencai, Guo Rixiu: *Experimental study on resistance reduction of planing craft by air injection.* Shipbuilding of China, 43(4), 2002.
17.Dong Wencai, Guo Rixiu: *Experimental investigation on the resistance reduction of stepped planing craft by formation of air cavity*. Journal of Hydrodynamics, 17(4), 2002.
18.Xia Xiang: *Matching performance of propulsion system for hyper-velocity step planing boat.* Chinese Journal of Ship Research, 3(2), 2008.
19.Shen Xiaohong, Wu Qirui: *A resistance regression formula for double stepped planing craft.* Chinese Journal of Ship Research, 5(2), 2010.
20.Zhao Lianen,Han Duanfeng: *Hydrodynamic principle and design of high-performance ships*. Harbin Engineering University Press, Harbin, 2000.
21.Troop 916 *of People's Liberation Army: Fluid mechanics of seaplane.* Translated by COMFORAER,1963.
22.Yue Guoqiang, Yao Chaobang, Dong Wencai: *Study of influence factors on resistance of deep-V planing craft in still water*. Chinese Journal of Ship Research, 4(3), 2009.

CONTACT WITH THE AUTHORS

Weijia Ma, Ph. D.
College of shipbuilding Engineering,
Harbin Engineering University,
Nan tong street Harbin, HLJ, P. R. CHINA,
e-mail: maweijia@live.cn

Huawei Sun, Ph. D.
AVIC Aerodynamics Research Institute, China,
Nan tong street Harbin, HLJ, P. R. CHINA,
e-mail: sunhuawei0051@163.com

POLISH MARITIME RESEARCH 4(80) 2013 Vol 20; pp. 52-61
10.2478/pomr-2013-0041

Second Generation Intact Stability Criteria: on the validation of codes for direct stability assessment in the framework of an example application

Gabriele Bulian, Ph.D.,
Alberto Francescutto, Prof.,
University of Trieste, Trieste, Italy

ABSTRACT

The Sub-Committee on Stability and Load Lines and on Fishing Vessels Safety (SLF) of the International Maritime Organization (IMO) has undertaken the development of so-called "Second Generation Intact Stability Criteria" (SGISC) with the intention of providing a new set of rules covering those phenomena which are not properly covered by present, mostly semi-empirical, requirements. The first two levels of the envisioned 3+1 tiers structure of SGISC are so-called "vulnerability assessment" levels: most of the discussion has so far been dedicated to these levels. At the highest level there is the so-called "Direct Stability Assessment", which is also strictly linked with the development of ship-specific "Operational Guidance". Recent discussion on the topic of "Direct Stability Assessment" (DSA) has touched the issue of "validation" of numerical codes to be employed at this level. Stimulated by, and in view of, the ongoing IMO discussion, this paper presents the results of a recent series of experiments in beam waves (mono-/bi-chromatic, irregular) and associated simulations based on a 6-DOF blended code. Nonlinear harmonic and sub-harmonic resonances are observed and simulated.

Key words: IMO; large amplitude ship motions; second generation intact stability criteria; nonlinear roll; sub-harmonic resonance; validation

INTRODUCTION

The Sub-Committee on Stability and Load Lines and on Fishing Vessels Safety (SLF) of the International Maritime Organization (IMO) has undertaken the development of so-called "Second Generation Intact Stability Criteria" (SGISC) with the intention of providing a new set of rules covering those phenomena which are not properly covered by present, mostly semi-empirical, requirements.

The envisioned framework of the SGISC is based on a 3+1 tiers approach, where different dangerous phenomena are treated separately, and where three levels of assessment are considered, with increasing complexity. These three levels are so-called "Level 1 Vulnerability Assessment", "Level 2 Vulnerability Assessment" and "Direct Stability Assessment". An additional level, bearing the name of the "Development of Operational Guidance", is also foreseen for those cases where the danger associated with specific phenomena cannot be controlled only by design countermeasures. In the envisioned structure, a ship sailing in a specific loading condition is expected to be considered as "safe" when at least one of the levels can be passed. Of course, firstly the simpler "vulnerability" levels are expected to be applied (and hopefully fulfilled). In case the vulnerability levels cannot be passed, then the following options are available:

- the design is modified;
- the loading condition is considered as not acceptable;
- the ship is tested at the higher tier(s), i.e. "Direct Stability Assessment", with possible development of ship-specific "Operational Guidance".

The majority of the ongoing discussion taking place at SLF and in the research community has concentrated so far on the development of vulnerability assessment methodologies, since these methods are expected to be applied to a wide population of ships (see, e.g., [1, 2, 3, 4, 5, 6] and references therein).

However, more recently, the discussion has also more directly addressed the "Direct Stability Assessment" (DSA), which is also strictly linked with the development of ship-specific "Operational Guidance". Key aspects in this discussion can be identified in:

- the outline of the characteristics of the codes which are expected to be used at these levels;
- the validation of the codes.

Regarding the expected characteristics of the codes, the preliminary specifications available in [7] indicate that typical hybrid (blended) simulation codes, following the line initiated in [8], have the characteristics adequate for being considered as suitable tools in this context.

Regarding the problem of "validation", one recent IMO document [9] has put forward a proposal where the "validation" of codes could be split into a "qualitative validation" and

a "quantitative validation". The former is intended to check that the physics embedded into the simulation code is appropriate for the simulation of the phenomenon under analysis. The latter is intended as a check of the degree of accuracy in the reproduction of the phenomenon. Some validation work directly connected with the development of SGISC can be found in [10]. At the same time, it is to be recalled that work aimed at the validation of codes for intact stability assessment, although not intended for a regulatory context, was carried out on different occasions by the ITTC (particularly since [11] up to the latest [12]). Moreover, a lively discussion on the matter of "Verification&Validation (V&V)" is undergoing, in parallel, in the ship stability community (e.g. [13, 14, 15, 16]). A benchmarking study for parametric roll assessment was also undertaken in the framework of the EU-funded SAFEDOR project [17].

Although validation is a fundamental aspect of Science, where mathematical models are continuously checked against real world phenomena since the time of Galileo Galilei, the matter of validation gets a different flavor when embedded in the rule making process, especially in case of IMO intact stability regulations. Indeed, IMO instruments for intact stability are significantly lacking from the point of view of indications regarding validation of simulation codes, and this can easily be explained by the fact that the use of codes for the simulation of ship dynamics is presently not considered as an option in the majority of IMO stability regulations. Exceptions can be found in case of, e.g. high-speed craft and mobile offshore drilling units. This situation is an evident indicator of the tendency of IMO stability requirements to be quite outdated compared to the general level of knowledge, "with an average time interval of 20 to 30 years between scientific evidence and practical application" [18]. Coming back to the issue of "validation", although this concept cannot be considered as part of present intact stability rules' background, it is interesting to underline that, in the process of the development of regulations, it is not uncommon to face the request of IMO Delegations for a proper "validation" of the developed rules. As discussed in [5], "validating a rule" is of course a process simply not possible, since a rule is a combination of a calculation method ("criterion" in SGISC nomenclature), which is a technical aspect which can be potentially validated in some cases, and the setting of a limit value ("standard" in SGISC nomenclature), which is a mainly political decision which cannot be "validated". The term "validation", in the IMO discussion, is, therefore, often misused.

Given the described situation, it was of interest to look at the results of a series of beam waves model experiments and associated numerical simulations, from the perspective of the undergoing discussion on "Direct Stability Assessment" approaches. Indeed, for a full Series-60 vessel, some experimental results were available from a previous experimental campaign [19]. More experimental tests have recently been carried out, with the ship in different loading conditions, with the aim of investigating the occurrence of sub-harmonic roll motion in beam waves under multi-frequency excitation (in particular bi-chromatic and irregular waves) [20, 21]. Associated with the experimental results, a series of numerical simulations have been carried out using a developed 6-DOF blended code for large amplitude motions and maneuvering in waves [22], which is based on suitable, in principle, modeling for the type of simulations expected to be necessary for "Direct Stability Assessment". The availability of simulations and experiments allows to put this material in the perspective of SGISC development, and to provide some feedback for the ongoing discussion.

VALIDATION OF CODES FOR DIRECT STABILITY ASSESSMENT

In the framework of SGISC, at so called "Direct Stability Assessment" (DSA) level, it is expected to use simulation models which are able to reproduce the behavior of the ship in waves, with particular attention to certain phenomena which have been identified as "dangerous" (see also [23]). These phenomena are:

- Pure loss of stability;
- Parametric rolling;
- Surf-riding/Broaching;
- Dead-Ship condition;
- Excessive accelerations.

Although this list might be incomplete, it covers quite a significant part of dangerous events, if considered separately. It should be said that "Excessive accelerations" is actually something different, since excessive accelerations could occur as a result of different „true" dangerous phenomena (e.g. in dead-ship condition, or during a parametric roll event). This aspect is however not discussed further in this paper.

According to [7], tools expected to be used at the DSA level should be based on "state-of-the-art" methods. Ideally, a general purpose software for large amplitude ship motions simulations in waves should be able to address all the aforementioned phenomena if the ship, loading condition and environmental conditions are such to make one of the above phenomena to appear. It is however known that, in the field of simulation of large amplitude ship motions in waves, it is still necessary to use mathematical models which, although being based on first-principles, need to be complemented by not negligible semi-empirical tuning/corrections/sub-models. This is valid, to a different extent, whatever computational model is used. Of course, the more we move towards the full application of first-principles approaches (this meaning, basically, direct computational fluid dynamics approaches addressing the fluid-structure interaction in waves), the less we need semi-empirical additions to the simulations. However, at the moment of writing, a direct complete computational fluid dynamics approach for the extensive simulation of ship behavior in irregular waves is simply not feasible for practical applications, due to the excessive requirement of computation resources/computational time and also due to numerical issues still waiting to be fully resolved in a mature way. This basically leaves the door open, today, only to "hybrid/blended methods", where, although in a simplified partially semi-empirical way, the most important characteristics of the problem are taken into account, namely: exact ship geometry, nonlinear rigid body dynamics, forces due to (undisturbed) pressure of waves on the instantaneously submerged hull, radiation and diffraction effects, viscous effects, maneuvering forces, rudder effects, wind actions, etc. Being such type of methods partially semi-empirical means that they are often better suited (tailored) for particular applications and/or ship types. For instance, software tools developed, tested and extensively applied for monohulls can be extremely poor in predictions for multihulls, without proper re-tuning (and/or partial re-development). Moving from the problem of different types of ships to the problem of different types of phenomena, methods which, for instance, are working well for dead-ship condition could be completely unsuitable for simulating, for instance, broaching. In particular this latter comment opens a big question, i.e. whether it is appropriate to develop (strongly) different DSA tools for different phenomena. Tailoring too much a tool for a specific application is, in general, dangerous, because the model could eventually overlook possible dangerous phenomena which were not

explicitly considered in the original development of the model, but which could nevertheless happen for certain ships. An archetypal example of this issue, relevant for this paper, is the 1-DOF modeling of roll in beam waves. It is of course necessary to develop a model for such condition taking into account the nonlinearities of restoring in waves (say $\overline{GZ}$). It is also known that in several situations (typically beam regular waves with sufficiently large metacentric heights $\overline{GM}$) even relatively simple nonlinear models provide good predictions if properly used/tuned in their parameters. However, despite possible good performances of the model in the "foreseen" conditions, if the model is developed neglecting the coupling with heave and the relative angle between the ship and the waves, it can completely miss the occurrence of some nonlinear phenomena (see [20, 21, 24, 25]). It is therefore necessary to try to avoid, in the development stage, as many simplifications as possible in order to leave as much of the original physics of the problem embedded in the mathematical model, letting the simulation tool "doing its job" without constraining its behavior. Of course, following this way inevitably increases the complexity of the model and, consequently, the debugging phase, the parameters selection phase, the overall computational time, the skills required for using the model, the possible introduction of "spurious" behaviors, etc. etc. It is therefore always a matter of engineering and scientific judgment to decide the level up to which simplifications can be (should be) carried out without compromising too much the capabilities and the accuracy of the model. In this context the process of "validation" helps in checking, although without necessarily giving a final answer to the question of whether the simplifications have been brought the model too far from the real physics.

Going now to the approach proposed in [9], we will report here the main aspects which are relevant for the present discussion. For more information the reader is referred to the original source [9] as well as to some early feedback [26]. The proposal in [9] regarding DSA tools is based on two main concepts:

1) The specification of minimum requirements for the simulation model;
2) The specification of validation requirements for considering the simulation model suitable for regulatory applications.

The specification of the abovementioned requirements is provided differently for different failure modes with some common requirements. It can be commented that this implicitly means that the proposal in [9] assumes as acceptable the development and subsequent validation of possibly different simulation tools for different dangerous phenomena/ conditions.

Before going to specific requirements for dead-ship condition (which is the situation dealt with in the present series of experiments / simulations), it is worth reporting a summary of the generic requirements proposed in [9].

First of all, [9] proposes to use the Airy model for modeling waves. It is worth mentioning here, as a comment, that the Airy model requires proper stretching (e.g. [27, 28, 29]) before being consistently usable for large amplitude motion simulations (e.g. [22, 30]) otherwise the zero-pressure condition at the free surface cannot be properly enforced. The stretching method could be different from code to code.

There are then a couple of interesting and useful reminders/ requirements in [9] regarding roll damping and hull forces. These notes remind the developers to avoid possible duplications of effects, a matter which was actually touched in the past in [31]. It is indeed important to avoid the possible (partial) overlapping of different models (e.g. seakeeping and maneuvering models) in the simulation code.

Regarding the specific case of dead-ship condition without considering wind (which is the situation dealt with in the present series of experiments / simulations), minimum requirements in [9] can be summarized as follows, with some comments (see the original text for the exact wording):

- *At least 5 DOFs should be used (surge can be avoided)*. As a comment to this requirement, it could be said that eliminating any DOF is always a "tricky" job. The way to eliminate/constrain DOFs is typically not unique and different developers can follow different approaches (e.g. partial elimination through elastic joints, complete elimination through virtual forces based on analytical conditions, simple dropping of terms in the equations of motions, ...).
- *Froude-Krylov and hydrostatic forces should be calculated on the actual underwater hull.* It is of course necessary to consider the instantaneous underwater hull, because this is the main source of roll restoring nonlinearities. Also, this approach implicitly introduces some coupling with other DOFs, in particular heave, which is something of interest in the framework of the present study. What should however be commented, is the wording used in [9], which implicitly considers it possible to separate the Froude-Krylov component from the hydrostatic component. While this separation is perfectly suited for linear calculations, where the undisturbed wave pressure field can be separated into the undisturbed calm water hydrostatic pressure and the wave disturbance, this is no longer possible in nonlinear simulations, particularly when considering a non-flat free surface. Trying to keep on using this separation can potentially create consistency issues and unforeseen problems (in case of, e.g., very large waves). For this reason, in nonlinear ship motions simulations, the "Froude-Krylov" pressure should always be considered (or, better, defined) as the total pressure of the undisturbed wave (i.e. without removing the "hydrostatic" component). This is particularly necessary when using stretching approaches as mentioned before. Moreover this would be more easily transferrable to fully nonlinear descriptions of the undisturbed wave pressure field.
- *Radiation and diffraction forces should be appropriately considered.* The introduction of radiation and diffraction effects, in a simplified way, has always been a struggle for developers. The typically most effective approach (though not necessarily the most correct one) is the introduction of diffraction and radiation terms from linear seakeeping pre-calculation. However, also in this case different developers have used different approaches. Typical different choices are whether to use constant coefficients or embed memory effects through convolution integrals (this latter nowadays considered more suitable, although slower from the computation point of view). A particular issue is associated with the reference system to be used for the calculation of radiation and/or diffraction terms based on the linear theory (body-fixed variables? earth fixed variables? variables in "almost-steadily" translating horizontal system? ...). Moreover, variable speed effects (typically with large drift angles) in the case of convolution-based approaches also represent a modeling issue where different approximations can be considered, which leads to inherently different codes/simulation methods.
- *Drift forces (longitudinal, heeling moment, yaw moment) should be based on model test results (CFD can be used if proved to be sufficiently accurate)*. Open issues are associated with this matter. Drift forces from model tests are often determined in quite "artificial" conditions and

a fundamental issue is how to consistently implement experiment (CFD simulation) data in large amplitude motions simulations. A relevant and instructive example touching a little bit this aspect is the application of the alternative experimental assessment of Weather Criterion through the procedure specified in MSC.1/Circ.1200 [32]. As briefly noted in [33], there is often space for "interpretation" on how to combine experiments, which are typically carried out in a free sinkage&trim condition in calm water, with calculations, which are typically dealing with different conditions, especially when wind forces and drift forces are to be combined. The lack of uniqueness in the modeling of these effects is likely to introduce some "modeling noise".

In addition to the above topics, the proposal in [9] also touches wind forces and, very briefly, the problem of proper generation of irregular waves.

Regarding requirements for validation, the proposal in [9] introduces the idea of splitting the validation process in two parts, namely:

1) "Qualitative validation";
2) "Quantitative validation".

In addition, the proposal in [9] introduces the idea of having a validation process which is basically "failure-mode specific", although some validation requirements are specified more generally, in terms of the type of characteristic the model is expected to embed. The introduction of a failure-mode specific validation approach has the pros of being very tailored and effective, but, on the other hand, it potentially opens the door to the possibility of overlooking some phenomena which are not originally intended to be represented by the mathematical model and/or checked through the validation process.

Regarding qualitative validation (limiting to aspects related to dead-ship condition - see [9] for exact wording):

- *Calculation methods where instantaneous underwater hull geometry is to be considered, shall be capable of consistently reproduce the angle dependence of roll restoring, roll oscillation frequency (backbone curve) and bending of the roll response curve (in addition variations of stability in waves should be properly handled).* Bending of roll response curve in beam waves due to restoring nonlinearities is nowadays well known [34]. The bending of the response curve in beam waves is associated, to a large extent, to nonlinearities of roll restoring (although drifting effects can also be of importance [35]). Moreover, nonlinear roll restoring also introduces a rolling-amplitude dependence of the natural roll oscillation frequency, which can be qualitatively (and partially quantitatively) observed through the analysis of (large-initial-angle) roll decays.
- *Heel caused by drift and wind should be reproduced.* This is of course necessary whenever ship motions are to be simulated in waves and/or wind.

Regarding quantitative validation (limiting to aspects related to dead-ship condition - see [9] for exact wording):

- *Results from experiments carried out according to ITTC guidelines should be considered as "correct values".* In [9] it is not reported exactly which procedure should be used, but the relevant procedure for this purpose, as suggested in [26], is likely the procedure given in [36]. It is to be said, however, that the procedure [36] is very qualitative in nature.
- *Response curve for synchronous roll is acceptable when differences in rolling amplitude are below [10%] if the rolling amplitude is below the angle of maximum GZ, and [20%] if the rolling amplitude is above the angle of maximum GZ.* Putting sharp quantitative limits is always difficult. In particular, 10% limits can be significantly strict, especially in case of relatively small rolling amplitudes. For instance, in case of a rolling amplitude of 10deg, the limit would be set to 1deg. This value, in some cases, is smaller than the reasonable accuracy for certain instrumentation in dynamic conditions (especially some inertial units strongly based on signal post-processing). Also, in standard experiments, unless the towing tank is very long and/or the absorbing beach is extremely efficient, such an uncertainty in rolling amplitude could easily be due to: transient effects, partial reflection, inaccuracies in wave generation, variability of waves along the tank, reflections from tank's sides, etc. etc. Also, in some cases, large differences at fixed frequencies can be observed due to the shifting in frequency of the simulated response curve with respect to the experimental response curve, for various reasons, such as: differences, between experiments and simulations, of $\overline{GM}$ and radii of inertia, inaccuracies in simulating drift and/or in numerically reproducing experimental drift-constraints, typically soft springs, etc. etc. As a result, percentage values should always be bounded by minimum absolute values, which, from experience, could be of the order of ±2 deg.
- *Differences between ensemble estimates of roll variance from experiments and simulations should be not statistically significant at 5% confidence level.* On this point, lack of more details prevents a detailed discussion.

Given the general complexity of the problem under analysis (nonlinear ship motions in waves) and of the tools intended to be used for the simulation (blended codes), and considering the need of application in a regulatory framework (for DSA and/or development of operational guidance in the framework of SGISC), it is therefore expectable that a "once for all" validation process will not provide sufficient robustness, so requiring appropriate interaction with the Administrations.

SIMULATION METHOD

Simulations have been carried out using a nonlinear 6-DOF blended simulation code (SHIXDOF - "nonlinear SHIp motion simulation program with siX Degrees Of Freedom"), under development at the University of Trieste [21, 22]. The simulation methodology can be considered to follow the line initiated by [8]. The main characteristics of the simulation method have been described in [21, 22], and here they are reported in view of the undergoing discussion on DSA methods in the development of SGISC [9, 26].

First of all, rigid body motion equations are considered fully nonlinear in six DOFs, using a main state vector expressed in a ship-fixed reference system S:Oxyz. As it is common in maneuvering simulations, the nonlinear rigid-body equations of motions are then supplemented by those necessary to translate and orientate the rigid body with respect to an earth-fixed reference system Σ:Ωζηζ. The system of equations then reads as follows:

$$\begin{cases} m\cdot\left[\mathbf{u}'_O+\boldsymbol{\omega}\wedge\mathbf{u}_O+\boldsymbol{\omega}'\wedge\mathbf{x}_G+\boldsymbol{\omega}\wedge(\boldsymbol{\omega}\wedge\mathbf{x}_G)\right]=\mathbf{f}_{ext} \\ \mathbf{I}_O\cdot\boldsymbol{\omega}'+\boldsymbol{\omega}\wedge(\mathbf{I}_O\cdot\boldsymbol{\omega})+m\cdot\mathbf{x}_G\wedge\mathbf{u}'_O+m\cdot\mathbf{x}_G\wedge(\boldsymbol{\omega}\wedge\mathbf{u}_O)=\mathbf{m}_{ext}(O) \\ \dfrac{d}{dt}(\xi_O,\eta_O,\zeta_O)^T=\underset{S\to\Sigma}{\mathbf{R}}(\psi,\vartheta,\phi)\cdot\mathbf{u}_O; \\ \dfrac{d}{dt}(\phi,\vartheta,\psi)^T=\mathbf{T}^{-1}_{\omega_S}(\psi,\vartheta,\phi)\cdot\boldsymbol{\omega} \end{cases} \quad (1)$$

where the superscript "T" indicates the transpose operator, the prime subscript indicates differentiation with respect to time in the ship-fixed reference system, m [kg] is the ship mass, $\mathbf{u}_O = (u, v, w)^T$ [m/s] is the speed of the centre of the reference system (which does not coincide, in general, with the centre of gravity of the ship), $\omega = (p, q, r)^T$ [rad/s] is the rigid body angular velocity, $\mathbf{x}_G = (x_G, y_G, z_G)^T$ [m] is the position vector of the centre of gravity in the ship-fixed reference system S: Oxyz, $\mathbf{I}_O$ [kg·m^2] is the tensor of inertia with respect to centre O of the ship-fixed reference system, $\mathbf{f}_{ext}$ [N] is the total force due to external effects and $\mathbf{m}_{ext}(O)$ [N·m] is the total moment with respect to O due to external effects. The matrices $\mathbf{R}_{S\to\Sigma}(\psi, \vartheta, \phi)$ and $\mathbf{T}^{-1}_{\omega S}(\psi, \vartheta, \varphi)$ are appropriate transformation matrices, depending on the Euler angles ψ [rad] (yaw), ϑ [rad] (pitch) and φ [rad] (roll), which are used to obtain the time derivative of the position of the point O in the earth fixed reference system Σ:$\Omega\zeta\eta\zeta$ and to get the time derivative of the Euler's angle from the angular velocity. It can be seen that the system of equations (1) considers the fully nonlinear rigid-body dynamics. As such, the rigid-body dynamical model is suitable to consider all the phenomena of interest in the DSA for SGISC and it is in line with the requirements proposed in [9].

The modeling of external forces is intended to give the code the capability of simulating nonlinear ship maneuvering in regular and irregular waves [21, 22]. The Froude-Krylov pressure (comprising the hydrostatic term) is calculated up to the instantaneous wetted surface of the hull in order to catch the effect of geometrical nonlinearities (in particular nonlinear roll restoring), which is a fundamental requirement to address large amplitude motions (particularly roll) in waves. This characteristic is in line with the requirements proposed in [9]. Using an approach along the line in [27], particular attention was given to embed a suitable stretching of the pressure and particle's velocity fields in order to guarantee, in particular, zero-pressure at the free surface (see discussion on this issue in [30]). Radiation terms (leading to added mass and wave damping) are based on linear hydrodynamic pre-calculations. In order to allow a quite consistent use of the code in irregular waves and/or in case of non-harmonic responses (e.g. sub-harmonic, ultra-harmonic, chaotic motions), radiation effects are embedded through convolution integrals following [37] and accounting for [38]. The linear maneuvering forces due to lift effects are based on linear derivatives from [39]. The roll moment induced by the maneuvering forces is taken into account. In order to avoid overlapping between the seakeeping and the maneuvering model, added mass terms are supposed to be dealt with by the seakeeping model, and this attention in the modeling takes into account the warnings in [9]. However, when simulating the motions in waves, the drift angle can become quite large. For this reason linear maneuvering forces are reduced at large drift angles taking into account [40]. Moreover, since the flow field in waves is characterized by spatial variability due to wave induced orbital velocities, an "equivalent surge-yaw-sway motion" relative to the water is updated at each simulation time step, in a way similar to [41]. Nonlinear drag terms, which in the modeling mimic nonlinear maneuvering forces, are based on a simplified modeling which accounts for the relative speed between water and instantaneously submerged ship centreplane. The obtained model is basically a simplified cross-flow drag model taking into account the instantaneous relative velocity between the ship and wave particles. This model implicitly introduces a nonlinear roll damping. Additional linear and nonlinear roll damping coefficients can be introduced for tuning purposes. Particular attention is given in setting these coefficients, because roll damping is partially provided, implicitly, by different models (seakeeping model, maneuvering model, simplified cross-flow model, ...). This is true also concerning forward speed lift effects, because additional roll damping is introduced by forward speed effects in sway forces from the maneuvering model. For this reason, coefficients are set, in general, by iterative tuning of simulated roll decays. This process takes into account the warnings in [9]. Finally, constraints can be introduced in different forms. With reference to the topic of the paper, springs can be introduced to limit certain motions (typically lateral drift and/or low frequency yaw). Other characteristics are available (e.g. lifting surfaces, propulsors, ...) which are however not relevant for the topic under discussion. Overall, it can be said that the mathematical modeling embedded in the simulation code is therefore in line with the main specifications in [9].

HULL FORM AND EXPERIMENTAL CONDITIONS

The hull form used in this study is a standard Series 60 with main characteristics reported in Table 1. The bodyplan and the $\overline{GZ}$ curve in the considered loading conditions are reported in Figure 1. The hull was tested in the past using the loading condition LC01 (see [19]). Recently, additional tests have been carried out in the loading condition LC02, which is characterized by a much lower $\overline{GM}$, and therefore a much more nonlinear $\overline{GZ}$. In both cases the $\overline{GZ}$ is of the "hardening" type (more than linear). All experiments have been carried out at the Hydrodynamic Laboratories of the University of Trieste.

Different types of experimental tests have been carried out for the two considered loading conditions. Letting ω_0 the roll natural frequency and:

- *Loading condition LC01 (large $\overline{GM}$)* [19]. Roll decays, monochromatic beam waves ($\omega_{wave} \sim \omega_0$). Model free to drift;
- *Loading condition LC02 (small $\overline{GM}$)* [21]. Roll decays, monochromatic beam waves ($\omega_{wave} \sim 2\omega_0$; $\omega_{wave} \sim 3\omega_0$), bi-chromatic beam waves ($\omega_{wave,\,2k} \sim 2\omega_0 + \omega_{wave,\,3k} \sim 3\omega_0$), irregular beam waves (spectral peak frequency $\sim 2\omega_0$). Model partially restrained at bow and stern.

Tests executed for LC01 were part of a study, associated with the development of MSC.1/Circ.1200 [32], regarding the application of simplified 1-DOF mathematical models for the analysis and modeling of roll decays and 1:1 resonant roll response under harmonic beam waves. On the other hand, tests

Tab. 1. *Main characteristics of the hull form. Nominal data at model scale*

Quantity → / ↓ Load Cond. ↓	Mass [kg]	Length L_{BP} [mm]	Breadth B [mm]	Draught T [mm]	Dry pitch radius of inertia R_{yy}/L_{BP} [nd]	Dry roll radius of inertia R_{xx}/B [nd]	$\overline{GM}$ [mm]	Natural roll period [s]	Config.
LC01	32.5	1625	250	100	N/A	N/A	16	1.5	Bare hull
LC02					0.250	0.362	4	3.1	

executed for LC02 were part of a study intended to address the possible occurrence of sub-harmonic resonance under bi-chromatic and multi-frequency excitations in beam seas [20, 21]. It is important to underline that in case of loading condition LC02, all simulations, which were carried out in advance, were based on a nominal frequency equal to $\omega_0 = 2.010$ rad/s (model scale), whereas the experiments were carried out considering a reference roll frequency $\omega_0 = 1.913$ rad/s (model scale). As a result, given the ratio ω_{wave}/ω_0, the actual wave length/frequency is not exactly the same in the experiments and simulations shown in the next section. Bearing this in mind, comparisons can be considered still meaningful.

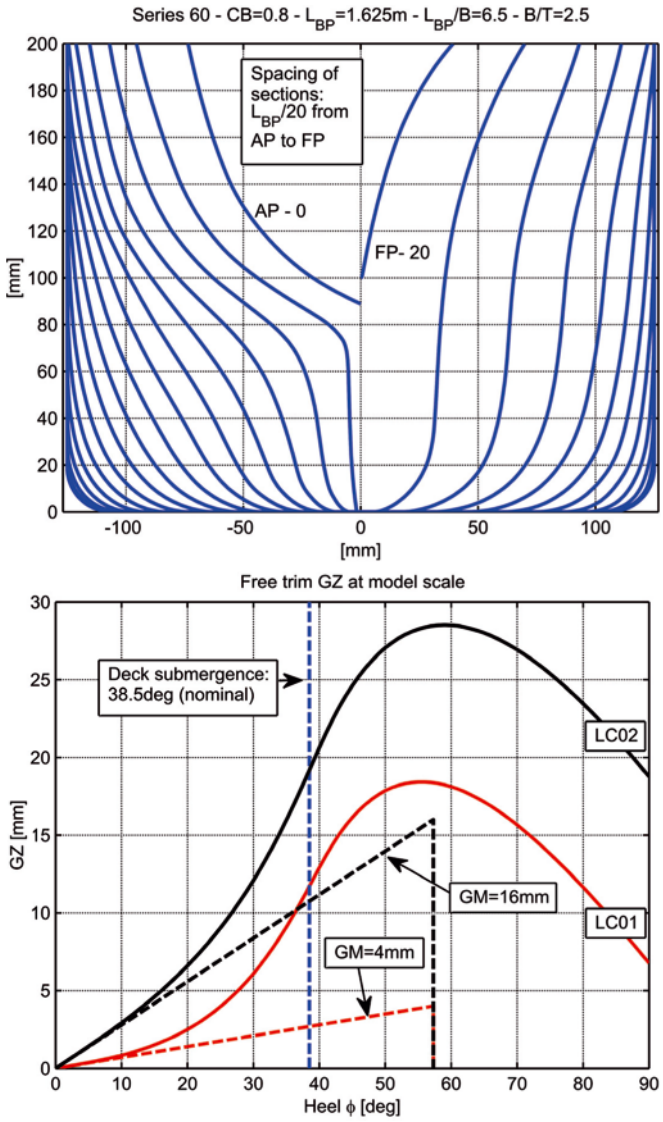

Fig. 1. *Bodyplan of the hull and $\overline{GZ}$ in the considered loading conditions. Model scale*

EXPERIMENTS AND NUMERICAL SIMULATIONS: SELECTED SAMPLE RESULTS

For the two considered loading conditions, LC01 and LC02 (see Table 1), numerical simulations have been carried out in order to compare the numerical predictions and the experimental results. In case of LC01, the (dry) roll moment of inertia was tuned to match the experimental roll natural frequency and roll damping coefficients have been tuned to fit the roll decays. On the other hand, in case of LC02, full tuning was not carried out, because the simulations were carried out before completing the analysis of roll decays. In particular, as said, the roll natural frequency in experiments and simulations is not exactly the same, and this indirectly influences the actual forcing wave length(s). Moreover, the tuning of damping parameters for LC02 was carried out to have a dimensionless roll damping, as a function of roll amplitude, in line with the data for LC01. However, the analyses carried out so far indicate that the roll damping used in the simulations could be smaller than the actual damping and that roll damping in the experiments could be associated with non negligible surface tension effects, which are not modeled in the simulations. The effect of inaccurate damping tuning in LC02 is therefore subject to further investigation. It can nevertheless be said that, in a practical application, it could be possible to imagine that roll damping coefficients from one loading condition could be transferred to another loading condition, in the absence of further information. Moreover, it is also possible that the predicted roll natural frequency could differ from the actually measured roll natural frequency. As such, the results reported in this paper for LC02 could be considered to represent a typical level of discrepancy induced by typical, not perfectly accurate, assumptions on main roll coefficients. In both loading conditions, soft springs for yaw have been introduced, but in LC01 the model is free to drift, while in LC02 soft springs prevents also the drift motion in accordance with the experimental setup. Herein some results are reported in view of the requirements proposed in [9].

First of all we want to check that the simulation model, as expected, is able to reproduce the effect of nonlinear roll restoring and nonlinear damping. Figure 2 shows two simulated roll decays, starting from the same initial angle, for the two loading conditions LC01 and LC02. Together with the time histories of roll, Figure 2 also shows a comparison of the amplitude dependence of oscillation frequency (normalized w.r.t. its value at zero amplitude) and of dimensionless equivalent roll damping, as obtained from processing of the simulated decays. It can be clearly seen that the amplitude dependence of both frequency and damping is modeled in the simulations. Stronger nonlinearities of restoring in condition LC02 lead to stronger relative increase of the oscillation frequency as the amplitude increases. As a consequence of the tuning of damping for condition LC02 on the basis of data from condition LC01, the dimensionless equivalent linear roll damping in both conditions is very close. The increase of the roll damping with the amplitude is a consequence of the presence of inherent nonlinear effects in the mathematical model plus the tuning of additional roll damping coefficients. Figure 3 shows a comparison between the experimental and simulated rolling amplitude in beam regular (monochromatic) waves for condition LC01. It can be seen that the comparison between the experimental results and the numerical simulations is good, although the maximum rolling amplitude for the steepness $s_w = 1/30$ is over predicted by the simulations (better tuning of the damping model could improve the agreement). The drifting speed at high frequency for $s_w = 1/30$ also tends to be over predicted by the simulations, as it can be noticed by the stronger Doppler effect in simulations compared with experiments. The major features of nonlinear rolling in beam waves, i.e. saturation of the amplitude and bending of the response curve, are reproduced. Moreover, as expected, the roll response curves tend to "fold around" the backbone curve obtained from the analysis of roll decays (when considering the oscillation frequency). All the reported outcomes are in line with the requirements in [9].

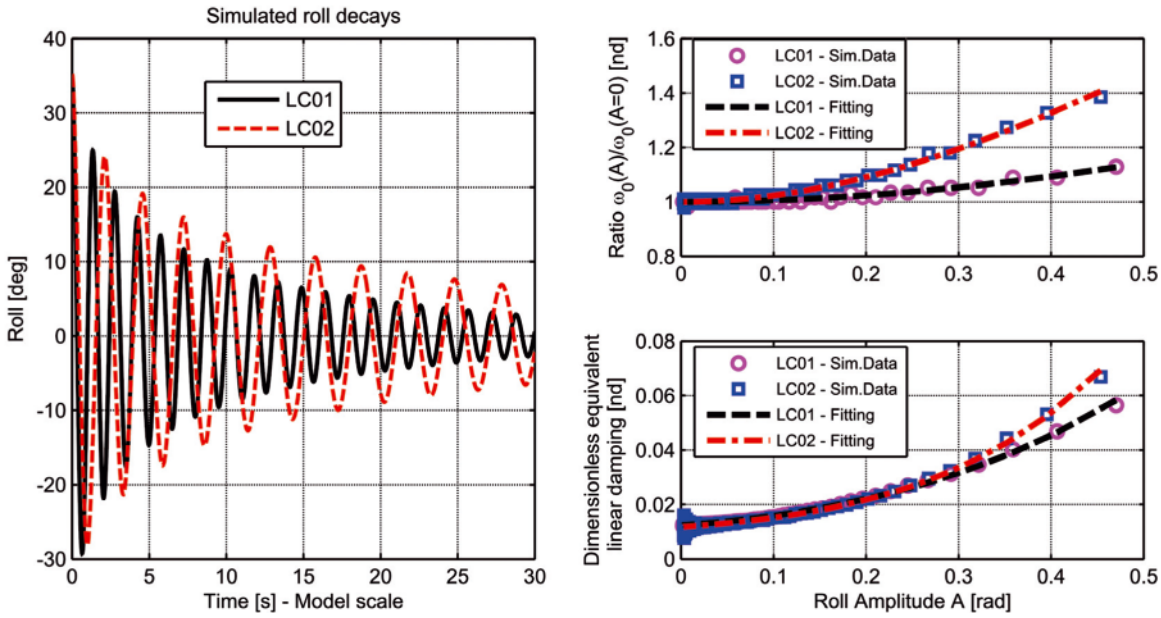

Fig. 2. Simulated roll decays with associated damping/frequency analysis

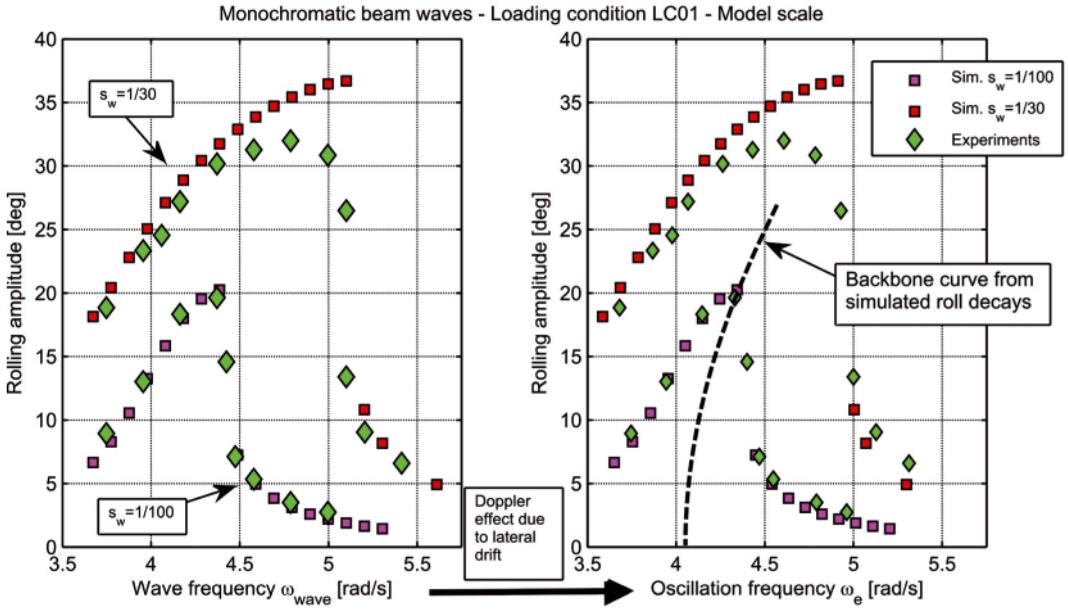

Fig. 3. *Experimental and simulated rolling amplitude in regular beam waves*

The experimental tests carried out in the loading condition LC01 have addressed a well known phenomenon, i.e. nonlinear 1:1 resonant roll in regular beam waves. On the other hand, the experiments carried out in the loading condition LC02, which is characterized by a small metacentric height and thus a strongly nonlinear $\overline{GZ}$ with hardening shape, have instead addressed the occurrence of sub-harmonic roll motion when waves are either bi-chromatic (a useful archetypal model) or irregular (which is a more realistic case). A limited series of tests have also been carried out in mono-chromatic beam waves [21].

In case of bi-chromatic waves [21], two harmonic components have been superimposed, each harmonic with the same ratio between (linear) wave height and wave length (i.e. steepness s_w). The frequencies of the two harmonic components, ω_{2k} and ω_{3k}, have been chosen as two and three times, respectively, a reference frequency ω_{ref}, which was defined in terms of the roll natural frequency ω_0, through a tuning ratio parameter k_{ratio} , i.e.:

$$\omega_{ref} = k_{ratio}\omega_0 \; ; \; \omega_{2k} = 2\omega_{ref} \; ; \; \omega_{3k} = 3\omega_{ref} \qquad (2)$$

The results from the experiments and the 6-DOF simulations are shown in Figure 4. The roll motion is reported in terms of roll standard deviation since, in principle, the time history could be characterized by multiple frequencies. In reality, due to the dominance of the sub-harmonic response at a frequency equal to ω_{ref}, the motion is almost mono-chromatic, hence the amplitude is approximately $\sqrt{2}$ times the roll standard deviation. The experimentally observed sub-harmonic roll response is reproduced by the simulation model. Discrepancies between the simulated roll motion and the experimental results could partially be due to a not very accurate tuning of roll damping, as already pointed out, and due to the difference in the roll natural frequency ω_0 between the experiments and simulations. The bending of the roll response curve observed in the experiments is reproduced by the simulations and the side of the bending, i.e. towards the high frequency region, is consistent with the shape of the roll restoring (hardening type, i.e. more-than-linear type).

Finally, a sample result from tests and simulations in irregular waves is reported in Figure 5. The figure shows

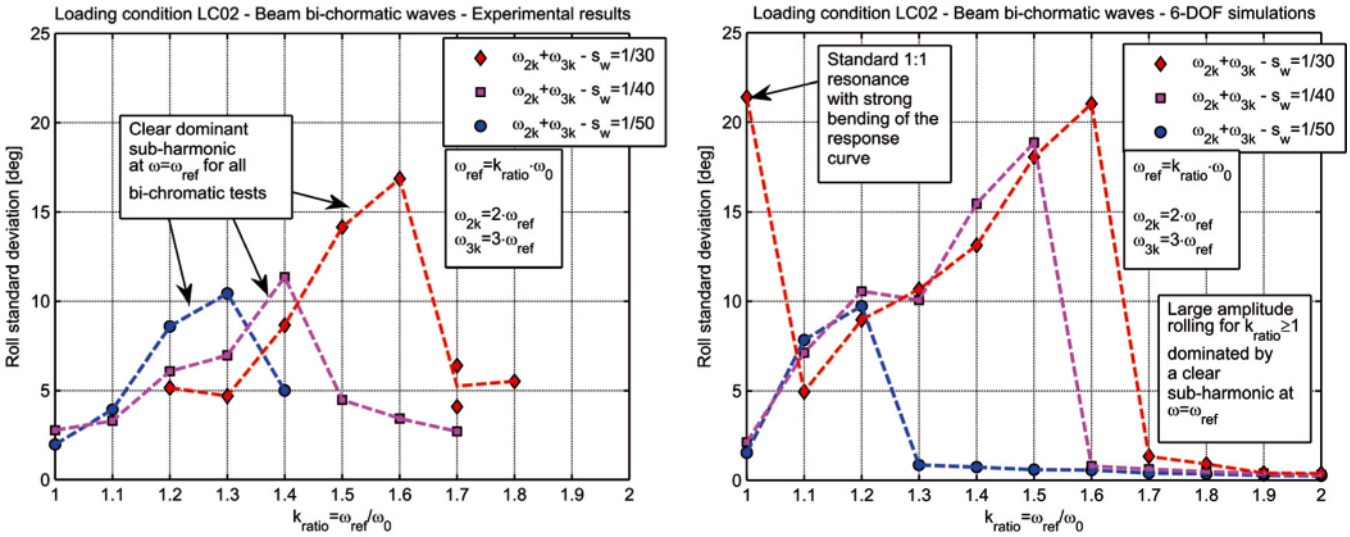

Fig. 4. *Experimental (left) and simulated (right) rolling amplitude. Bi-chromatic beam waves*

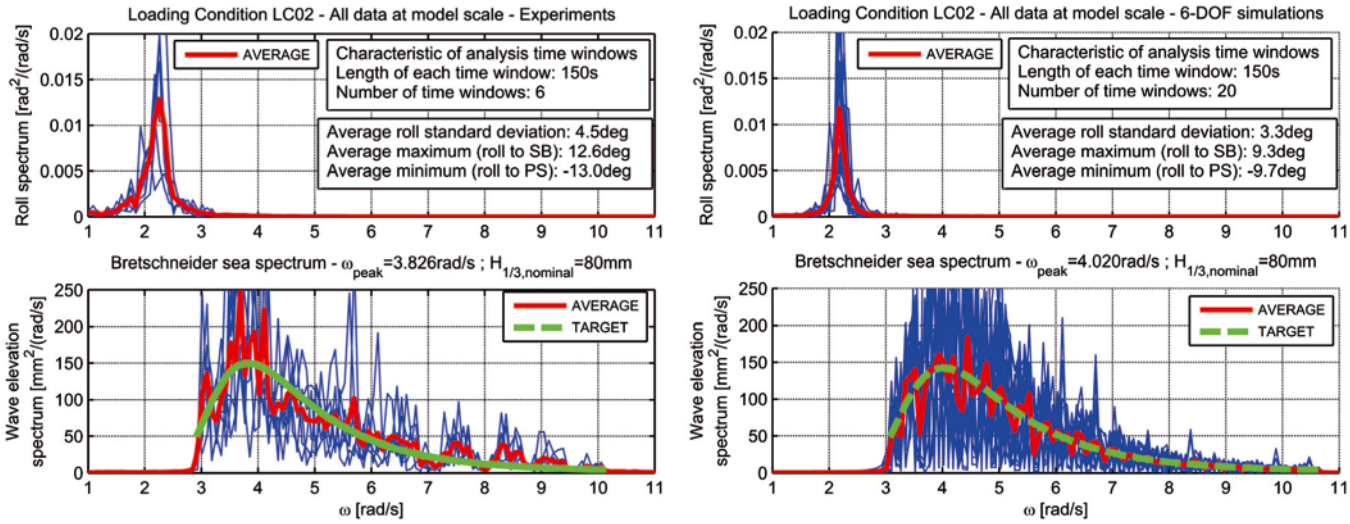

Fig. 5. *Experimental (left) and simulated (right) roll and sea spectra. Irregular beam waves*

the roll spectrum as obtained from the experiments and the simulations when the sea spectrum has a Bretschneider shape, with significant wave height 80mm and peak spectral frequency equal to twice the roll natural frequency (simulations: $\omega_0 = 2.010$ rad/s ; experiments: $\omega_0 = 1.913$ rad/s). It can be seen that the roll motion is completely governed by the sub-harmonic response. This characteristic is observed in experiments and reproduced by simulations. Quantitative agreement between experiments and simulations is good.

It is now worth looking at the results reported in Figure 4 and Figure 5, and link them with the previous discussion regarding the level of simplification which is to be considered as acceptable in the mathematical model for DSA. First of all it must be reported that a relatively "standard" 1-DOF nonlinear roll model based on an absolute angle approach was not able to reproduce the observed sub-harmonic resonances, while a model based on a relative angle approach showed some characteristics of the observed phenomenon, but only from a qualitative point of view [21]. Coming back to the simulations reported in this paper, the mathematical model used in the 6-DOF simulations was developed, originally, without having in mind the possibility of (or need for) simulating the occurrence of sub-harmonic rolling under bi-/multi-chromatic beam sea excitation. Nevertheless, due to the quite general approach, the simulation method has proven to be able to predict the existence of this type of phenomenon, although this was not in the mind of the developer at the moment of the development. If the modeling had been developed only with the intention of simulating 1:1 resonance in beam regular/irregular waves, it is quite possible that the simplifications introduced for tailoring the model to such application could have led to a simulation tool unable to predict the observed behavior. Therefore, as already said, in case of tools intended for DSA application, it is often better (necessary) to keep the underlying mathematical modeling as general as reasonably possible, letting the simulation tool "doing its job" without constraining its behavior.

CONCLUSIONS

In the framework of the development of "Second Generation Intact Stability Criteria" (SGISC), the IMO has started addressing the topic of "Direct Stability Assessment" (DSA), with particular attention to the characteristics and the validation of those numerical tools which are expected to be used for this purpose. In the 3+1 tiers framework of SGISC (vulnerability level 1 and 2, DSA + ship-specific operational guidance), the DSA level is supposed to be applied only in a relatively small fraction of cases and results from calculations carried out at this level are expected to help, if necessary, in the

development of ship-specific "Operational Guidance". Tools to be used at this level are expected to represent the state-of-the-art in the field of simulation of maneuvering and large amplitude ship motions in waves, bearing in mind the need for practical application purposes.

Stimulated by the ongoing discussion, this paper has commented some recent proposals put forward at IMO, linking them with some experimental results and numerical simulations based on a 6-DOF blended code. Topics like the quantitative level of agreement between experiments and simulations, the level of simplification and the risk of inconsistencies in the mathematical models to be used, etc. have been addressed. Several open issues remain on the table, but the example reported in this paper, where a ship with low metacentric height and strongly nonlinear restoring exhibits sub-harmonic resonance in beam bi-chromatic and irregular waves, indicates that too high simplifications in the mathematical models to be used at DSA could lead to the missing of some phenomena, if such phenomena are not in the mind of the developer at the time of developing. For this reason, in case of tools intended for DSA application, it is often better (necessary) to keep the underlying mathematical modeling as general as reasonably possible, letting the simulation tool "doing its job" without constraining its behavior.

The comparison between experiments and simulations, as reported in this paper, has also tried to briefly follow the idea of separating qualitative and quantitative validation, as recently put forward at IMO, for tools to be used at DSA level. The general characteristics of the mathematical model used in the simulation code make it suitable for application at the DSA level and the agreement between the experiments and the simulations has also shown to be in general good.

Acknowledgements

The financial support from "Università degli Studi di Trieste - Finanziamento per Ricercatori di Ateneo (FRA 2011)" is acknowledged. The authors would like to thank Mr. Marco Sinibaldi for the help in the execution of the experimental campaign for loading condition LC02.

REFERENCES

1. SLF54/INF.12: *Information collected by the intersessional Correspondence Group on Intact Stability*, Submitted by Japan, 11 November 2011, London, UK
2. SLF54/INF.12: *Information collected by the intersessional Correspondence Group on Intact Stability*, 11 November 2011, IMO, London, UK
3. SLF54/WP.3: *Report of the working group* (part 1), 19 January 2012, IMO, London, UK
4. Peters, W.S., Belenky, V., Bassler, C., Spyrou, K.: *On Vulnerability Criteria for Parametric Roll and Surf-riding*, Proc. 12th International Ship Stability Workshop, Washington, USA, June 2011.
5. Bulian, G., Francescutto, A.: *Considerations on Parametric Roll and Dead Ship Conditions for the Development of Second Generation Intact Stability Criteria*, Proc. 12th International Ship Stability Workshop, Washington, USA, June 2011.
6. Shigunov, V., Rathje, H., El Moctar, O., Altmayer, B.: *On the Consideration of Lateral Accelerations in Ship Design Rules*, Proc. 12th International Ship Stability Workshop, Washington, USA, June 2011.
7. SLF52/WP.1-Annex 2: *Preliminary Specifications for the New Generation Intact Stability Criteria*, 28 January 2010, London, UK
8. de Kat, J.O., Paulling, J.R.: *The Simulation of Ship Motions and Capsizing in Severe Seas*, Trans. SNAME, Vol. 97, 1989, pp. 139-168
9. SLF54/INF.12-Annex 21: *United States view on direct stability assessment procedures*, Submitted by the United States, 2011
10. Umeda, N., Izawa, S., Sano, H., Kubo, H., Yamane, K., Matsuda, A.: *Validation Attempts on Draft New Generation Intact Stability Criteria*, Proc. 12th International Ship Stability Workshop, Washington, USA, June 2011.
11. ITTC: *Specialist Committee on Prediction of Extreme Ship Motions and Capsizing - Final Report and Recommendations to the 23rd ITTC*, Proc. 23rd ITTC, Venice, Volume II, 2002, pp. 619-748
12. ITTC: *Specialist Committee on Stability in Waves - Final Report and Recommendations to the 26th ITTC*, Proc. 26th ITTC, Rio de Janeiro, Volume II, 2011, pp. 523-560
13. Telste, J. G., Belknap, W. F.: *Potential Flow Forces and Moments from Selected Ship Flow Codes in a Set of Numerical Experiments*, Carderock Division, Naval Surface Warfare Center Report NSWCCD-50-TR–2008/040, 2008, 15'240 p.
14. Belknap, W, Telste, J.: *Identification of Leading Order Nonlinearities from Numerical Forced Motion Experiment Results*. Proc. 27th Symposium on Naval Hydrodynamics, Seoul, Korea, 2008
15. Reed, A.M.: *A Naval Perspective on Ship Stability*, Proc. 10th International Conference on Stability of Ships and Ocean Vehicles (STAB2009), St.Petersburg, 2009, pp.21-44
16. Story, W.R., Xing, Z., Wu, W., McCue, L.: *Validation: A Historical Look and Two Suggested Techniques*, Proc. ITTC Workshop on Seakeeping - V&V for Nonlinear Seakeeping Analysis, October 2010, Seoul, Korea, pp. 214-246
17. Spanos, D., Papanikolaou, A.: *SAFEDOR International Benchmark Study on Numerical Simulation Methods for the Prediction of Parametric Rolling of Ships in Waves*, Revision 1.0, 30 June 2009, http://www.naval.ntua.gr/sdl/sibs.
18. Francescutto, A.: Intact Ship Stability: *The Way Ahead*, Marine Technology, Vol.41, 2004, pp.31-37
19. Tzamtzis, S.: *Development and testing of a procedure for the alternative assessment of Weather Criterion on experimental basis*, Diploma Thesis, University of Trieste and National Technical University of Athens, Academic Year 2003-2004.
20. Bulian G., Francescutto, A.: *Effect of roll modelling in beam waves under multi-frequency excitation*, Ocean Engineering, Vol. 38, Issue 13, September 2011, pp. 1448–1463
21. Bulian, G., Francescutto, A., Sinibaldi, M.: *Roll motion of a ship with low metacentric height in bi-chromatic beam waves*, Proc. of the 11th International Conference on the Stability of Ships and Ocean Vehicles (STAB2012), 23-28 September 2012, Athens, Greece, pp. 187-200
22. Bulian, G., Francescutto, A.: *SAFEDOR benchmark on parametric roll - Brief description of the simulation methodology employed in the code SHIXDOF under development at DINMA*, Internal Technical Report, Department DINMA, University of Trieste, Trieste, Italy, 2008.
23. IMO: *International Code on Intact Stability, 2008 - 2009 Edition*, 2009, ISBN 978-92-801-1506-2
24. IMO SLF54/INF.12-Annex 3: *On the Consideration of Lateral Accelerations in Ship Design Rules*, Submitted by Germany, 2011, (SLF54/INF.12 submitted by Japan)
25. Fujiwara, T, Ikeda, Y.: *Effects of roll damping and heave motion on heavy parametric rolling of a large passenger ship in beam waves*, Proc. 9th International Ship Stability Workshop, Hamburg, Germany, 2007
26. SLF54/INF.12-Annex 22: *Comments on the United States Submission for Direct Stability Assessment Procedures*, Submitted by Japan, 2011
27. Wheeler, J.D.: *Method for Calculating Forces Produced by Irregular Waves*, Offshore Technology Conference, Dallas, Texas, US, Paper No. 1006, 1969
28. Du, S.X., Hudson, D.A., Price, W.G., Temarel, P.: *Implicit expressions of static and incident wave pressures over the instantaneous wetted surface of ships*, Proc. IMechE Part M: J. Engineering for the Maritime Environment, Vol. 223, 2009, pp. 239-256
29. Faltinsen, O.M.: *Sea Loads on Ships and Offshore Structures*, Cambridge University Press, 1990

30. Matusiak, J.: *On the non-linearities of ship's restoring and the Froude-Krylov wave load part*, 2010, Proc. ITTC Workshop on Seakeeping - V&V for Non-linear Seakeeping Analysis, October 19-21, Seoul National University, Seoul, Korea, pp. 151-159
31. Ayaz, Z., Vassalos, D., Spyrou, K.J.: *Manoeuvring behaviour of ships in extreme astern seas*, Ocean Engineering, Vol. 33, 2006, pp. 2381-2434
32. IMO MSC.1/Circ.1200: *Interim Guidelines for Alternative Assessment of the Weather Criterion*, 24 May 2006, London, UK
33. Bulian, G., Francescutto, A., Fucile, F., Cafagna, F., Genuzio, D.H., Maccari, A.: *Heeling moment in the alternative assessment of the Weather Criterion: direct experiments and numerical simulations*, Proc. 4th International Maritime Conference on Design for Safety and 3rd Workshop on Risk-Based Approaches in the Marine Industries - Part I, 18-20 October 2010, Trieste, Italy, pp. 107-121
34. Francescutto, A., Serra, A.: *Experimental tests on ships with large values of B/T, OG/T and roll period*, Proc. 6th International Stability Workshop, New York, 2002
35. Kuroda, T., Ikeda, Y.: *Extreme Roll Motion in Wide Frequency Range Due to Drift Motion*, Proc. 6th International Stability Workshop, New York, 2002
36. ITTC: Recommended Procedures - Model Tests on Intact Stability - 7.5-02-07-04.1", 2008
37. Cummins, W.E.: *The Impulse Response Function and Ship Motions*, Schiffstechnik, Vol. 47, 1962, pp. 101-109
38. Bailey, P.A., Price, W.G., Temarel, P.: *A Unified Mathematical Model Describing The Manoeuvring of a Ship Travelling in a Seaway*", Trans. RINA, 1998, Vol. 140, pp. 131-149
39. Clarke, D., Gedling, P., Hine, G., "The Application of Manoeuvring Criteria in Hull Design Using Linear Theory", Trans. RINA, Vol. 125, 1983, pp. 45-68
40. Karasuno, K., Okano, S., Miyoshi, J., Maekawa, K.: *Predictions of ship's hull hydrodynamic forces and maneuvering motions at slow speed based on a component-type mathematical model*, Proc. MARSIM2003, Kanazawa, Japan, 25-28 August, 2003, RC-4-(1-11)
41. Artyszuk, J.: *A Non-Uniform Current in Ship Manoeuvring*, Proc. MARSIM2006 - International Conference on Marine Simulation and Ship Manoeuvrability, Terschelling, the Netherlands, June, 2006

CONTACT WITH THE AUTHORS

Gabriele Bulian, Ph.D.
Alberto Francescutto, Prof.
Department of Engineering and Architecture
University of Trieste
Via A. Valerio, 10
34127 Trieste, ITALY
e-mail: gbulian@units.it ; francesc@units.it

POLISH MARITIME RESEARCH 4(80) 2013 Vol 20; pp. 62-70
10.2478/pomr-2013-0042

Effect of material on hydro-elastic behaviour of marine propeller by using BEM-FEM hybrid software

Hassan Ghassemi, Prof.,
Morteza Ghassabzadeh, Ph.D.,
Maryam Gh. Saryazdi, Ph.D.,
Amirkabir University of Technology, Tehran, Iran

ABSTRACT

This paper studies the effect of material on the hydro-elastic behaviour. The geometry of flexible propeller changes due to hydrodynamic and inertial forces acting on the propeller. By using prepared software (called HYDRO-BEM and ELASTIC-FEM) the hydro-elastic features of the propeller made of various materials are analyzed. In the software the hybrid boundary element and finite element methods are used. First, the load acting on the propeller is determined by using the BEM and deformed propeller geometry is then obtained by the FEM. In the next step, the load on the deformed propeller is determined by the BEM and a new shape is obtained. The iterative procedure is repeated till the blade deflection and hydrodynamic characteristics (thrust, torque and efficiency) of the propeller become converged. Four different materials are examined. It is concluded that the hydro-elastic behaviour of the composite propeller is strongly affected by its flexibility due to light material.

Keywords: hydro-elasticity; propeller characteristics; deformed blade;
HYDRO-BEM software; ELASTIC-FEM software

INTRODUCTION

Marine propeller is a lifting body which generates thrust to overcome ship's resistance. It consists of a number of blades which rotated by the shaft. The loads acting on the blades are the hydrodynamic and mechanical forces. The performance of propellers is usually determined on the basis of their geometry in rigid state. However, in operating conditions the geometry of the flexible propeller will be deformed due to hydrodynamic loads. The hydro-elastic analysis considers the effect of fluid flow on the structures and the interaction of the fluid and structures. Therefore, it is essential to study the effect of deformations on the performance of propeller to optimize its design.

In primary research works the forces acting on the blades and their stress-strain reactions are calculated by using analytical and experimental relations. Sontvedt [1] achieved, using the shell elements, the results for prediction of quasi-static and dynamic stresses in marine propeller blades. Young [2] presented a coupled boundary element method (BEM) and finite element method (FEM) for the numerical analysis of flexible composite propellers in uniform flow and wake inflow. This research is extended to the fluid–structure interaction analysis of flexible, composite marine propellers subjected to hydrodynamic and inertial loads. The hydrodynamic blade loads, stress distributions, and deflection patterns of flexible composite propellers can be predicted by the method [3]. A coupled structural and fluid flow analysis was performed to assess the hydro-elastic behaviour of a composite marine propeller [4]. A MAU 3-60 propeller was analyzed with different stacking sequences of composite lay- up. The hydro-elastic behaviour of the propeller with balanced and unbalanced stacking sequences were investigated and discussed by Lin *at al.* [5]. Mulcahy *et al.* [6] carried out a comprehensive work on the hydro-elastic tailoring of the flexible composite propeller.

Blade stress-strain relation of the marine propeller was analyzed by Chau [7]. Recently, Koronowicz *et al.* [8] presented the comprehensive computer program to account for the hull-propeller-rudder system in the propeller design process. The program outcome includes the hydrodynamic performance, cavitation effect, blade strength and efficiency optimization.

The SPD (Ship Propeller Design) software has been recently prepared by Ghassemi (the first author of this paper) and applied to various propulsors such as propeller-rudder system (PRS) [9], high-skew propeller [10], contra-rotating propeller [11] and surface piercing propeller (SPP) [12]. This software uses the BEM including boundary layer theory to determine the hydrodynamic analysis of marine propeller.

In recent years, polymer materials have entered to the marine market due to some advantages. Polymer propeller is nowadays used for the marine crafts especially for the SPPs. The SPD laboratory team (at AUT) is focused on the research analysis of characteristic hydro-elastic problems of various propulsors.

In this paper the effect of elastic deformation on the propeller performance such as its efficiency, thrust and torque coefficients is examined for various materials by using the hydro-elastic analysis. To determine the shape of the propeller, in a boundary element code an iteration method is used in which the hydrodynamic forces acting on the blades are determined by modelling the fluid-structure interaction. The deformation of the blades is then calculated by using a finite element model. The geometry of the deformed propeller is determined for four different materials and the effect of deformations on the propeller performance is examined for several values of advance coefficient. The software for the BEM-FEM analysis is described in Section 2, numerical results are discussed in Section 3, and conclusions are given in Section 4.

HYDRO-BEM AND ELASTIC-FEM SOFTWARE

Boundary element for hydrodynamic analysis

The thrust and torque generated by the propeller depend on two parameters of pressure and friction. The thrust is almost entirely due to the pressure distribution. For this reason, the potential theory may be used to calculate the hydrodynamic characteristics of the propeller. The BEM is applied to boundary surface of the propeller and its trailing vortex surface which should be discretized into quadrilateral elements (Fig. 1 and 2). Then boundary value problems should be solved to determine the velocity potential. Since the propeller is a lifting body the Kutta condition should be satisfied - as an essential boundary condition - for the propeller. By using the boundary element techniques and boundary layer theory the hydrodynamic pressure and tangential stress are determined as follows:

$$P_h = 0.5\rho\,(2\vec{V}_R.\nabla\phi - \nabla\phi.\nabla\phi) \tag{1}$$

$$\tau = 0.5\rho C_f \vec{V}_R^{\,2} \tag{2}$$

where:

$\nabla\phi$ – derivative of the velocity potential,
ρ – density of water,
C_f – frictional coefficient determined from ITTC empirical formulae,
$\vec{V}_R$ – inflow velocity equal, in case of propeller, to:
u_a, u_t – induced velocities determined by means of the derivative of velocity potential, as shown in Fig. 3.

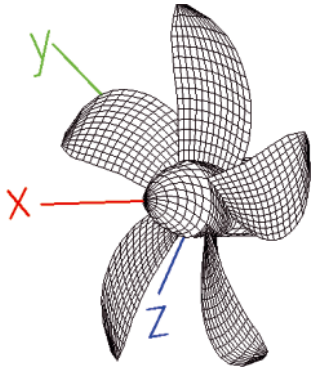

Fig. 1. *The global Cartesian system of the propeller*

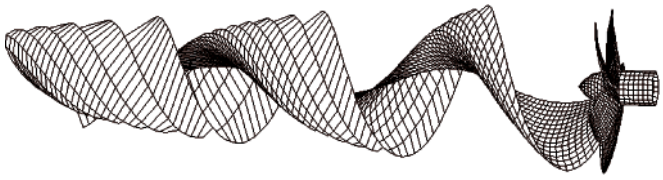

Fig. 2. *Trailing vortex wake of the propeller*

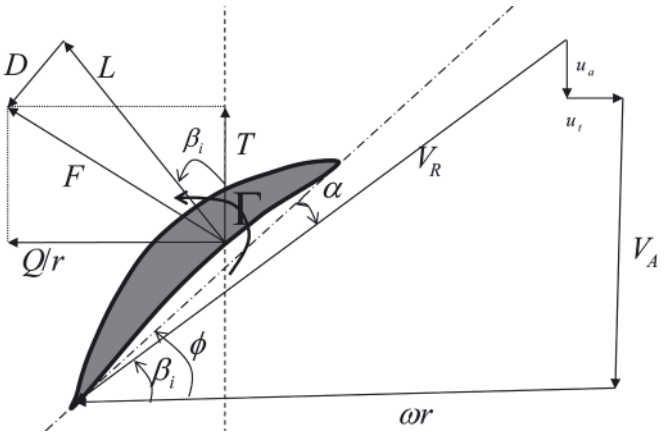

Fig. 3. *Inflow velocity and hydrodynamic forces acting on the blade at radius r*

Finally, the total thrust and torque of the propeller are determined as follows:

$$T = \int_S P_h dS_x + \int_S \tau dS_x \tag{3}$$

$$Q = \int_S P_h.r.dS_{yz} + \int_S \tau.r.dS_{yz} \tag{4}$$

The following non-dimensional coefficients are used to express the general characteristics of the propeller:

Thrust coefficient:

$$K_T = \frac{T}{\rho n^2 D^4} \tag{5}$$

Torque coefficient:

$$K_Q = \frac{Q}{\rho n^2 D^5} \tag{6}$$

Efficiency:

$$\eta = \frac{TV_A}{2\pi nQ} = \frac{J}{2\pi}\frac{K_T}{K_Q} \tag{7}$$

Advance coefficient:

$$J = V_A/nD \tag{8}$$

As an example, the propeller efficiency curve for the rigid propeller is shown in Fig. 4.

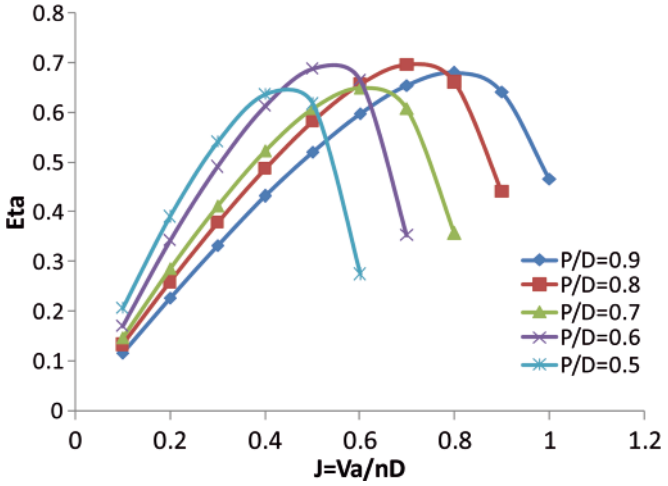

Fig. 4. *Propeller efficiency curve obtained from SPD software*

Finite element for elastic analysis

The finite element method (FEM) is used for structural analysis in elastic domain. For this purpose, a finite element program is prepared for the elastic analysis. A macro is generated and sent to the FEM program in which the blade

geometry is generated automatically by using the general characteristics of the propeller. And, the boundary conditions and loads are applied. The FEM model of propeller is then analyzed and the resulting data are sent to the output file.

In the generated macro the geometry model is formed according to the coordinates x, y, z of the points used in the BEM model. Therefore the results from the FEM can be simply transferred to the BEM software. The geometry model is meshed regularly with the 3D solid element of 20 nodes. It is clear that the loading conditions of blades depend on their position. In every revolution the maximum load is applied to each blade once. In the vertical and downward position the critical load is applied to each blade. In this situation the gravity and centrifugal forces act in the same direction. In addition the summation of the atmospheric pressure (P_0), hydrostatic pressure (due to head of water above the hub axis) and hydrodynamic pressure (P_h) are applied onto the surface blade. Hydrodynamic pressure values are calculated by using the BEM program and sent to the FEM. The total pressure is determined for each element as follows:

$$P = P_h + P_0 + \rho.g.(Y_{CE} + H) \tag{9}$$

where:
H – depth of the hub axis below the free surface,
Y_{CE} – position of element centre in y - direction.

It should be noted that for the horizontal shaft the Coriolis effect is eliminated because the linear velocity and rotary velocity vectors are parallel to each other.

The procedure of the proposed method

The algorithm of the proposed method is shown in Fig. 5. First, the undeformed blade is analyzed in the HYDRO-BEM software in which the fluid-structure interaction is considered to determine the hydrodynamic forces, efficiency, K_{T1} and K_{Q1} coefficients. The deformations of the blade are then determined by using the ELASTIC-FEM software. In the second step, the hydrodynamic forces, efficiency, K_{T2} and K_{Q2} coefficients are determined based on the deformed shape of blade obtained from the BEM software. The deformations of the blade are calculated in the FEM software again based on new calculated hydrodynamic forces. By comparing the results from the two steps the convergence of values of the selected parameters (i.e. the maximum deflection, efficiency, K_T and K_Q), is checked. The procedure continues until convergence of values of the selected parameters is obtained. In the final step the deformed shape of blade and other parameters are calculated.

NUMERICAL RESULTS

In this study a five-blade propeller is selected to examine the effect of deformations on the propeller performance. The main dimensions of the propeller and the blade profile data are given in Tab. 1 and 2, respectively. The analysis is performed for four different materials: 13 % Chromium stainless steel, copper-nickel-aluminium alloys, high tensile- copper- brass and a polymer. The propeller material properties are listed in Tab. 3.

Tab. 1. *Main dimensions of the propeller*

Number of blades	5
Diameter [m]	0.35
Hub ratio (r_h/R)	0.2
Expanded Area Ratio (EAR)	0.65
Skew angle [deg.]	15
Rake angle [deg.]	10

Tab. 2. *Maximum thickness, chord and pitch ratios of the propeller*

r/R	Thickness ratio (t/D)	Chord ratio (c/D)	Pitch ratio (P/D)
0.2	0.041	0.3183	0.5312
0.25	0.0385	0.3478	0.5528
0.30	0.036	0.375	0.5756
0.35	0.0334	0.3998	0.5981
0.40	0.0309	0.4218	0.6194
0.45	0.0284	0.4409	0.638
0.50	0.0258	0.457	0.6519
0.55	0.0233	0.4695	0.6608
0.60	0.0208	0.4774	0.6668
0.65	0.0182	0.4786	0.6711
0.70	0.0157	0.4702	0.6737
0.75	0.0132	0.451	0.6731
0.80	0.0106	0.4197	0.6677
0.85	0.0081	0.3622	0.6573
0.90	0.0056	0.2513	0.6406
0.95	0.0044	0.2412	0.6301
1.00	0.003	0.0238	0.6059

Tab. 3. *Material properties of the propellers*

Material	E (Gpa)	Poison coeff. (ν)	Specific gravity (ton/m³)	Tensile strength (Mpa)
13% Chromium Stainless steel	196.133	0.3	7.7	690
Copper-nickel-aluminium alloys	122.58	0.33	8.25	640
Copper high-tensile brass	102.97	0.35	7.6	540
Polymer material	3.19	0.39	1.15	95

In the analysis, for the sake of simplicity and time saving, only one blade of the propeller is modelled. The forces acting onto the propeller include the hydrodynamic loads (thrust and torque), centrifugal and gravity forces. The maximum force acts on the blade in the vertical and downward position because the centrifugal and gravity forces are in the same direction. The blade is deformed mostly due to the thrust and torque and the centrifugal force may be of special importance for high-rotating-speed. It is noted that skew and rake of propeller lead to an additional bending moment exerted to the blade.

Based on the flow chart presented in Fig. 5, the three-dimensional propeller and loads acting on the un-deformed blade are calculated by means of the HYDRO-BEM software and then sent to the ELASTIC-FEM software. The geometry model of the blade is shown in Fig. 6 (a) and (b). Because of the complicity of the blade shape the blade geometry is

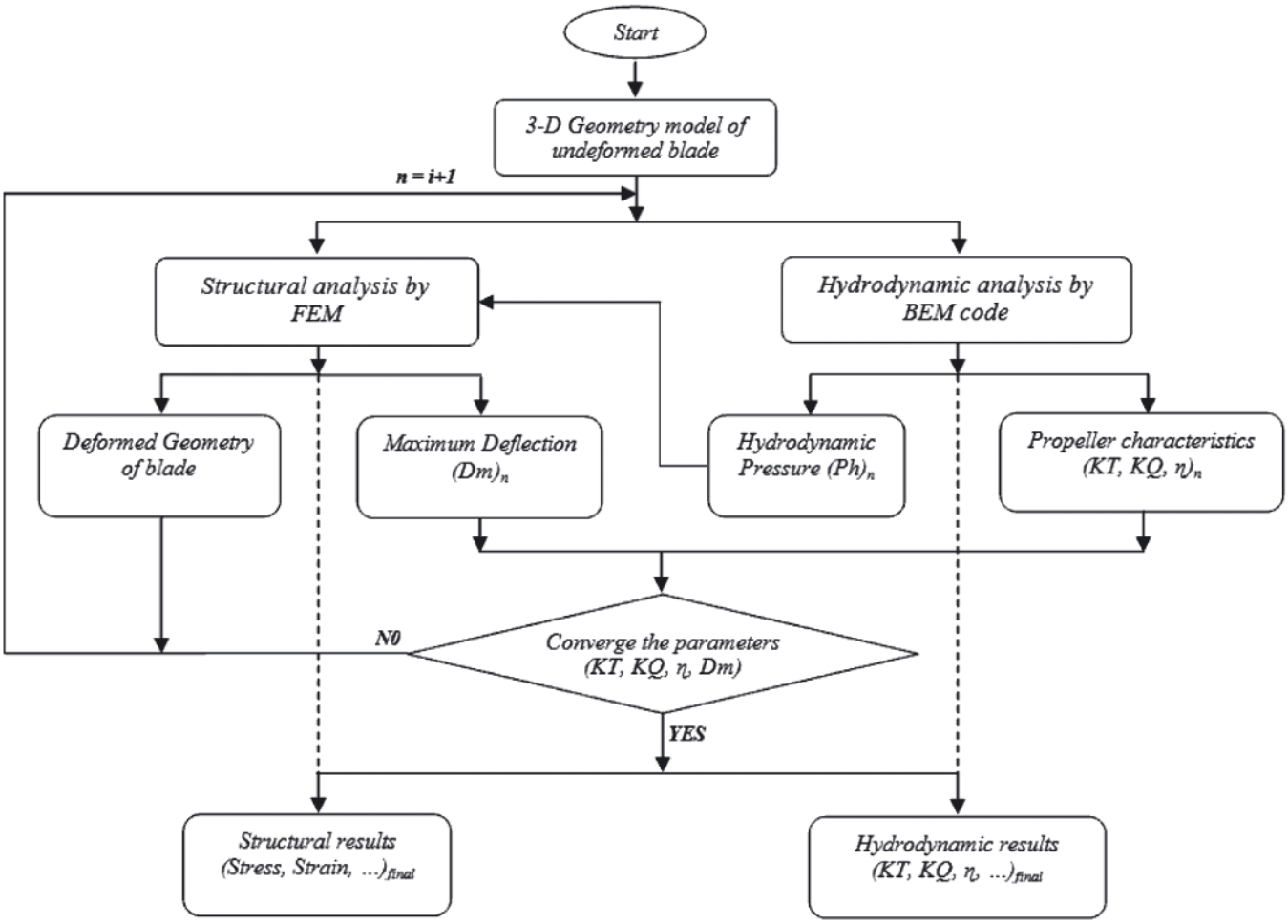

Fig. 5. Flow chart of the proposed computational method

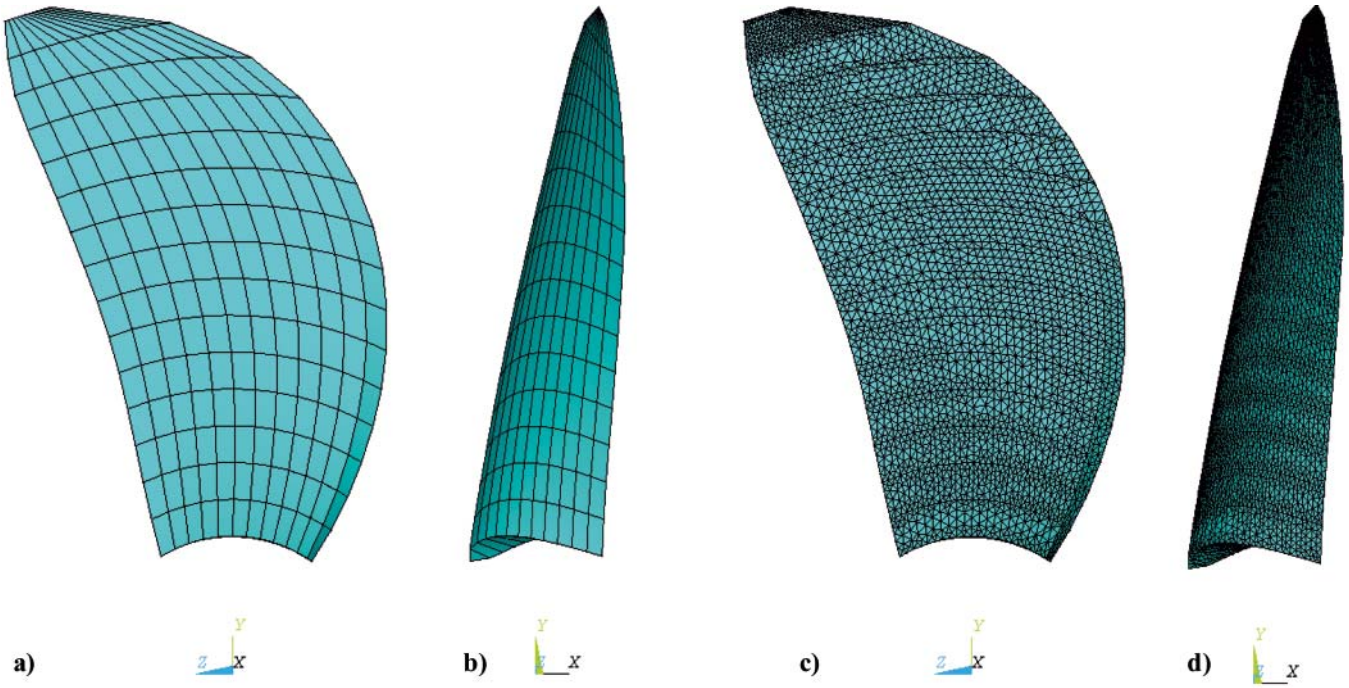

Fig. 6. The mesh generated on the blade surface (a, b), and the finite element mesh of the blade (c, d)

divided into several volumes. This helps to create an accurate model of the blade geometry. Fig. 6 (c) and (b) show the finite element model of the blade. To achieve a grid independent on the model, several FEM models with different element size are formed. The size of elements is then reduced step by step until the results converge appropriately.

The root of blade is assumed fixed. The hydrodynamic pressure is calculated by using the boundary element software. The elastic analysis of the blade is then performed by the finite element software to calculate deformation of the blade. This procedure is repeated until values of the maximum deformation, efficiency, thrust coefficient and torque coefficient converge.

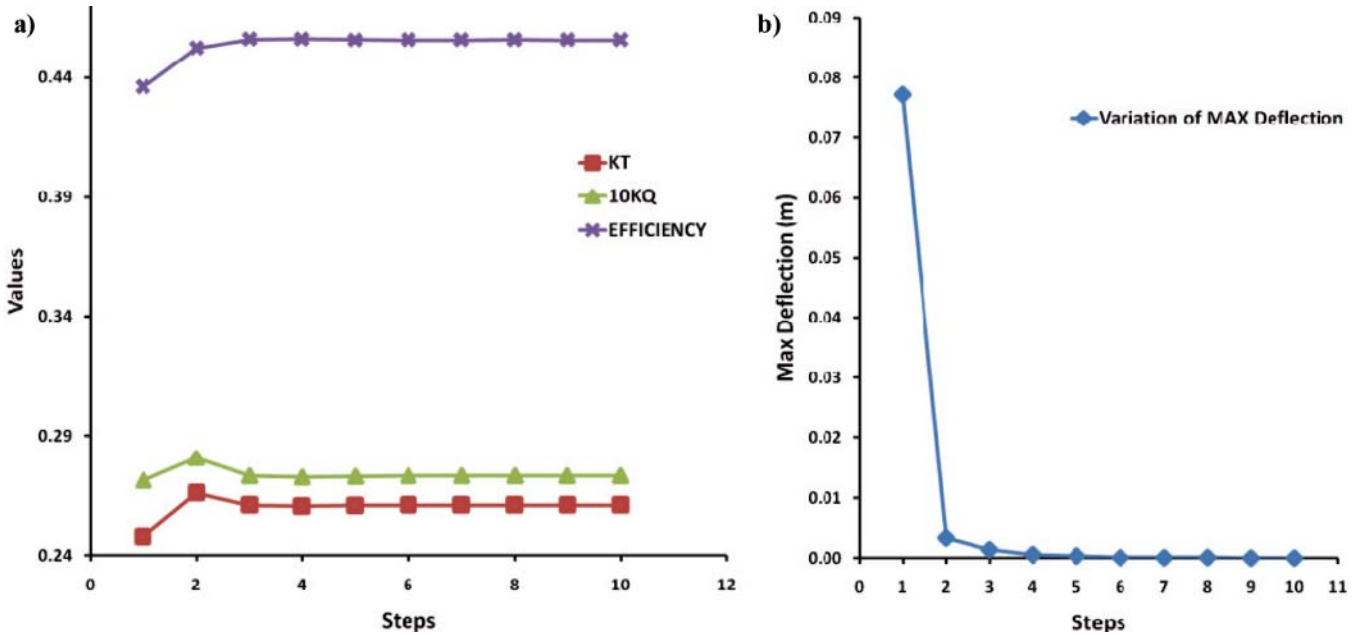

Fig. 7. *Calculation convergence steps of the K_T, K_Q, efficiency and maximum deflection for polymer (nylon) blade at J = 0.3*

Fig. 7 shows the convergence of the values of these parameters for the polymer blade at J = 0.3. The variations of the parameters vanish after 10 steps of hydro-elastic analysis. The hydro-elastic analysis of each blade is performed for the five values of advance coefficient: J = 0.3, 0.4, 0.5, 0.6 and 0.7. Fig. 8 shows the pressure distribution on the face and back side of the undeformed and deformed polymer propeller. Fig. 9 shows the total pressure vector on the surface of steel blade at J = 0.3

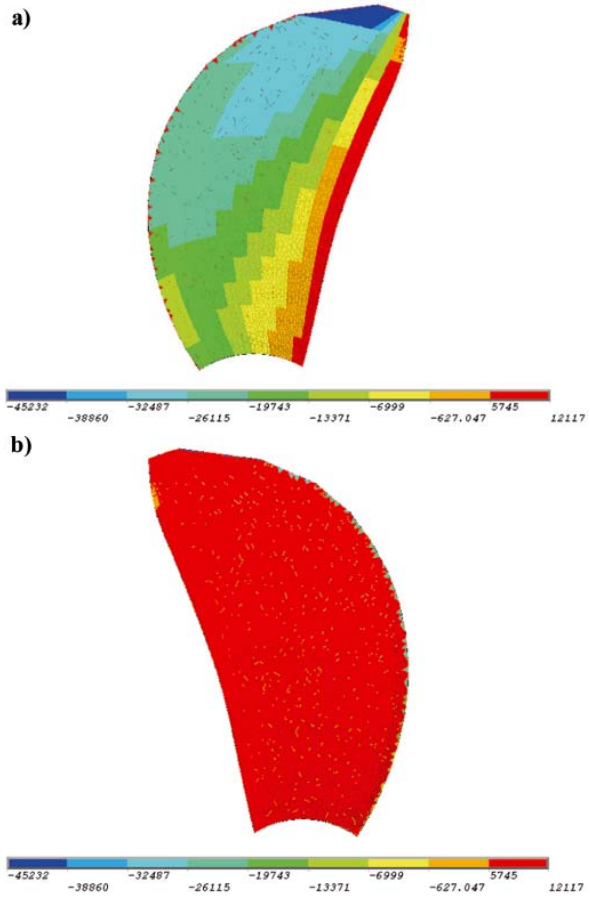

Fig. 8. *The hydrodynamic pressure distribution on polymer blade:* ***a)*** *undeformed back side,* ***b)*** *undeformed face side,* ***c)*** *deformed back side,* ***d)*** *deformed face side*

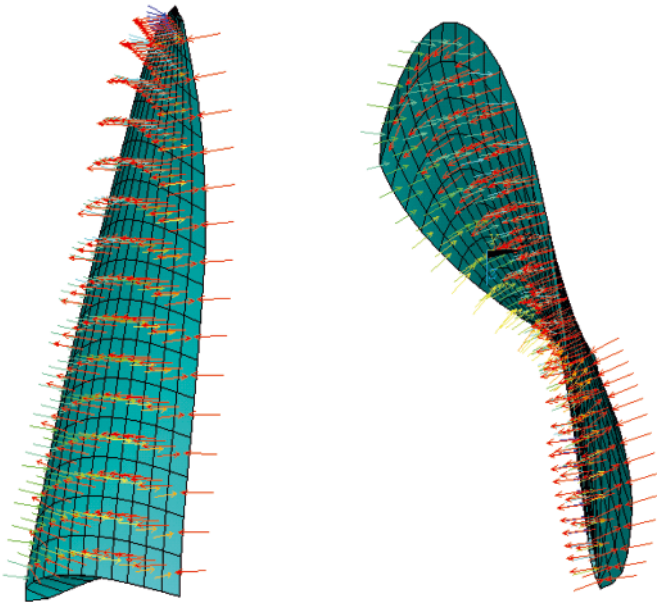

Fig. 9. *Pressure applied to the blade surface at J = 0.3*

The undeformed and deformed shape of polymer blade for J = 0.3 is shown in Fig. 10. The maximum principal stress of the copper–brass blade at J = 0.3 is shown in Fig. 11. The principal stress is negative on the back side of the blade except near the trailing and leading edges. The maximum tensile stress occurs in the middle of blade root at the face side. The similar stress field can be achieved from the hydro-elastic analysis of the blade for other values of J, however the maximum stress decreases with the increasing of advance coefficient values. The deformation field of the copper-brass blade is shown in Fig. 12. The deformation increases toward the blade tip due to increase of centrifugal force, hydrodynamic pressure and cantilever-mode behaviour of the blade.

The maximum deflection of the blade versus the advance coefficient (J) is shown in Fig. 13 for three different metal materials. Because the maximum deflection of the polymer blade is much greater, it is separately shown in Fig. 14. The thrust coefficient versus the advance coefficient J for deformed and undeformed propeller, is shown in Fig. 15. It is found

Fig. 10. Deformed and undeformed shape of the polymer blade at J = 0.3

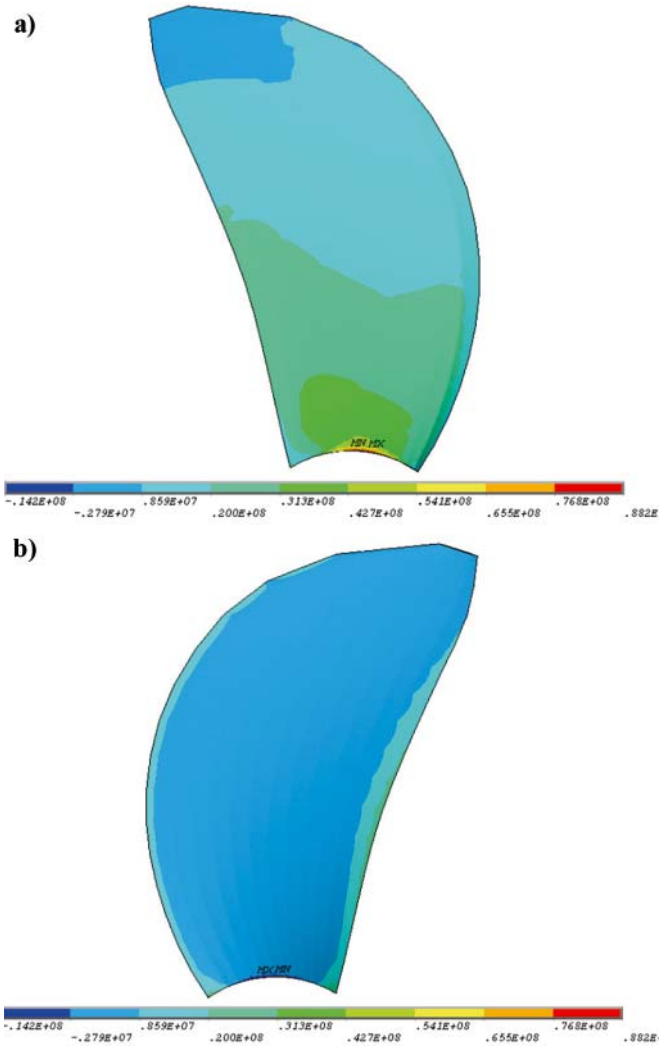

*Fig. 11. Maximum principal stress of the cooper brass blade at J = 0.3, **a)** at the face side, **b)** at the back side*

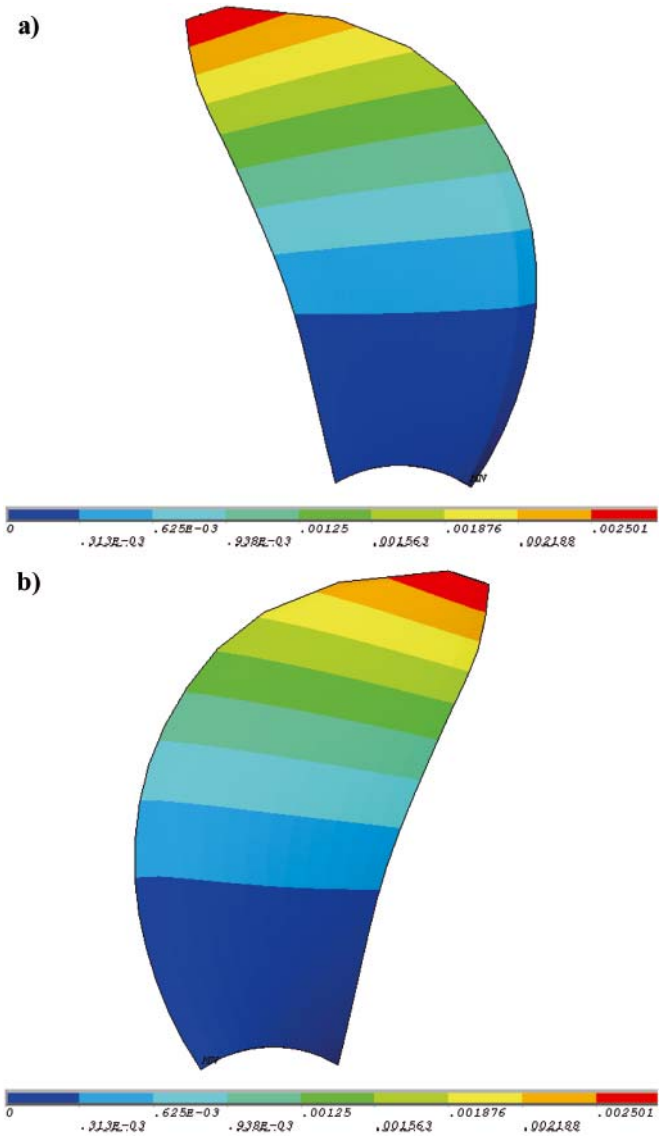

*Fig. 12. Deformation of the copper brass blade at J = 0.3, **a)** at the face side, **b)** at the back side*

that the thrust coefficient decreases with the increasing of advance coefficient, J. Except the polymer propeller, the thrust coefficient of the deformed blade is greater than that of the undeformed blade for all advance coefficient values. However, the thrust coefficient of the polymer blade is greater than that of the undeformed blade for $J < 0.52$ and smaller than that for $J > 0.52$. Moreover, the changes of this parameter for the polymer blade are greater than for other blades. Fig. 16 shows the torque coefficient versus the advance coefficient, J for deformed and undeformed propellers. The torque coefficient variations are similar to those of the thrust coefficient. The propeller efficiency versus the advance coefficient J is shown in Fig. 17. The maximum efficiency of undeformed blade occurs at $J = 0.52$. For $J < 0.4$, the efficiency of the deformed metal propellers is equal to that of the undeformed one, but for $J > 0.4$ the efficiency of the deformed propeller is higher than that for the undeformed one. The efficiency of the deformed polymer (blade) propeller is higher than that of the undeformed one for $J < 0.52$. However, for $J > 0.52$ the efficiency of the deformed polymer propeller is less than that of the undeformed one.

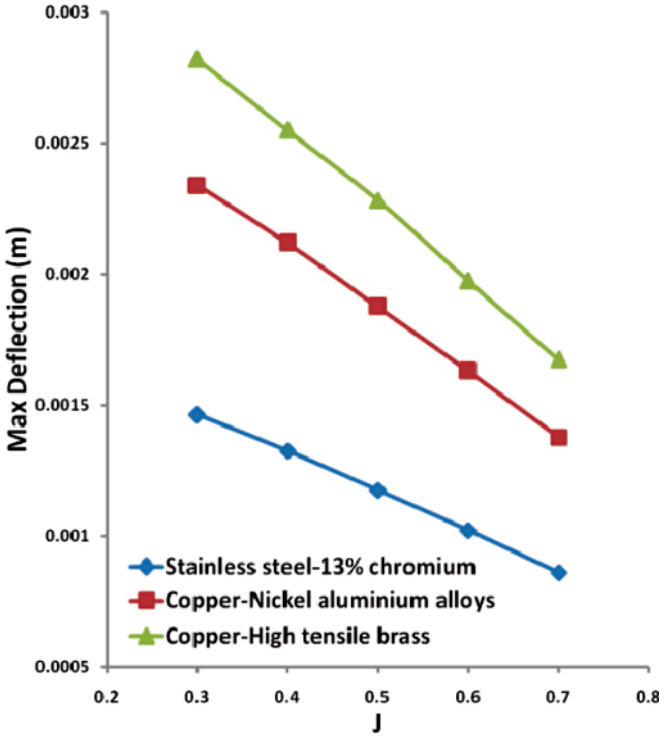

Fig. 13. Maximum deflection versus advance coefficient for the used metal materials

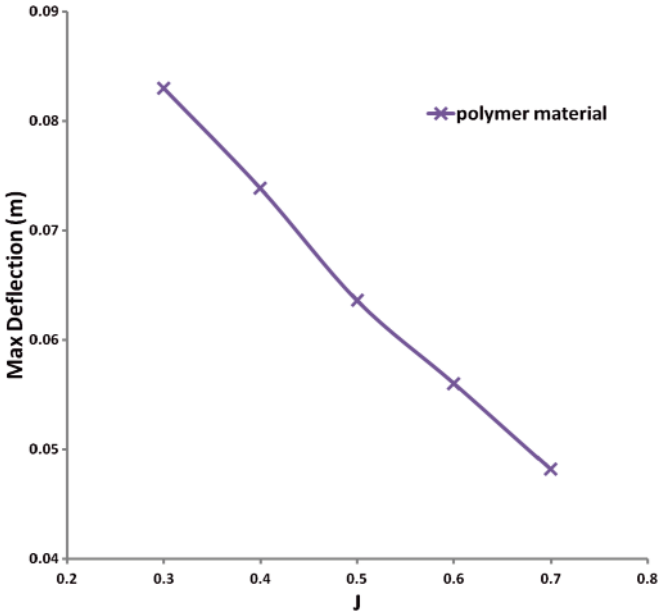

Fig. 14. Maximum deflection versus advance coefficient for the used polymer material

The relative variations of propeller characteristics, related to un-deformed blade, are calculated as follows:

$$\begin{cases} \Delta K_{Tr} = \dfrac{K_T - K_{T0}}{K_{T0}} \times 100 \\ \Delta K_{Qr} = \dfrac{K_Q - K_{Q0}}{K_{Q0}} \times 100 \\ \Delta \eta_r = \dfrac{\eta - \eta_0}{\eta_0} \times 100 \end{cases} \tag{10}$$

where index of "0" stands for undeformed blade.

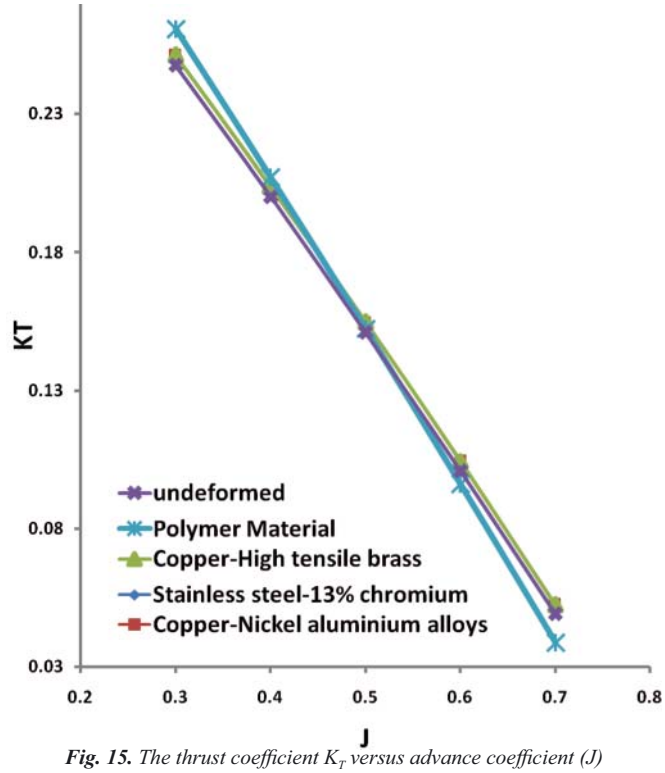

Fig. 15. The thrust coefficient K_T versus advance coefficient (J) for the used materials

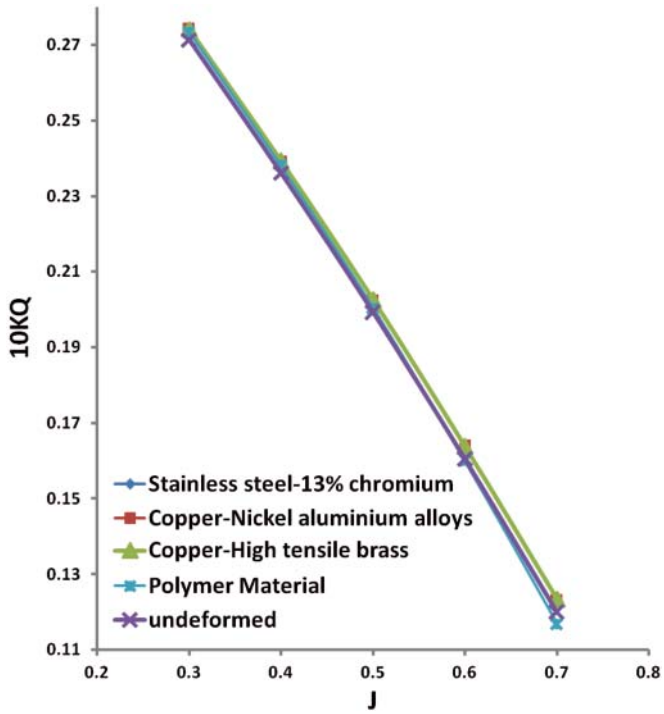

Fig. 16. The torque coefficient K_Q versus advance coefficient (J) for the used materials

Fig. 18, 19 and 20 show the curves of ΔK_{Tr}, ΔK_{Qr} and $\Delta \eta_r$ versus J, respectively. It is found that the effect of deformation on ΔK_{Qr} is lower than that on ΔK_{Tr} and $\Delta \eta_r$. The parameters increase along with J increasing for the metal propellers, but the trend is opposite for the polymer propeller.

In order to show the effect of material, the ratio of elastic modulus and specific density (E/ρ) is calculated for four materials. The variation of ΔK_{Tr} and $\Delta \eta_r$ at various advance coefficient values are listed in Tab. 4 and 5, respectively. It is found that ΔK_{Tr} and $\Delta \eta_r$ decrease along with E/ρ increasing for $J < 0.5$, and increase for $J > 0.5$.

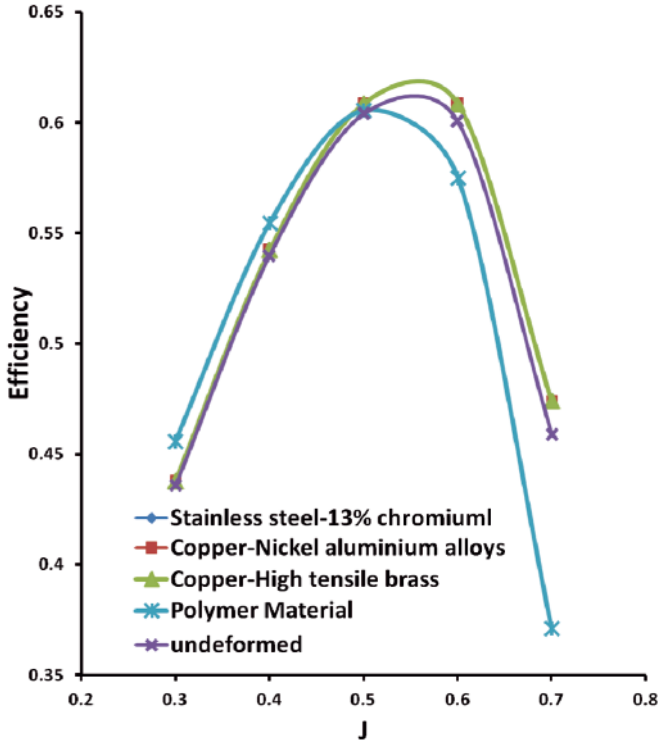

Fig. 17. Efficiency versus advance coefficient (J) for the used materials

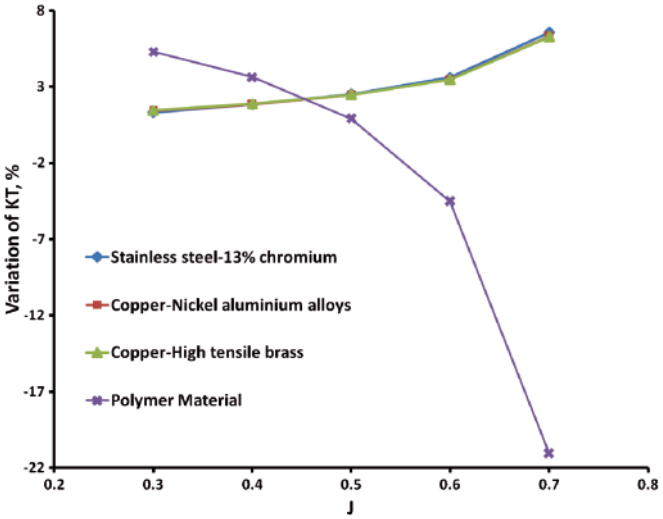

Fig. 18. ΔK_T (K_T variations) versus advance coefficient J for the used materials

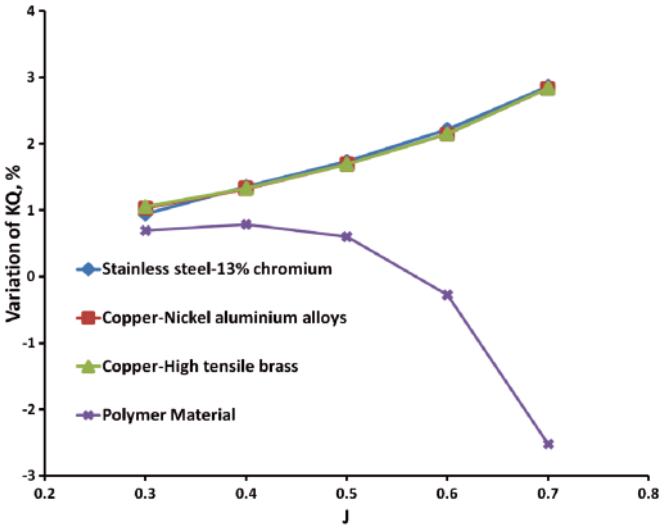

Fig. 19. ΔK_Q (K_Q variations) versus advance coefficient J for the used materials

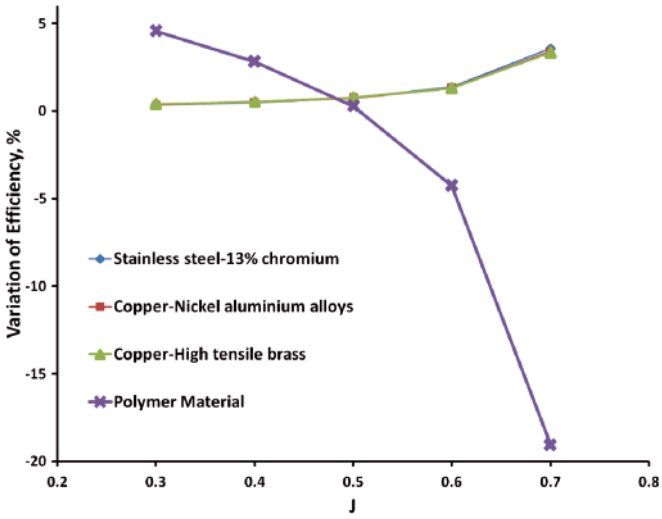

Fig. 20. Variations of efficiency, $\Delta\eta$, versus advance coefficient J for the used materials

CONCLUSIONS

A fluid-structure interaction in case of flexible marine propellers made of various materials have been analyzed by using the combined (BEM-FEM) software. The hydrodynamic load was determined by using the BEM and the structural

Tab. 4. Thrust coefficient (ΔK_T) for the propellers of four considered materials at various advance coefficient values

E/ρ	J = 0.3	J = 0.4	J = 0.5	J = 0.6	J = 0.7
25.47182	1.303891	1.834449665	2.4950364	3.607889781	6.54376013
14.85818	1.396738	1.839448166	2.455327598	3.479036574	6.320907618
13.54868	1.44518	1.864440668	2.468563865	3.459213004	6.26012966
2.773913	5.288229	3.628911327	0.893448048	-4.529685796	-21.06969206

Tab. 5. Efficiency ($\Delta\eta_T$) for the propellers of four considered materials at various advance coefficient values

E/ρ	J = 0.3	J = 0.4	J = 0.5	J = 0.6	J = 0.7
25.47182	0.357814579	0.476402328	0.743512891	1.370250741	3.571272838
14.85818	0.362401945	0.513476439	0.751792545	1.315307516	3.388130641
13.54868	0.392219827	0.5301598	0.7666959	1.2936632	3.327083242
2.773913	4.564429561	2.819486153	0.283164152	-4.26059738	-19.0446082

response was analyzed by using the FEM. The deformation of propeller affects its hydrodynamic characteristics. In this paper, by considering the hydrodynamic and mechanical forces, the flexible propeller performance is examined. For performing the hydro-elastic analysis of the propeller a combined BEM - FEM method is proposed in which an iteration approach is used to predict the deformed shape of propeller. The hydrodynamic force is calculated by modelling solid-fluid interaction in the BEM software. The deformation of the propeller is then determined by using the finite element software (FEM). Three metal propellers and one propeller made of polymer material are analyzed by using the proposed method. From the performed analyses the following conclusions can be derived:

- The deformation of propeller has a lower effect on its torque coefficient (K_Q) and a greater effect on its efficiency.

- It seems that the value of the advance coefficient J at which the maximum efficiency occurs has an important impact on the variation of characteristics of the deformed propeller. In the case study, the maximum efficiency occurs at J = 0.5, and ΔK_{Tr} and $\Delta\eta_r$ decreases with the increasing of E/ρ ratio for J < 0.5 and increases for J > 0.5.

BIBLIOGRAPHY

1. Sontvedt, T.: *Propeller blade stress application of finite element methods.* Computers & Structures, Vol. 4, pp. 193-204, 1974.
2. Young, Y.L.: *Hydro-elastic behaviour of the flexible composite propeller in wake inflow*. 16th conf. on composite materials, Kyoto, Japan, 2007.
3. Young, Y.L.: *Fluid-structure interaction analysis of flexible composite marine propellers*. Journal of Fluids and Structures, Vol. 24, 799–818, 2008.
4. Blasques, J. P., Berggreen C., Poul Andersen, P.: *Hydro-elastic analysis and optimization of a composite marine propeller.* Marine structure, Vol. 23, 2010.
5. Lin H. J., Lai W. M., Kuo, Y. M.: *Effect of stacking sequence on nonlinear hydro-elastic behaviour of composite propeller*. Journal of Mechanics, Vol. 26, No. 3, September 2010.
6. Mulcahy, N. L. and Prusty B. G. and Gardiner C. P.: *Hydro-elastic tailoring of flexible composite propellers.* Ships and Offshore Structures, Vol. 5, No. 4, 359–370, 2010.
7. Chau, T. B.: *2-D versus 3-D stress analysis of a marine propeller blade.* Zeszyty Naukowe Akademii Morskiej w Gdyni, No. 64, July 2010.
8. Koronowicz, T., Krzemianowski, Z., Tuszkowska, T., Szantyr, J.A.: *A complete design of ship propellers using the new computer system*. Polish Maritime Research, Vol. 16, No. 1 (59); pp.29-34, 2009.
9. Ghassemi, H., Ghadimi, P.,: *Computational hydrodynamic analysis of the propeller-rudder and the AZIPOD systems*. Ocean Engineering, Vol. 34, pp.117-130, 2007.
10. Ghassemi, H.: *The Effect of Wake Flow and Skew Angle on the Ship Propeller Performance.* Scientia Iranica, Vol. 16, No. 2, pp.149-158, 2009.
11. Ghassemi, H.: *Hydrodynamic performance of coaxial contra-rotating propeller (CCRP) for large ships.* Polish Maritime Research, Vol. 16, No. 1 (59), pp.22-28, 2009.
12. Ghassemi, H.: *Hydrodynamic characteristics of the surface-piercing propellers for the planing craft*. J. Marine Sci. Appl., Vol. 7, pp.147-156, 2008.

CONTACT WITH THE AUTHORS

Hassan Ghassemi, Prof.,
Department of Ocean Engineering,
Amirkabir University of Technology, Tehran, IRAN
e-mail: gasemi@aut.ac.ir,
http://hmaa.itgo.com/ghassemi.html
tel.: +98-21-64543112, fax: +98-21-66412495

Morteza Ghassabzadeh, Ph.D.,
Marine Industry Research Centre,
Amirkabir University of Technology, Tehran, IRAN
e-mail: morteza_ghassab@yahoo.com

Maryam Gh. Saryazdi, Ph.D.,
Vehicle Technology Research Institute,
Amirkabir University of Technology, Tehran, IRAN
e-mail: mghsaryazdi@aut.ac.ir

POLISH MARITIME RESEARCH 4(80) 2013 Vol 20; pp. 71-79
10.2478/pomr-2013-0043

Critical review of propeller performance scaling methods, based on model experiments and numerical calculations

Tomasz Bugalski, Ph.D.,
Ship Design and Research Centre CTO SA, Poland,
Heinrich Streckwall, Ph.D.,
Hamburg Ship Model Basin, Germany,
Jan A. Szantyr, Prof.,
Gdansk University of Technology, Poland

ABSTRACT

The article presents the results of experimental and numerical investigation of propeller scale effects, undertaken in co-operation of the Hamburg Ship Model Basin (HSVA), Germany, and Ship Design and Research Centre (CTO SA), Poland. The objective of the investigation was to test the adequacy of the methods currently used to account for the propeller scale effect and to develop possible improvement of the methods. HSVA has conducted model experiments in the large cavitation tunnel together with panel method and CFD calculations. CTO SA has performed model experiments in the towing tank, together with lifting surface and CFD calculations. Both institutions have suggested different new approaches to the problem and different new procedures to account for the propeller scale effects. In the article the procedures are presented together with the description of the underlying experimental and theoretical research.

Keywords: propeller scale effects; open water tests; computational fluid dynamics

INTRODUCTION

Despite a rapid development of the computational fluid dynamics (CFD) the open water model experiments remain the basic source of information about the hydrodynamic characteristics of ship propellers. This information is later used for determination of the powering performance of real, full scale ships. As the complete hydrodynamic similarity between model experiments and full scale operation of propellers cannot be achieved, the appropriate methods for correction of the so called scale effect had to be developed and implemented in order to convert the hydrodynamic characteristics of a propeller model into their full scale equivalent. The differences between the model and full scale propeller characteristics arise mainly due to a marked difference in model and full scale Reynolds numbers, hence they are connected to viscous flow effects in both scales. The differences are illustrated in Fig. 1, showing the scale effect on propeller efficiency. The ideal (inviscid) efficiency does not depend on scale, therefore it is shown as a horizontal line. The real (viscous) flow around propeller model and full scale propeller exhibits pronounced scale effects. Accurate determination of the scale effects is the subject of research described in this paper.

Scale effects may be studied in experimental and numerical way. Suitably controlled experiments in model scale are relatively easy, but their full scale equivalents are almost impossible to conduct. Therefore, the CFD and other numerical methods may be helpful in studying the problem. The research described in this paper has been undertaken by two ship hydrodynamic centres, namely the Hamburg Ship Model Basin (HSVA), Germany, and Ship Design and Research Centre (CTO SA), Gdansk, Poland. The joint project included model experiments conducted both in cavitation tunnels and towing tanks, together with CFD and lifting surface/surface panel potential flow calculations. The objective was to assess the adequacy of currently used methods for scale effect corrections to the geometry of contemporary ship propellers and, if possible, to suggest modifications of these methods.

RESEARCH AT THE HAMBURG SHIP MODEL BASIN (HSVA)

Introductory considerations

Usually the model - test - based prediction of the power at the full scale propeller involves tests in two Reynolds number ranges. In the ship self-propulsion mode the model propeller has to obey Froude similarity and appropriately defined Reynolds numbers $Re_{0.7}$ are around $5*10^5$ (see below for definition). In addition to support the power prediction process open water tests are performed in the towing tank at moderate Reynolds numbers ($Re_{0.7} \approx 1*10^6$). In both cases there exists a Reynolds number range characterized by a mixture of turbulent and laminar flow on the propeller blade surface (laminar from the leading edge to a certain transition range and turbulent after switching).

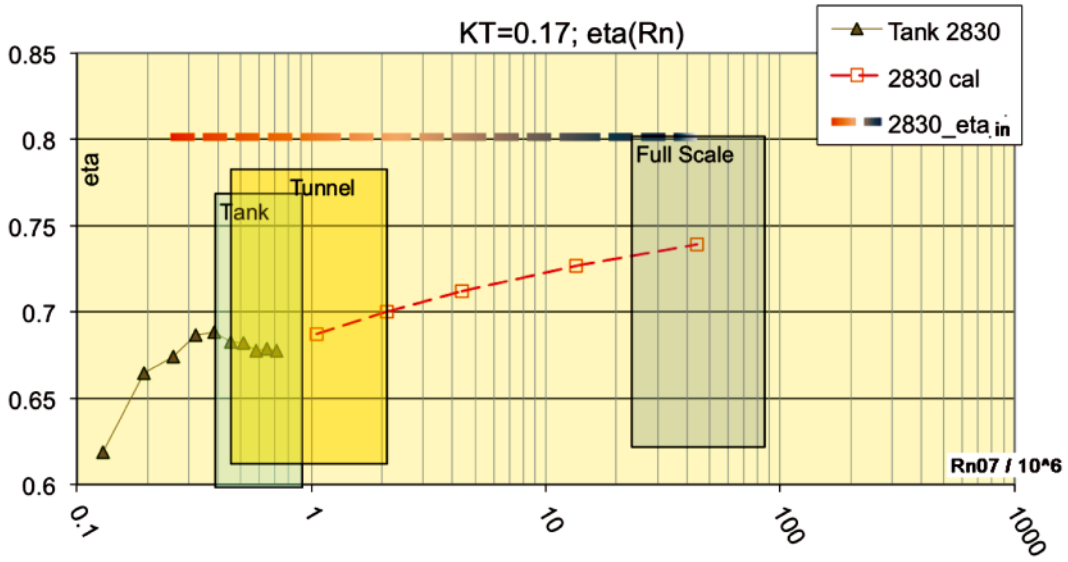

Fig. 1. *Example of scale effect on propeller open-water efficiency, showing the ideal (inviscid) efficiency and real (viscous) efficiency for model tank, cavitation tunnel and full scale*

Scaling procedures for propeller efficiency are to provide a good estimation for surface friction effects. In any scale they have to divide the propeller performance into two contributions. One part is valid under the absence of surface friction and thus is only counting forces normal to the propeller blade surface. For simplicity the low-order scaling methods consider this (dominating) share as not influenced by the Reynolds number. To arrive at the other share one has to estimate tangentially directed blade surface forces. The local magnitude of such forces may give a complex surface pattern, especially if the above mentioned transition results in a more or less equal share of laminar and turbulent flow on the blade.

A strip method was considered as a good compromise between treating surface friction in a reasonably detailed way and being still robust and quick. Accordingly, such a procedure was to be developed up to a quality and robustness which would allow using it as a new standard method and replace HSVA's former scaling procedure according to Lerbs/Meyne [5].

Principles of a new strip method

The quality of a scaling method may be expressed by its ability to deduce the inviscid propeller (no surface friction acting) from any Reynolds number level. To quantify a Reynolds number level a unique Reynolds number may be defined by $Re_{0.7}$.

$$Re_{0.7} = \frac{c_{0.7}}{\nu}\sqrt{\omega^2 r_{0.7}^{\ 2} + u^2}$$

where:
- ω – angular frequency,
- u – axial inflow velocity,
- $r_{0.7}$ – 70% of propeller radius,
- $c_{0.7}$ – chord at $r_{0.7}$,
- ν – kinematic viscosity).

The bigger problem for scaling is considered to occur at model scale level, but it can hardly be proved whether a method performs well in this range or not. The problem with ranking scaling methods is related to the fact that the inviscid propeller is hard to access experimentally and numerically.

Using a strip method gives at least a chance to resolve the mixture of laminar and turbulent flow at any radial position. As a basic characteristic of friction on a propeller blade a Reynolds number range is to be considered (instead of relying on one unique Reynolds Number like $Re_{0.7}$). Basically the Reynolds number changes strongly along the radius due to the local rotational speed. The strip method accounts for this situation. Furthermore, it accounts for the blade outline as well as for the blade pitch distribution and sums up friction effects from the set of strips that built up the blade.

This principle is displayed in Fig. 2, showing a coarse arrangement of strips and a color code to indicate the significance of each strip. Each strip has its local pitch and converts section drag into a local mixture of axial and circumferential force components. Finally, the latter shares are summed up to arrive at a thrust coefficient correction ΔK_T and a torque coefficient adjustment ΔK_Q for the whole propeller.

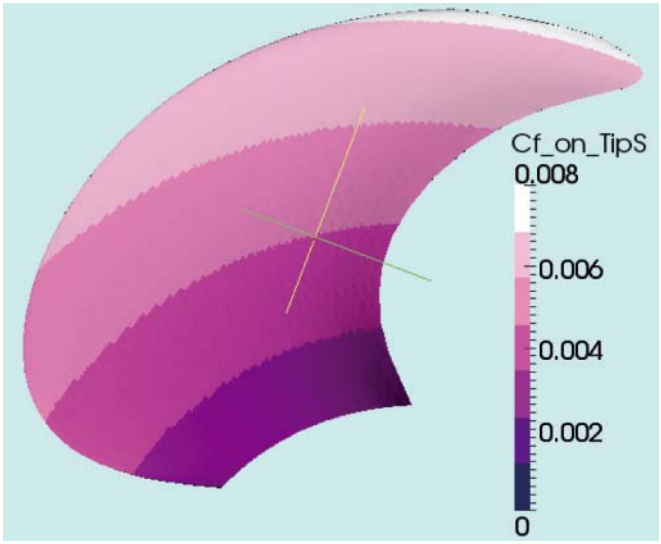

Fig. 2. *Principle of the strip method representing the relevance of different strips for the total viscosity effect (significance increases with brightness)*

Concept of the new HSVA procedure based on the strip method

In a review of HSVA's former standard procedure (the Lerbs/Meyne-method) the following improvements, together with the introduction of a strip method, were considered:
- address full scale in a more definite manner compared to the standard methods (Lerbs/Meyne-method [5] formerly used at HSVA, or ITTC'78-method [4]),

- withdraw the charts-based process to identify an 'ideal' propeller for further interpretation of the open water test and for full scale performance prediction (an essential idea behind the Lerbs/Meyne-method to recognize the above mentioned inviscid propeller),
- instead, rely on a more conventional scaling process, i.e. use friction lines to arrive at all scales starting with the measured open-water performance,
- introduce different friction lines for the open-water test mode and the propulsion test mode to resolve for different levels of incoming turbulence in either case.

The idea to use two friction lines for either the open water mode or the propulsion mode shall reflect different characters of the incoming flow. The lines are related to different degrees of turbulence in the arriving flow affecting the mixture of laminar and turbulent regimes on the blade surface. Fig. 3 gives the basic friction lines representing section drag in a normalized form, which is to be linked to the drag D of a strip (supposed to act in the direction of the nose-tail line) by means of:

(1)

where:
c – represents the chord of the strip,
dr – its radial extension
V_0 – the relevant velocity, the latter including rotation and advance of the strip.

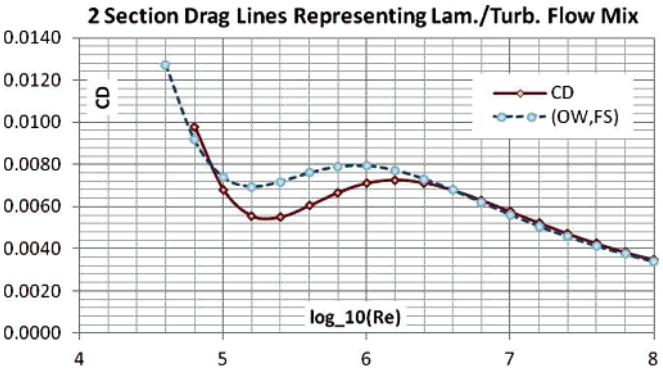

Fig. 3. *Lines for section drag coefficient used in the new strip method: the full* ***red line*** *stands for the full scale and open water case (OW, FS), the dashed* ***blue line*** *- for the propulsion test mode (RP). Each line reflects a specific mixture of laminar and turbulent flow.*

Validation and correlation of the new HSVA procedure

The inviscid propeller concept is detailed in Fig. 4. One might avoid this idea and reduce the process of scaling to finding the difference between friction forces in model scale and in full scale. This view may however suggest certain simplicity and it is recommended here to retain the "back and forth"- view as given in Fig. 4.

For an experimental based access to the inviscid propeller it is considered reasonable to reduce mixture effect from simultaneous appearance of laminar and turbulent flow as far as possible. In the experiments it was aimed at the largest Reynolds numbers achievable with existing propeller hardware and test facilities. It was expected that by doing so the above mentioned mixtures effects were reduced and the prospects for ranking scaling procedures were enhanced. At HSVA the large model propellers were tested in the largest conventional cavitation tunnel (where the measuring equipment can stand higher forces and moments as the towing tank hardware). Ensuring that turbulent flow becomes dominant on the blade surface it was considered that empirical lines for pure turbulent blade surface friction can be used to arrive at a good estimation of viscous forces.

Evaluating these tests it was soon noticed that the standard ITTC'78 method and the 'Lerbs/Meyne'- method previously applied at HSVA, may treat full scale friction effects too conservatively. For the ITTC'78 method this is obvious from Fig. 4, where for propeller 2004 the full scale η was predicted slightly below model scale efficiency (using the standard roughness setting). This finding rather supports the necessity of a detailed treatment of viscous effect in the range of full scale Reynolds numbers (which was not addressed in the Lerbs/Meyne-method). It gives no further arguments for the necessity of a strip method.

Besides the propeller efficiency scaling process, the evaluation of propulsion test results for a full scale power prediction involves other correction steps, among which are wake-scaling and added resistance. It was an essential demand for the modification of propeller efficiency scaling, that it should not lead to a general shift of predicted full scale power (in the mean sense). This led to the necessity to run a lot of comparative evaluations of propulsion tests results in both ways, applying the previous process and the new strip method.

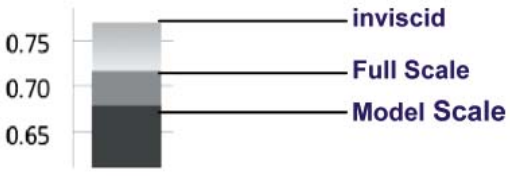

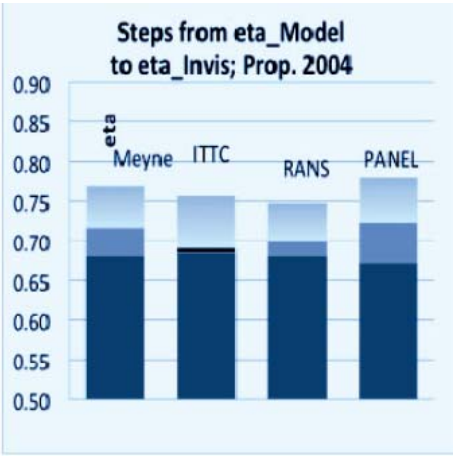

Fig. 4. *Illustration of the inviscid propeller concept (left). The model scale efficiency is measured, the estimation and subtraction of model scale surface friction forces gives the in-viscid performance and a guess for full scale friction effects reduces the inviscid efficiency to the full scale efficiency. The diagram on the right holds for propeller 2004 (D = 0.382m), operated at 18 Hz ($Re_{0.7}$ = 2.3*10) in HSVA's large conventional tunnel. Various methods were used to execute the steps explained on the left. For propeller 2004 the full scale efficiency level in the ITTC column (reflecting the application of the ITTC'78 scaling procedure) is hardly visible as it was predicted slightly below model scale efficiency.*

For a particular propeller Fig. 5 gives a comparison of either method when applied over the whole range of advance ratios J. The focus is on the efficiency $\eta = J \cdot K_T/2\pi K_Q$, where in the figure $\eta_{OPEN\ WATER}$ stands for the unaltered measured quantity; η_{FS} and $\eta_{PROPULSION}$ are related to full scale and propulsion test, respectively. It may be considered a drawback of the previous approach, that in some particular cases (the given example belongs to this set) the steps between the 3 relevant efficiencies seem to be of reversed order. The strip method predicts the propulsion mode efficiency closer to $\eta_{OPEN\ WATER}$ and further from η_{FS} and not opposite, as the former approach does.

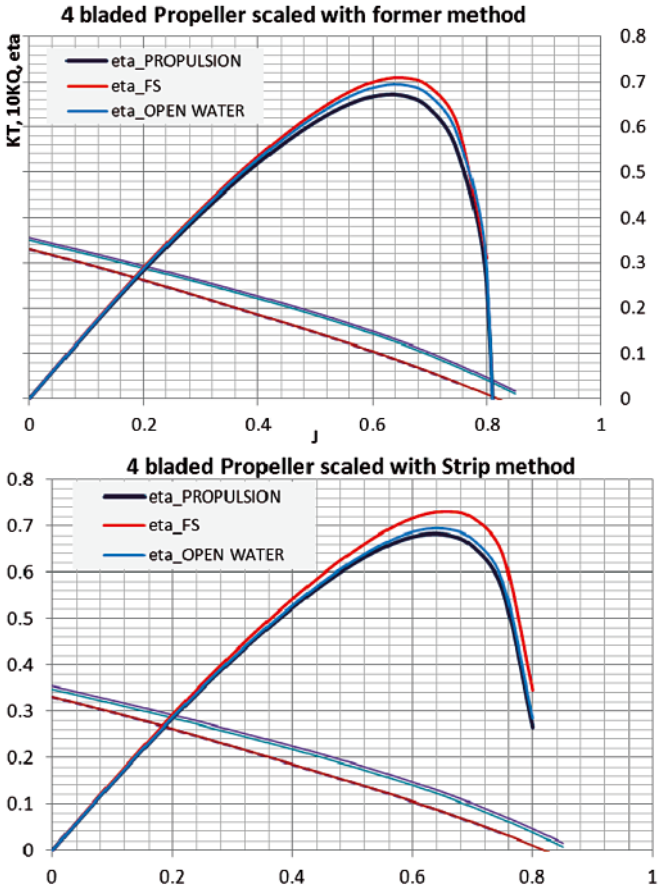

Fig. 5. Full scale efficiency versus propulsion test efficiency for 4-blade propeller obtained from the former HSVA scaling procedure and due to the new strip method

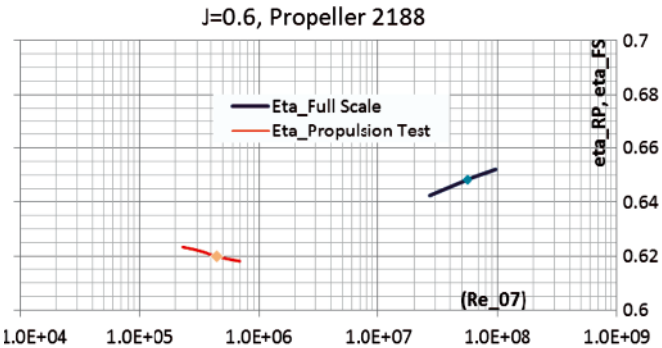

Fig. 6. The open-water efficiency plotted for a specific advance ratio over the Reynolds number on 70% of the propeller radius, considering ranges typical for full scale or model scale (propulsion mode) conditions

Fig. 6 depicts one advance ratio and shows the variation of the open water efficiency with the Reynolds Number at 70 % of the propeller radius. A typical full scale range and a typical model scale range (for a propulsion mode) are considered. This figure reflects the character of the above given section drag lines. Note that when using a separate friction line (the RP-line) the efficiency for propulsion conditions is generally worsened. The RP-line however shows a local minimum for typical propulsion test Reynolds numbers.

It was considered reasonable to post-process RANS results in a manner that section drag can be presented strip-wise to allow for a direct comparison with the strip method. The procedure is demonstrated in Fig. 7. The integration of forces generated by shear is confined to a strip and local velocities and the strip area are taken for reference to calculate a section drag coefficient by using the above given C_D - formula. For the same propeller the C_D values obtained from the strip method approach may be collected.

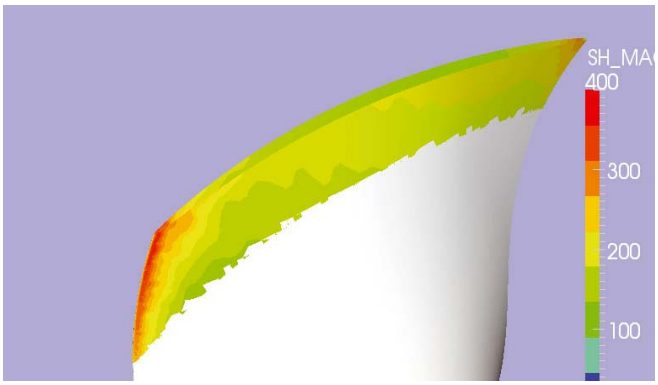

Fig. 7. Shear force distributions from RANS results, used to derive a strip - wise resolution of section drag (due to shear) for comparison with strip method results

Fig. 8 gives C_d results plotted against the radius, referencing RANS calculations performed with the HSVA's in-house solver FreSCo and strip method assumptions by using the above given section drag lines. As the RANS solver was assuming turbulent flow starting from the leading edge it was expected that it would reveal a different behaviour over the radius. The relation of measured shaft power from trials to predicted shaft power from propulsion tests should improve with the new correction method, though (in the mean sense) the predictions should not deviate too much from the HSVA's former procedure.

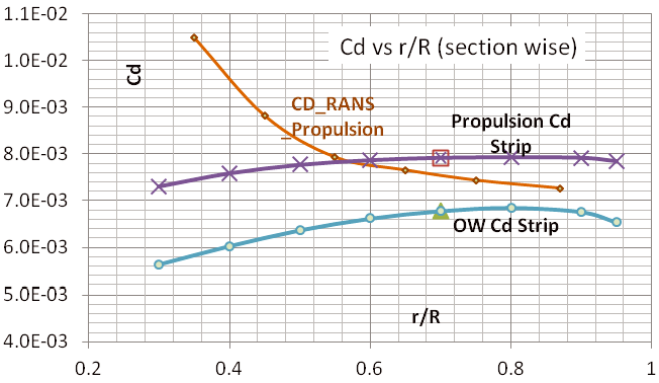

Fig. 8. Instead of plotting section drag vs. Reynolds number one may indirectly consider the section drag coefficient in function of the radius

Fig. 9 (up) gives all 112 trial cases available at HSVA, re-evaluated with the new method from model tests and then compared with the actual measured power. Fig. 9 (down) displays the former correlation obtained with the Lerbs/Meyne approach. Comparing both figures one can state that the application of the strip method improved the correlation (1.6 % under this prediction vs. 2.5 % under prediction of power) but the results stayed only 0.9 % apart, as both procedures tend to under-predict.

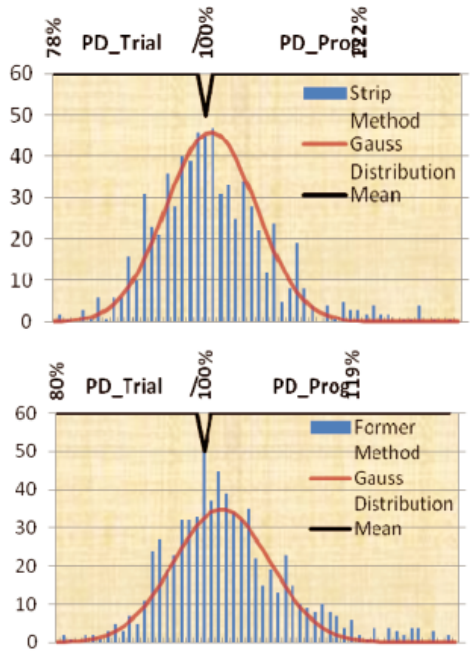

Fig. 9. *Comparison of the strip method (up) and the former method (down) in terms of their ability to match 100% correlation in average. The mark (∇) indicates the position for a case where 100% match of predicted and measured power was achieved ($PD_{Trial} = PD_{Prog}$). The actual mean for the ratio trial-power vs. predicted power (PD_{Trial}/ PD_{Prog}) is to be taken from the maximum of the Gauss-distribution*

RESEARCH AT THE SHIP DESIGN AND RESEARCH CENTRE (CTO SA)

Alternative formulae for lift and drag of propeller blade sections

The currently used ITTC78 procedure [4] for development of scale effect corrections for propeller thrust and torque is often criticized in three aspects:

- the formulae for propeller scale effect are based on the equivalent blade section at 0.75 radius, therefore they may be inadequate for contemporary propeller geometries, especially these with high skewback and strongly non-uniform radial pitch distributions,
- the formulae used for calculation of blade section drag may be not accurate enough,
- the scale effect on blade section lift may have to be included ([8]).

The alternative formula for blade section drag coefficient, in model and full scale alike, considered in this paper in Variants 3 and 4 below, has the following form (taken from [1]):

$$C_D = 0.05808\left(1 - 0.2\frac{t}{c}\right)\frac{1}{Re^{0.1458}} \tag{2}$$

The formula for scale effect on blade section lift coefficient considered in this paper in Variant 3 below, has the following form (also taken from [1]):

$$C_{LV} = 2\pi\mu_1(\alpha + \mu_2\,\alpha_0) \tag{3}$$

where:

$$\mu_1 = 1 - \exp\left(-0.0691 + 12.46\frac{t}{c} - 0.1855\log Re\right) \tag{4}$$

$$\mu_2 = 1 + \frac{t}{c}\left(\frac{t}{c} - 0.05\right)\frac{1}{(0.04664\log Re - 0.4378)^2} \tag{5}$$

$$Re = \frac{c}{\nu}\sqrt{\omega^2 r^2 + u^2} \tag{6}$$

Model propellers used in the experiments and calculations

Altogether three propeller models were analyzed at CTO SA: one of them (P629) has a more traditional geometry, resembling the B Wageningen - series propellers, and the other two are highly skewed propellers CP312 and CP416. Only the results for highly skewed propellers are presented in this article. The geometry of the propeller CP312 is shown in Fig. 10, and the geometry of propeller CP416 is presented in Fig. 11. The geometry and results for the propeller P629 may be found in [3].

Towing tank model experiments at CTO SA

The open water experiments with the above presented propeller models were conducted in the large towing tank of CTO SA. The standard open-water diagrams of both propeller models were measured. Apart from that, the influence of Reynolds number on the propeller hydrodynamic characteristics was measured for the given advance coefficients by changing the rotational speed of the models within the range permitted by the available measuring equipment and the maximum possible advance velocity of the towing tank carriage. The Reynolds

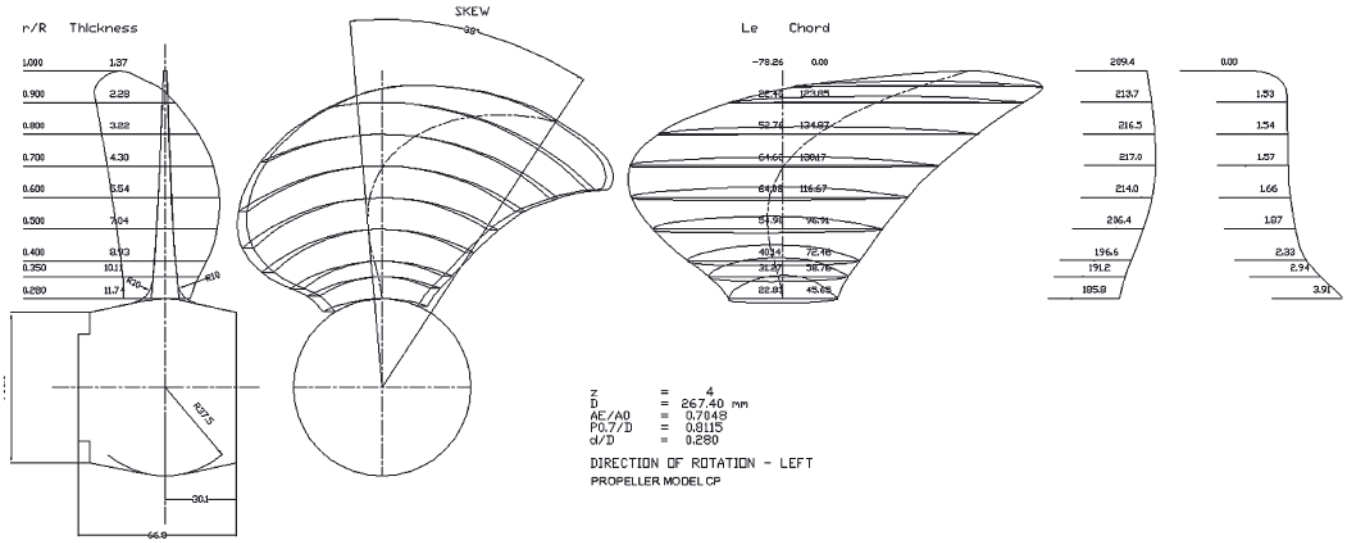

Fig. 10. *Model propeller CP312 tested and analyzed at CTO SA*

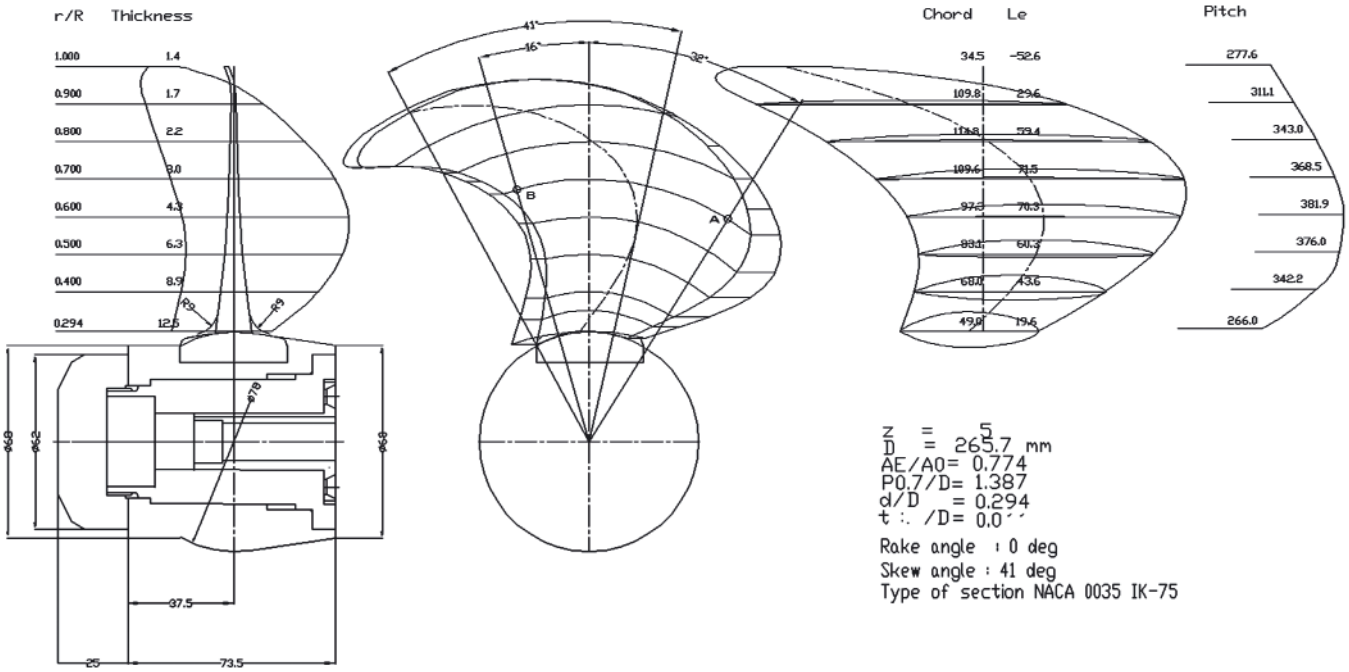

Fig. 11. *Model propeller CP416 tested and analyzed at CTO SA*

Tab. 1. *Reynolds numbers in tank tests and in calculations at CTO SA (all values *10⁶)*

Open-water tests in towing tank							
Propeller	J	n = 4 [1/s]	n = 6 [1/s]	n = 8 [1/s]	n = 10 [1/s]	n = 12 [1/s]	n = 16 [1/s]
CP312	0.50	-	-	0.573	0.707	0.852	1.135
		n = 4 [1/s]	n = 6 [1/s]	n = 8 [1/s]	n = 10 [1/s]	n = 12 [1/s]	n = 16 [1/s]
CP416	0.70	0.225	0.338	0.450	0.563	0.676	-
CFD calculations for model scale							
		n = 13 [1/s]	n = 20 [1/s]	n = 30 [1/s]	n = 40 [1/s]	n = 50 [1/s]	n = 60 [1/s]
CP312	0.50	0.973	1.497	2.245	2.984	3.742	4.491
CP416	0.90	0.862	1.326	1.988	2.651	3.314	3.977

numbers achieved in experiments for both propeller models are given in Tab. 1 together with the numbers used in calculations.

The results of towing tank experiments are presented in Fig. 12 and 13. They confirm the expected tendencies of all coefficients, but they do not reach the Reynolds numbers considered in calculations below. Therefore they cannot be used for direct validation of the results of different variants of calculation presented below in Fig. 16, 17, 18 and 19.

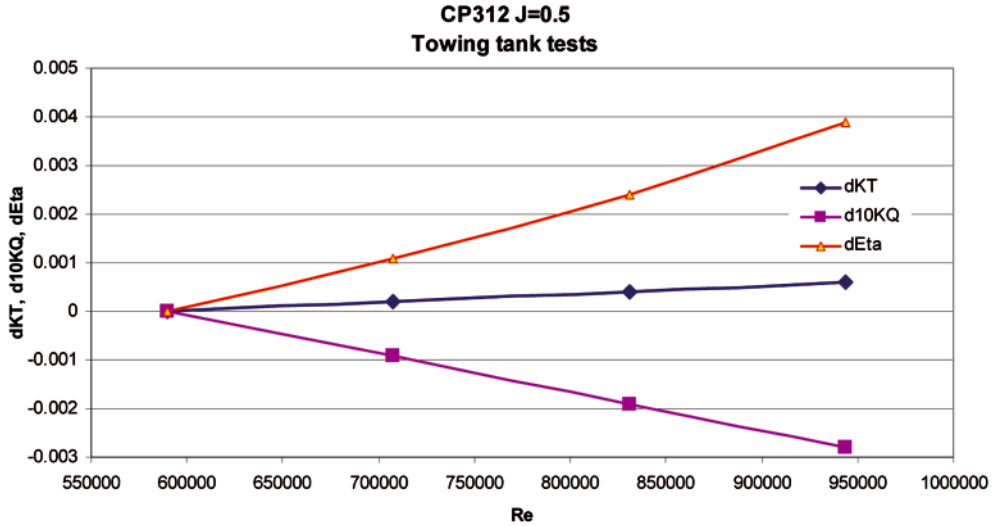

Fig. 12. *Scale effect corrections for the thrust coefficient, torque coefficient and efficiency of the propeller model CP312 based on measurements in the towing tank at different Reynolds numbers*

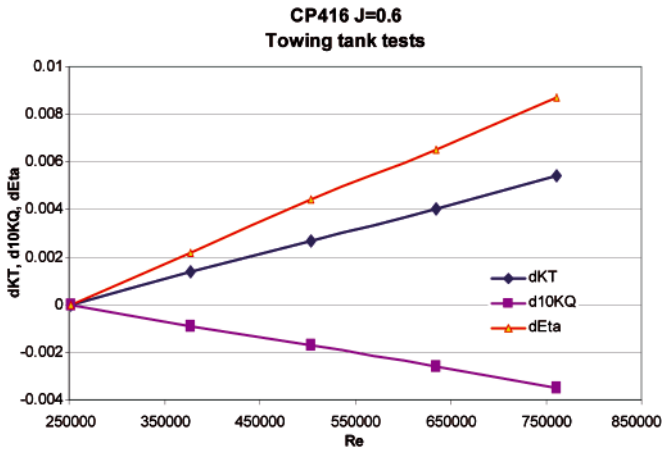

Fig. 13. Scale effect corrections for the thrust coefficient, torque coefficient and efficiency of the propeller model CP 416 based on measurements in the towing tank at different Reynolds numbers

Lifting surface and CFD calculations at the Ship Design and Research Centre (CTO SA)

The well-established and thoroughly validated lifting surface program UPCA92 for analysis of propeller operation in non-uniform velocity field [9], was used. The program was modified in such a way that it produced the complete open-water diagram of propellers at the required scale. In the calculations the propeller rate of rotation was usually kept constant and the advance velocity was varied in order to produce the required values of the advance coefficient. Four different algorithms for prediction of scale effect corrections were incorporated into the program:

- the classical ITTC78 procedure (hereinafter Variant 1), based on the equivalent blade section at radius 0.75
- the ITTC78 formulae used locally for the respective blade sections and whose results are integrated along the blade radius – similarly as in the above described HSVA's strip method (hereinafter Variant 2),
- alternative formulae for blade section drag and lift integrated along the blade radius (hereinafter Variant 3),
- alternative formula for blade section drag only integrated along the blade radius (hereinafter Variant 4).

The program was used for calculations in model scale for 13, 20, 30, 40, 50 and 60 rps and for calculation of three different simulated full-scale situations, corresponding to propeller diameters of 3, 5 and 8 [m]. The full-scale calculations were performed for standard propeller blade roughness value of 30 microns.

Tab. 2. *Reynolds numbers in simulated full-scale calculations (all values *10⁸)*

Propeller	D = 3.0 [m]	D = 5.0 [m]	D = 8.0 [m]
CP312	0.3768	0.6781	1.050
CP416	0.3378	0.5633	0.9012

In the CFD calculations the meshing and flow simulations are performed with the Reynolds Averaged Navier-Stokes (RANS) solver StarCCM+ from CD-Adapco. The code solves the RANS and continuity equations in integral form on a polyhedral mesh by means of the finite volume technique. The Reynolds stress problem is solved by means of "realizable" k-ε turbulence model. As in the open-water situation the propeller inflow is uniform the moving reference frame approach is applied. The solution domain was chosen such as to extend 10 propeller diameters in front of the propeller, 3 diameters in the radial direction and 5 diameters behind the propeller. The computational grid was constructed of about 900 000 polyhedral elements. The details of the calculation technique may be found in [2].

The CFD calculations were carried out for advance coefficients in the range from J = 0.0 to J = 1.0, following the above defined model and full-scale conditions for the lifting surface calculations. The computed thrust and torque on the propeller were converted into the dimensionless thrust coefficient, torque coefficient, and the propeller open-water efficiency was calculated. The study of the flow field shows that the phenomena occurring in the flow (pressure distribution, tip vortices etc) are typical for propeller flow and can be considered qualitatively correct.

In Fig. 14 is shown the calculated distribution of the local viscous shear stress and pressure distribution on the suction side of the model propeller CP416. The distribution of shear stress supports the idea of dividing the blade surface into strips and calculating friction forces separately for each strip. The analogous results for full scale presented in Fig. 15 do not support the idea of dividing the blade surface into strips in an equally clear way. However, it is visible that the shear stresses are distributed over the blade surface in a strongly non-uniform way and describing them with a single drag coefficient is a very far reaching approximation.

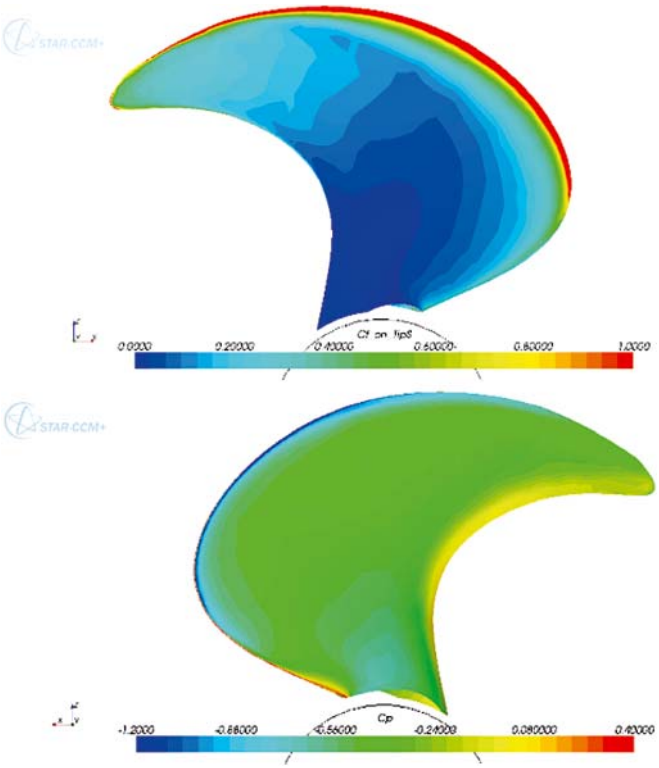

Fig. 14. CFD calculations for propeller model CP416: blade surface shear stress distribution based on tip speed (up) and pressure distribution on the suction side (down)

Results of computations obtained at the Ship Design and Research Centre (CTO SA)

The results of computations for the propeller CP312 are shown in Fig. 16 and 17 in the form of scale effect corrections related to the model scale values of respective parameters at the lowest Reynolds number, i.e. at 13 rps. The scale effect corrections are shown for the design advance coefficient of the propeller equal to J = 0.5. Fig. 16 shows the corrections for

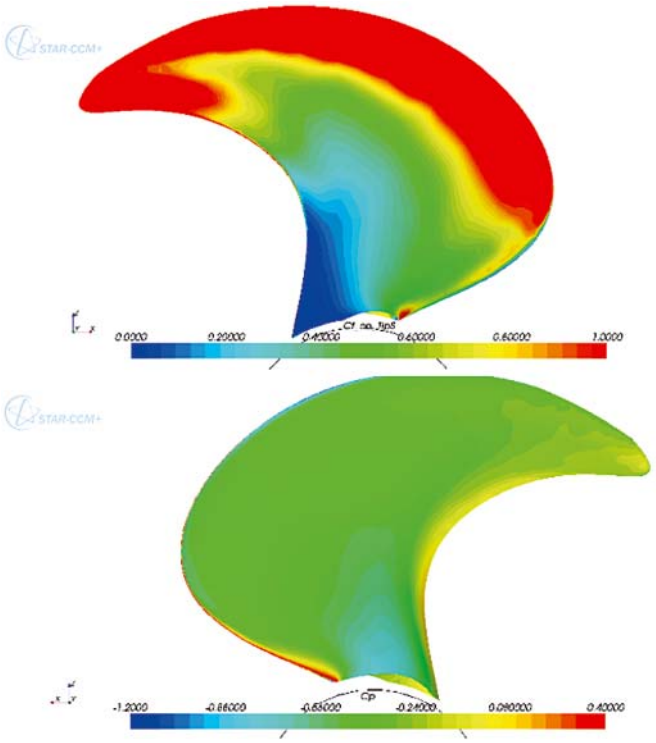

Fig. 15. CFD calculations for full scale (D = 5m) propeller CP416: blade surface shear stress distribution based on tip speed (up) and pressure distribution on the suction side (down)

propeller torque coefficient and Fig. 17 - for propeller open-water efficiency.

The scope of the calculations and the form of presentation of the results for propeller CP416 in Fig. 18 and 19 are identical to those for propeller CP312. The design advance coefficient is now J = 0.9.

The above presented results of lifting surface and CFD calculations may be summarized in the following way, assuming CFD results as the level of reference:

- the classical ITTC78 formulae produce too high corrections for propeller torque, effectively under-estimating this parameter in full scale; this may lead to the development of hydrodynamically "too heavy" propeller designs;
- the classical ITTC78 procedure significantly over-estimates the increase in propeller open-water efficiency in full scale as compared with model scale; this may cause too optimistic predictions of ship powering performance;
- the integration of the locally defined ITTC78 corrections along the propeller radius does not produce visible changes in the results when the presence of laminar/turbulent flow in model scale is not taken into account;
- variant 3 based on the alternative formulae for blade section lift and drag produces too high corrections for propeller thrust, but comparison with ITTC78 - based results shows that some smaller scale effect on lift may need to be included in the scaling procedure in order to improve correlation of the thrust correction with CFD results,
- the alternative formula for blade section drag, used in Variants 3 and 4, seems to predict scale effect corrections for torque much better than the original ITTC78 formula.

GENERAL CONCLUSION

The research performed both at HSVA and CTO SA leads to the following general conclusions:

- the currently used procedures for propeller scale effect corrections require modifications in order to keep up with the advanced propeller designs and advanced experimental and numerical techniques;
- to develop the reliable new procedures is difficult due to the complicated nature of the involved physical phenomena;
- the incorporation of the new formulae for blade section drag coefficients, taking into account the mixed laminar/turbulent flow in model scale, is a promising concept which requires further investigation;
- the incorporation of the scale effect on blade section lift may be also the way to improve the current scale effect procedures.

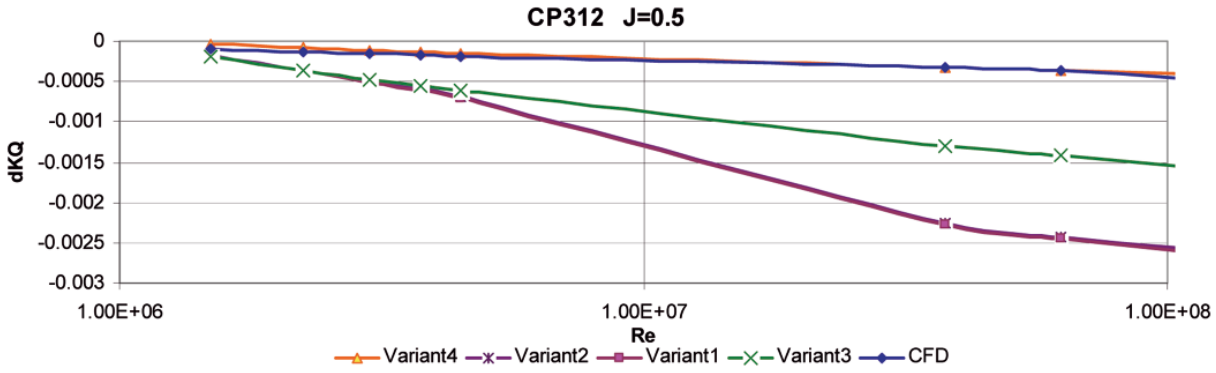

Fig. 16. Results of calculations for the scale effect correction on the torque coefficient of the CP312 propeller

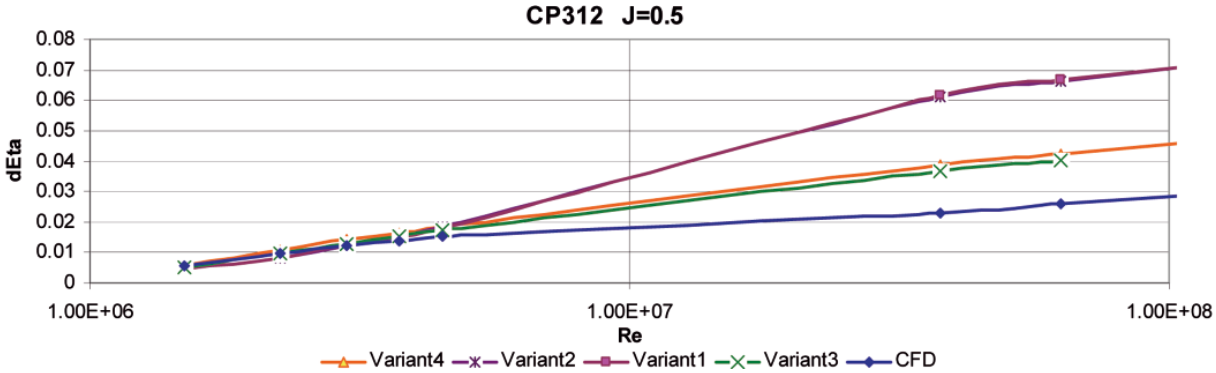

Fig. 17. Results of calculations for the scale effect correction on the open- water efficiency of the CP312 propeller

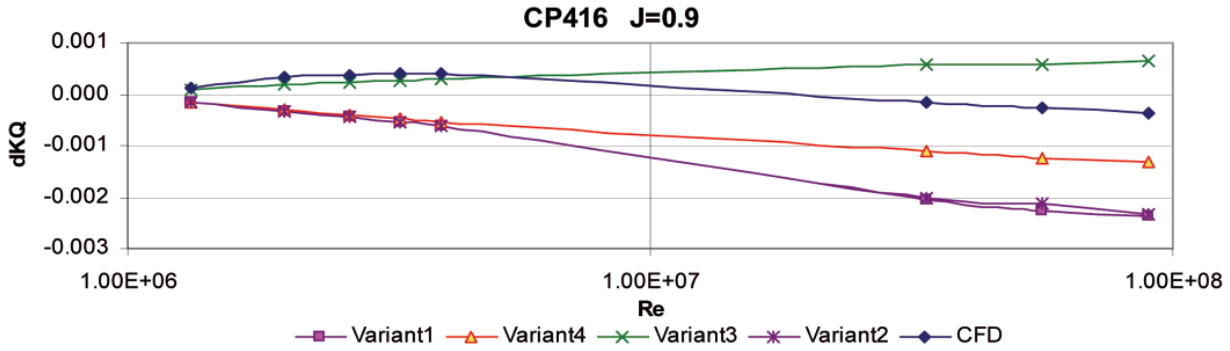

Fig. 18. *Results of calculations for the scale effect correction on the torque coefficient of the CP416 propeller (J = 0.9)*

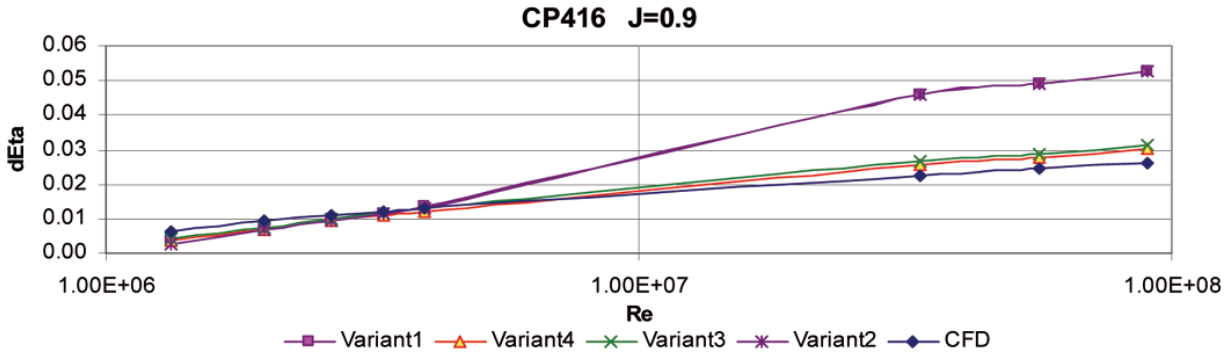

Fig. 19. Results of calculations for the scale effect correction on the open-water efficiency of the CP416 propeller (J = 0.9)

Acknowledgements

The authors acknowledge with gratitude that the research presented in this paper was supported by the ERA-NET MARTEC and by the Polish National Centre for Research and Development (NCBiR) grant No. N R10 0039 06/2009.

NOMENCLATURE

C_{LV} = 2π (+)
α – angle of attack [rad]
α_0 – zero lift angle [rad]
c – blade sectionchord [m],
D – propeller diameter (D = 2R) [m]
J – advance coefficient [-]
K_T – thrust coefficient $K_T = T/\rho n^2 D^4$
K_Q – torque coefficient $K_Q = Q/\rho n^2 D^5$
μ_1, μ_2 – corrections for viscosity effects [-]
n – propeller rate of rotation [rps - revolutions per second]
η – propeller open water efficiency [-]
r – radius defining propeller blade section [m]
ρ – density of water [kg/m^3]
t – maximum blade section thickness [m],
ω – angular frequency related to the shaft frequency n, $\omega = 2\pi n$ [rad/s]
u – propeller advance velocity [m/s]
ν – coefficient of kinematic viscosity
Re – Reynolds number

BIBLIOGRAPHY

1. Bavin W.F. *et al*: *Grebnye winty -sovremennyje mietody razcziota* (in Russian), Izd. Sudostrojenije, Leningrad 1983
2. Bugalski, T., Hoffmann, P.: *Numerical Simulation of the Interaction Between Ship Hull and Rotating Propeller*. Proceedings of the Second International Symposium on Marine Propulsors, SMP'11, Hamburg, Germany, 2011, pp. 256-26
3. Bugalski T., Szantyr J.A.: *Numerical Analysis of Scale Effects in Open Propellers*. Proc. International Symposium on Ship Hydrodynamics HYDRONAV 2012, Ilawa, September 2012
4. ITTC Performance Committee: *Report of the Performance Committee*. Proceedings of the 15th ITTC, 1978
5. Meyne, K.: *Experimentelle und theoretische Betrachungen zum Maßstabseffekt bei Modellpropeller- Untersuchungen* (in German) Schiffstechnik, Vol. 15, 1968.
6. *PREFUL - Propeller Efficiency in Full Scale.* European research project under the MARTEC network, 2010 ÷ 2012
7. Streckwall H., Dymarski P., Greitsch L.: *Review of propeller performance scaling including RANS calculations and high speed tunnel tests*. HydroComp 2012, Propeller Workshop, Glasgow, 11 June, 2012.
8. Szantyr J.*: Lift Based Propeller Scale Effect and its Influence on the Propulsive Characteristics of Ships*, Trans. West Japan Society of Naval Architects, No. 84 (1992), pp. 239-246
9. Szantyr J., Centkowski J.: *UPCA92 – the Lifting Surface Program for Hydrodynamic Analysis of Marine Propellers. Part II – Description of the Algorithm*, (in Polish). Report of IFFM ? No. 22/92

CONTACT WITH THE AUTHORS

Tomasz Bugalski Ph.D.,
Ship Design and Research Centre CTO SA,
Szczecinska 65,
80-392 Gdansk, POLAND,
e-mail: tomasz.bugalski@cto.gda.pl

Heinrich Streckwall, Ph.D.,
Hamburg Ship Model Basin
(Hamburgische Schiffbau-Versuchsanstalt GmbH),
Bramfelder Str. 164,
D-22305 Hamburg, GERMANY,
e-mail: Streckwall@hsva.de

Jan A. Szantyr, Prof.,
Faculty of Mechanical Engineering,
Gdansk University of Technology,
Narutowicza 11/12,
80-233 Gdansk, POLAND,
e-mail: jas@pg.gda.pl

POLISH MARITIME RESEARCH 4(80) 2013 Vol 20; pp. 80-86
10.2478/pomr-2013-0044

Efficient heuristic for non-linear transportation problem on the route with multiple ports

Srećko Krile, Assoc. Prof.,
University of Dubrovnik, Croatia

ABSTRACT

We need a better transport planning tool for loading maximization and transport cost minimization on the voyage route with multiple loading/unloading (discharging) ports. The implemented heuristic algorithm is able to find out an appropriate routing sequence with maximal earnings and profit. In the same time it looks for minimal loading/discharging and transshipment costs, but with fulfillment of cargo demands in a number of ports on the route. The efficient algorithm for optimal transport of N cargo loads (e.g. contingent of containers) for ships with limited capacity is being developed. This efficient tool may significantly reduce transport costs and ensure maximal profit to freight forwarders. Also, it can be applied for supply chain management of different goods from numerous vendors. The proposed algorithm shows acceptable complexity that means that such optimization tool can be used in shipping supported with limited computing power.

Key words: Non-linear Transportation Problem; Multi-destination Routing Problem; Minimum Cost Multi-Commodity Flow Problem; Capacity Management of Container Ships

INTRODUCTION

Pre-shipment planning is a key element for efficient cargo management and successful transport with transportation means of limited capacity (ship, train, airplane etc.). This paper deals about maritime shipping industry but it could be easily extended for another transportation system.

One of the most important problems in cargo transportation is to find the sequence of cargo distribution between multiple sources and multiple destinations which minimizes the transportation cost and better utilizes the ship capacity. The capacity management problem in shipping is extended to transportation problem of different cargo types transported by one mean on the route with multiple sources (loading ports) and multiple destinations (ports of discharge).

In example from Fig. 2 we have 5 ports. Loads of containers (contingents) are waiting to be transported as it is shown on Fig. 1. The loading amounts are given in percentage of total ship capacity. If all contingents have the same freight cost it is clear that the ship will avoid port 3, to reduce the transportation cost. The port 4 has to be on the route because the efficiency will be increased with load 4-5. The ship is barely full, only free ship capacity of 10 % is present from 1-2 and 10 % from 4-5. But if we have higher freight cost for contingent 3-4 the routing sequence will include the port 3, as it is shown with dotted line on Fig. 2. In that case the profit is more important that the idle (unused) capacity on the board. Details are shown in Fig. 6 – Fig. 8.

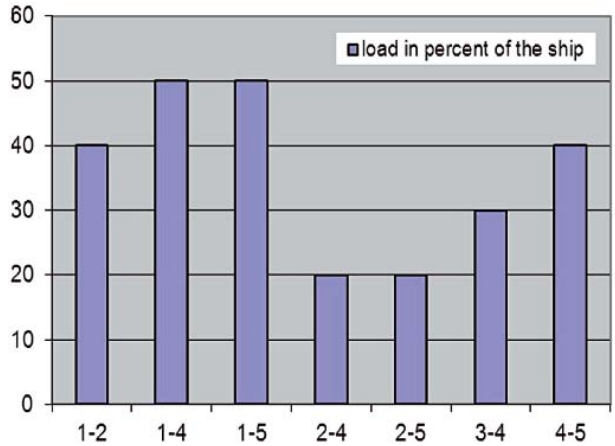

Fig. 1. *Potential transfer of container contingents between ports given in percentage of the total ship capacity*

Such a problem appears in route management for multi-purpose ships, tramper ships, container ships, where different contingents of cargo are transported by the ship with limited capacity; see [14]. Also, such an optimization tool can help to freight forwarder companies to select and manage the right mix of suppliers and to identify warehousing and distribution facilities best suited to customer needs. Very famous freight forwarders have extensive road and rail feeder network with links to their hubs, sub-hubs and gateways distributed all over the world; see [10, 11, 12].

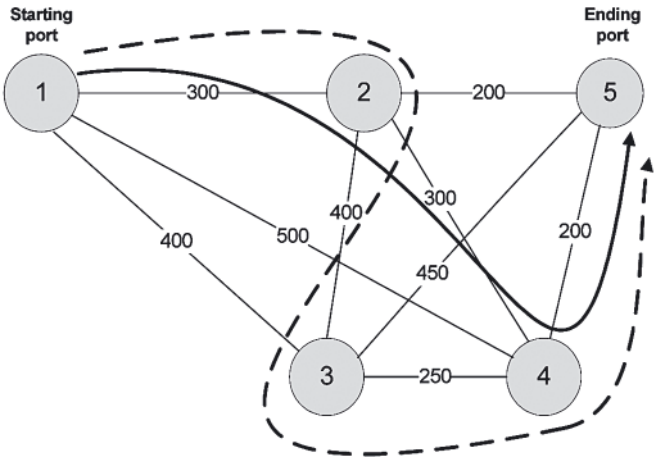

Fig. 2. *Port distances. Trivial routing solution is represented with full line if all freight costs are equal for all contingents. Dotted line marks the routing solution if contingent from port 3 to port 4 is more valuable than others*

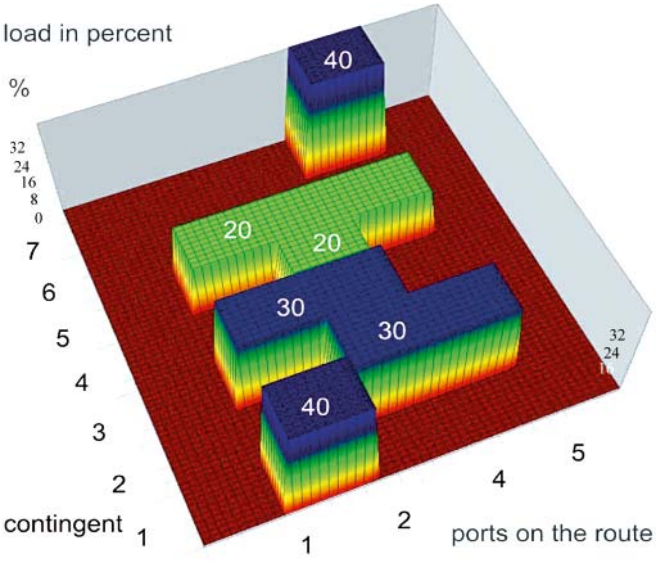

Fig. 3. *Trivial routing sequence 1-2-4-5 and the load amounts on board the ship during voyage*

The amount of different cargo loads (e.g. container) is in firm correlation because the total capacity of the ship is limited, e.g. in GT (Gross Tonnage) or in TEU (Twenty-foot Equivalent Unit). Taking into account cargo demands (unloading) for each cargo, and various loading ports with sufficient amount of cargo (number of containers) waiting to be loaded, we need an optimal transportation plan to minimize shipping and loading/unloading expenses, transshipment cost and cost of ship's stay in port (connected with duration of loading process). It can help in definition of ship capacity arrangement or for comparison of ships with different cargo capacity.

The non-linear transportation problem (NTP) with multiple (several) ports of loading (sources) and multiple destinations (sinks) is a very hard (NP-hard) problem so it is still the subject of many scientific papers. The problem can be solved using different techniques, see [5] and [16] In special circumstances the NTP can be seen as Minimum Cost Multiple Commodities Flow Problem (MCMCF); see [1] and [2]. In this paper we applied such network optimization approach. The mathematical model is formulated in section 2. The algorithm implementation is explained in section 3. Testing results and explanation of basic heuristic approach can be seen in section 4. Due to the presence of certain limitations the improvement of the algorithm is made in section 5. This approach, consisting of successive iterations, decreases the calculation complexity to an acceptable level.

MATHEMATICAL MODEL

Different kinds of good (e.g. container contingents) are differentiated with i for i = 1, 2,..., N. The ship with defined cargo capacity is shipping from the first to the last port marked with K M, with a possible set of intermediate (transshipment) ports. The objective is to find a loading and transshipment strategy that minimizes the total cost incurred over the whole voyage route consisting of M ports on the path (M ≤ K). We need the loading plan for various cargo/container contingents in each port to serve N cargo loads from the loading port to destinations (ports of discharge). The loading strategy consists of the load/discharge plan for each port and for each cargo contingent. The starting port on the route can be only for loading and the last port on the route can be only for discharging; other ports on the route may be for both.

The transportation problem can be represented by a flow diagram of non-oriented acyclic network. The problem can be solved using the network optimization technique as the shortest path problem; The problem can be solved using different techniques, see [13]. Figure 4 gives a network flow representation of MCMCF for N different cargo loads and M ports along the path. The common node "O" is the source of cargo for each cargo load with possible limitations. Some source ports can have limitation on charging capacity, but most of them are hub ports with capacity exceeding ship's earning capacity. Each load has the strictly defined discharging port. In Figure 4 the i-th row of nodes represents the capacity state of i-th type of cargo/container after loading in port m. Links between the nodes represent the amount of cargo transported between the ports (in TEU).

Such a transportation problem can be seen as the capacity expansion problem (CEP). For each cargo load we need appropriate ship space so it looks like expansion (load) or reduction (unload) of ship capacity in given bounds. Expansion and reduction can be done for each contingent separately but the free space can be reused for another contingent if previous load was discharged.

In the mathematical model of CEP the following notation is used:

- i, j and k = indices for cargo load. The N facilities are not ranked, just present different types of cargo/container contingents from 1, 2,..., N.
- m = indices the port of loading (charging) or discharging. The number of port of calls on the voyage including the departure port is M (m = 1,.., M).
- u, v = indices for ports in sub-problem, 1 ≤ u,..., v ≤ M. All ports on the route are transshipment ports except 1 and M.
- $x_{i,m}$ = quantity of i-th load of cargo amounts (e.g. containers contingent) being loaded on board in port m (TEU). Total loading amount in port m:

$$X_m = \sum_{i=1}^{N} x_{i,m} \tag{1}$$

- $Lx_{i,m}$ = limitations for each port and each cargo load. For convenience, the $x_{i,m}$ is assumed to be integer.
- $r_{i,m}$ = unloading of i-th cargo contingent in port m. For convenience, the $r_{i,m}$ is assumed to be integer. All unloading demands must be satisfied after discharging in last port on the route. Total discharging amount (unloading) in the port m.

$$R_m = \sum_{i=1}^{N} r_{i,m} \tag{2}$$

- $I_{i,m}$ = the amount of cargo load i at arrival in port m (or, equivalently, at departure from port m-1). Before the first

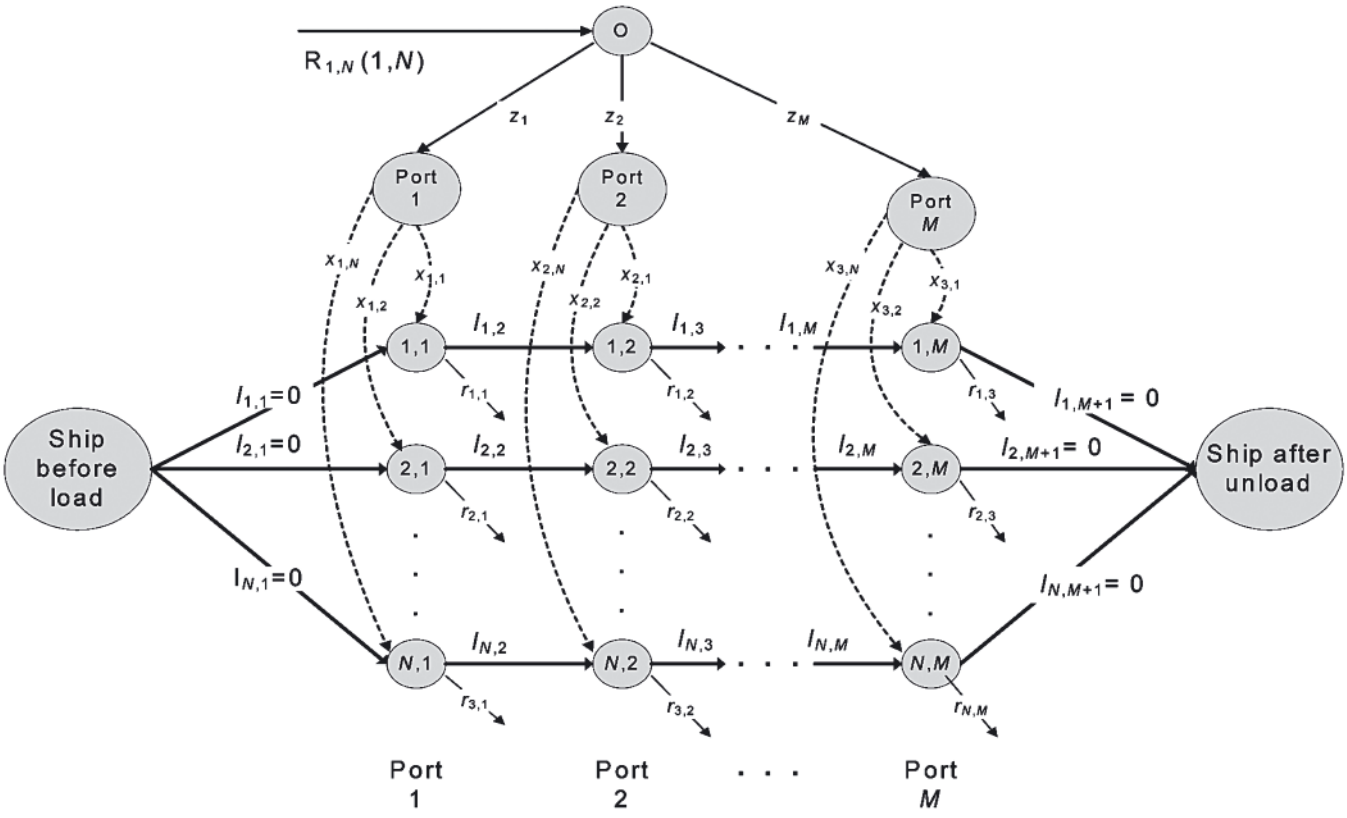

Fig. 4. *A network flow presentation of the trasnportation problem*

port of loading, $I_{i,m} = 0$. After the last port $I_{i,M+1} = 0$ for i = 1,…, N. Capacity values cannot be negative.

- step I_i = the lowest step of possible capacity charging and discharging for capacity type i. In numerical examples it can be set, e.g. step I_i = 10 % of total capacity of the ship.
- z_m = the total loading/unloading amount for all types of cargo (containers) in port m, i.e.,

$$Z_m = \sum_{i=1}^{N} x_{i,m} + r_{i,m} \tag{3}$$

- Q = ship's deadweights in tons:

$$Q = \sum_{i=1}^{N} Q_{i,m} \tag{4}$$

- $Q_{i,m}$ = element of ship deadweight used for i-th cargo contingent
- a_i = weight per unit of the i-th type of cargo unit (container)
- ship's transport capacity (GT or TEU) used for i-th cargo load:

$$W_{i,m} \le \frac{Q_{i,m}}{a_i} \tag{5}$$

- ship's transport capacity (GT or TEU):

$$W = \sum_{i=1}^{N} W_{i,m} \tag{6}$$

- used ship capacity between ports m and m + 1; for any m, m = 1, …, M:

$$I_m = \sum_{i=1}^{N} I_{i,m} \tag{7}$$

- shipping efficiency between ports m and m + 1:

$$e_m = \frac{I_m}{W} \tag{8}$$

- unused ship capacity in port m:

$$IDLE_m = \sum_{i=1}^{N} W_{i,m} - \sum_{i=1}^{N} I_{i,m} \tag{9}$$

- $lg_{i,m}$ = average number of cargo units (TEU) of i-th type of cargo (container) that can be loaded on board or discharged from board on daily basis in port m.

The total cost over time includes:

a) Transshipment cost on distance between ports m and m+1:

$$c_m = C_m \cdot d_m / s \tag{10}$$

where:

C_m = transportation cost of the ship during voyage (per day);

d_m = distance (in nautical miles or km);

s = speed of ship (in knots). Here it is not correlated with the number of cargo units (containers) on board, the influence on speed, oil consumption, agent taxes and freight expenses, but these effects could be easily incorporated. In our examples the constant speed of the ship is incorporated in the value C_m.

b) Loading and discharging cost in port m:

$$h_m = H_m \sum_{i=1}^{N} \left(\frac{x_{i,m} + r_{i,m}}{lg_{i,m}} \right) \tag{11}$$

where:

H_m = cost of ship stay in port m (per day).

The expenses for total duration of voyage and ship's stay in port during loading can be expressed as:

$$T = \sum_{m=1}^{M-1} \left(\frac{d_m}{s} + \sum_{i=1}^{N} \frac{x_{i,m} + r_{i,m}}{lg_{i,m}} \right) \tag{12}$$

c) Freight cost for transshipment of cargo type i is making profit $f_{i,m}$ to forwarder company. We want to incorporate minimization of expenses with maximal profit in the same optimization process, so we have to introduce the freight cost. We can do that by the exponential cost function showing the economy of scale:

$$f_{i,m} = A_{i,m} + B_{i,m} \cdot I_{i,m}^{a_{i,m}} \tag{13}$$

where $a_{i,m}$ represents the factor of concavity for an appropriate cargo type i and for appropriate transshipment conditions on the route (m = 1, …, u, v, …, M). In some cases the constant value A_i could be used as the freight cost f_i without the influence of cargo amount on board. The optimization process will find out the most attractive cargo loads for shipping revenue.

The optimization problem can be formulated as minimization of the objective cost function - as follows:

$$\min \sum_{i=1}^{N} \sum_{m=1}^{M-1} \{c_m(d_m) + h_m(z_m) - f_{i,m}(I_{i,m})\} \tag{14}$$

so that we have:

$$I_{i,m+1} = I_{i,m} + x_{i,m} - r_{i,m} \tag{15}$$

$$I_{i,1} = I_{i,M+1} = 0 \tag{16}$$

$$\text{for } m = 1, 2,.., M;\ i = 1, 2,..., N$$

Generally, we try to find out the optimal loading/unloading sequence with maximal freight costs and minimal expenses; see [4] and [5]. It is a very demanding dual max/min transportation problem but it can be solved in a very simple way. The minimization of the expenses should have a strong influence on maximal profit.

ALGORITHM DEVELOPMENT

Instead of a nonlinear convex optimization that can be very complicated and time-consuming, the network optimization methodology has been efficiently applied. The main reason for such an approach is the possibility of use of discrete capacity values for a limited number of contingent loads, which improves significantly the optimization process. The multi-constrained problem (MCP) can be formulated as the Minimum Cost Multi-Commodity Flow Problem (MCMCF). Such a problem (NP-complete) can be easily represented by the multi-commodity single (common) source/multiple destination network; see [2] and [3].

The definition of the single-constrained problem for CEP is to find a path P from starting to end port such that:

$$w(P) = \min \sum_{m=1}^{M+1} \sum_{i=1}^{N} w_{i\,m}(I_{i,m}, x_{i,m}, r_{i,m}) \tag{17}$$

where:

$$I_{i,m} \le L x_{i,m} \tag{18}$$

satisfying the additional condition:
max. distance of:

$$P = \sum_{m_1}^{m_2} lon_i \le LON \tag{19}$$

$$\text{for } i = 1, \ldots, N;\ m = 1, \ldots, M$$

where LON is the maximal length of the voyage in miles.

A path obeying the above conditions is said to be feasible. Note that there may be multiple feasible paths between the starting port and the ending port (node).

Generalizing the concept of the capacity states after loading/unloading of each contingent (load) m between ports on the route we define as a capacity point - α_m.

$$\alpha_m = (I_{1,m}, I_{2,m},..., I_{N,m}) \tag{20}$$

$$\alpha_1 = \alpha_{M+1} = (0, 0,..., 0) \tag{21}$$

Let C_m be the number of capacity point values at port m (load value for each contingent after departure from the port); see Fig. 4. Only one capacity point is for the starting port and one for the ending port on the route: $C_1 = C_{M+1} = 1$. The total number of capacity points is:

$$C_p = \sum_{m=1}^{M+1} C_m \tag{22}$$

Horizontal links (branches) represent capacity flows between two neighbor ports.

Formulation (21) implies that zero values are before loading at the starting point and after unloading at the ending point.

The network optimization can be divided into two steps. At first step the minimal transportation weights $d_{u,v}$ between all pairs of capacity points (neighbor ports on the route) are calculated. It is obvious that in CEP we have to find many cost values $d_{u,v}(\alpha_u, \alpha_{v+1})$ that emanate two capacity points of neighbor links (common router), from each node (u, α_u) to node $(v + 1, \alpha_{v+1})$ for $v \ge u$. Calculation of this value is the capacity expansion sub-problem (CES).

The most of the computational effort is spent on computing the sub-problem values. That number depends on the total number of capacity points, see (22). The total number of all possible $d_{u,v}(\alpha_u, \alpha_{v+1})$ values representing CES between two capacity points is:

$$N_d = \sum_{m=1}^{M} C_m \cdot C_{m+1} \tag{23}$$

At second step we are looking for the shortest path in the network with the former calculated weights.

As the number of all possible $d_{u,v}(\alpha_u, \alpha_{v+1})$ values depends on the total number of capacity points it is very important to reduce that number (C_p). This can be done through imposing of appropriate capacity bounds or by introduction of additional constraints (e.g. max. shipment delay). Through numerical test-examples we'll see that many loading / unloading solutions cannot be a part of the optimal expansion sequence. It is the way how the algorithm can be significantly improved. So we can obtain the near-optimal result with significant computational savings. The objective function for CES can be formulated as follows:

$$d_{u,v} = \max \left\{ \sum_{m=u}^{v} \left[\sum_{i=1}^{N} f_{i,m}(f_{i,m}) - c_m(d_m) + \right. \right. \left. \left. - h_m(z_m) - g_m(G_m) \right] \right\} \tag{24}$$

where:

$$I_{i,m+1} = I_{i,m} + D_{i,m}(x_{i,m}, r_{i,m}) \tag{25}$$

$$D_{i,m} = \sum_{i=1}^{N} (x_{k,m} - r_{l,m});\ k \ne l \tag{26}$$

$$\text{for } m = 1, 2,..., M+1;\ k, l = 1, 2,..., N.$$

For every CES many different solutions can be derived depending on D_i value. Each of them represents the capacity

state of each contingent onboard the ship with loading and unloading values (amounts) in appropriate port.

In the objective function the total cost includes some different costs (weights). We want to incorporate minimization of expenses with maximization of the profit in the same optimization process. All expenses have to have negative polarity; see (24). The freight cost is denoted with $f_{i,m}(I_{i,m})$. We can differentiate the freight cost for each container load (contingent).

The transportation cost is denoted with c_m (d_m), while the loading and discharging cost is denoted with $h_m(z_m)$. The idle capacity cost g_m (I_{max}-I_m) could be taken in account, but only as a penalty cost to force the usage of the maximum capacity (prevention of unused/idle capacity). The port taxes can be incorporated with h_m. Costs are often represented by the fix-charge cost or by a constant value. It should be assumed that all function costs are concave and non-decreasing (some of them reflecting economies of scale) and they differ from one port to another. The objective function is necessarily the non-linear cost. With variation of cost parameters the optimization process could be easily managed, looking for benefits of the most appropriate transportation solution; see [6]. Instead of maximization of the profit we can use minimization of the reciprocal value or minimization of negative value of the objective function (24). In both cases it leads to maximization of the profit.

Suppose that all links (sub-problems) in diagram from Fig. 5. are calculated, the optimal solution for CEP can be found by searching for the optimal sequence of capacity points and their associated link state values; see Fig. 2. Then the Dijkstra's or Floyd's algorithm, or any similar algorithm, can be applied; see [7] and [13].

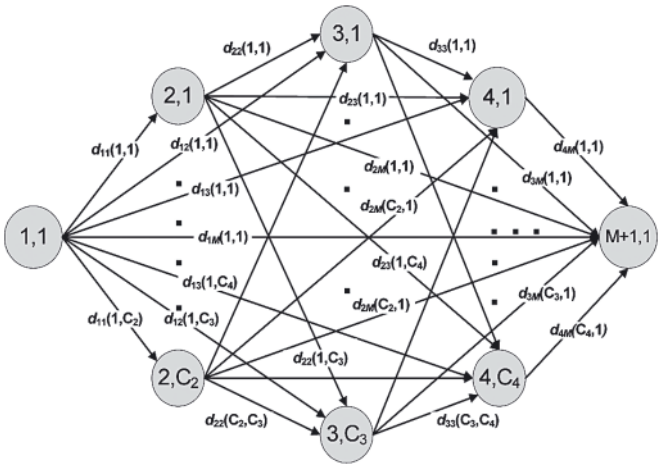

Fig. 5. *The CEP problem can be seen as the shortest path problem for an acyclic network in which the nodes represent all possible values of capacity points. Links connecting neighbor ports on the route represent CES values*

The complexity of the proposed algorithm is $O(C_p^2)$. As we said before C_p is in a strong correlation with the number of ports M and the number of contingents N but also with the capacity increment step I_i that can vary from contingent to contingent.

If the contingent capacity is given in TEU we have the problem with large number of capacity states. Instead, we use contingent amounts given in the percentage of the total ship capacity; see Fig. 1.

In this research the load amount on board does not influence on voyage speed neither to oil consumption but it could be easily incorporated. The loading strategy consists of loading/unloading plans for each port and for each contingent. The starting port on the route can be only for loading purpose and the last port is only for unloading; other transshipment ports may be for both.

Some limitations on the ship capacity can exist, but today most ports have loads not exceeding the ship capacity.

RESULTS OF BASIC HEURISTIC

In the route definition shown, for example in Fig. 2 we have the starting port 1 and the ending port 5, but any of three middle ports can also be included in the route.

All distances between ports are defined in miles. From Fig. 1 we can see traffic demands (possible transfer of contingents) given in the percentage of the total ship capacity. That information is gathered through market research or from statistics. From input data we can see seven contingents waiting for transport. It is obvious that the loads have to be transported on relation: 1-2 (40 %); 2-5 (50 %); 1-4 (50 %); 2-4 (20 %) 1-5 (20 %), 3-4 (30 %) and 4-5 (40 %), but we have no demands from port 2 to port 3. For simplicity all costs elements are equal ($A_{i,m} = 0$, $B_{i,m} = 15.0$/ % of capacity; $C_{i,m} = 3.0$/km; $H_{i,m} = 1.0$/ % of capacity; $G_{i,m} = 0$; and concavity for all costs $a_{i,m} = 0.85$.

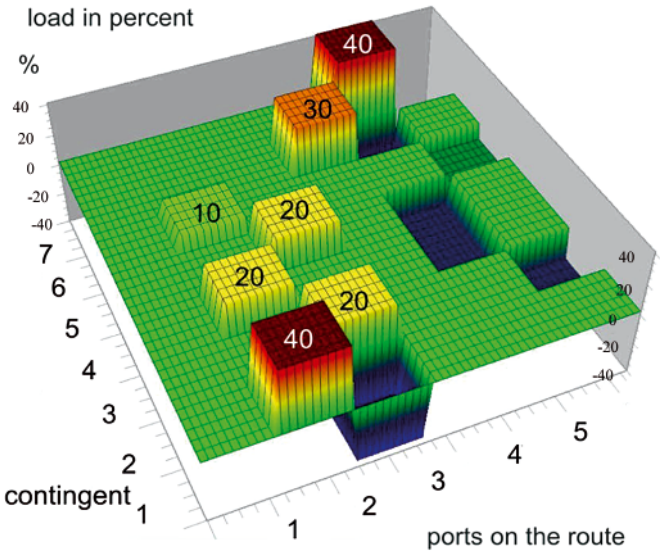

Fig. 6. *Optimal solution given by loading and unloading amounts in each port on the route*

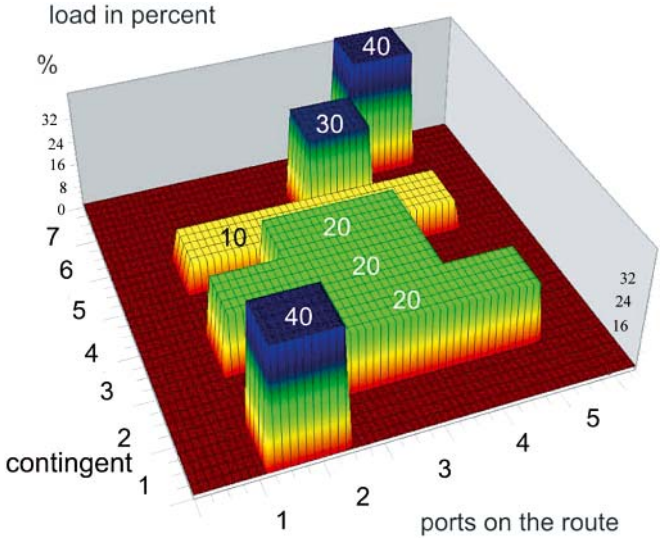

Fig. 7. *Ship's occupancy on the route with particular contingents onboard*

Only the freight cost for contingent 6 (3-4) is $B_{i,m} = 30{,}0$ that is significantly higher. In this example we force travelling across the port 3 as we have contingent from 3-4 with valuable load. According to all transport costs and the price determination (freight cost, oil consumption, transshipment cost, port taxes

etc.) we can design the route which will be the most profitable. Figures 6 and 7 present the resulting (best) route. Fig. 6. shows the loading and unloading amounts in appropriate port and Fig.7 shows the load amounts of every contingent on board the ship during the voyage. For the basic option we used the same capacity increment step I_i for all contingents and it is 10 %. We are aware that such capacity resolution is not satisfactory and, in general, we should be far away from the optimal result. In that case we have 1438 capacity states and 1438 x 1438 CES values.

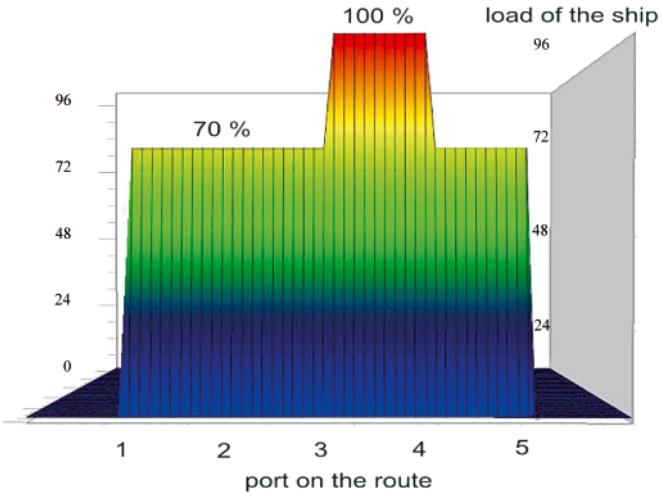

Fig. 8. *Efficiency of the ship on the route*

For our test-example the best routing option is from port 1 to port 2, to port 3, to port 4, and, finally, to port 5. The solution does not extract port 3 because it is more profitable to go this way (in spite of longer distance).

Figure 8 presents the efficiency of the ship, so idle capacity during the voyage is obvious. Only from port 3 to port 4 we have no idle capacity (100 %) on board. For this example the cost elements are similar but they can be differentiated from port to port and from contingent to contingent.

ALGORITHM LIMITATIONS AND POSSIBLE IMPROVEMENT

As we said before, the crucial element is the number of capacity points C_p. In our numerical example the starting capacity increment is 10 % and the number of capacity point is 1438. Calculation of so many CES values could be very demanding but it is still acceptable. If we decide to have smaller capacity increment step I_i the number of capacity points drastically increases.

For example, the capacity of a large container ship can be 5.000 - 10.000 TEU. The VLCS class (Very Large Container Ships) has more than 10.000 TEU. If we use the capacity increment of 10 % it means 500 - 1000 TEU. Normally we need better resolution e.g. 50 - 100 TEU or less. In that case we have to use step I_i = 1 % or 0,1 % of ship capacity. If we decide to apply for step I_i the value of 1 % instead, the number of capacity states rises up to approx. 15 000, which means that we have to calculate approx. 15 000 x 15 000 CES values. Such approach has no perspective in case of shipping supported with average computation power.

As we usually have limitation in reliable computation up power (average PC) we have to decrease that number somehow. It is clear that we need another approach to increase the resolution, but the corresponding computing complexity has to be acceptable.

So we decided to calculate it in a number of steps (with successive iterations). The first step is shown in Fig. 6 and Fig. 7. The numerical values are shown in table 1. After that we can shorten the range of capacity points using some of artificial intelligence techniques. For example, the calculated routing sequence shows that the second contingent is in amount of 20 % so we can use the range from 15 – 25 only. For some contingents we use step I_i = 5 % and for some 1 %. Capacity limitations for each contingent are given in table 1. In that case we have the number of capacity points C_p = 3483 (instead of millions). It is obvious that the problem complexity is still acceptable; see table 1. Also, we got significantly better result.

Tab. 1. *Results for the routing sequence in three successive iterations*

	1. iteration	**Cost elements**				**2. iteration**		**3. iteration**		
Load i	**Max. capacity**	**$B_{i,m}$ $f_{i,m}$ = $B_{i,m}I_i^{ai,m}$**	**C_i c_i = $C_i d_m^{ai,m}$**	**H_i h_i = $H_i Z_i^{ai,m}$**	**C_p**	**Load/Max. capacity Delta = 5**	**C_p**	**Load/Max. capacity Delta = 2**	**C_p**	**Load**
1	40 (0-40) I_{step} = 10 %	15.	3.	2.	C_1 = 89 C_2 = 291 C_3 = 968 C_4 = 89 C_5 = 1	40 (35-40) I_{step} = 5 %	C_1 = 132 C_2 = 1188 C_3 = 2126 C_4 = 36 C_5 = 1	40 (38 – 40) I_{step} = 1 %	C_1 = 75 C_2 = 625 C_3 = 1293 C_4 = 75 C_5 = 1	40
2	50 (0-50) I_{step} = 10 %	15.	3.	2.		20 (15-25) I_{step} = 5 %		20 (18-22) I_{step} = 1 %		18
3	50 (0-50) I_{step} = 10 %	15.	3.	2.		20 (15-25) I_{step} = 1 %		17 (15-19) I_{step} = 1 %		17
4	20 (0-20) I_{step} = 10 %	15.	3.	2.		20 (15-20) I_{step} = 1 %		18 (16-20) I_{step} = 1 %		18
5	20 (0-20) I_{step} = 10 %	15.	3.	2.		10 (5-15) I_{step} = 1 %		15 (13-17) I_{step} = 1 %		17
6	30 (0-30) I_{step} = 10 %	30. (15.)	3.	2.		30 (25-30) I_{step} = 5 %		30 (28-30) I_{step} = 1 %		30
7	40 (0-40) I_{step} = 10 %	15.	3.	2.		40 (35-40) I_{step} = 5 %		40 (38-40) I_{step} = 1 %		40
Total CES					1438		3483		2069	
Profit						**1926,33**		**1931,53**		**1932,39**

In the next step (third iteration) we applied the smaller range of capacity e.g. 18 - 22. Also, we can use smaller increment step I_i = 1 % for all contingents. In that case we have 2069 capacity states that is still an acceptable number. It means that number of possible sub-problems Nd is about 4 million (instead of hundreds of millions). From Fig. 9 we can see that the routing sequence slightly differs from the previous result and the profit is increasing again. From Fig. 10 it is clear that the idle capacity of the ship on the route is lower. With this step by step method we can increase the resolution of the capacity states significantly and because of that we can reach much closer to the optimum.

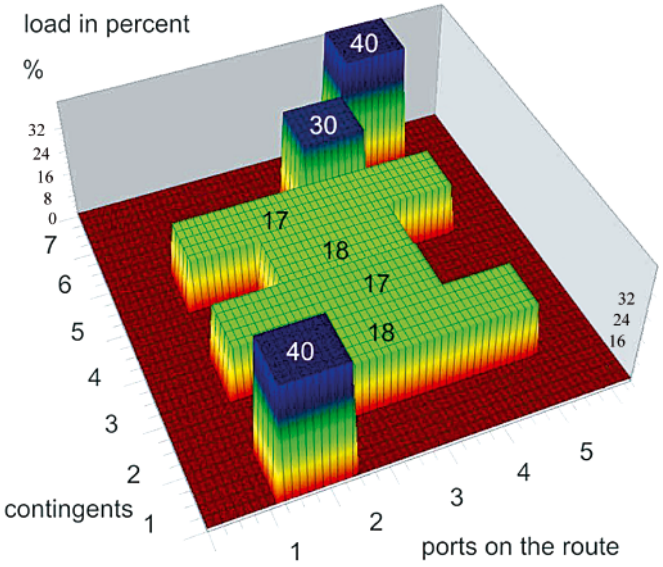

Fig. 9. *After third iteration the profit is increased*

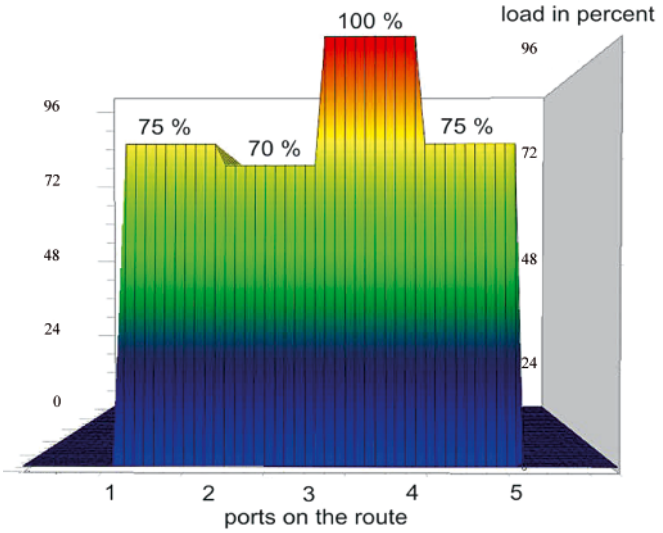

Fig. 10. *Efficiency of the ship is better than before*

Through many test examples it is clear that the presented approach functions very well and the complexity of the calculation process is under control. Without such step by step calculation method the complexity may be too big.

CONCLUSIONS

The proposed algorithm shows ability to solve very complex transportation problems with many loading/unloading ports and with many contingents of the load. The most important benefit is that the algorithm can solve nonlinear problems which normally occur in practice. Also, the existing limited calculation power in shipping surrounding makes the algorithms with huge complexity useless. The present approach consisting of a number of successive iterations decreases the calculation complexity to an acceptable level. In the same time it ensures to forwarder managers very fine modulation of many input values, leading the optimization process in wanted direction.

With such optimization tool the shipping companies (freight forwarder) can ensure significant savings on multiport routes and be more profitable by following the demands and easily adapt to their changes. Also, such innovative solutions can optimize the supply chains and reduce the logistic costs.

REFERENCES

1. Ouorou A., Mahey P., Vial J.Ph.: *A Survey of Algorithms for Convex Multi-commodity Flow Problems, Markup Languages*, Vol. 46, No. 1,, pp. 126-147, (2000).
2. Castro J., Nabona N.: *An Implementation of Linear and Nonlinear Multi-commodity Network Flows*, European Journal of Operational Research, Vol. 92, No.1, pp. 37-53, (1996).
3. Fleisher L.: *Approximating multi-commodity flow independent of the number of commodities*, Siam J. Discrete Math. Vol. 13, No. 4, pp. 505-520, (2000).
4. Fonoberova M., Lozovanu D.: *The maximum flow in dynamic networks*, Computer Science Journal of Moldova 3(36), pp. 387–396, (2004).
5. Garaix T., Artiques C., Feillet D. & Josselin D.: *Vehicle routing problems with alternative paths: An application to on-demand transportation*. European Journal of Operational Research. Volume 204, No. 1, pp. 62-75, (2009).
6. Krile S.: *Application of the Minimum Cost Flow Problem in Container Shipping*, Proc. of 46th ELMAR' 04 (International Symposium of Electronics in Marine), pp. 466-471, Zadar, (2004).
7. Krile S.: *Optimal Voyage Planning in Container Shipping*, Proc. of 25th International Conference of Automation in Transportation, Zagreb–Copenhagen, pp. 32*Slika 3. Kontingenti tereta koji čekaju na prijevoz* - 35, (2005).
8. Krile S.: *Logistic Support for Loading/Unloading in Shipping with Multiple Ports / Logistika za ukrcaj i iskrcaj na plovidbi s više luka*, Proc of. 31st International Conference of Automation in Transportation (KOREMA), Pula – Milan, pp. 94–97, (2011).
9. Krile S.: Krile M.: *Better Profitability of Multi-Stop Flight Routes*, Proc. of. International Conference of Automation in Transportation (KOREMA), Zagreb - Wien, pp. 97-100, (2012).
10. Yan S Chen H.C, Chen Y.H, & Lou T.C.: *Optimal scheduling models for ferry companies under alliances*. Journal of Marine Science and Technology, Vol. 15, No. 1, pp. 53-66, (2007).
11. Yan S. and Chen H.: *A scheduling model and a solution algorithm for inter-city bus carriers*. Transportation Research Part A: Policy and Practice, Volume 36, No. 9, pp. 805-825, (2002).
12. Yang S, Tang C.H, & Lee M.C.: *A flight scheduling model for Taiwan airlines under market competitions*. The International Journal of Management and Science. Vol. 35, No. 1, pp. 61-74, (2007).
13. Zangwill I. W.: *Minimum Concave Cost Flows in Certain Networks*, Management Science, Vol. 14, pp.429-450, (1968).
14. Zenzerovic Z. and Beslic M.: *Contribution to the Optimization of the Cargo Transportation Problem*, Promet - Traffic - Traffico, Vol. 15, No 1, Portorož, Trieste, Zagreb, pp. 13-17, (2003).
15. Zhang X., Xiea F., Jiab R.: *Hybrid Genetic Algorithm for Minimum Saturated Flow in Emergency Network*, IJACT: International Journal of Advancements in Computing Technology, Vol. 4, No. 21, pp. 133 ~ 144, (2012).
16. Xiea F., an Jiab R.: *Nonlinear fixed charge transportation problem by minimum cost flow-based genetic algorithm*, Computers & Industrial Engineering, Vol. 63, No. 4,, pp. 763–778, (2012).

CONTACT WITH THE AUTHOR

Srećko Krile, Assoc. Prof.,
University of Dubrovnik (Sveučilište u Dubrovniku)
Electric Engineering and Computing Department
Ćira Carića 4, 20000 Dubrovnik, Hrvatska
Tel: 385 20 445-739, Fax: 385 20 435-590,
e-mail: srecko.krile@unidu.hr

POLISH MARITIME RESEARCH 4(80) 2013 Vol 20; pp. 87-94
10.2478/pomr-2013-0045

Legal aspects of low-emission shipping in the light of provisions of "sulphur directive" adopted by the European Union

Beata Madejska, M. Sc.,
Independent lawyer

ABSTRACT

Shipping emits a variety of air pollutants: sulphur dioxide (SO_x), nitrogen oxides (NO_x), carbon dioxide (CO_2) and particulate matter PM. Air pollutant emissions from maritime transport can be transported over long distances and thus increasingly contribute to air quality problems. Key environmental regulations (international and European) coming into force in this decade address emissions of SO_x, NO_x, CO_2 and PM to control and limit their impact in the atmosphere. In the European Union, accordingly to the legal regulations, in the sulphur emission control areas the required SO_x content of fuel will be reduced from 1.5 % to 0.1 % beginning January 2015. Globally, from 2020 onwards, ships operating in all other European Sea areas will have to use fuels with sulphur content of 0.5 % or less.

Key words: ship emissions; sulphur dioxide; nitrogen oxides; sulphur directive; MARPOL Annex VI; protection of the environment; control on sulphur emissions

BACKGROUND

The main sources of air pollution are transport, power generation, industry, agriculture, and heating. All these sectors emit a variety of air pollutants – sulphur dioxide, nitrogen oxides, carbon dioxide and particulate matter. Shipping is a large and growing source of different kinds of atmospheric emissions. Air pollutant emissions from maritime transport can be transported over long distances and thus increasingly contribute to air quality problems in the European Union. Sulphur emissions are harmful to our health and to the wider environment, and need to be reduced. It is right that the shipping industry is being required to reduce its emissions in the way that other industries and transport sectors have already done. Current forecasts indicate that shipping in the EU will produce more emissions than all land-based sources by 2020 (*source: Clean Air from Europe impact assessment, p. 31, 2005*). Ship emissions contribute to acid rain (which damages crops and buildings), air pollution, ground-level ozone (smog), and marine eutrophication in the European Union. One of the European areas which is highly susceptible to the environmental impacts of ship emissions is the Baltic Sea.

The Baltic Sea with a total area of about 370,000 km^2 is one of the world's largest brackish water basins, but it is also a small sea on a global scale. The Baltic is almost entirely land-locked and the water exchange is very limited. It is also a high priority for the EU, owning to its status as a Sulphur Emission Control Area, due to high pollution of the region. The Commission describes the Baltic Sea and also the North Sea and English Channel as "very fragile ecosystems", because of their significance for recognized ecological (unique ecosystem) and socio-economic reasons (recreation, tourism).

In order to achieve the desired effect on the environment, emissions regulations must be agreed and applied internationally.

INTERNATIONAL LEGISLATION (IMO CONVENTION)

The issue of controlling air pollution from ships, in particular, noxious gases from ships' exhausts was discussed in the lead up to the adoption of the 1973 MARPOL Convention. However it was decided not to include regulations concerning air pollution at the time.

Meanwhile, air pollution was being discussed in other arenas. The 1972 United Nations Conference on the Human Environment in Stockholm marked the start of active international cooperation in combating acidification, or acid rain. Between 1972 and 1977, several studies confirmed the hypothesis that air pollutants could travel several thousand kilometers before deposition and damage occurred. This damage includes effects on crops and forests. In 1979, a ministerial meeting on the protection of the environment, in Geneva, resulted in the signing of the Convention on Long-range Transboundary Air Pollution by 34 governments and the European Community. This was the first international legally binding instrument to deal with problems of air pollution on a broad regional basis (*source: IMO website*).

The MARPOL Convention is the main international convention covering prevention of pollution of the marine

environment by ships from operational or accidental causes. It is a combination of two treaties adopted in 1973 and 1978, respectively, and also includes the Protocol of 1997 (Annex VI). It has been updated by amendments through the years.

The International Convention for the Prevention from Ships (MARPOL) was adopted on 2nd November 1973 at IMO and covered pollution by oil, chemicals, harmful substances in packaged form, sewage and garbage. The original Convention was signed on 17 February 1973, but did not come into force due to lack of ratifications. As a combination of 1973 Convention and the 1978 Protocol, the current MARPOL convention (commonly known as MARPOL 73/78) entered into force on 2 October 1983. As of May 2013, 152 states, representing 99,2 percent of the world's shipping tonnage, are parties to the convention.

Annex VI Prevention of Air Pollution from Ships entered into force 19th May 2005. The revision of Annex VI was adopted in October 2008 and entered into force on 1st July 2010.

The regulations in this Annex set limits on sulphur dioxide and nitrogen oxide, emissions from ship exhausts as well as particulate matter.

Annex VI contains provisions allowing for special Sulphur Emission Control Areas (SECAs) to be established with more stringent controls on sulphur emissions. In these areas the sulphur content of fuel oil used onboard ships must not exceed 1.5 % by mass. Alternatively, ships must fit an exhaust gas cleaning system or use any other technological method to limit sulphur dioxide emissions.

The Baltic Sea Area is designated as a Sulphur Emission Control Area in the Protocol. The North Sea was adopted as Sulphur Emission Control Area in July 2005.

EUROPEAN LEGAL PROVISIONS CONCERNING REDUCTION OF SHIP EMISSIONS

At the European Union level there have been subsequent steps to regulate sulphur content in liquid fuels to reduce its emissions in the atmosphere during the past twenty years. Historically, the sulphur content of certain liquid fuels was regulated by Directive 93/12/EC, adopted in 1993 (*Council Directive 93/12/EEC of 23 March 1993 relating to the sulphur content of certain liquid fuels, OJ 121, 11.5.1999*), which placed restrictions on the marketing of diesel fuels used in road vehicles and gas oil used for off-road transport (but excluding aviation).

In the following years it has been deemed important to lay down limits for the sulphur content of other liquid fuels, in particular heavy fuel oil, marine gas oils and gas oils, on the basis of cost effectiveness studies and also in view of the regulation in Annex VI on sulphur content of marine fuel in the IMO's MARPOL Protocol of 1997. The result was the Sulphur Content of Liquid Fuels Directive No 32 adopted on 26 April 1999 (*Council Directive 1999/32/EC of 26 April 1999 relating to a reduction in the sulphur content of certain liquid fuels and amending Directive 93/12/EEC*). It established limits for sulphur content in heavy fuel oil (1.0 % after 1st January 2003) and gas oil, including marine gas oil (0.2 % after 1st January 2000 and 0.1 % after 1st January 2008). In the latter case derogations for Greece throughout its territory, for Spain with regard to the Canary Islands, for France with regard to the French Overseas Departments, and for Portugal with regard to the archipelagos of Madeira and Azores were also included since the new limits may present technical and economic problems for these regions. In the Directive was also included a recommendation to continue the initiative to have the North Sea including English Channel declared as sulphur emission control area (ECA). The requirements concerning the sulphur content of gas oil and heavy fuel oil, heating oil and marine fuels appeared in the Directive to follow the incorporation into EU law of rules adopted by the International Maritime Organization. The incorporation of IMO standards aimed, inter alia, at reinforcing the restricted international monitoring and enforcement regime.

Member States were obliged to transpose the Directive into national legislation before 1st June 2000.

The list of national enforcement measures in exemplary EU Member States, embracing the provisions of the Directive 93/12/EEC, are shown in the table below:

Item	Country	National execution measures
1.	**DENMARK**	1. Bekendtgorelse af 22 juni 2000 om begraensning av svovindholdet I visse flydende braendstoffer (Legal act: *Bekendtgřrelse*; Official Journal: *Administrative measures*)
2.	**GERMANY**	1. Dritte Verordnung zur Durchfuhrung des Bundes-Immissionsschutzgesetzes (Verordnung über den Schwefelgehalt bestimmter flüssiger Kraft- oder Brennstoffe - 3 BlmSchV) vom 24/06/2002 BGbl. Teil I n° 41 du 28/06/2002 p. 2243 (Legal act: *Verordnung*; Official Journal: *Verwaltungsmassnahmen*, Entry into force: *24/06/2002*; Reference: *(SG(2002)A/07440)* 2. Zweite Verordnung zur Änderung der Verordnung über die Beschaffenheit und die Auszeichnung der Qualitäten von Kraftstoffen réf.: Bundesgesetzblatt I S. 2243 of 28 June 2002. Date d'adoption de l'acte:24/06/02 (Legal act: *Verordnung*; Official Journal: *Verwaltungsmassnahmen*
3.	**ESTONIA**	1. Välisõhu kaitse seadus (Legal act: *seadus*, number: *RTI, 19.05.2004, 43, 298* ; Official Journal: *Elektrooniline Riigi Teataja*, number: *RTI, 19.05.2004, 43, 298,* Entry into force: *30/09/2004*; Reference: *(MNE(2004)52690)* 2. Säästva arengu seadus (Legal act: Legal act: *seadus*, number: *RT I 1995, 31, 384*; Official Journal: *Elektrooniline Riigi Teataja*, number: *RT I 1995, 31, 384*, Entry into force: *01/01/2001*; Reference: *(MNE(2003)54275)* 3. VÄLISÕHU KAITSE SEADUS (Legal act: *seadus*; Official Journal: *Elektrooniline Riigi Teataja*, Publication date: *08/01/2004*; Reference: *(MNE(2003)55186)* 4. Vedelkütuse nõuetekohasuse tõendamise protseduuride ja korra kinnitamine (Legal act: *Majandusministri määrus*; Official Journal: *Elektrooniline Riigi Teataja*, Publication date: *01/11/1998*; Reference: *(MNE(2003)54970)* 5. Tarbijakaitseseadus (Legal act: *seadus*, number: *RTI, 15.03.2004, 13, 86*; Official Journal: *Elektrooniline Riigi Teataja*, number: *RTI, 15.03.2004, 13, 86*, Entry into force: *15/04/2004*; Reference: *(MNE(2003)55290)*

Item	Country	National execution measures
3.	**ESTONIA**	6. Nõuded vedelkütusele (Legal act: *Majandus- ja Kommunikatsiooniministri määrus*, number: *RTL 2004, 134, 2080*; Official Journal: *Elektrooniline Riigi Teataja*, number: *RTL 2004, 134, 2080*, Entry into force: *22/10/2004*; Reference: *(MNE(2003)55190)* 7. PIIRIÜLESE ÕHUSAASTE KAUGLEVI 1979. AASTA KONVENTSIOONI ÕHUSAASTEAINETE KAUGLEVI SEIRE JA HINDAMISE EUROOPA KOOSTÖÖPROGRAMMI (EMEP) PIKAAJALISE FINANTSEERIMISE PROTOKOLLIGA ÜHINEMISE SEADUS (Legal act: *seadus*, number: *RTII, 03.01.2001, 1, 2* ; Official Journal: *Elektrooniline Riigi Teataja*, number: *RTII, 03.01.2001, 1, 2,* Publication date: *01/06/2002*, Entry into force: *01/06/2002*; Reference: *(MNE(2003)54884)* 8. Keskkonnajärelevalve seadus (Legal act: *seadus*, number: *RT I 2001, 56, 337*; Official Journal: *Elektrooniline Riigi Teataja*, number: *RT I 2001, 56, 337*, Entry into force: *01/01/2004*; Reference: *(MNE(2003)54269)*
4.	**IRELAND**	1. The Air Pollution Act (Sulphur Content of Heavy Fuel and Gas Oil) Regulations, 2001 S.I. n° 13 of 2001, Reference: *SG(2001)A/01569)*
5.	**FINLAND**	1. Landskapslag om tillämpning i landskapet Aland av vissa riksförfattningar rörande atgärder mot förorening av luften 02/04/1991 AFS Nr 32 de 1991 du 25/04/19991; SG(00)A/16230 du 03/01/2001 et idem SG(2001)A/1657 du 07/02/2001 (Official Journal: *Ĺlands Författningssamling (ĹFS)*, number: *32/1999*, Publication date: *25/04/1999*, Entry into force: *02/04/1991)* 2. Alands Landskapsstyrelses Beslut om ändring av Alands landskapsstyrelses beslut om tillämpning i landskapet Aland av vissa statsradsbeslut rörande atgärder mot förorening av luften 12/10/2000 AFS Nr 72 de 2000 du 21/11/2000; SG(00)A/16230 du 03/01/2001 et idem SG(2001)A/1657 du 07/02/2001 (Official Journal: *Ĺlands Författningssamling (ĹFS)*, number: *72/2000*, Publication date: *21/11/2000*, Entry into force: *12/10/2000)* 3. Valtioneuvoston asetus râskaan polttoöljyn ja kevyen polttoöljyn rikkipitoisuudesta (766/200) 24/08/2000 Suomen Säädöskokoelma 30/08/2000 N° 766, page 1986; SG(2001)A/1657 du 07/02/2001 (Legal act: *Valtioneuvoston asetus*, number: *766/200*, Entry into force: *24/08/2000)* 4. Statsradets förodning nr 766 (Reference: *(SG(2000)A/11718)*
6.	**FRANCE**	1. Arręté du 11 aoűt 1999 modifiant l'arręté du 29 aoűt 1957 modifié fixant les caractéristiques du fioul domestique JORF 08/09/1999 - SG(00)A/8601 du 10/07/00 Legal act: Arręté, number: 1; Official Journal: Journal Officiel de la République Française (JORF), Publication date: 08/09/1999, Page: 00, Entry into force: 01/08/1999 2. Arręté du 25 avril 2000 relatif aux caractéristiques des fiouls lourds JORF 27.06/2000 p.7056 - SG(00)A/8601 du 10/07/00 Legal act: *Arręté, number: 2; Official Journal: Journal Officiel de la République Française (JORF), Publication date: 27/06/2000, Page: 7056, Entry into force: 05/04/2000;* Reference: *(SG(00)A/8601)* 3. Arręté du 19 juin 2000 relatif aux caractéristiques du diesel marine léger JORF 27.06/2000 p.9648 - SG(00)A/8601 du 10/07/00 Legal act: *Arręté, number: 1; Official Journal: Journal Officiel de la République Française (JORF), Publication date: 27/06/2000, Page: 9648, Entry into force: 09/06/2000; Reference: (SG(00)A/8601)* 4. Arręté du 15 aoűt 2000 modifiant l'arręté du 25 juillet 1997 relatif aux prescriptions générales applicables aux installations classées pour la protection de l'environnement soumises ŕ déclaration sous la rubrique n° 2910 (combustion) JORF du 25/09/2000 page 15313 - SG(01)A/71 du 05/01/2001 Legal act: *Arręté*, number: *1*; Official Journal: *Journal Officiel de la République Française (JORF)*, Publication date: *25/09/2000*, Page: *15313*, Entry into force: *05/08/2000* 5. Arręté du 19 juin 2000 relatif aux caractéristiques du gazole pęche Legal act: *Arręté*, number: *1*, Entry into force: *09/06/2000*; Reference: *(SG(2000)A/08601)*
7.	**LATVIA**	1. Par vides aizsardzību (Legal act: *Likums*; Official Journal: *Latvijas Vēstnesis*, number: *33*, Publication date: *29/08/1991*; Reference: *(MNE(2003)50370)* 2. Administratīvo pārkāpumu kodekss (Legal act: *Likums*; Official Journal: *Latvijas Vēstnesis*, Publication date: *01/07/1985*; Reference: *(MNE(2003)50416)* 3. Ministru Kabineta 2006.gada 26.septembra noteikumi Nr. 801 Noteikumi par sēra satura ierobežošanu atsevišķiem šķidrās degvielas veidiem (Legal act: *Ministru Kabineta noteikumi*, number: *801*; Official Journal: *Latvijas Vēstnesis*, number: *161*, Publication date: *10/10/2006*, Entry into force: *11/10/2006*; Reference: *(MNE(2006)56669)* 4. Likums "Par atbilstības novērtēšanu" (Legal act: Official Journal: *Latvijas Vēstnesis*, number: *139 Likums*;, Publication date: *20/08/1996;* Reference: *(MNE(2003)50596)* 5. Grozījumi likumā „Par piesārņojumu" (Legal act: *Likums*; Official Journal: *Latvijas Vēstnesis*, number: *62*, Publication date: *19/04/2006*, Entry into force: *03/05/2006*; Reference: *(MNE(2006)54960)*

Item	Country	National execution measures
7.	**LATVIA**	6. Ministru Kabineta 2004.gada 2.marta noteikumi Nr. 125 „Noteikumi par sēra satura ierobežošanu noteiktiem šķidrās degvielas veidiem" (Legal act: *Ministru Kabineta noteikumi*; Official Journal: *Latvijas Vēstnesis*, number: *37*, Publication date: *09/03/2004*; Reference: *(MNE(2003)50860)* 7. Likums Par piesārņojumu (Legal act: *Likums*; Official Journal: *Latvijas Vēstnesis*, number: *51*, Publication date: *29/03/2001*; Reference: *(MNE(2003)50252)* 8. Ministru Kabineta 2002. gada 20. augusta noteikumi Nr. 379 „Kārtība, kādā novēršama, ierobežojama un kontrolējama gaisu piesārņojošo vielu emisija no stacionāriem piesārņojuma avotiem" (Legal act: *Ministru Kabineta noteikumi; Official Journal: Latvijas Vēstnesis*, *number: 122,* Publication date 30/08/2002; Reference: (MNE(2003)50757).
8.	**LITHUANIA**	1. LIETUVOS RESPUBLIKOS APLINKOS MINISTRO,LIETUVOS RESPUBLIKOS ŪKIO MINISTRO IRLIETUVOS RESPUBLIKOS SUSISIEKIMO MINISTROĮSAKYMAS NR. D1-201/4-128/3-170 DĖL LIETUVOS RESPUBLIKOS APLINKOS MINISTRO, LIETUVOS RESPUBLIKOS ŪKIO MINISTRO IR LIETUVOS RESPUBLIKOS SUSISIEKIMO MINISTRO 2001 M. RUGPJŪČIO 31 D. ĮSAKYMO NR. 438/268/266 „DĖL KURO IR DEGALŲ KOKYBĖS APLINKOSAUGINIŲ RODIKLIŲ PATVIRTINIMO" PAKEITIMO (Legal act: *Įsakymas*, number: *D1-2001/4-128/3-170/2004*; Official Journal: *Valstybės žinios*, number: *71*, Publication date: *30/04/2004*, Entry into force: *01/05/2004*; Reference: *(MNE(2004)57754)* 2. Lietuvos Respublikos aplinkos ministro, Lietuvos Respublikos ūkio ministro ir Lietuvos Respublikos susisiekimo ministro 2008 m. lapkričio 27 d. įsakymas Nr. D1-638/4-589/3-468 "Dėl Lietuvos Respublikos aplinkos ministro, Lietuvos Respublikos ūkio ministro, Lietuvos Respublikos susisiekimo ministro 2006 m. rugpjūčio 31 d. įsakymo Nr. D1-399/4-336/3-340 „Dėl Lietuvos Respublikoje vartojamų naftos produktų, biodegalų ir skystojo kuro privalomųjų kokybės rodiklių patvirtinimo" pakeitimo (Legal act: *Įsakymas*, number: *D1-638/4-589/3-468/2008*; Official Journal: *Valstybės žinios*, number: *138*, Publication date: *02/12/2008*, Entry into force: *01/12/2008*; References: *(MNE(2009)50157* 3. Lietuvos Respublikos aplinkos ministro, Lietuvos Respublikos ūkio ministro ir Lietuvos Respublikos susisiekimo ministro 2006 m. rugpjūčio 31 d. įsakymas Nr. D1-399/4-336/3-340 +quote;Dėl Lietuvos Respublikoje vartojamų naftos produktų, biodegalų ir skystojo kuro privalomųjų kokybės rodiklių patvirtinimo+quote (Legal act: *Įsakymas*, number: *D1-399/4-336/3-340/2006*; Official Journal: *Valstybės žinios*, number: *95*, Publication date: *09/09/2006*, Entry into force: *10/09/2006*; Reference: *(MNE(2006)55918)* 4. Lietuvos Respublikos aplinkos oro apsaugos įstatymas Nr. VIII-1392 (Legal act: *Įstatymas*, number: *VIII-1392/1999*; Official Journal: *Valstybės žinios*, number: *98*, Publication date: *19/11/1999*, Entry into force: *19/11/1999*; Reference: *(MNE(2003)50017)* 5. Aplinkos ministro, ūkio ministro, susisiekimo ministro 2001 m. rugpjūčio 31 d. įsakymas Nr. 438/268/266 „Dėl kuro ir degalų kokybės aplinkosauginių rodiklių patvirtinimo" (Legal act: *Įsakymas*, number: *438/268/266/2001*; Official Journal: *Valstybės žinios*, number: *77*, Publication date: *07/09/2001*, Entry into force: *08/09/2001*; Reference: *(MNE(2003)50028)* 6. Ūkio ministro, aplinkos ministro ir susisiekimo ministro įsakymas Nr. 4-105/131/3-172 dėl Lietuvoje vartojamų naftos produktų ir skystojo kuro privalomųjų kokybės rodiklių patvirtinimo (Legal act: *Įsakymas*; Official Journal: *Valstybės žinios*, number: *30*, Publication date: *28/03/2003*; Reference: *(MNE(2003)50029)* 7. Lietuvos Respublikos Vyriausybės 2010 m. lapkričio 3 d. nutarimas Nr. 1540 „Dėl Lietuvos Respublikos Vyriausybės 2004 m. balandžio 7 d. nutarimo Nr. 388 +quote;Dėl Ataskaitų, susijusių su Europos Sąjungos aplinkos sektoriaus teisės aktų įgyvendinimu, teikimo Europos Komisijai tvarkos patvirtinimo ir informacijos, kurios reikia ataskaitoms Europos aplinkos agentūrai parengti, teikimo+quote; pakeitimo" (Legal act: *Nutarimas*, number: *1540/2010*; Official Journal: *Valstybės žinios*, number: *130*, Publication date: *06/11/2010*, Entry into force: *07/11/2010*; Reference: *(MNE(2010)57171)*
9.	**POLAND**	1. Rozporządzenie Ministra Transportu i Budownictwa z dnia 4 maja 2006 r. w sprawie wymagań dotyczących zawartości siarki w paliwie dostarczanym na statek (Legal act: *Rozporządzenie*; Official Journal: *Dziennik Ustaw*, number: *2006/79/555*; Reference: *(MNE(2006)53109)* 2. Ustawa z dnia 27 kwietnia 2001 r. Prawo ochrony środowiska (Legal act: *Ustawa*; Official Journal: *Dziennik Ustaw*, Publication date: *20/06/2001*; Reference: *(MNE(2003)51903)* 3. Rozporządzenie Ministra Gospodarki z dnia 17 grudnia 2002 r. w sprawie szczegółowych wymagań jakościowych dla niektórych paliw ciekłych (Legal act: *Rozporządzenie*; Official Journal: *Dziennik Ustaw*, Publication date: *24/12/2002*; Reference: *(MNE(2003)51909)* 4. Ustawa z dnia 16 marca 1995 r. o zapobieganiu zanieczyszczaniu morza przez statki (Legal act: *Ustawa*; Official Journal: *Dziennik Ustaw*, number: *1995/47/243*, Publication date: *09/05/1995*, Entry into force: *09/08/1995*; Reference: *(MNE(2004)50877)* 5. Rozporządzenie Ministra Gospodarki z dnia 21 lutego 2007 r. w sprawie metod badania jakości lekkiego oleju opałowego, ciężkiego oleju opałowego oraz oleju do silników statków żeglugi śródlądowej (Legal act: *Rozporządzenie*, number: *2007/41/262*; Official Journal: *Dziennik Ustaw*, number: *2007/41/262*; Reference: *(MNE(2007)52490)*

Item	Country	National execution measures
9.	**POLAND**	6. Rozporządzenie Ministra Gospodarki z dnia 21 lutego 2007 r. w sprawie sposobu pobierania próbek lekkiego oleju opałowego, ciężkiego oleju opałowego oraz oleju do silników statków żeglugi śródlądowej (Legal act: *Rozporządzenie*, number: *2007/41/261*; Official Journal: *Dziennik Ustaw*, number: *2007/41/261*; Reference: *(MNE(2007)52489)* 7. Rozporządzenie Ministra Gospodarki z dnia 4 stycznia 2007 r. w sprawie wymagań jakościowych dotyczących zawartości siarki dla olejów oraz rodzajów instalacji i warunków, w których będą stosowane ciężkie oleje opałowe (Legal act: *Rozporządzenie*, number: *2007/4/30*; Official Journal: *Dziennik Ustaw*, number: *2007/4/30*; Reference: *(MNE(2007)50728)* 8. Ustawa z dnia 25 sierpnia 2006 r. o systemie monitorowania i kontrolowania jakości paliw (Legal act: *Ustawa*, number: *2006/169/1200*; Official Journal: *Dziennik Ustaw*, number: *2006/169/1200*; Reference: *(MNE(2007)50623)*
10.	**SWEDEN**	1. Miljöbalken 1998:908 (Legal act: *Administrative measures)* 2. Förordningen 2000:372 om ändring i förordningen 1998:946 om svavelhaltigt bränsle (Legal act: *Administrative measures)*

Following the entry into force of MARPOL Annex VI in May 2005 a new Directive 2005/33/EC (*Directive 2005/33/EC of the European Parliament and of the Council of 6 July 2005 amending Directive 1999/32/EC, OJ L 191, 22.7.2005*), was promulgated in July 2005, amending Directive No 32 adopted in 1999 (hereinafter referred to as the Sulphur Directive).

The Directive 2005/33/EC of the European Parliament and of the Council of 6th July 2005, amending the Sulphur Directive, introduced, inter alia, the IMO concept of Sulphur Emission Control Areas (SECAs) and the associated stricter fuel standards. The maximum sulphur content of marine fuels was limited to a maximum of 1.5 % for ships operating in the Baltic Sea as from 2006 and in the North Sea and the English Channel as from 2007. In addition, and in recognition of the need to further improve air quality for the protection of human health beyond the SECAs, some requirements that went beyond the IMO rules were introduced of which the most important are:

1. The obligation for ships at berth or anchorage in EU ports to use fuels containing maximum 0.1 % sulphur;
2. The obligation for passenger ships on regular services to EU ports to use fuels containing a maximum sulphur content of 1.5 %;
3. The introduction of a possibility to test and use the emission abatement technologies.

Member States were obliged to transpose the Directive into national legislation by 11 August 2006.

The list of national enforcement measures in the exemplary EU Member States, covering the provisions of the Directive 2005/33/EC, are shown in the table below:

Item	Country	National execution measures
1.	**DENMARK**	1. Bekendtgřrelse om svovlindholdet i faste og flydende brćndsler (Legal act: *Bekendtgřrelse*, number: *1663*; Official Journal: *Lovtidende A*, number: *1663*; Reference: *(MNE(2007)50430)*
2.	**GERMANY**	1. 8. Schiffssicherheitsanpassungsverordnung (Legal act: *Verordnung*; Official Journal: *Bundesgesetzblatt Teil 1 (BGB 1)*, Publication date: *30/06/2006*; Reference: *(MNE(2006)54300)*
3.	**ESTONIA**	1. Vedelkütustele esitatavad keskkonnanőuded muutmise määrus (Legal act: *Keskkonnaministri määrus*, number: *RTL, 21.07.2006, 57, 1044*; Official Journal: *Riigi teataja*, number: *RTL, 21.07.2006, 57, 1044*, Entry into force: *24/07/2006*; Reference: *(MNE(2006)55927)* 2. VÄLISŐHU KAITSE SEADUSE JA KESKKONNAJÄRELEVALVE SEADUSE MUUTMISE SEADUS (Legal act: *seaduse parandus*, number: *RTI, 01.03.2007, 19, 95* ; Official Journal: *Elektrooniline Riigi Teataja*, number: *RTI, 01.03.2007, 19, 95,* Entry into force: *11/03/2007*; Reference: *(MNE(2007)52271)* 3. VEDELKÜTUSE SEADUS (Legal act: *seaduse parandus*, number: *RT I 2003, 21, 127*; Official Journal: *Elektrooniline Riigi Teataja*, number: *RT I 2003, 21, 127*, Entry into force: *01/12/2006*; Reference: *(MNE(2007)53042)*
4.	**IRELAND**	1. Sulphur Content of Heavy Fuel Oil, Gas Oil and Marine Fuels Regulations 2008.SI 119 of 2008 Legal act: *Statutory Instrument (Regulation or Order)*, number: *119 of 2008*; Official Journal: *Iris Oifigiúl*, Publication date: *02/05/2008*, Entry into force: *01/05/2008*; Reference: *(MNE(2008)52765)*
5.	**FINLAND**	1. Concordance table (Legal act: *Concordance table*; Reference: *(MNE(2006)55597)* 2. Valtioneuvoston asetus raskaan polttoöljyn, kevyen polttoöljyn ja meriliikenteessä käytettävän kaasuöljyn rikkipitoisuudesta / Statsrĺdets förordning om svavelhalten i tung brännolja, lätt brännolja och marin dieselbrännolja (689/2006) (Legal act: *Valtioneuvoston asetus*, number: *689/2006*; Official Journal: *Suomen Saadoskokoelma (SK)*, number: *689*, Publication date: *08/08/2006*, Page: *02128-02131*, Entry into force: *11/08/2006*; Reference: *(MNE(2006)55594)* 3. Kaupparekisterilaki / Handelsregisterlag (129/1979) (Legal act: *Laki*, number: *129/1979*; Official Journal: *Suomen Saadoskokoelma (SK)*, number: *129*; Reference: *(MNE(2006)55595)* 4. Valtioneuvoston asetus aluksista aiheutuvan ympäristön pilaantumisen ehkäisemisestä / Statsrĺdets förordning om förhindrande av miljöförorening frĺn fartyg (635/1993) ja sen muutokset / och sina förändringar: Valtioneuvoston asetukset / Statsrĺdets förordningar 1167/2003, 292/2005 ja 688/2006 (Legal act: *Valtioneuvoston asetus*, number: *635/1993*; Official Journal: *Suomen Saadoskokoelma (SK)*, number: *635*; Reference: *(MNE(2006)55592)*

Item	Country	National execution measures
5.	**FINLAND**	5. Laki aluksista aiheutuvan ympäristön pilaantumisen ehkäisemisestä / Lag om förhindrande av miljöförorening frĺn fartyg (300/1979) ja sen muutokset / och sina förändringar: laki / lag 21.4.1995 (696/1995), laki / lag 24.6.1999 (433/2000) ja/och laki / lag 18.3.2005 (238/2005) (Legal act: *Laki*, number: *300/1979*; Official Journal: *Suomen Saadoskokoelma (SK)*, number: *300*; Reference: *(MNE(2006)55587)*
6.	**SPAIN**	1. Real Decreto 1027/2006, de 15 de septiembre, por el que se modifica el Real Decreto 61/2006, de 31 de enero, en lo relativo al contenido de azufre de los combustibles para uso marítimo Legal act: *Real Decreto*, number: *1027/2006*; Official Journal: *Boletín Oficial del Estado (B.O.E)*, number: *232/2006*, Publication date: *28/09/2006*, Page: *33889-33891*, Entry into force: *29/09/2006*; Reference: *(MNE(2006)56332)*
7.	**LATVIA**	1. Ministru Kabineta 2006.gada 26.septembra noteikumi Nr. 801 Noteikumi par sēra satura ierobežošanu atsevišķiem šķidrās degvielas veidiem (Legal act: *Ministru Kabineta noteikumi*, number: *801*; Official Journal: *Latvijas Vēstnesis*, number: *161*, Publication date: *10/10/2006*, Entry into force: *11/10/2006*; Reference: *(MNE(2006)56669)* 2. Grozījumi likumā „Par piesārņojumu" (Legal act: *Likums*; Official Journal: *Latvijas Vēstnesis*, number: *62*, Publication date: *19/04/2006*, Entry into force: *03/05/2006*; Reference: *(MNE(2006)54960)*
8.	**LITHUANIA**	1. Lietuvos Respublikos aplinkos ministro, Lietuvos Respublikos ūkio ministro ir Lietuvos Respublikos susisiekimo ministro 2006 m. rugpjūčio 31 d. įsakymas Nr. D1-399/4-336/3-340 +quote;Dėl Lietuvos Respublikoje vartojamų naftos produktų, biodegalų ir skystojo kuro privalomųjų kokybės rodiklių patvirtinimo+quote (Legal act: *Įsakymas*, number: *D1-399/4-336/3-340/2006*; Official Journal: *Valstybės žinios*, number: *95*, Publication date: *09/09/2006*, Entry into force: *10/09/2006*; Reference: *(MNE(2006)55918)*
9.	**POLAND**	1. Ustawa z dnia 16 marca 1995 r. o zapobieganiu zanieczyszczaniu morza przez statki (Legal act: *Ustawa*; Official Journal: *Dziennik Ustaw*, number: *1995/47/243*, Publication date: *09/05/1995*, Entry into force: *09/08/1995*; Reference: *(MNE(2004)50877)* 2. Ustawa z dnia 25 sierpnia 2006 r. o systemie monitorowania i kontrolowania jakości paliw (Legal act: *Ustawa*, number: *2006/169/1200*; Official Journal: *Dziennik Ustaw*, number: *2006/169/1200*; Reference: *(MNE(2007)50623)* 3. Rozporządzenie Ministra Gospodarki z dnia 4 stycznia 2007 r. w sprawie wymagań jakościowych dotyczących zawartości siarki dla olejów oraz rodzajów instalacji i warunków, w których będą stosowane ciężkie oleje opałowe (Legal act: *Rozporządzenie*, number: *2007/4/30*; Official Journal: *Dziennik Ustaw*, number: *2007/4/30*; Reference: *(MNE(2007)50728)* 4. Rozporządzenie Ministra Transportu i Budownictwa z dnia 4 maja 2006 r. w sprawie wymagań dotyczących zawartości siarki w paliwie dostarczanym na statek (Legal act: *Rozporządzenie*; Official Journal: *Dziennik Ustaw*, number: *2006/79/555*; Reference: *(MNE(2006)53109)* 5. Rozporządzenie Ministra Infrastruktury z dnia 25 marca 2009 r. w sprawie wymagań dotyczących zawartości siarki w paliwie żeglugowym (Legal act: *Rozporządzenie*, number: *2009/58/477*; Official Journal: *Dziennik Ustaw*, number: *2009/58/477*; Reference: *(MNE(2009)51685)* 6. Protokół z 1997 r. uzupełniający międzynarodową konwencję o zapobieganiu zanieczyszczaniu morza przez statki, 1973, zmodyfikowaną przynależnym do niej protokołem z 1978 r. (Legal act: *Nowelizacja*, number: *2005/202/1679*; Official Journal: *Dziennik Ustaw*, number: *2005/202/1679*; Reference: *(MNE(2005)55439)* 7. Rozporządzenie Ministra Gospodarki z dnia 21 lutego 2007 r. w sprawie sposobu pobierania próbek lekkiego oleju opałowego, ciężkiego oleju opałowego oraz oleju do silników statków żeglugi śródlądowej (Legal act: *Rozporządzenie*, number: *2007/41/261*; Official Journal: *Dziennik Ustaw*, number: *2007/41/261*; Reference: *(MNE(2007)52489)* 8. Rozporządzenie Ministra Gospodarki z dnia 21 lutego 2007 r. w sprawie metod badania jakości lekkiego oleju opałowego, ciężkiego oleju opałowego oraz oleju do silników statków żeglugi śródlądowej (Legal act: *Rozporządzenie*, number: *2007/41/262*; Official Journal: *Dziennik Ustaw*, number: *2007/41/262*; Reference: *(MNE(2007)52490)*
10.	**SWEDEN**	1. Förordning (2006:1198) om ändring i förordningen (1998:946) om svavelhaltigt bränsle (Legal act: *Förordning*, number: *2006:1198*; Official Journal: *Svensk författningssamling (SFS)*, number: *2006:1198*, Entry into force: *01/01/2007*; Reference: *(MNE(2006)58141)* 2. Förordning om ändring i förordningen (1998:946) omsvavelhaltigt bränsle (Legal act: *Förordning*; Official Journal: *Svensk författningssamling (SFS)*, Publication date: *09/11/2006*, Entry into force: *01/01/2007*; Reference: *(MNE(2006)57638)*

The latest significant revision of the Sulphur Directive arises from the amendments to MARPOL Annex VI done in 2008, which imposed more stringent limits of sulphur content on fuels which are to be used in the Emission Control Areas. The EU rendered mandatory IMO rules on marine fuels through the Directive no 12, effective as of 17th December 2012, amending Sulphur Directive No 32 adopted in 1999 (*Directive 2012/33/EU of the European Parliament and of the Council of 21 November 2012 amending Council Directive 1999/32/EC as regards the sulphur content of marine fuels*).

The key elements of the new directive are:

- the sulphur limit in the Emission Control Areas (ECAs) is now 1.0 % falling to 0.10 % in 2015 (it was 1.5 % under the EU sulphur directive prior to this amendment);
- the marine fuel used in the EU must meet the global 3.50 % sulphur limit, except for on ships using an exhaust gas cleaning system operating in closed mode;
- a 0.50 % sulphur limit will be implemented in all EU waters (outside Emission Control Areas (ECAs) by 2020, even if the IMO decides to delay the global limit;
- passenger ships operating outside ECAs but on regular service between EU ports continue to be subject to a 1.50 % sulphur limit until 2020, when the EU-wide 0.50 % sulphur limit applies;
- ships at berth in EU ports are required to use only fuels with a maximum 0.1 % sulphur content;
- marine diesel oils sold in the EU must not exceed 1.50 % sulphur (as before).

By 18th June 2014 at the latest, Member States will have to amend their existing legislation on the quality of marine fuels to align it with the new Directive. The Directive provides legal certainty for the required investments by ship owners, port operators and refineries.

From 2015 onwards, Member States are asked to ensure that ships use fuels with a sulphur content of not more than 0.10 % in the Baltic Sea and the North Sea including English Channel. Equivalent, compliance methods, such as exhaust cleaning systems, are accepted.

From 2020 onwards, ships operating in all other European Sea areas will have to use fuels with sulphur content of 0.50 % or less.

The list of national enforcement measures in EU Member State, covering the provisions of the Directive 2012/33/EU, is shown in the table below:

Item	Country	National execution measures
1.	**SLOVAKIA**	1. Vyhláška Ministerstva životného prostredia Slovenskej republiky č. 231/ 2013 Z. z. o informáciách podávaných Európskej komisii, o požiadavkách na vedenie prevádzkovej evidencie, o údajoch oznamovaných do Národného emisného informačného systému a o súbore technicko-prevádzkových parametrov a technicko-organizačných opatrení Legal act: *vyhláška*, number: *231/2013*; Official Journal: *Zbierka zákonov SR*, number: *55*, Publication date: *22/08/ 2013*, Entry into force: *01/09/2013*; Reference: *(MNE(2013)57747)*

Council Directive 1999/32/EC of 26 April 1999 relating to a reduction in the sulphur content of certain liquid fuels lays down the maximum permitted sulphur content of heavy fuel oil, gas oil, marine gas oil and marine diesel oil used in the Union. Emissions from shipping due to the combustion of marine fuels with a high sulphur content contribute to air pollution in the form of sulphur dioxide and particulate matter, which harm human health and the environment, and contribute to acid deposition. Without the measures set out in this Directive, emissions from shipping would soon have been higher than emissions from all land-based sources. Air pollution caused by ships at berth is a major concern for many harbour cities when it comes to their efforts to meet the Union's air quality limit values. Under Directive 1999/32/EC, the Commission is to report to the European Parliament and the Council on the implementation of that Directive and may submit with its report proposals for amending it, in particular as regards the reduction of sulphur limits for marine fuel in SOx Emission Control Areas (SECAs), in accordance with the work of the International Maritime Organisation (IMO). In 2008, the IMO adopted a resolution to amend Annex VI of the Protocol of 1997 to amend the International Convention for the Prevention of Pollution from Ships, 1973, as modified by the Protocol of 1978 relating thereto (MARPOL), containing regulations for the prevention of air pollution from ships. The revised Annex VI to MARPOL entered into force on 1 July 2010. The revised Annex VI to MARPOL introduces, inter alia, stricter sulphur limits for marine fuel in SECAs (1.00 % as of 1 July 2010 and 0.10 % as of 1 January 2015) as well as in sea areas outside SECAs (3.50 % as of 1 January 2012 and, in principle, 0.50 % as of 1 January 2020). Most Member States are obliged, in accordance with their international commitments, to require ships to use fuel with a maximum sulphur content of 1.00 % in SECAs as of 1 July 2010. In order to ensure coherence with international law as well as to secure proper enforcement of new globally established sulphur standards in the Union, Directive 1999/32/EC should be aligned with the revised Annex VI to MARPOL. In order to ensure a minimum quality of fuel used by ships either for fuel-based or technology-based compliance, the marine fuel the sulphur content of which exceeds the general standard of 3,50 % by mass should not be allowed for use in the Union, except for fuels supplied to ships using emission abatement methods operating in closed mode. Amendments to Annex VI to MARPOL regarding SECAs are possible under IMO procedures. In the event that further changes, including exemptions, are introduced with regard to the application of SECA limits in Annex VI to MARPOL, the Commission should consider any such changes and, where appropriate, without delay make the necessary proposal in accordance with the TFEU to fully align Directive 1999/32/EC with the IMO rules regarding SECAs. The introduction of any new emission control areas should be subject to the IMO process under Annex VI to MARPOL and should be underpinned by a well-founded case based on environmental and economic grounds and supported by scientific data. In accordance with regulation 18 of the revised Annex VI to MARPOL, Member States should endeavour to ensure the availability of marine fuels which comply with this Directive. In view of the global dimension of environmental politics and shipping emissions, ambitious emission standards should be set at a global level. Passenger ships operate mostly in ports or close to coastal areas and their impacts on human health and the environment are significant. In order to improve the air quality around ports and coasts, those ships are required to use marine fuel with a maximum sulphur content of 1.50 % until stricter sulphur standards apply to all ships in territorial seas, exclusive economic zones and pollution control zones of Member States.

Complying with the low sulphur limits for marine fuels, particularly in SECAs, can result in a significant increase in the price of such fuels, at least in the short term, and can have a negative effect on the competitiveness of short sea shipping in comparison with other transport modes, as well as on the competitiveness of the industries in the countries bordering SECAs. Suitable solutions are necessary in order to reduce compliance costs for the affected industries, such as allowing for alternative, more cost-effective methods of compliance than fuel-based compliance and providing support, where necessary. Based inter alia on reports from Member States, the Commission will closely monitor the impacts of the shipping

sector's compliance with the new fuel quality standards, particularly with respect to possible modal shift from sea to land-based transport and will, if appropriate, propose proper measures to counteract such a trend.

The costs of the new requirements to reduce sulphur dioxide emissions could result in modal shift from sea to land-based transport and could have negative effects on the competitiveness of the industries. The Commission should make full use of instruments such as Marco Polo and the trans-European transport network to provide targeted assistance so as to minimise the risk of modal shift. Member States may consider it necessary to provide support to operators affected by this Directive in accordance with the applicable State aid rules.

CONTACT WITH THE AUTHOR

Beata Madejska, M. Sc.
lawyer specialized in the EU legal regulations
mobile: +48 606 273 740
e-mail: beata.madejska@interia.pl

The Ship Handling Research and Training Centre at Ilawa is owned by the Foundation for Safety of Navigation and Environment Protection, which is a joint venture between the Gdynia Maritime University, the Gdansk University of Technology and the City of Ilawa.

Two main fields of activity of the Foundation are:

- Training on ship handling. Since 1980 more than 2500 ship masters and pilots from 35 countries were trained at Iława Centre. The Foundation for Safety of Navigation and Environment Protection, being non-profit organisation is reinvesting all spare funds in new facilities and each year to the existing facilities new models and new training areas were added. Existing training models each year are also modernised, that's why at present the Centre represents a modern facility perfectly capable to perform training on ship handling of shipmasters, pilots and tug masters.

- Research on ship's manoeuvrability. Many experimental and theoretical research programmes covering different problems of manoeuvrability (including human effect, harbour and waterway design) are successfully realised at the Centre.

The Foundation possesses ISO 9001 quality certificate.

Why training on ship handling?

The safe handling of ships depends on many factors - on ship's manoeuvring characteristics, human factor (operator experience and skill, his behaviour in stressed situation, etc.), actual environmental conditions, and degree of water area restriction.

Results of analysis of CRG (collisions, rammings and groundings) casualties show that in one third of all the human error is involved, and the same amount of CRG casualties is attributed to the poor controllability of ships. Training on ship handling is largely recommended by IMO as one of the most effective method for improving the safety at sea. The goal of the above training is to gain theoretical and practical knowledge on ship handling in a wide number of different situations met in practice at sea.

For further information please contact:
The Foundation for Safety of Navigation and Environment Protection

Head office:
36, Chrzanowskiego Street
80-278 GDAŃSK, POLAND
tel./fax: +48 (0) 58 341 59 19

Ship Handling Centre:
14-200 IŁAWA-KAMIONKA, POLAND
tel./fax: +48 (0) 89 648 74 90
e-mail: office@ilawashiphandling.com.pl
e-mail: office@portilawa.com

I am pleased to invite you to the 20th International Conference on Hydrodynamics in Ship Design and Operation – HYDRONAV 2014. The conference is organised by Wrocław University of Technology, in cooperation with Gdańsk University of Technology, The Foundation for Safety of Navigation and Environment Protection, and Ship Design and Research Centre S.A. It will be held on 24th and 25th of June 2014 in Wrocław, Poland.

Wrocław University of Technology

Objectives & Topics

The conference is thought to provide a forum for paper presentation and discussion on development and application of experimental and theoretical hydrodynamics in design and operation of ships and other marine vehicles or structures. Conference papers will refer to the following topics:

- Ship resistance
- Marine propellers and propulsion
- Steering devices and manoeuvrability
- Stability, seakeeping and safety of navigation
- Hydrodynamics problems in operation
- Interaction with environment

GDANSK UNIVERSITY OF TECHNOLOGY

Deadlines

The prospective participants and authors of conference papers are asked to comply with the following schedule:

Submission of abstracts ..... by January 31, 2014
The acceptance of abstracts ..... by February 28, 2014
Submission of full-length manuscripts ..... by April 15, 2014
Registration ..... by April 15, 2014
Payment of fee ..... by June 15, 2014

SHIP HANDLING RESEARCH AND TRAINING CENTRE
ILAWA - POLAND

Contact

For more information, please visit the conference web site at **http://hydronav.pwr.wroc.pl** or contact the Conference Secretariat:

Conference Secretariat HYDRONAV 2014
Wrocław University of Technology
Institute of Machine Design and Operation
Wybrzeże Wyspiańskiego 27
50-370 Wroclaw, Poland;
http://hydronav.pwr.wroc.pl
phone: +48 71 3202667; fax: +48 71 3227645; e-mail: hydronav@pwr.wroc.pl

Sincerely yours,
Prof. Jan Kulczyk – Chairman of the Organizing Committee